Modelling the impacts of climate change on blue and green water interchange, crop yields, and virtual water trade under drought and post-drought conditions in Nelson River Basin

by

Pouya Khalili

A dissertation submitted in partial fulfillment of the requirements for the degree of

Doctor of Philosophy

Department of Earth and Atmospheric Sciences

University of Alberta

ABSTRACT

The unfolding climate change crisis poses a growing challenge to water and food security, and yet the reliability of the global breadbaskets and their relation with water resources in the future is poorly understood. The global breadbaskets are defined as key production regions for food grains and recognized for their vital contribution to global food security. In the mid-to-high latitude regions, especially in the higher latitudes of the temperate zone, the global breadbaskets are projected to receive an overall increased precipitation and improved crop yields under the effects of global warming scenarios, which is often perceived as beneficial to crop production and export potentials in the future (Myers et al., 2017; IPCC, 2021). However, the extreme warm-dry events, anticipated as a consequence of global warming, can significantly affect the agro-hydrological processes, crop yields, and therefore export potential of the crops from these regions. This research examines the potential impacts of future droughts and post-droughts on hydrology, crop yields, and their linkages through assessing net virtual water export (NVWE), the water embodied in the production process of the crops that are exported to international countries. The study takes Nelson River Basin (NRB), a large agricultural watershed in western Canada and a global breadbasket located in higher latitudes of the temperate zone, as an example and it provides insights for future planning and informed decisions for water and food security.

To understand the hydrological processes affecting crop yield and soil nutrients (i.e., nitrogen in this study) and their relation with changes in climate, this study employs a semi-distributed process-based agro-hydrologic model to an agricultural catchment in the NRB, i.e., Red Deer River Basin (RDRB), in the province of Alberta, Canada. Specifically, the research explores the effects of climate change and availability of soil water, as well as nitrogen fertilizer application scenarios on crop yields. The study examines the impacts on rainfed spring wheat, which is a

dominant crop grown in most of NRB and in the RDRB. The results indicate that nitrogen stress may dominate other stress factors in producing rainfed wheat yields in the future as compared to the historical conditions that water-stress has been a dominant factor in the region. This is likely due to the overall increase in the soil moisture in the future that when compounded with a warmer temperature, triggers crop growth and potential yields, demanding more nitrogen in the soil. However, a regional assessment of the soil water availability, which affects nutrient and water uptakes by crops and their evapotranspiration rates (ET, green water), and the effects on hydrological water balance under extreme climatic events such as droughts in the future, is required.

In a closed hydrological system, i.e., a watershed, the blue water (BW, or net annual freshwater generated in a catchment) and green water (GW, or actual evapotranspiration) are interlinked through numerous climate, soil, and plant processes. Their relationship has reportedly been non-stationary, with an anticipated shift from BW to GW in the future. Given that GW accounts for over 70% of water consumption in global food production, further research in this study scrutinizes the interlinkages between BW and GW and their potential shifts, primarily in response to future extreme warm-dry events. The results indicate dissimilarity in the physical processes that link GW and BW across different ecohydrological regions, and therefore, disproportional projected changes in BW and GW, and their linkages across regions. Mountainous and natural lands exhibit a shift from BW to GW, due to legacy soil moisture from earlier seasons and groundwater contributions. Conversely, in crop lands, there is a significant decrease in both BW and GW with no notable shift from BW to GW, posing severe threats to local and regional food production.

Lastly, the research evaluates the effects of drought and subsequent post-drought conditions on crop production and its relation to watershed hydrology (i.e., blue water- also defined as water yield (WYLD) in this study) through assessment of NVWE. Contrary to prevalent long-term average projections of a wetter future for higher latitude regions of the temperate zone, the investigation of the longest and the most severe drought (LMD) in this study, indicate a substantial reduction in precipitation, Y (rainfed wheat and canola in this study), as well as WYLD in the future. The reductions in these agro-hydrological variables are likely to be more severe than historical drought conditions under SSP126. The slight improvement under the SSP585 scenario due to the CO_2 effects on plant photosynthesis processes is not uniform across region and crop types. In central areas, which are prominent for crop production, the canola Y demonstrated less improvement as compared to the wheat Y, which is also compounded with a greater VWC of canola than wheat. The larger VWC of canola suggests larger crop water consumption in production of a tonne of crop, resulting in a considerable reduction of WYLD as compared to wheat crop and relative to the other regions across NRB. Overall, the regional scale WYLD, Y, and VWC show improvement during SSP585 droughts as compared to those of SSP126; however, they remain considerably lower than the average historical conditions regardless of crop type and the geographic location.

During post-droughts, the study reveals variable recovery times for WYLD, Y, and NVWE in the future, with the WYLD demonstrating the slowest recovery time as compared to Y and NVWE during the years after the LMD. Given the projected frequent droughts in the future, the slow recovery of the WYLD after droughts can be a limiting factor for sustainable production and export potentials as it can deteriorate environment and several economic sectors. Our study lays a strong basis for examination of a strategic crop selection and diversification, which can be considered as

an adaptation measure for conservation of WYLD for an integrated water and food security in the future.

PREFACE

This PhD research utilizes the agro-hydrological models of the Red Deer River Basin (RDR) and the Nelson River Basin (NRB) created by Pouya Khalili. The dissertation follows a paper-based structure, with several chapters already published or under review in respected journals.

Chapter 2, entitled "Non-stationary response of rain-fed spring wheat yield to future climate change in northern latitudes," was published in the Science of the Total Environment journal. The citation for this work is: Khalili, P., Masud, B., Qian, B., Mezbahuddin, S., Dyck, M. & Faramarzi, M. (2021). Science of The Total Environment, 772, p.145474.

Chapter 3, "Assessment of blue water-green water interchange under extreme warm and dry events across different ecohydrological regions of western Canada", is accepted for publication in the Journal of Hydrology. The proposed citation is: Khalili, P., Razavi, S., Davies, E.G., Alessi, D.S., & Faramarzi, M. (2023). Journal of Hydrology.

Finally, Chapter 4, “Modelling the impacts of future droughts and post-droughts on hydrology, crop yields, and their linkages through assessing virtual water trade in agricultural watersheds of high latitude regions”, has been thoroughly reviewed and revised, and is now ready to be submitted to a peer-reviewed journal in hydrology research.

Pouya Khalili is the primary author of this dissertation and of all three manuscripts, who performed all of the analyses, wrote the draft manuscripts, and revised them in later versions; and Dr. Monireh Faramarzi is corresponding author who reviewed and provided constructive comments and revision of this dissertation and the early drafts of the three manuscripts that form the main body of this dissertation.

DEDICATION

I dedicate this dissertation to my beloved family, with special acknowledgement to my wife, Paniz. Her unwavering support and love have been indispensable throughout this journey. Without her, the completion of this work would not have been possible.

ACKNOWLEDGEMENTS

I wish to express my deepest gratitude to my supervisor, Dr. Monireh Faramarzi, whose exceptional supervision and dedicated involvement in this project made my participation in this program possible. Her consistent support, encouragement, and novel ideas have spurred insightful discussions and propelled future water-food research.

I am equally thankful to my supervisory committee members, Dr. Daniel Alessi and Dr. Evan Davies, for their insightful feedback and invaluable suggestions, which significantly contributed to the preparation and success of this PhD research. The continuous dedication of Dr. Faramarzi, Dr. Alessi, and Dr. Davies, as displayed in supervisory committee meetings, was crucial to the success of this program.

Furthermore, I wish to acknowledge Dr. Paul Myers for graciously accepting to chair my PhD thesis defense. I would like to extend my gratitude to my external examiner, Dr. Raghavan Srinivasan, and my arm's length examiner, Dr. Wenming (William) Zhang. I appreciate their willingness to devote their time and expertise in evaluating my dissertation.

My heartfelt thanks also go to my colleagues at the Watershed Science and Modelling Laboratory, particularly Dr. Badrul Masud and Dr. Quan Cui, for their assistance at various stages of this research project. Finally, my appreciation extends to Dr. Majid Iravani, whose moral and emotional support has been a beacon throughout my journey.

TABLE OF CONTENTS

LIST OF TABLES

LIST OF FIGURES

Figure 2.10. Share of the variance related to GCMs, RCPs, DSs, and 95PPUs for projected SWY changes in the study watershed, under baseline N application scenario, NS1, and NS2.

Figure 2.11. Share of the variance (% ANOVA) related to GCMs, RCPs, DSs, and 95PPUs for projected SWY changes in high (H), mid-high (MH), mid-low (ML), and low (L) W and N_stress regions under the baseline scenario, NS1, and NS2.

Figure 3.1. (A) Map of the Nelson River Basin including geographic extents, major watersheds, rivers, reservoirs, dams, lakes, hydrometric stations, (B) the land use map and land use classes considered in the model according to the Government of Canada (2019) classification, and the Census Agricultural Region (CAR), for which the agricultural management and crop yield time series are available from government of Canada for calibration and validation in this study.

Figure 3.2. A color map demonstrating model performance for the entire calibration and validation period for spring wheat yield/SWY (upper row) and streamflow (lower row). The color cells (count in the legend) represent the combination of the number of stations (or number of CARs) and number of times of occurrence during the study period, while whitespace denotes where no data exists.

Figure 3.4. Temporal variation of the compound warm-dry events during the growing season (May to September) for the historical (1987-2016) and future (2070-2099) periods. A, B, C, D, E, and F represent the results that are derived based on the EC-Earth3, MRI-ESM2.0, BCC-CSM2-MR, CNRM-CM6-1, EC-Earth3-veg, and CanESM2 models, respectively. Note that warm-dry events are calculated for all years of the historical and future periods but for better visualization, only a limited number of warm-dry events are shown in the picture.

Figure 3.6. Simulated long-term average hydrologic water balance data during growing season (calculated as the averages over five months during the crop growing season) for historical period (left column), and their anomalies from AH under extreme dry-warm years (column 2-4 from the left). The maps in horizontal rows are: average GW (ET, mm/month), precipitation (mm/month), soil water (mm/month), BW (mm/month), water stress (days/month), and snowmelt (mm/month) during growing season.

Figure 3.7. Sub-basin scale simulated blue to green water ratio (BW/GW) for the growing season. (a) long-term (1987-2016) average historical ratios (AH); (b) Anomalies of historical extreme warm-dry years ratios from those of AH; (c) Anomalies of future (2070-2099) extreme warm-dry years ratios under SSP126 from those of AH (EF126); (d) Anomalies of future (2070-2099) extreme warm-dry years ratios under SSP585 from those of AH (EF126) (EF585). The % anomalies in b, c, and d were calculated as: [(Extreme Scenario-AH)/AH]×100. Figures c and d are based on multi-model ensemble mean values. The circles represent streamflow anomalies in 150 select outlets (%).

Figure 3.8. Comparison of simulated hydrologic variables for mountainous lands (a), natural lands (b), and crop lands (c) under AH, EH, EF126, and EF585 scenarios. AH is averaged over

30 years. EH, EF126 and EF585 are averaged over extreme warm-dry years. All extreme scenarios are anomalies from AH, and all future extreme scenarios are based on ensemble means. All data are reported for growing season.

Figure 4.1. (A) Map of the NRB including the land use land cover classes considered in the model according to the Government of Canada (2019) classification, rivers, reservoirs, lakes, and hydrometric stations; (B) geographic extent, and the Census Agricultural Region (CAR), for which crop yield time series are available from Government of Canada (2019) for calibration and validation in this study; (C) spring wheat and (D) canola crop spatial density maps (%) showing the density of cultivated lands in the study area.

Figure 4.2. Simulated long-term average monthly WYLD (mm) and precipitation (mm) during the crop growing season (monthly averages during May-Sept): historical (first column), future SSP126 scenario (second column), future SSP585 scenario (third column), and the anomalies from the historical baseline for both future SSP126 (fourth column) and SSP585 (fifth column) scenarios.

Figure 4.3. Simulated long-term average annual (1987-2016) crop yields for spring wheat and canola (tonne/ha) during crop growing seasons: historical baseline (first column from left), future SSP126 scenario (second column), future SSP585 scenario (third column), and anomalies from the historical baseline for both future SSP126 (fourth column) and SSP585 (fifth column) scenarios.

Figure 4.4. Long-term average simulated virtual water content (VWC; m^3/tonne) and net virtual water export (NVWE; m^3) for spring wheat and canola under historical and future scenarios (SSP126 and SSP585), accompanied by their projected anomalies as compared to the historical values (%) (right two columns).

Figure 4.6. Simulated WYLD (left) and Y (right) versus cumulative precipitation in six selected CARs across the basin. The data are presented for the five consecutive post-drought years (D scenario, red) and the same years assuming no prior drought (ND scenario, blue) under the SSP126 future scenario. Only spring wheat Y is presented due to its prevalence in the basin. Each dot represents a sub-basin within a CAR.

Figure 4.7. Simulated net virtual water export (NVWE) anomalies between D and ND scenarios (i.e., calculated as NVWE (D) - NVWE (ND)) in six selected CARs across the basin. The data are presented for five consecutive post-drought years under the SSP126 future scenario. Only spring wheat NVWE anomalies ($\times 10^5$ m^3) is presented due to its prevalence in the basin. Each dot represents a sub-basin within a CAR.

LIST OF ACRONYMS

95PPU: 95 percent prediction uncertainty
AFSC: Alberta Financial Service Cooperation
AH: Average historical
ANOVA: Analysis of Variance
ARB: Assiniboine river basin
BW: Blue water
CAR: Census agricultural region
CMIP6: Coupled Model Intercomparison Project Phase 6
CV: Coefficient of variation
D scenario: Drought scenario; Considers the actual occurrence of drought in time series data.
DEM: Digital elevation map
DHMI: Dry-hot magnitude index
DS1: Downscaled climate data with further bias correction
DS2: Downscaled climate data without further bias correction
L95PPU: The 2.5% level presented a lower band of uncertainty range
EF: Extreme events under historical period
EF126: Extreme events under SSP126
EF585: Extreme events under SSP585
ET: Actual evapotranspiration
GCM: Global climate models
GW: Green water
HRU: Hydrologic response unit
KGE: Kling-Gupta efficiency
LHS: Latin hypercube sampling
LMD: longest and most severe droughts
masl: Meters above sea level
MSE: Mean square error
N: Nitrogen
N_stress: Nitrogen stress
ND scenario: non-drought scenario; Assumes that the drought years never happened in time series data
NRB: Nelson River basin
NRLB: Nelson river local basin
NS1: 20% decreased N fertilizer application rate from the baseline scenario
NS2: 20% increased N fertilizer application rate from the baseline scenario
NSE: Nash-Sutcliffe efficiency
NVWE: Net virtual water export
NVWT: Net virtual water trade

PBIAS: percent bias
PCIC: Pacific Climate Impacts Consortium
PET: Potential evapotranspiration
R^2: Coefficient of determination
RCP: Representative Concentration Pathway
RDR: Red Deer River
RRB: Red river basin
RUE: Radiation-use efficiency
SA: Sensitivity analysis
SPEI: Standardized Precipitation Evapotranspiration Index
SPI: Standardized precipitation index
SRB: Saskatchewan river basin
SSI: The sum of squares of interactions
SSP: Shared socioeconomic pathway
SST: Total sum of squares
SS_X: the sum of squares from an individual source X
SUFI-2: Sequential uncertainty fitting program
SWAT: Soil and Water Assessment Tool
SWY: Spring wheat yield
T_stress: Temperature stress
U95PPU: The 97.5% level indicated a higher band of uncertainty range
USDA: United states department of agriculture
VWC: Virtual water content
VWT: Virtual water trade
W_stress: Water stress
WFDEI: WATCH Forcing Data ERA-Interim
WP: Water productivity
WRB: Winnipeg river basin
WYLD: Water yield
Y: Crop yield

CHAPTER I – INTRODUCTION

1.1. Overview

Climate change, characterized by its escalating severity of extreme weather phenomena such as droughts and intensified heat conditions, poses a profound threat to the stability of global ecosystems (IPCC, 2021). Such evolving climatic dynamic bears significant implications for socioeconomic sectors and ecosystem services (Rosenzweig et al., 2020). Different socioeconomic sectors (i.e., agricultural crop production, industries, and municipality) are linked through their reliance on two crucial types of water resources including green water (GW) and blue water (BW). In a watershed, the GW is defined as the total actual evaporation from soil and open water bodies and transpiration by plants. The GW is an in-situ source of water, which is supplied from rainfall precipitation, snowmelt infiltration, as well as high groundwater levels. The BW is defined as the net freshwater generated in a hydrologic catchment and stored in streams, lakes/reservoirs, and aquifers. The BW components that do not account for groundwater storage is also called water yield (WYLD).

Traditional water policies and development plans have often centered around managing BW through water transfer projects, storage through construction of dams and distribution through channels, or through groundwater pumping; all of which are utilized for various socioeconomic sectors (Mekonnen and Hoekstra, 2016). However, GW plays a critical role in global water consumption, particularly in the agricultural sector. In fact, 70% of the agricultural sector relies on GW resources for its water needs (Jägermeyr et al., 2021). The BW and GW are interconnected through numerous biogeochemical and physical processes within a watershed, and their availability is limited in time and space (Schyns et al., 2019). As climate change amplifies the frequency and severity of droughts (Spinoni et al., 2020), these two distinct, yet interconnected

water resource components, become increasingly critical; and maintaining their balance to support not only food production, but also other socioeconomic sectors and ecosystem services remains imperative. Therefore, it is crucial to develop an interdisciplinary approach for a thorough assessment of linkages between blue and green water resources, while also assessing their relationship with crop yields and export potentials for global food security. Numerous studies assessed water resources under future global warming scenarios without linking them to crop production (Arnell and Gosling, 2013; Greve et al., 2014; Schewe et al., 2014). Other studies developed a thorough assessment of actual and potential crop yields and management options for filling crop yield gaps, but without considering how the crop yield potentials might be affected by changes in hydrological processes and the GW-BW variations under future climate change scenarios (Burek et al., 2016; Mekonnen and Hoekstra, 2016; Oki and Kanae, 2006). Only limited studies suggested a comprehensive assessment of water-food relations and their variation and feedback mechanism using multidisciplinary approaches and under extreme climate events in the future (Orth and Destouni, 2018; Rockström, 2003).

The virtual water trade (VWT), i.e., water embedded in the production process of crops that are traded between and within nations (Allen, 1996), is a measure, which relates crop yields to their BW and GW consumptions in irrigated and rainfed production systems, respectively. Most earlier VWT studies, centered around three main subjects including: (1) assessing the feasibility of using the concept as a management tool for balancing global water resources through trade of water intensive commodities from water abundant to water scarce regions (Allan, 1996, Chapagain et al., 2006), (2) investigating water availability of nations and their food import pattern, with an ultimate goal to understand if food imports follow water availability restrictions of the nations (Mekonnen and Hoekstra, 2020), and (3) socioeconomic drivers of VWT and the impacts on both

importing and exporting nations (D'Odorico et al., 2019). However, this study uses VWT as an inter-disciplinary approach that connects crop growth, crop yields, and crop export potentials, to the GW consumption and their relation to hydrological processes and, therefore, to BW availability at a watershed scale.

Central to this exploration is the Red Deer River Basin (RDR), a pivotal agricultural catchment within the large-scale Nelson River Basin (NRB). Here, a process-driven agro-hydrological model charts the multitude of natural and human-induced factors—from increased CO_2 levels, shifting temperatures, and altered precipitation patterns to varying agricultural practices. These elements jointly influence BW and GW resources and the subsequent crop yields, emphasizing their interdependence across the catchment. The broader implications of these relations, especially under extreme climatic events, become imperative in the larger context of the NRB—a vast region in western Canada, rich in agriculture and playing a pivotal role in global food supplies. With origins in the Rocky Mountains, it spans diverse ecological zones, from vital agricultural lands to ecologically rich forests and wetlands, making it a unique study area for this study. Given the evolving dynamics of climate change, there is an emphasis on understanding the impacts of global warming scenarios, particularly in relation to crop yield, BW, and net virtual water export (NVWE) during future warm-dry events and after droughts. Utilizing scenarios like SSP126 and SSP585, this research not only endeavors to understand potential shifts in the GW-BW during these climatic extremities but also aims to explore the interrelations of crop yield, NVWE, and BW following the termination of droughts.

This study facilitates examination of the interactions between agro-hydrological processes and their implications for water and food security under future global warming scenarios. The insights derived, especially about the interplay of GW-BW, crop yields, and NVWE under

changing climatic conditions, are not confined to the NRB; they have a global resonance. The variation between VWC of different crops, their association with hydrological metrics, and export potential serve as a foundation for potential strategies, including crop diversification, to ensure water and food security in the future. This study lays a strong basis for examination of such adaptation strategies, for long-term planning and management of water and food resources.

1.2. Overarching Goal and the Main Research Objectives

The overarching goal of this research is to study the dynamics of GW-BW balance and their relationship with crop yields and NVWE under historical and future conditions. The study aims to assess their changes under future extreme climatic events, particularly warm and dry spells, as well as their recovery status during post drought conditions. The study involves an explicit assessment of the interplay among multiple components, such as soil water content, watershed hydrological processes like runoff and infiltration, crop yield response to climatic variables (including temperature, precipitation, and CO_2 concentrations), and soil nutrients. By diving deep into these processes and their interactions and linkages, this research seeks to shed light on the collective response of the watershed agro-hydrologic processes, especially in the face of droughts and their subsequent repercussions. The study spotlights the NRB, a significant agricultural watershed in western Canada and a main breadbasket in mid-to-high latitude region, which supplies food to over 170 countries around the globe and is home to ~70 Mha of agricultural lands in Canada. The ecohydrological diversity of the basin, with its geographic location situated in the higher latitudes of the global temperate zone, and being one of the largest river basins in North America, provides strong basis for a comprehensive assessment of BW and GW resources and their linkages under various ecohydrological settings. This includes the study of processes involved in the climate-water-food system, such as increased CO_2 concentration, elevated temperature, altered

precipitation, crop growth response to elevated atmospheric CO2 and the resulting impacts on stomatal closure, nutrient demands, and evapotranspiration (ET) scheme, as well as altered soil water dynamics and shifting snowmelt patterns. These factors are integral to understanding the dynamics of BW and GW resources, crop yields, and their linkages across regions.

To achieve the overarching goal of this study, the research is guided by the following main objectives, forming the three main chapters of this research (see section 1.3):

Objective 1: To provide an improved understanding of non-stationary crop yield response to climate change-induced agro-hydrological processes and management factors at a regional scale. To achieve this main objective the specific objectives are as follow:

- quantify yield response to variations in climate models, emission scenarios, downscaling methods, and agro-hydrologic model parameters,
- investigate spatiotemporal variability of the projected yield responses to understand physical, biochemical, and physiological processes driving crop yield responses in the future
- to draw a conclusion on the non-stationarity in agricultural crop yields under changing climate and agronomic management practices

Objective 2: To characterize changes in GW-BW relationships under future warm-dry events across different landscape and ecological settings such as mountainous lands, natural lands, and crop lands in large watersheds. To achieve this main objective, the specific objectives are to:

- quantify spatiotemporal variations of BW and GW linkages under different ecohydrological settings, including in mountains and foothills (i.e., mountainous lands),

agricultural plains (i.e., crop lands), and other natural landscapes such as forests and wetlands (i.e., natural lands)

- discuss the spatiotemporal variations of driving factors and how they affect changes in GW-BW relationships
- quantify GW-BW anomalies under possible future extreme warm-dry events from their historical averages

Objective 3: To examine the impacts of future droughts and post-droughts on crop yields, crop production and export potentials, and their effects and relations to water resources (i.e., GW-BW) through analysis of NVWE. To achieve this main objective, the specific objectives are to:

- analyze the past and projected changes in BW (i.e., water yield in this study) under average, drought, and post drought conditions
- assess the past and projected changes in crop yields, under average, drought, and post drought conditions
- evaluate the impacts of drought and post-drought conditions on NVWE and its linkages with Y and WYLD under historical and future scenarios in the NRB as one of the important breadbaskets of the world which exports agricultural crops to over 170 countries around the world

The research utilizes the Soil and Water Assessment Tool (SWAT) agro-hydrologic model for process simulation associated with BW, GW, and Y, and the outputs are further analysed to achieve the specific objectives listed above. SWAT is a process-based, semi-distributed agro-hydrological model that lends itself as a suitable tool to climate change impact assessment in this research because:

1. It integrates many related physical processes including watershed hydrology, climate, soil nutrient cycling, crop and vegetation growth, and agricultural and water management practices
2. It has been successfully applied both worldwide and in Canada
3. Calibration and uncertainty analysis of the processes have been performed, and the related tools have been developed and continuously updated

1.3. Thesis Structure

Chapter 2 presents the modelling and the analyses performed to achieve the objective 1 and is drafted in the form of a manuscript, which is published in the *Science of The Total Environment* journal. It presents the simulation and analysis of crop yield response to variation in soil water and nutrient processes due to changes in climate and management factors under global warming scenarios. It also describes the uncertainties inherent in the hydrologic and climate change model projections.

Chapter 3 covers modeling data and analysis performed to achieve objective 2. The findings are presented in the form of a manuscript, which is accepted for publication in the *Journal of Hydrology*. This chapter analyzes the linkages between GW and BW across various ecohydrological regions in the NRB, exploring the processes and factors influencing their spatiotemporal variations and assessing potential deviations from historical averages under future extreme warm-dry events.

Chapter 4 presents results of objective 3, and is presented in the form of a draft manuscript. This chapter is currently undergoing the final minor revisions and is ready for submission to a peer-reviewed journal. Chapter 4 investigates the effects of extreme drought and post-drought conditions on crop yields and crop export potentials under future global warming scenarios. The

chapter assesses the linkages on blue water disruptions by analysing NVWE in the NRB. It also provides discussion and implications of improved yields and export potentials on watershed hydrology and BW availability for other socioeconomic sectors and ecosystem.

Chapter 5 synthesizes the research findings from previous chapters, providing general conclusions concerning water-food relations and the potential changes under future extreme droughts and post-drought conditions in the Nelson River Basin, with the possibility to extend to other agricultural watersheds of high latitude regions in temperate zone with similar ecohydrological conditions. A number of shortcomings encountered in modeling the water and crop production are pointed out. Finally, an outlook is provided pointing out the potential applicability of the modeling framework developed in this study to examine various management scenarios (e.g., cropping pattern adjustment) to improve water-food security.

CHAPTER II – MANUSCRIPT 1

Non-stationarity response of rain-fed spring wheat yield to future climate change in northern latitudes

Pouya Khalili[1], M. Badrul Masud[1], Budong Qian[2], Symon Mezbahuddin[3, 4], Miles Dyck[4], Monireh Faramarzi[1*]

[1] Watershed Science and Modeling Laboratory, Department of Earth and Atmospheric Sciences, Faculty of Science, University of Alberta, Edmonton, AB T6G 2R3, Canada

[2] Ottawa Research and Development Centre, Agriculture and Agri-Food Canada, Ottawa, ON K1A 0C6, Canada

[3] Natural Resource Management, Alberta Agriculture and Forestry, Edmonton, AB

[4] Department of Renewable Resources, Faculty of Agricultural Life and Environmental Sciences, University of Alberta, Edmonton, AB, Edmonton, AB T6G 2R3 Canada.

[*]Corresponding author: faramarz@ualberta.ca

2.1 Abstract

The non-stationary response of crop growth to changes in hydro-climatic variables makes yield projection uncertain and design and implementation of adaptation strategies debatable. This study simulated time-varying behavior of the underlying cause-and-effect mechanisms affecting spring wheat yield (SWY) under various climate change and nitrogen (N) application scenarios in the Red Deer River basin in agricultural lands of the western Canadian Prairies. A calibrated and validated Soil and Water Assessment Tool and Analysis of Variance decomposition methods were utilized to assess contribution of crop growth parameters, Global Climate Models, Representative Concentration Pathways, and downscaling techniques to the total SWY variance for the 2040-2064 period. The results showed that the cause-and-effect mechanisms, driving crop yield, shifted from creating a water stress (W_stress) historically dominated system (27 days of W_stress days) to nitrogen stress (N_stress) dominated status (27 to 35 N_stress days) in the future period. It was shown that while higher precipitation, warmer weather, and early snowmelts, along with elevated

CO_2 may favor SWY in cold regions in the future (up to 50% more yields in some sub-basins), the yield potentials may be limited by N_stress (only up to 0.7% yield increase in some sub-basins). The N_stress might be partially related to the N deficiency in the soil, which can be compensated by N fertilizer application. However, inadequate N uptake due to limited evapotranspiration under elevated atmospheric CO_2 might pose restrictions to SWY potentials even in the least N deficient regions. This study uncovers important information on the understanding of spatiotemporal variability of hydrogeochemical processes driving crop yields and the non-stationary response of yields to changing climate. The results also underscore spatiotemporal variability of N_stress due to N deficiency in the soil or N uptake by crops, both of which may restrain SWY by changes in atmospheric CO_2 concentrations in the future.

Keywords: Variance decomposition, water stress, nitrogen stress, temperature stress, hydrologic processes

2.2 Introduction

Climate change is expected to increase the frequency of extreme climatic events such as droughts (Kang and Sridhar, 2018) and floods (Karamouz et al., 2019) that may significantly jeopardize freshwater availability and food production (IPCC, 2014). Agriculture and food production can be disrupted due to the direct and indirect effects of climate change. Direct effects of changes in climate pattern, such as increased heat stress (Yang et al., 2017), frequent extreme temperatures (S. Zhang et al., 2016), intermittent heavy rainfall and waterlogging of soils (Li et al., 2019), and changes in atmospheric composition and CO_2 fertilization (Swann et al., 2016) can alter crop physiology and drastically decrease or in some cases enhance crop yields in the future. Indirect effects such as changes in ice and snowmelt dynamics and hydrologic regime (Wang et al., 2017), as well as pests and diseases (Jabran et al., 2020), may also impact crop production. However, the magnitude and the way crops are impacted by these factors depend not only on geographic location, crop type, and stage of the growing season but also on numerous processes and factors that collectively affect crop growth and yield and their response to such alterations. To design proper adaptation strategies for future food security, understanding key processes and stressors affecting crop yields, and assessing the non-stationary response of yields and crop developments to changes in climate variables and atmospheric CO_2 fertilization across spatiotemporal scales is pivotal.

Various studies showed that climate-driven changes in agro-hydrology and the consequent impact on crop yields did not follow a consistent pattern, indicating that their response to climate change is not stationary (Fezzi and Bateman, 2015; McCarl et al., 2008; Milly et al., 2008, 2015; Montanari and Koutsoyiannis, 2014). The non-stationary approach requires relating the time-varying behavior of the underlying cause-and-effect mechanisms that influence changes in crop

yield (Serinaldi and Kilsby, 2015), which can be very different from their historical compartments. Studies have argued that identifying cause-and-effect mechanisms is key to inferring their future evolution and making hydrological, agronomic, and ecological predictions beyond their historical records (McCarl et al., 2008; Ganguli and Coulibaly, 2017; Hofgaard et al., 2019). In fact changes in the mean and variance of a given variable, e.g., crop yield might be driven by different processes or similar processes of different magnitude and intensity in the future as compared to their historical compartments. Consequently, it is imperative to study cause-and-effect mechanisms associated with agricultural and hydroclimatic evolution, i.e., non-stationarity in yield projections. Past studies assumed universal favorable effects of increased atmospheric CO_2 concentration on biomass and crop yield development (Högy et al., 2009; Jablonski et al., 2002). In theory, depending on crop type and their species, increases in atmospheric CO_2 concentration, in addition to changes in radiative forcing, can affect crop photosynthesis processes and evapotranspiration schemes favorably (Swann et al., 2016). Both C4 crops (those that are CO_2-saturated in their plant cells, such as maize and millet) and C3 crops (those that are CO_2-deficit in their plant cells, such as wheat) may benefit from CO_2 fertilization by either enhancing photosynthesis (more evident in C3 crops) (Roudier et al., 2011), or improving water use efficiency (evident on both C3 and C4 crops) due to reduced evapotranspiration (Kimball, 2016; Nowak et al., 2004). However, crop yield advantage due to elevated CO_2 concentration may not fully offset the negative impacts of other unfavorable climate factors (e.g., water shortage, excessive warming) (Arora et al., 2020). Yang et al. (2017) predicted maize yield reduction under future climate despite an elevated CO_2 concentration, which indicated dependence of yield increments on factors other than changes in atmospheric CO_2 concentrations. Crop yields are thus expected to present regionally variable non-linear responses to the compound effects of changes in climatic variables (i.e., precipitation and

temperature), atmospheric CO_2 concentration, and soil environment under future climates (Broberg et al., 2019; Li et al., 2020; Porter and Semenov, 2005). Yields of crops such as wheat and soybean may increase due to longer growing seasons and larger accumulation of crop heat units under future climates, especially in higher latitudes, until the crop growth and yield become limited by plant nutrient availability (He et al., 2018). While earlier studies elaborated on the beneficial effects of elevated CO_2 on crop growth and crop water-use efficiency (Deryng et al., 2016; Long et al., 2004; Tubiello et al., 2007), recent empirical studies indicated that under low N application, the favorable effects of elevated CO_2 on crop yields and their productivity would be constrained (Manderscheid et al., 2018). Moreover, the water and nutrient storage capacity of soils affect crop growth sustainability during periods of adverse conditions, and they either buffer or reinforce the impacts of climate variability (Folberth et al., 2016; Wang et al., 2009). Therefore, it is crucial to study the non-stationary response of crop yields to climate change with a thorough assessment of their response to atmospheric CO_2 and its warming effects when compounded with other hydrological, crop phenological, and agronomic management factors in the future. Rigorous conceptualization of the way plants may respond to the changes in CO_2, and their adaptability to the new and altered conditions are imperative to understanding the full impacts that various interconnected global change factors may have on plant growth in future projections (Geng et al., 2019; Leakey et al., 2009). Soil physical and biogeochemical processes, eco-physiology, and agronomic management practices are among the most critical factors driving biomass development and crop yield response to climate change. Examining the extent to which each of these processes and factors or groups of processes may affect crop growth across spatiotemporal scales will help better understand and improve predictive capacity on the non-linear response of crop yields and

their non-stationary pattern in the future. This will enhance confidence in yield predictions for adaptive management of water and food challenges in the future.

Process-based agro-hydrological, climate, and crop growth models are among the best available means for regional assessment of the response of crop yields to changes in climate and water resources (Angulo et al., 2013; Challinor et al., 2010; Tao et al., 2009). These models simulate dynamic interactions of the processes involved in the soil-plant-atmosphere continuum in response to changes in atmospheric, hydrologic, and management conditions. Therefore, they facilitate assessing crop response to changes in plant water and nutrients availability, agronomic management, and climate, which affect plant physiological processes and their phenological properties (Frieler et al., 2017). However, these models are subject to uncertainty due to the differences in mechanistic approaches used to simulate feedbacks among physical and biochemical processes in agro-ecosystems. Overall, crop growth simulation models can be categorized into three major groups: (i) carbon-driven models (Bouman et al., 1996; Ceglar et al., 2019; Van Ittersum et al., 2003), (ii) radiation-driven models (Jin et al., 2016; Monteith and Moss, 1977), and (iii) water-driven models (Abedinpour et al., 2012; Garcia-Vila et al., 2019; Starr et al., 2020). Carbon-driven models, such as WOFOST (Diepen et al., 1989) and SWAP (Van Dam et al., 1979), have a hierarchical structure in which the higher-level responses, such as leaf and canopy CO_2 assimilation and dark respiration, result from the combination of very detailed underlying parameters such as the effects of leaf angles, location latitudes, and crop row orientation. Most of these models are highly complex and require a wide range of measured data at the plant level, such as plant phenological parameters along with detailed site-specific climate data and soil properties among others (Kanda et al., 2018). Although recent computational advancements have made agro-hydrological simulations of large regions attainable, the application of these models is still mostly

limited to plot- and field-scale studies, predominantly due to the limited availability of detailed plant physiological measurements to drive the model simulation at larger spatial scales. In radiation-driven models, such as SWAT-EPIC (Williams et al., 1989) and STICS (Brisson et al., 1998), plant- and canopy-level detailed physiological processes are presented with a more simplified approach (Steduto, 2003). For instance, net plant CO_2 assimilation is simplistically incorporated into a coefficient called radiation-use efficiency (RUE) (Kukal and Irmak, 2020). In these models, plant growth is determined from leaf area development, light interception, and conversion of intercepted light into chemical energy and hence plant biomass, assuming a species-specific radiation use efficiency. These crop growth simulators have their advantages in fewer data requirements at the plant level while efficiently simulating and scaling up key eco-physiological responses to large regional scales. Besides these models also simulate key processes driving soil-plant-atmosphere water and nutrient cycles adequately in simpler algorithms. On the other hand, in water-driven models, such as AquaCrop (Steduto et al., 2009), and CropSyst model (Stöckle et al., 2003), some of the key physiological processes such as root water uptake and crop water use through transpiration are only represented by a water productivity (WP) parameter (Steduto, 2003). These models assume that the spatiotemporal variability of above-ground and below-ground biomass production due to the changes in soil water balance is proportional to the single WP parameter. Moreover, these models do not simulate how changes in key climatic variables such as radiation and atmospheric CO_2 concentration affects crop growth and yield (Raes et al., 2018). Hence the application of these models is restricted by the oversimplification of key physical and biogeochemical processes, which may underestimate the response of crop yield to changes in future climate.

In this study, we aimed to revisit plant-water-soil-atmosphere relation and study non-stationary behavior of the crop growth by providing a comprehensive assessment of SWY response to complex and interactive feedback between water, nitrogen, temperature, and atmospheric CO_2 concentration under future climate change and agronomic management scenarios. The overarching goal of this study is to provide an improved understanding of non-stationary crop yield response to climate change-induced agro-hydrological processes and management factors at a regional scale. We implemented the Soil and Water Assessment Tool (SWAT), a radiation driven model, and utilized an Analysis of Variance (ANOVA) decomposition approach (see section 2.3.4) to apportion total variance in crop yield projections into its various sources and to understand yield response to its driving forces. To achieve this goal our specific objectives are to (1) setup, calibrate, and validate a process-based SWAT agro-hydrologic model for rain-fed wheat yield simulation at a watershed scale, (2) quantify yield response to variations in climate models, emission scenarios, downscaling methods, and agro-hydrologic model parameters, (3) investigate spatiotemporal variability of the projected yield responses to understand physical, biochemical, and physiological processes driving crop yield responses in the future, and (4) to draw a conclusion on the non-stationarity in agricultural crop yields under changing climate and agronomic management practices.

To accomplish our objectives, we focused our modeling efforts on the Red Deer River (RDR) basin in Alberta, a western province of Canada. The RDR basin is representative of agricultural lands in the Prairies of Canada, which is considered as a main breadbasket of the world, and is characterized by heterogeneous soil, climate, and geospatial conditions, as well as cold region hydrology (e.g., Pomeroy et al., 2007) and intermittent droughts. Moreover, it is one of the most productive regions in western Canada in terms of SWY, with its croplands benefited from both

rainfall and snowmelt that are projected to alter under changing climate, hence, making this basin a suitable study area to address our research objectives.

2.3 Methods and data

2.3.1 Study area and data collection

The Canadian prairies are central to global grain production and a major breadbasket of the world. The region exports crop and agricultural commodities to over 170 countries around the world on an annual basis (Masud et al., 2019). Our research is carried out in the RDR basin with an area of 47,000 km^2, located in the croplands of Canadian prairies in the southern part of the province of Alberta between 50-53 ^oN and 110-115 ^oW (Figure 2.1). The elevation ranges from 574 meters above sea level (masl) to 1700 masl in the crop production areas and it reaches 3280 masl at the highest altitudes in the western parts of the RDR basin. The agricultural lands in the RDR basin are the dominant land use-land cover type covering the majority of the basin except for higher altitudes in the west. Spring-wheat, as the main crop in Canada, is predominantly produced in Canadian prairies and in the RDR basin, which is highly dependent on hydroclimate variables and phenological parameters (Masud et al., 2018). The watershed's long-term average daily temperature has a minimum of -25 ℃ and a maximum of 35℃ with an average annual precipitation of 400 mm. During the growing season, the precipitation is roughly 250 mm, and the average daily temperature ranges from 2 ℃ at its lowest in the western parts (nearest to the Rocky Mountains) to 34℃ at its highest in the middle of the watershed. Snowmelt plays a vital role in supplying water needs early in the growing season in RDR (Masud et al., 2018). Moreover, black soils are mostly dominating the croplands of the RDR basin (Alberta Agricultural and Rural Development, 2004). These soil types are specified among the most productive soils worldwide and are considered the reason for agricultural suitability in the RDR basin (Bentley et al., 1971).

In this study, the historical climate data, including daily precipitation, temperature, solar radiation, humidity, and wind speed were taken from Faramarzi et al. (2015). They used a suite of four climate time series from local meteorological, gridded products, and satellite data covering the province to reproduce historical streamflow records by implementing a calibrated SWAT hydrologic model. Other data, including a topographic map, vegetation cover, and soil characteristics, were obtained from Faramarzi et al. (2017) (See Table A.1). The potential heat units, fertilizer application rate, and maximum amount of annual fertilizer application were adapted from Masud et al. (2019) and the Government of Alberta (Alberta Agricultural and Rural Development, 2004). In addition, yearly crop yields (ton/ha), used to calibrate and validate the simulated rain-fed spring-wheat, were obtained from Alberta Agriculture and Rural Development (AARD) at the level of Census Agricultural Region (CAR) for the 1983-2007 period (Figure 2.1c).

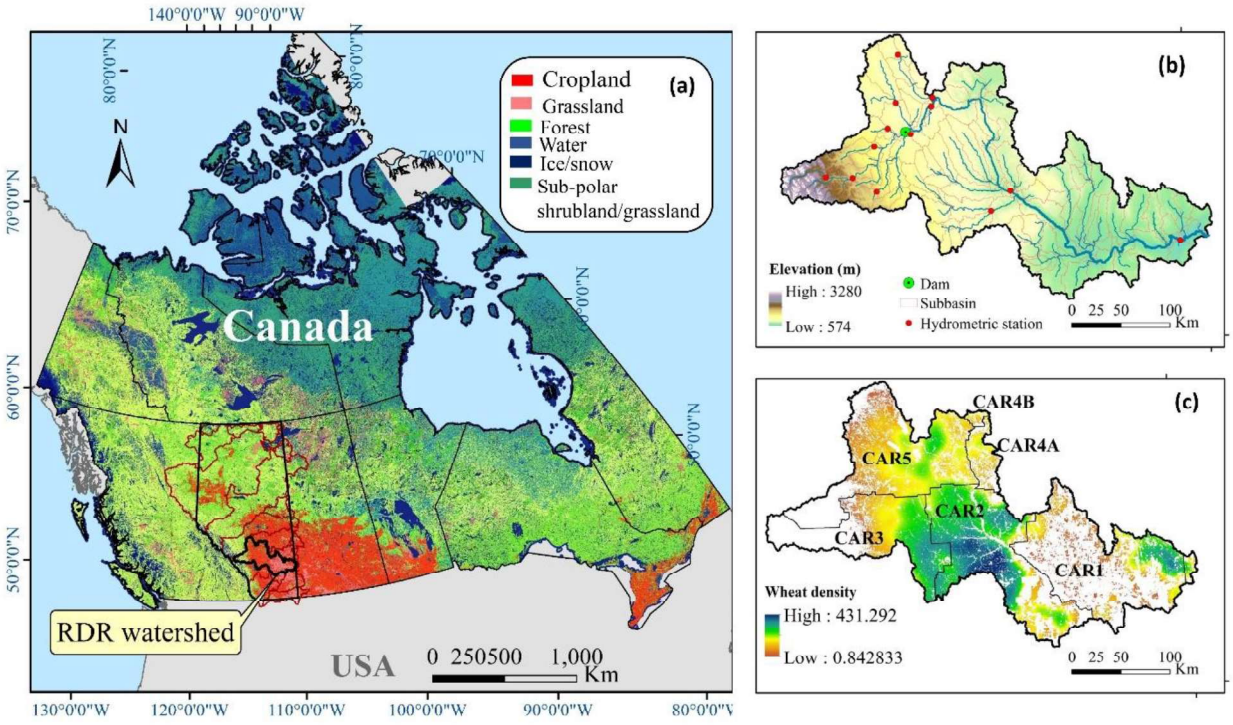

Figure 2.1. Geographic extend of the RDR basin, located in croplands of the Canadian Prairies, is one of the main river basins in the province of Alberta (a); topographic domain, main rivers,

and modeled sub-basins of the study area (b); and spring wheat crop spatial density map and the five Census Agricultural Region of the study watershed (c).

2.3.2 Simulation of climate change impacts

For future projections of wheat yields, the climate data were incorporated from an ensemble of nine Global Climate Models (GCMs) of the Fifth Assessment Report (Stocker et al., 2013), under two Representative Concentration Pathways including of RCP2.6 and RCP8.5, for the 2040-2064 period (see Table A.2). In this study, we set the concentration of CO_2 to 350, 450, and 750 ppm for the historical, future RCP2.6, and future RCP8.5 periods in simulations based on the possible range provided by IPCC (2014), respectively. Climate data were statistically downscaled based on historical daily gridded climate data for Canada, and they are available through Pacific Climate Impacts Consortium (PCIC) at roughly 10 km resolution (Hopkinson et al., 2011; McKenney et al., 2011). To test the effect of the downscaling procedure on crop yield simulation and its response to the aforementioned factors, the PCIC data were further downscaled to Alberta conditions based on daily historical climate data from earlier studies by Ammar et al. (2020) and Masud et al. (2018). In their study, the delta method (Quilbé et al., 2008; Chen et al., 2011a) was used for bias correction of the projected climate time series. It is noteworthy that the RCP2.6 and RCP8.5 were selected in our study to represent the largest plausible range for greenhouse gas emissions. The former describes a best-case scenario with a rising radiative forcing pathway of 2.6 W/m^2 in 2100, and the latter defines a worst-case scenario in which greenhouse gas emissions continue to increase rapidly with a radiative forcing reaching 8.5 W/m^2 in 2100 (IPCC, 2014).

2.3.3 SWAT model setup, calibration, validation, and uncertainty analysis

The ArcSWAT 2012 (Rev. 664) was implemented to simulate hydrological processes and crop yield for both historical (1983-2007) and future (2040-2064) periods. SWAT is a physically-based, continuous-time, semi-distributed model (Arnold et al., 1998), which is widely applied for

analyses of the impacts of climate change, water management, and agricultural management on hydrological (Aryal et al., 2019; Fang et al., 2018; Faramarzi et al., 2017) and crop growth (Masud et al., 2018 & 2019; Chen et al., 2019; Shahvari et al., 2019) processes. The crop growth simulation algorithms in SWAT are adapted from the EPIC crop growth model (Williams et al., 1984). SWAT uses a crop-specific base temperature to calculate the number of accumulated heat units (Monteith and Moss, 1977). Plant growth is estimated using leaf area development, light interception, and conversion of intercepted light into biomass assuming a plant species-specific radiation use efficiency (Neitsch et al., 2011a). Optimal biomass and potential yields are simulated under ideal growing conditions consisting of adequate water and nutrient supply, and a favorable climate, i.e., optimum temperature (Neitsch et al., 2011a). Water stress, temperature stress, and nutrient stress factors are then simulated to model actual development of above ground and below ground biomass, and crop yields on a daily basis. Biomass development commences once the temperature exceeds the plant specific base temperature from planting to harvest date (growing season), or until the time it reaches the crop-specific, maximum heat units. Actual water uptake by the crop is simulated based on potential evapotranspiration, biomass-dependent water requirement, and water availability in the soil layers on daily basis. The potential evapotranspiration is simulated using the Penman-Monteith method (Beven, 1979).

Using a topographic map and the threshold drainage area of 200 km^2, the watershed was delineated into 142 sub-basins that were later characterized using soil, vegetation, slope properties, as well as climate parameters. Crop yield simulations were then enabled in each sub-basin by assigning crop-specific phenological and agricultural management data such as planting and harvesting dates, fertilizer and pesticide application, irrigation, tillage, and harvest and kill operations. In SWAT, potential crop yield is usually not achieved because of constraints induced

by water, nutrients, and temperature stresses. W_stress can be related to water deficiency or water surplus. The water deficiency stress is simulated based on comparing actual and potential plant transpiration for each day (Eq. 2.1):

$$W\_stress = 1 - \frac{E_{act}}{E_p} \quad (2.1)$$

Where, W_stress is the water stress for a given day, E_p is the maximum plant transpiration on a given day (mm), and E_{act} is the actual amount of transpiration on a given day (mm). The E_{act} is simulated based on soil physical properties, soil water availability, plant biomass development, and climate factors. The soil water availability is based on soil hydrologic water balance, which is calculated based on surface runoff, snowmelt, infiltration to the soil, lateral flow, groundwater recharge, evaporation from the soil, transpiration from plants, and capillary recharge from groundwater due to capillary effects (see Neitsch et al., 2011). Water surplus stress is simulated as the function of saturation over field capacity in the soil profile. Similarly, N_stress is calculated based on comparing the actual mass of nitrogen stored in plant material and the optimal mass of nitrogen stored in the plant for a given day (Eq. 2.2,2.3):

$$N\_stress = 1 - \frac{S}{s + \exp(3.53 - 0.02s)} \quad (2.2)$$

$$S = 200\left(\frac{bio_N}{bio_{N,opt}} - 0.5\right) \quad (2.3)$$

Where, S is a scaling factor for N_stress on a given day, $bio_{N,opt}$ is the optimum mass of nitrogen stored in plant material for the current growth stage (kg N/ha), bio_N is the actual mass of nitrogen stored in plant material for the current growth stage (kg N/ha). The bio_N is calculated based on the amount of N uptake from the soil which is simulated based on the transpiration and the amount of nitrate in the soil. The nitrate content of the soil is computed as a product of N

fertilizer application and the nitrogen transformation processes in the soil i.e., nitrification, atmospheric deposition, immobilization, and mineralization on daily basis. Therefore, the simulated N_stress in the model is either related to inadequate availability of the N in the soil or limited N uptake due to changes in plant phenological features (e.g., stomatal conductance) or hydroclimate factors (e.g., inadequate soil moisture or reduced transpiration (Neitsch et al., 2011). The temperature stress (T_stress) is a function of the daily average air temperature and the optimal temperature for plant growth (Eq. 2.4-2.6).

$$T\_stress = 1 \qquad when\ \overline{T}_{av} \le T_{base} \tag{2.4}$$

$$T\_stress = 1 - exp\left[\frac{-0.1054 \times \left(T_{opt} - \overline{T}_{av}\right)^2}{\left(\overline{T}_{av} - T_{base}\right)^2}\right] \qquad when\ T_{base} \le \overline{T}_{av} \le T_{opt} \tag{2.5}$$

$$T\_stress = 1 - exp\left[\frac{-0.1054 \times \left(T_{opt} - \overline{T}_{av}\right)^2}{\left(2T_{opt} - \overline{T}_{av} - T_{base}\right)^2}\right] \qquad when\ T_{opt} \le \overline{T}_{av} \le 2.T_{opt} - T_{base} \tag{2.6}$$

Where $\overline{T}_{ave}$ is the mean air temperature for day (°C), T_{base} is the crop's minimum temperature for growth (°C), and T_{opt} is the crop's optimal temperature for growth (°C).

In the model, the N fertilizer application in each sub-basin was enabled by specifying an N_stress threshold (Auto_NSTRS parameter) factor which is as a fraction of potential plant growth. When actual plant growth fell below this threshold level because of N_stress in a sub-basin, N fertilizer was applied until the cumulative volume of N application reached an allowable N defined in one year based on measured data. For the simulation of historical crop yields (i.e., baseline scenario), we set the maximum allowable N application based on an earlier study by Masud et al. (2019), where a realistic volume of N fertilizer application was adapted based on literature review and personal communication with regional farmers. Therefore, we assume that

setting the N fertilizer application in the model based on the actual yearly N volumes, limits the N application rates and it simulates a realistic rate of application in the real world.

Table 2.1. Selected parameters for calibration of crop yields in each CAR, in this study.

No.	Parameter	Underlying SWAT parameter
1	v__DAY{[],1}.mgt	Plant growing season date
2	v__DAY{[],5}.mgt	Day harvest takes place
3	v__HEAT_UNITS{[],1}.mgt	Total heat units for plant to reach maturity
4	v__HI_TARG{[],1}.mgt	Harvest index target ((kg/ha)/(kg/ha))
5	v__AUTO_NSTRS{[],11}.mgt	N_stress factor of plant that triggers fertilization
6	v__AUTO_NAPP{[],11}.mgt	Maximum amount of mineral N allowed in any one application (kg N/ha)
7	v__AUTO_NYR{[],11}.mgt	Maximum amount of mineral N allowed to be applied in any one year (kg N/ha)
8	v__AUTO_EFF{[],11}.mgt	Application efficiency
9	v__AFRT_SURFACE{[],11}.mgt	Fraction of fertilizer applied to top 10 mm of soil
10	r__CN2.mgt	SCS runoff curve number for moisture condition II
11	v__ESCO.hru	Soil evaporation factor
12	v__EPCO.hru	Plant uptake compensation factor
13	v__OV_N.hru	Manning's n value for overland flow
14	v__LAT_TTIME.hru	Lateralflow travel time (days)
15	v__LAT_SED.hru	Sediment concentration in lateral and groundwaterflow (mg/L)
16	r__CANMX.hru	Maximum canopy storage (mm H2O)
17	r__HRU_SLP.hru	Average slope steepness (m/m)
18	r__SOL_BD(1).sol	Soil bulk density in layer 1 of soil profile (g/cm3)
19	r__SOL_CBN(1).sol	Organic carbon content in layer 1 of soil profile (% soil weight)
20	r__SOL_ALB(1).sol	Moist soil albedo in layer 1 of soil profile
21	r__ANION_EXCL.sol	Fraction of porosity from which anions are excluded
22	r__SOL_K(1).sol	Saturated hydraulic conductivity in layer 1 of soil profile (mm/h)
23	r__SOL_CRK.sol	Potential or maximum crack volume of the soil profile
24	r__USLE_K(1).sol	USLE equation soil erodibility (K) factor in layer 1 of soil profile
25	r__SOL_AWC().sol	Available water capacity of the soil layer (mm H2O/mm soil)
26	v__SHALLST.gw	Initial depth of water in the shallow aquifer (mm H2O)
27	v__ALPHA_BF.gw	Baseflow alpha factor (1/days)
28	v__SHALLST_N.gw	Initial concentration of nitrate in shallow aquifer (mg N/L or ppm)
29	v__GW_SPYLD.gw	Specific yield of the shallow aquifer (m3/m3)
30	v__GWSOLP.gw	Concentration of soluble phosphorus in groundwater (mg N/L or ppm)
31	v__HLIFE_NGW.gw	Half-life of nitrate in the shallow aquifer (days)

For calibration, validation, and uncertainty analysis, Sequential Uncertainty Fitting (SUFI-2) in combination with a parallel processing scheme was used (see Du et al., 2020). A set of 31 sensitive hydrological and crop parameters were initially selected based on a literature review for

rain-fed spring-wheat growth simulation in each CAR (see Table 2.1). The Latin Hypercube Sampling (LHS) method was implemented to generate 1000 parameter sets from an initially meaningful range assigned to each parameter based on a literature review (Alberta Agricultural and Rural Development 2004; Masud et al., 2018). Sampled parameters were used to force the model and 1000 simulations were performed in each calibration iteration. The model performance of each simulation was evaluated using p-factor and r-factor. The p-factor is the percentage of observed data bracketed within the simulated range of output variables due to the use of 1000 parameter sets (i.e., observed versus simulated streamflow and crop yields). It varies from 0 to 1 and ideally the p-factor of 1 is targeted through the calibration process. The r-factor is another statistic that is calculated based on the average width of output uncertainty divided by the standard deviation of the corresponding measured data. The output uncertainty is calculated as 95 percent of the cumulative distribution of the simulated streamflow and yields from the 1000 model runs, and is called parameter prediction uncertainty (95PPU hereafter). The r-factor maps all sources of model uncertainty resulting from parameter inputs, model structure, and observed data to the output uncertainty. The r-factor varies within the interval $(0,\infty)$, and the larger r-factor indicates more uncertainty in the model prediction. Therefore, a value of 0 is expected in an ideal model with perfect performance. Unlike streamflow simulation, the standard deviation of crop yields is relatively small and it can arbitrarily increase the r-factor as compared to streamflow studies. Therefore, any r-factor values within the range of 1-3 is desirable for crop yield simulations (Faramarzi et al., 2010). To calibrate the model, the simulated streamflow and crop yields were compared with their observed time series. The Nash-Sutcliffe Efficiency (NSE) and bR^2 (Faramarzi et al., 2015 and 2017) were used as objective functions for calibration of streamflow

at 13 hydrometric stations, and the mean square error (MSE) was used as the objective function (Eq. 2.7):

$$MSE = \frac{1}{n}\sum_{i=1}^{n}(O_i - S_i)^2 \tag{2.7}$$

Where n is the number of observed crop yields in each CAR, O is the observed crop yield, and S is the simulated crop yield. For comparison purposes, crop yield simulations at the sub-basin scale were aggregated to the CAR scale. We performed three iterations for model calibration and uncertainty assessment. The optimum MSE in the first calibration iteration was used to decide about further calibration-uncertainty iterations on how to narrow the uncertainty while optimizing performance statistics (i.e., p-factor and r-factor). The model was calibrated from 1995 to 2007, and the optimized parameter ranges resulted from the last iteration were used for model validation from 1983 to 1994. A warm-up period of three years (1983-1985) was considered to lower the influence of initial state variables. The calibration of streamflow using NSE and bR^2 is extensively discussed in Faramarzi et al. (2015) and Faramarzi et al. (2017). This paper focuses on presenting the results of SWY calibrations.

2.3.4 ANOVA for the decomposition of total yield variances and model scenarios

Statistical analyses such as the ANOVA decomposition method is commonly used to analyze the proportion of yield response to the effects of individual and multiple factors after they are simulated under various scenarios. The ANOVA decomposition approach is useful for studying how and to what extent crop yields respond to various factors such as climate projections of Global Climate Models (GCMs), alternative Representative Concentration Pathways (RCPs), various downscaling techniques, hydrological and crop growth model parameters, as well as input data, and their structure (Vetter et al., 2017; Corbeels et al., 2018; Tao et al., 2018). It can also analyze

the sensitivity of yields to various agricultural adaptation options and agronomic management practices (i.e., cropping calendar, fertilizer application, other management practices). The ANOVA method has a lower number of assumptions comparing to other similar approaches (i.e., classical Bayesian approach) for decomposition analysis and is a relatively new method with a growing interest in utilizing this approach for such decomposition analyses (Aryal et al., 2019; Ashraf Vaghefi et al., 2019; Wang et al., 2018).

The ANOVA method was used to assess how wheat yield corresponds to various hydrological and crop-related processes and factors under changing climate and CO_2 concentrations. This method apportioned the total variances of projected yield into its originating sources resulting from nine GCMs, two RCPs (Table A.2), two bias correction methods (DSs) including of with (DS1) and without (DS2) further bias correction, and two 95PPUs. The two 95PPUs are calculated at the 2.5% and 97.5% levels of the cumulative distribution of an output variable resulted from 1000 parameters of the model (95PPU). The 2.5% level presented a lower band of uncertainty range (L95PPU) and the 97.5% level indicated a higher band of uncertainty range (U95PPU). These two levels of 95PPU were used for analyses of variance in the ANOVA as follow:

$$SST = SS_{PPU} + SS_{GCM} + SS_{RCP} + SS_{DS} + SSI \quad (2.8)$$

In ANOVA, the total sum of squares (SST) and the sum of squares from individual sources, including crop model parameters (SS_{95PPU}), GCMs (SS_{GCM}), RCPs (SS_{RCP}), and DSs methods (SS_{DS}) are quantified alongside the effect of their interactions (SSI) in Eq. 2.8 (Aryal et al., 2019; Ashraf Vaghefi et al., 2019; Wang et al., 2018). Then, the share of variance from each source is calculated as $100\times(SS_i/SST_i)$, where I is the individual source of variance.

$$SSI = SS_{PPU*GCM} + \cdots + SS_{RCP*DS} + SS_{PPU*GCM*RCP} + \cdots + SS_{GCM*RCP*DS} + SS_{PPU*GCM*RCP*DS} \quad (2.9)$$

The sum of squares of interactions (SSI) is a combination of two, three, four, and five combinations (Eq. 2.9), making 2^n-n-1 combinations in total (n is the number of individual variance sources).

To evaluate the potential impacts of the soil nutrient variations on crop yield when it is compounded with elevated CO_2, changes in precipitation and temperature pattern due to climate change, and resulting changes in soil hydrological water balance, we developed two N application model scenarios, in addition to the GCMs, RCPs, DSs, and 95PPUs scenarios. Two N application scenarios included a 20% decreased and 20% increased N fertilizer application rate from the baseline (historical) scenario in the model, referred to NS1 and NS2 hereafter, respectively. We quantified crop yield changes using the ANOVA approach by developing 72 model scenarios as presented in Figure 2.2. Overall, simulated results of 72 SWAT models (9 GCM×2 RCP×2 DS×2 95PPU) under three scenarios including baseline (historical) N application, NS1, and NS2, were analyzed to apportion variances at different spatial (e.g., sub-basin and watershed) and temporal (e.g., yearly) scales.

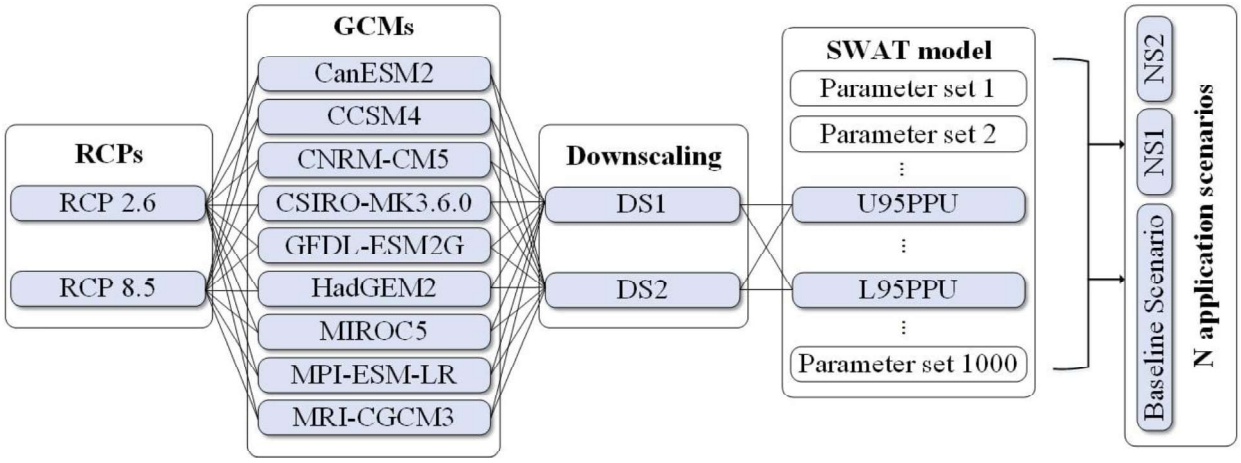

Figure 2.2. Development of SWAT model scenarios for decomposition analysis of projected crop yield variances. Three N application scenarios were tested for future yield projections including baseline N, NS1 and NS2.

2.4 Results and discussion

2.4.1 Model calibration, validation, and uncertainty analysis

The SWY calibration results showed an average p-factor of 100% and an average r-actor of 2.15 in all CARs, which indicates satisfactory model performance (Table 2.2). With a large p-factor for both calibration (0.98) and validation (0.87) periods, the r-factor was greater for validation (3.38) than the calibration (2.15) period indicating better performance in the calibration than the validation period. The larger uncertainty in the validation period is mainly due to the yield statistics that may not be well-reported, changes in management practices that were potentially different in the validation period than the calibration, and crop varieties that may have been different in validation than calibration period (Masud et al., 2018). This also caused a slightly larger MSE in the validation period as compared to calibration results. Overall, the results for both calibration and validation were satisfactory as the model was able to reproduce most of the observed data within predicted uncertainty and represented their inter-annual variations in different CARs (Figure 2.3).

Table 2.2. Calibration and validation statistics of rain-fed spring-wheat for the historical period.

	Calibration			Validation		
County	p-factor	r-factor	MSE	p-factor	r-factor	MSE
CAR1	1.00	1.58	0.02	0.89	1.01	0.07
CAR2	1.00	2.33	0.03	0.89	4.91	0.06
CAR3	1.00	2.98	0.08	0.56	3.75	0.29
CAR4	1.00	1.91	0.04	1.00	3.26	0.09
CAR5	0.92	1.97	0.19	1.00	3.98	0.07
Average	0.98	2.15	0.07	0.87	3.38	0.22

Overall, the hydrological model performance was desirable for streamflow simulation during the calibration and validation periods from 1983 to 2007. The NSE values ranged from 0.02 to 0.64 and bR^2 values varied from 0.01 to 0.64 across hydrometric stations. The p-factor and r-factor values ranged from 0.22 to 0.94, and 0.51 to 3.74, respectively (see Table A.3). All calibration results indicated an acceptable model performance at the study basin. More details regarding the calibration and validation of the hydrologic model can be found in an earlier study by Faramarzi et al. (2015, 2017).

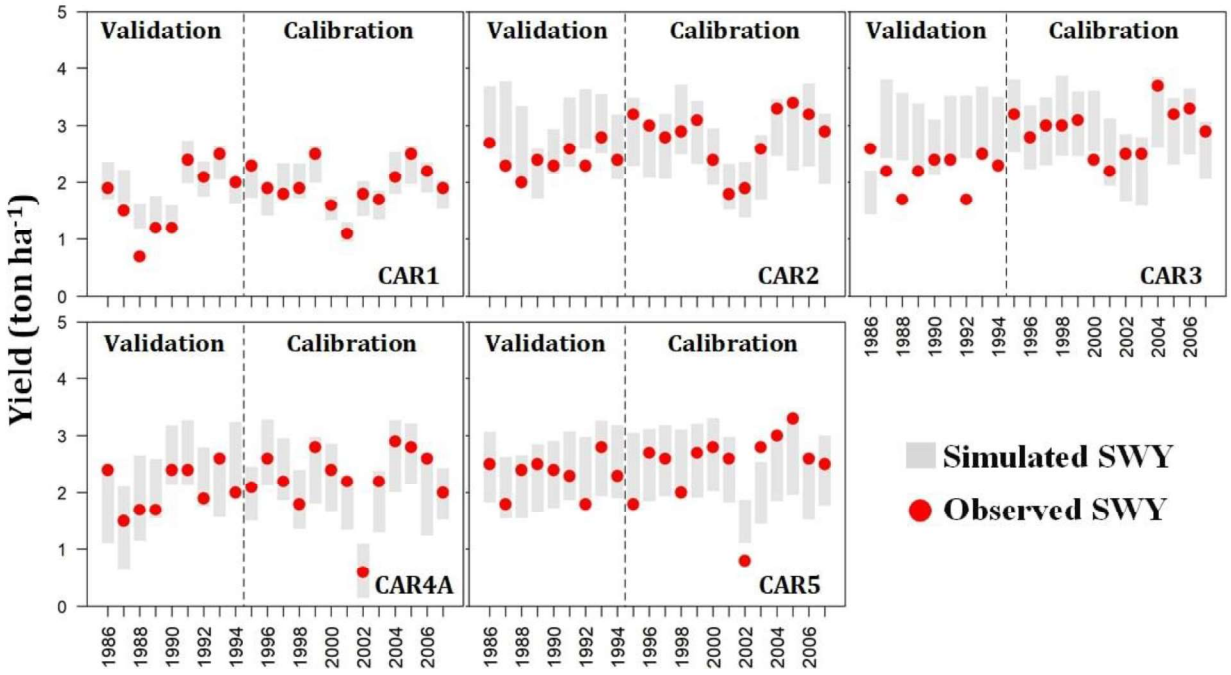

Figure 2.3. Comparison of observed (red circles) and simulated (grey bands) rain-fed SWY during calibration and validation periods in the five CARs.

2.4.2 Spatial characteristics of the future climate change, stress factors, and their interactions

Mean annual temperature and precipitation during the growing season ranged from 7ºC to 21℃ and 180 mm to 400 mm, respectively for the historical period (Figure 2.4). The ensemble mean temperature from 9 GCMs showed a mean increase in all of the sub-basins under RCP8.5 ranging from 0.4℃ to 3.2℃ for the future period (Figure 2.4a). However, the RCP2.6 indicates a smaller increase in temperature comparing to RCP8.5, ranging from -1℃ in the center of the basin to 1.8℃, in upstream and downstream of the watershed (Figure 2.4a). Growing season precipitation increased in the entire watershed under RCP2.6 (except the mountainous regions). Under RCP8.5, the magnitude of precipitation decreased in north-western sub-basins in the upstream where the total historical precipitation is high and increased in the downstream sub-basins where the magnitude of total historical precipitation is low (Figure 2.4b). The projected ensemble mean data

revealed higher temperatures for most of the sub-basins, which are potentially beneficial to crop development, especially in a cold region as it can escalate the accumulation of growing degree-days and heat units (He et al., 2018). However, soil water availability is key to the extent of yield increments resultant from temperature gain in the future.

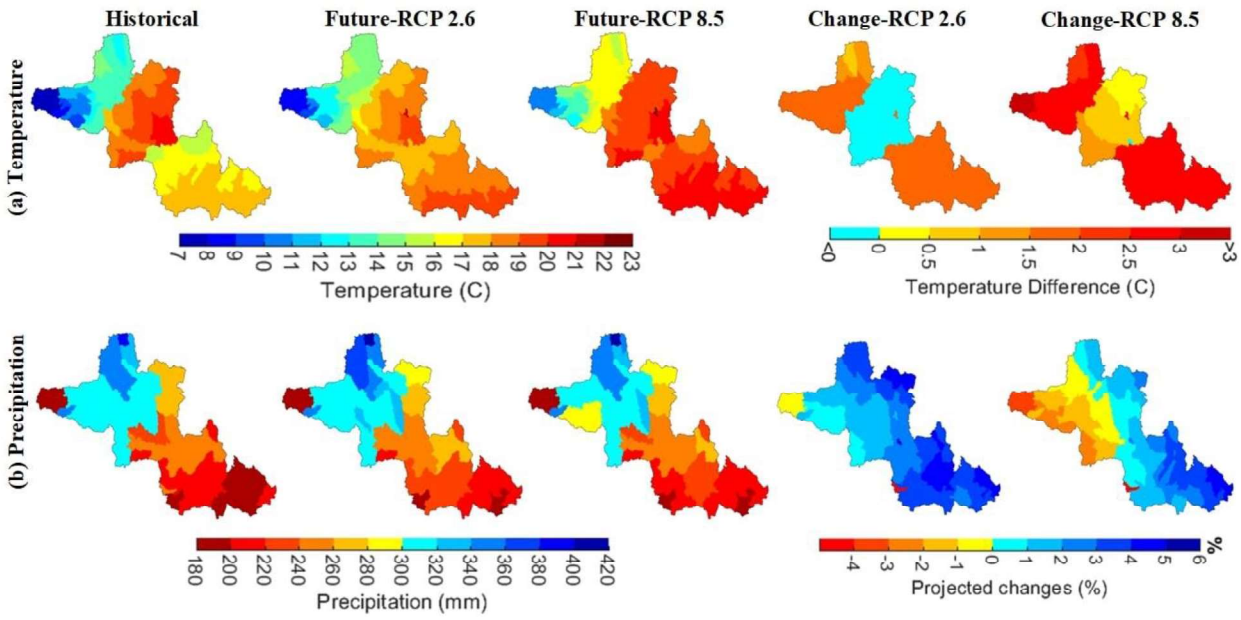

Figure 2.4. Comparison of historical and future mean temperature (a), and precipitation (b) under RCP2.6 and RCP8.5 scenarios. The maps in the right column, show anomalies from the historical values (1983-2007 period), and the future data are based on ensemble mean values averaged over 2040-2064 period.

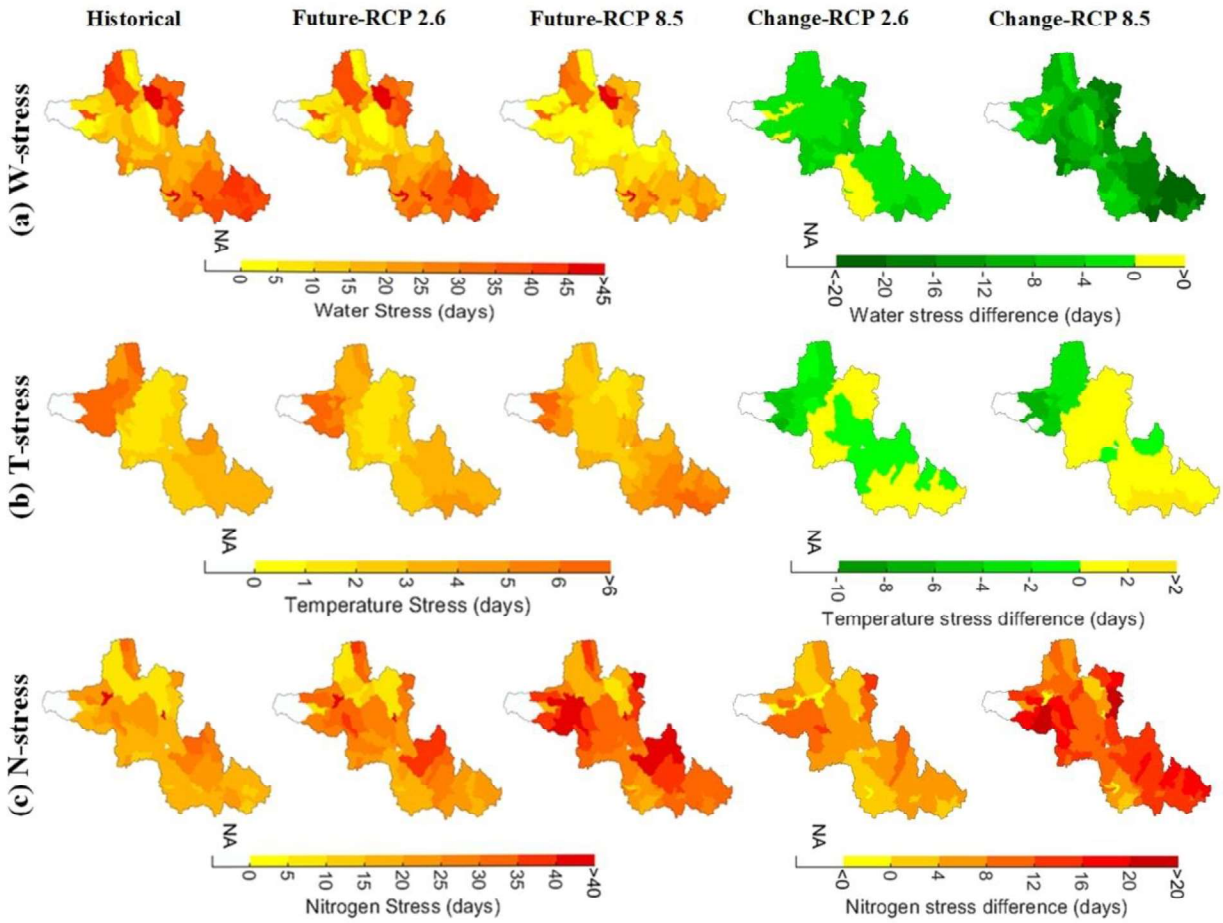

Figure 2.5. Comparison of the average annual number of water stress days (a), temperature stress days (b), and nitrogen stress days (c) under RCP2.6 and RCP8.5 scenarios. The maps in the right column, show projected changes from the historical values (1983-2007 period) and the future data are based on ensemble mean values averaged over 2040-2064 period.

The simulated W_stress days, which is also considered as one of the major yield-limiting factors among other stress factors (e.g., T_stress and N_stress), was 27 W_stress days for the historical period (Figure 2.5a) in the study watershed. This extensive water stress, however, is less apparent under future scenarios with the watershed average annual of 24, and 16 W_stress days under RCP2.6, and RCP8.5, respectively (Figure 2.5a). The model results showed earlier snowmelts and infiltration under future scenarios increased soil water availability resulted in the reduction of W_stress days in some sub-basins. In other sub-basins, the reduced W_stress days were due to the reduction in crop evapotranspiration rates (see discussions in the following

sections). With the watershed average annual of less than 4 T_stress days (Figure 2.5b), the T_stress remained moderate across watershed for both historical and future periods, except in mountainous areas where the temperature was colder (Figure 2.4a) in the historical period and they became warmer under future scenarios. In addition, N_stress days, which is considered as another primary yield-limiting factor, were amplified under both RCP scenarios in the future period. As seen in Figure 2.5c, the watershed annual average of 19 N_stress days during the historical period was increased to 27 days and 35 days under RCP2.6 and RCP8.5 scenarios, respectively. This increase in N_stress can be partially attributed to the potential enhancement of biomass caused by atmospheric CO_2 fertilization (Roudier et al., 2011), which required more nitrogen uptake from the soil and or related to the decline in soil moisture and evapotranspiration rates that are discussed in the following sections.

2.4.3 Temporal characteristics of the future climate change, stress factors, and their interactions

The temporal analysis of precipitation, N uptake, and W/N/T_stress variability in growing season over historical and future periods can provide insights about the underlying relationship between these variables and ultimately, the evolution of the crop yield and its response to its driving processes. The W_stress days were the highest from 2040 to 2042 and 2057 to 2059 due to the reduced precipitation (Figure 2.6) with reduced precipitation. N_stress days were the highest during low N uptake years (i.e., 2047 to 2056), and the lowest during high N uptake years (i.e., 2040 to 2042) (Figure 2.6). The RCP2.6 scenario demonstrates that the average precipitation and N uptake is 261 mm/year and 90.8 kg N/ha, respectively, which is well within the ranges of spring wheat N uptake in western Canada (Canadian Fertilizer Institute, 1998; Government of Alberta, 2020). The RCP8.5 scenario, on the other hand, demonstrates a slight decrease in both precipitation

and N uptake compared to RCP2.6 with the average of 255 mm/year and 88 kg N/ha, respectively. The lower N uptake under RCP8.5 as compared to RCP2.6 is in contrast with the fact that crops demand more nutrients from the soil to produce greater biomass which is usually expected under a higher atmospheric CO_2 scenario (RCP8.5) (Neitsch et al., 2011a; Ngosong et al., 2019). Our contrasting result is likely due to the lower transpiration under RCP8.5, in response to less stomatal conductance, which has reduced N uptake because of its direct relationship with the transpiration (Bower, 2008; Houshmandfar et al., 2018). Therefore, the potential N demand under RCP8.5 is not met due to a reduced N uptake rate because of the decreased transpiration, which results in more N_stress days under RCP8.5 compared to RCP2.6. On the contrary, RCP8.5 shows substantially fewer W_stress days than RCP2.6. This is due to the reduction in stomatal conductance stemming from higher CO_2 emission under RCP8.5 (Uddin et al., 2018), which results in an enhanced water use efficiency (Deryng et al., 2016) and less W_stress while experiencing lower average precipitation under RCP8.5 as compared to RCP2.6 (see Figure 2.6).

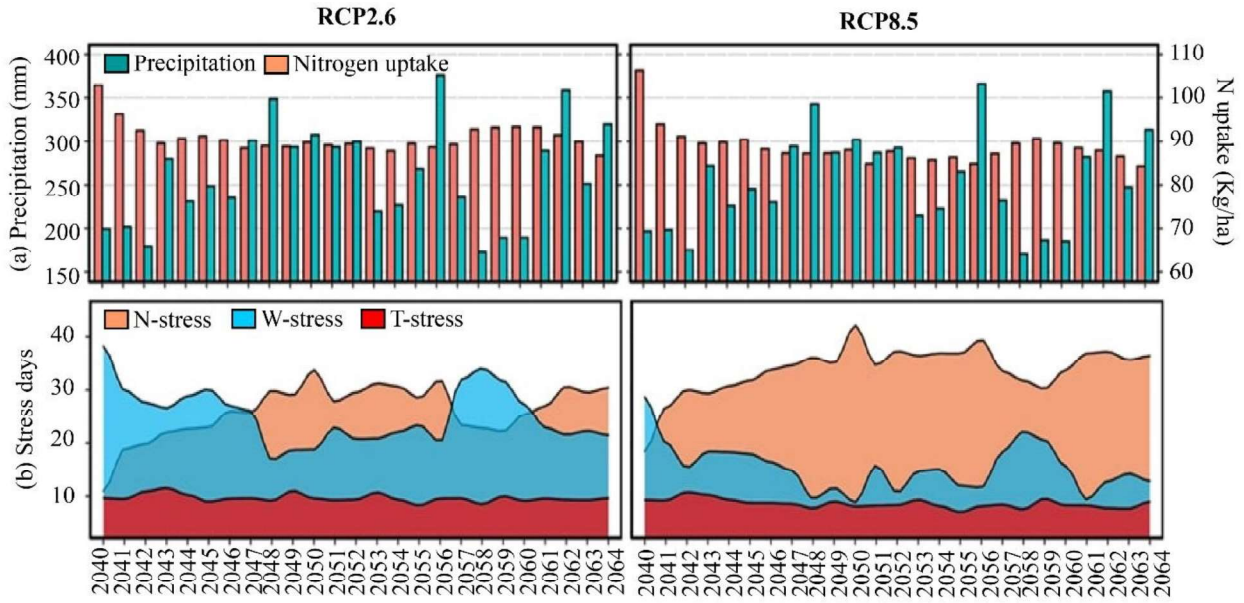

Figure 2.6. Comparison of future (a) annual precipitation (mm) and nitrogen uptake from the soil (kg N/ha), and (b) yearly changes in W-N-T stress days under RCP2.6 and RCP8.5 future scenarios (2040-2064).

2.4.4 Yield response to stress factors and its non-stationary behavior under future climate change scenarios

The simulated mean historical SWY indicated that maximum yields occurred upstream of the watershed, whereas the southern part of the watershed presented the minimum yields (Figure 2.7). Further, the mean ensemble model results, stemming from the nine GCMs simulations using the best parameter set of the agro-hydrologic model and averaged over two DSs, projected an increase of SWY in almost all of the sub-basins under both RCP scenarios (Figure 2.7). This upsurge in SWY is more pronounced in RCP8.5 (27% more yield at the watershed level) than RCP2.6 (11% more yield at the watershed level) scenarios. Potentially, the main reason is higher atmospheric CO_2 under RCP8.5 scenario than RCP2.6 compounded with less evapotranspiration under high CO_2 concentration due to stomatal closure, as well as a larger availability of soil moisture (Figure 2.5a) (Lambers et al., 2008). Comparison of W_stress, T_stress, and N_stress projections (Figure 2.5) with the crop yield (Figure 2.7) indicates that the increase of crop yield (0 to 50%) in most of the sub-basins under both RCP scenarios can partially be explained by CO_2 fertilization and both temperature and precipitation gains. However, in the upstream sub-basins, the high yield gain under RCP8.5 is likely due to the effects of CO_2 compounded with lower W_stress (Figure 2.5a), due to the higher annual mean precipitation (Figure 2.4b), as well as lower N_stress days in these specific sub-basins (Figure 2.5c). Nevertheless, the potential yield increase in these sub-basins may have been partially limited as the larger atmospheric CO_2 may restrict yield potentials by lowering N uptake due to a decline in crop evapotranspiration (Uddin et al., 2018) (Figure 2.5c).

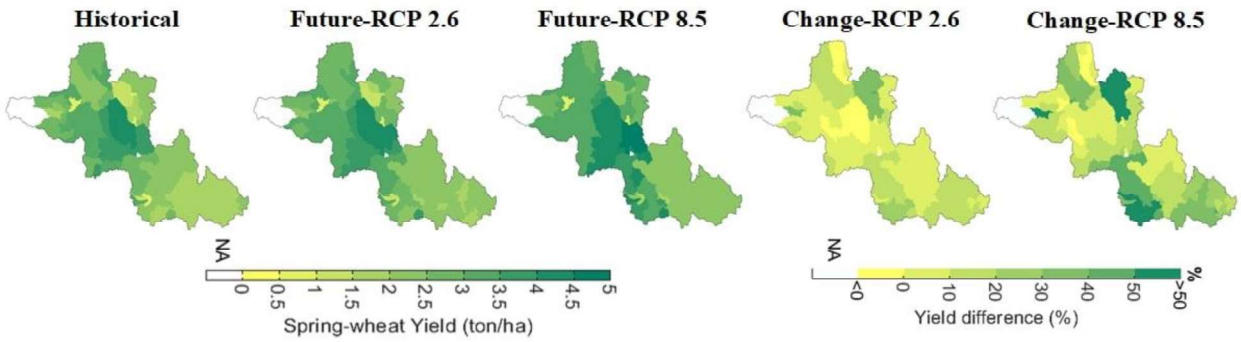

Figure 2.7. Comparison of historical and projected wheat yield under RCP2.6 and RCP8.5 scenarios. The maps in the right column show projected changes (%) from the historical yields (1983-2007 period) and the future data are based on ensemble mean values averaged over 2040-2064 period.

To further study the response of SWY to spatiotemporal dynamics of W-N stress factors, we analyzed our simulated results in four quarters including high (H), mid-high (MH), mid-low (ML), and low (L) water and nitrogen stress sub-basins (Figure 2.8). Due to the very different geospatial and hydrological characteristics of each region, the simulated historical SWY showed varying results in each region (Figure 2.8a-h) for the historical period. The high W_stress regions (Figure 2.8a) showed the lowest average of historical SWY (1.7 ton/ha) and the low W_stress regions (Figure 2.8d) demonstrated the highest average historical SWY (3.2 ton/ha) during 1986-2007 period. However, the average historical SWY in high N_stress regions (Figure 2.8e) was 2.6 ton/ha which declined to 2.1 ton/ha in low N_stress regions (Figure 2.8h). This indicates an inverse relation between W_stress days and SWY, which is not the case for N_stress days. As also discussed by Faramarzi et al. (2010), this is partly because simulated yields are quantified as a product of aboveground biomass and harvest index (Neitsch et al., 2011a), both of which are a function of W_stress. However, other stress factors such as N_stress and T_stress (Neitsch et al., 2011a) are only taken in the biomass calculation into account. Therefore, the modeled SWY is numerically more affected by W_stress variations than N_stress changes. In addition, the suppression of yield in high N_stress sub-basins can be partially attributed to the N deficiency in

the soil that hinders the beneficial effects of a larger soil water availability for yield gain. Therefore, it can be concluded that yield gain is not only stimulated by soil moisture but also nitrogen availability in the soil. The 72 projected SWY scenarios (grey lines in Figure 2.8i-x) also imply varying results in terms of the magnitude and temporal variations across regions (Figure 2.8i-x). The high W_stress regions (Figure 2.8i and Figure 2.8q) showed the lowest ensemble average SWY of 2.1 ton/ha under RCP2.6 and 2.4 ton/ha under RCP8.5, and the low W_stress regions (Figure 2.8l and Figure 2.8t) demonstrated the highest ensemble average SWY of 3.2 ton/ha under RCP2.6 and 3.4 ton/ha under RCP8.5 during 2040-2064 period. However, the ensemble average SWY in high N_stress regions (Figure 2.8m and Figure 2.8u) was 2.6 ton/ha and 2.7 ton/ha under RCP2.6, and RCP8.5, respectively, which slightly declined or remained almost the same in the low N_stress region (Figure 2.8p and Figure 2.8x) with average SWY of 2.5 ton/ha, and 2.8 ton/ha. In addition, the high N_stress regions showed a smaller range of SWY variation in each year resulting from 72 simulated scenarios (grey lines in Figure 2.8m and Figure 2.8u). In other words, the range of SWY projections, resulting from 72 model scenarios, was smaller in the high N_stress regions as compared to other regions. The small range indicates only a slight difference between GCMs, RCPs, DSs, and 95PPUs projections. This is most likely due to the high N deficiency in the soil or low N uptake by crops, both of which restrain the beneficial effects of soil water availability on SWY varied among nine GCMs, two RCPs, two DSs, and 95PPUs in the model. It is noteworthy that the majority of the selected 72 scenarios are only presenting the effects of climate change and they are more influential on soil water alterations (W_stress) than soil nutrients (N_stress). Likewise, a lower variation between model scenarios is observed under RCP8.5 as compared to the RCP2.6 scenario in the high N_stress regions (see Figure A.1).

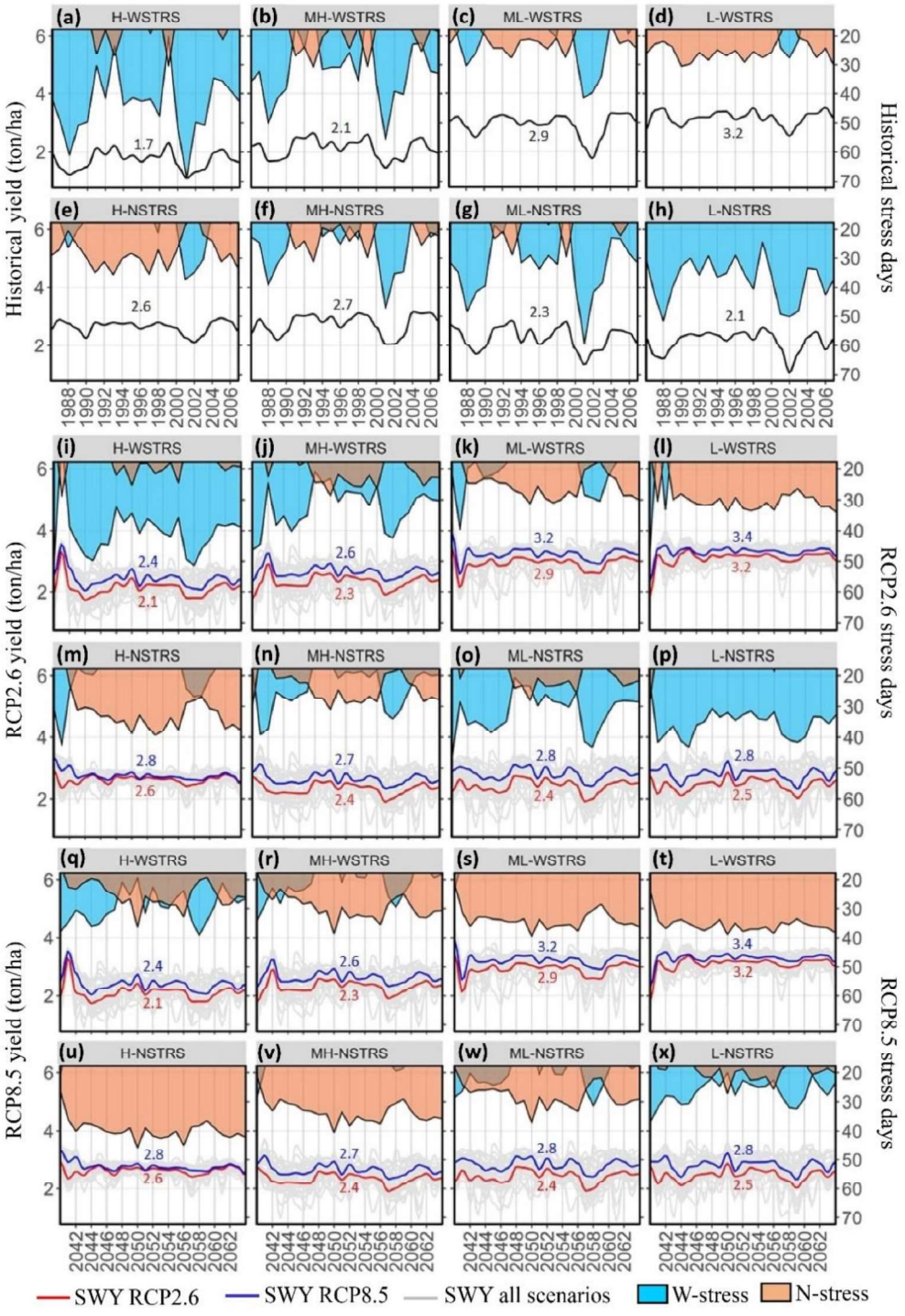

Figure 2.8. Comparison of historical SWY and projected SWY in high, mid-high, mid-low, and low W/N_stress regions and each region's respective W-N_stress days. Black, red and blue lines illustrate the average of historical and 36 projected SWY scenarios under RCP2.6 and RCP8.5, respectively. The number inside each sub-figure shows the average SWY during the respective time span. Grey signals in each panel are simulated SWY under the 72 scenarios.

It appears that the effect of elevated CO_2 is not uniform across regions. As also discussed by McCarl et al. (2008), a shift in the average and variability of SWY distribution has developed from the historical period to the future, indicating a non-stationary trend of crop yields in our study region. In addition, the results indicated that the cause-and-effect mechanism, driving crop growth and yield development, has changed in the future period from their historical compartments. It is shown that the system behavior has shifted from being historically a W_stress dominated setting (wider blue in Figure 2.8a-h) to a N_stress dominated status (wider orange in Figure 2.8q-x) in the future. Low W_stress regions were found to be the least affected regions from the changing climate (Figure 2.8d,l,t), as the average projected SWY has almost had no increase from the historical period (3.2 ton/ha), under RCP2.6 (3.2 ton/ha) and very limited increase under RCP8.5 (3.4 ton/ha). Note that while there is a substantial reduction in projected snowmelt from the historical time (Faramarzi et al., 2017; Zaremehrjardy et al., 2020), the soil water availability in these sub-basins has increased under future scenarios mainly due to earlier snowmelts and infiltration that increases soil water availability for the growing season. However, the anomalies in SWY was maximum in high W_stress regions with historical SWY of 1.7 ton/ha (Figure 2.8a) that increased to 2.1 ton/ha, and 2.4 ton/ha under RCP2.6, and RCP8.5, respectively (Figure 2.8i,q). This indicates that historically low W_stress regions may not benefit as much as high W_stress regions from earlier snowmelts and higher water-use efficiency under future scenarios (Uddin et al., 2018). In addition, the watershed may be partly detrimental to lower N uptake due to low water uptake stemming from stomatal closure under elevated CO_2 concentration (Bower, 2008; Houshmandfar et al., 2018) as discussed in section 2.4.3. Moreover, potential enhancement of biomass, which is expected under an enhanced atmospheric CO_2 fertilization (Roudier et al., 2011) and increased temperature in cold environments, may demand more N nutrient, which suggests that crop N

deficiency (N_stress) may become the primary limiting factor in the region. These alterations in physical and biogeochemical processes, as well as phenological characteristics and physiological processes of the crop, suggest time-varying yield behavior to the underlying cause-and-effect processes that generate it. It also implies that the same or different levels of crop yield may be attained under very different agro-hydrologic settings in the future as compared to the historical period. Therefore, adaptation measures based on inference from historical experience and data may be doubtful (Milly et al., 2008, 2015), as the results showed a non-stationary behavior of SWY.

2.4.5 ANOVA of the yield response to hydrologic model parameters, GCM, RCP, DS scenarios

The median of the ANOVA values showed that emission scenarios (RCP2.6 and RCP8.5) followed by global climate models (GCMs) created the largest variations in SWY projections. This is because the higher atmospheric CO_2 under RCP8.5 substantially intensifies future biomass development and crop yields as compared to RCP2.6 (see section 2.4.4), which results in a large difference between RCP2.6 and RCP8.5 projections. This results in a large range of SWY projections under RCP scenarios as compared to other driving forces such as GCMs, DSs, and 95PPUs (Figure 2.9). The large share of the SWY variance due to DSs implies considerable temporal variations of SWY under DS1 and DS2 (see Figure A.2) but the overall variance indicated by median value remains minimum as compared to the other drivers (Figure 2.9). The spatial distribution of DSs contribution to the total variance in Figure A.3 also indicates higher discrepancies between simulated SWY under DS1 and DS2 mostly in the northern RDR basin. This is rather evident in the regions where there are higher W_stress (Figure 2.5a), and less impediment from N deficiency (Figure 2.5c; also see Figure A.4). However, the relation between

W_stress, N_stress with the DSs contribution to the total variance is not as clear as their relations with GCMs, and RCPs share of the variance (see Figure A.4). This is probably due to the poor DS2 climate dataset (as they have not downscaled to local climate conditions) that inconsistently differs from DS1 in different years (see Figure A.2) and different locations (Figure A.3).

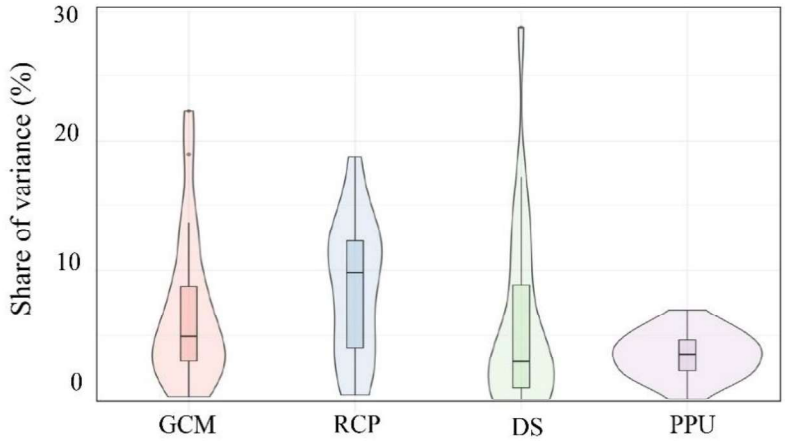

Figure 2.9. Variance decomposition in SWY for future (2040-2064) yield projections under different GCMs, RCPs, DSs, and 95PPUs factors. Box boundaries indicate the 25th and 75th percentiles; the black line within the box marks the median; whiskers below and above the box indicate the 10th and 90th percentiles. The violin plot outlines kernel probability density.

As shown in Figure 2.9, the GCM is the second largest reason for SWY variations. However, as also discussed in section 2.4.4 (Figure 2.8), with increasing N_stress, the variations of the SWY due to alteration in climate projection factors (e.g., GCMs) are limited in all regions because inadequate N restrain optimal growth and development of crops (Wang et al., 2009). Therefore, in sub-basins that are suffering from high W_stress in the historical period (mostly located in the southwestern part of the RDR basin, see Figure 2.5a), a higher contribution of GCMs and RCPs to the total SWY variance is observed only when their N_stress is relatively low (see Figure A.3 and Figure A.4). This is likely because when N is not a limiting factor, depending on the GCM types, crops can either grow towards their potential under favorable soil water and climate condition in the future or their yields are inhibited by high temperature and low precipitation, resulting in a

large range of variations from GCMs. The 95PPUs, as another source of variance, showed lower variance contribution as compared to GCMs, RCP, and DSs (Figure 2.9). While 95PPUs reflect cumulative effects of several parameters related to both N and W in the SWAT agro-hydrologic model of the basin (see Table 2.1), one can hypothesize that contribution of 95PPUs to the total SWY variance in both high N_stress and high W_stress should be relatively high. However, as also discussed in section 2.4.4, with increasing N_stress, the changes in water-related parameters are less influential on the SWY variation due to the nutrient deficiency, and vice versa. Thus, depending on the level of water and nutrient availability in the soil, the N related parameters and W related parameters may offset the effects of one another on SWY variation, resulting in a limited contribution of 95PPUs to the total variance in almost all the sub-basins (Figure 2.9 and Figure A.3).

2.4.6 ANOVA of the future yield response to different nitrogen application scenarios

N is a major nutrient that limits crop yield in western Canada. Most field crops in western Canada are sensitive to N deficiency in the soil and N deficient crops are highly responsive to N fertilizer (Nowak et al., 2004; Deryng et al., 2016; Reich et al., 2014). Hence, it is expected that future yields are affected by application rates of supplemental nutrients, especially N. Therefore, we hypothesized that CO_2 fertilization effects weaken when plant growth is restricted by N deficiency and this may cause a relatively similar SWY under both RCP2.6 and RCP8.5 scenarios (Figures 2.8m and 2.8u). To test this hypothesis, we studied the effects of two opposing N application rates on future SWY projections with 20% less N fertilizer application than baseline (NS1) and 20% more N fertilizer application (NS2) during the growing season. Note that the baseline scenario assumes historical N application rates and volumes for future yield projections.

Our results showed that under NS1, the contribution of 95PPUs in the overall SWY variances increases while it decreases or remains unchanged for GCMs, RCP, and DSs (Figure 2.10). The reasons for such increases in 95PPUs contribution is related to the availability of N in the soil and model parameters. As discussed in earlier sections (see section 2.4.4), crop response to climate factors and CO_2 changes depends on nutrient availability in the soil. The more N deficiency in the soil under NS1, creates more sensitivity of yield to small changes in N availability due to perturbing N related parameters in the model. Note that the 95PPUs are the only factors that reflect the effect of changes in N through its N-related parameters in the model, such as AUTO_NSTRS, AUTO_NAPP, and AUTO_NYR (see Table 2.1), as compared to GCMs, RCP, and DSs. Therefore, any further decline in N under NS1, increases the share of 95PPUs in variance as compared to GCMs, RCPs, and DSs.

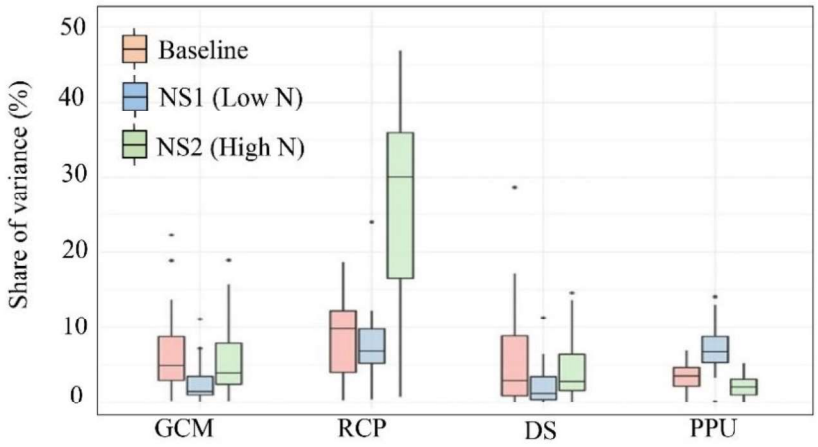

Figure 2.10. Share of the variance related to GCMs, RCPs, DSs, and 95PPUs for projected SWY changes in the study watershed, under baseline N application scenario, NS1, and NS2.

A larger share of variance from RCPs as compared to GCMs and DSs in NS1 is also due to the higher sensitivity of the yield to CO_2 emission scenarios than climate model projections and the downscaling techniques, even when the agronomic management factors such as N fertilizer application is restricted under NS1. The smaller share of RCPs in NS1 as compared to the baseline

scenario is due to a decrease in yield projection under NS1 due to N deficiency. This yield decline is more evident under RCP8.5, where more potential exists for yield to boost under elevated CO_2 availability, but N deficiency limits crop from reaching its potential as also shown in a study in agricultural lands in Australia by Wang et al. (2018).

The NS2 demonstrates the smallest share of physical parameters related to the processes in the agro-hydrologic model (95PPUs), while emission scenarios (RCPs) contribute the largest share to the overall cascade of SWY variances (Figure 2.10). A comparison of the results also indicates that the share of variance due to RCPs highly increased in the NS2 as compared to the baseline. The main reason is that under NS2, the additional N in the soil escalates biomass production and yield under RCP8.5, when elevated CO_2 force yield increases in the future (Ngosong et al., 2019). However, the increased N under this scenario does not considerably influence yields under RCP2.6 where atmospheric CO_2 is not a significant driving force for crops to grow to their potentials. This results in a large range of variation in SWY projections under RCP2.6 and RCP8.5, which results in a substantial increase in RCPs share of variance under NS2 as compared to baseline (Figure 2.10). Hence, it can be hypothesized that N_stress could be a dominant limiting factor in future scenarios (see Figure 2.5a, and 2.5c) due to lower W_stress and higher N demand under CO_2 fertilization. This has been also emphasized in studies by Kant et al. (2012) and Uddin et al. (2018). To test this hypothesis in more detail, we further investigated our results at the four L, ML, MH, and H sub-regions in our study area (Figure 2.11). The results showed that the share of SWY variance from different sources depends on not only climatic and management conditions, but also geographical locations and land, soil, and hydrologic specifications. The results showed that under NS2 the changes in the median share of the variance of the yields from their baseline compartments are larger under GCMs (Figure 2.11a) as compared to DSs (Figure 2.11c) and 95PPUs (Figure

2.11d), especially in high W_stress sub-basins. This higher share of the variance under GCMs is due to a large divergence in the projected temperature and precipitation among different GCMs than DSs and 95PPUs. Further, the ANOVA results of GCMs (Figure 2.11e) showed a limited discrepancy in the share of variance between the baseline scenario, NS1, and NS2 in high N_stress regions as compared to low N_stress regions. This suggests a significant impact of N deficiency on limiting yield variation under different precipitation and temperature scenarios forced by GCMs (see Figure 2.11e). This is evident even when water availability is not a limiting factor in regions with low W_stress and high N_stress regions (see Figure 2.8m and Figure 2.8u) (Sharma and Bali, 2017; Smith et al., 2019).

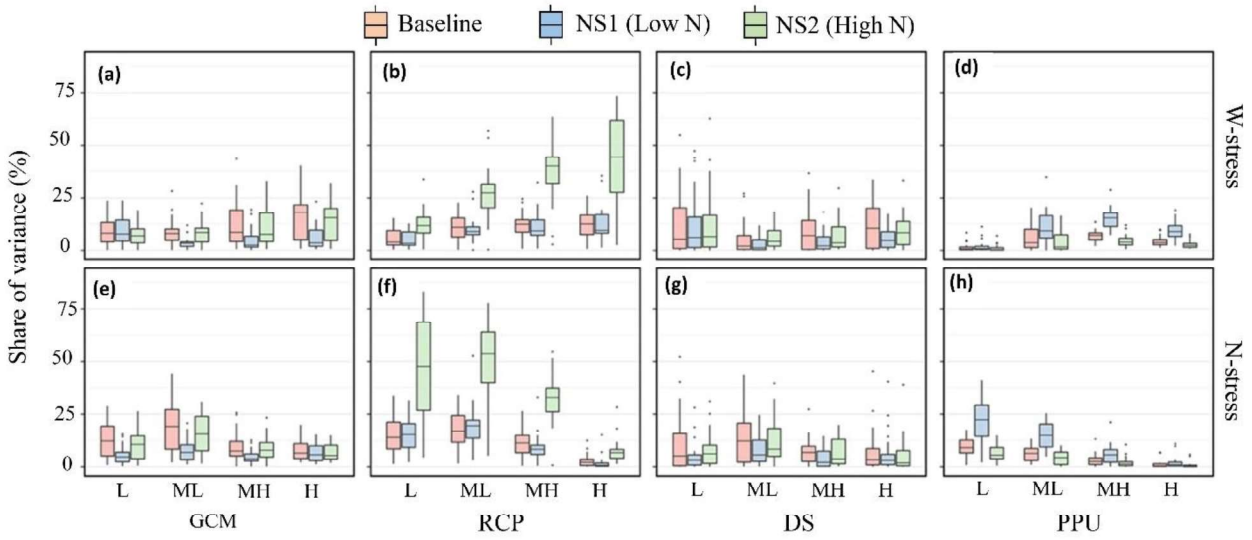

Figure 2.11. Share of the variance (% ANOVA) related to GCMs, RCPs, DSs, and 95PPUs for projected SWY changes in high (H), mid-high (MH), mid-low (ML), and low (L) W and N_stress regions under the baseline scenario, NS1, and NS2.

Comparison of ANOVA results for RCPs (Figure 2.11b) showed that under NS2 the increase of SWY variances was considerably higher in high W_stress regions as compared to low W_stress sub-basins (Figure 2.11b). This is due to the CO_2 fertilization effect of RCP8.5 on crop water-use efficiency (Uddin et al., 2018) that promotes SWY, especially in W_stress regions, as it can reduce

crop water consumption. This coincides with earlier studies that revealed higher atmospheric CO_2 concentration (i.e. RCP8.5) can reduce crop water loss per unit of carbon gain, especially in W_stress regions, which results in a higher sensitivity of SWY to W_stress variations (Swann et al., 2016; Ahmed et al., 2019; Reich et al., 2014; Urban et al., 2017). The share of RCP to yield variations in W_stress regions can further increase when there is sufficient N in the soil and it is not a limiting factor, e.g., in low N_stress regions (see Figure 2.8i and Figure 2.8q). Therefore, increasing the N application rate can be considered as a potential adaptation measure to confront climate change especially in W_stress regions (Guan et al., 2017).

2.5 Comparison of this study with the literature

Warmer and drier climate can cause higher potential evapotranspiration under low soil water availability that can produce crop water stress, which can be crucial during key stages of the crop's development (Chou et al., 2013; Pongrácz et al., 2014; Anjum et al., 2017). Our results indicate increasing SWY even in regions experiencing slightly reduced precipitation in future scenarios (Figure 2.4-2.7). This suggests the important role of multiple players on crop yields and its non-stationary behavior under changing climate. For instance, the sub-basins that historically suffered from high W_stress could show yield increases due to an improved water-use efficiency because of the effects of elevated CO_2 concentration on plant CO_2 assimilation (see Figure 2.4-2.7). In addition to CO_2 fertilization effects, changes in timing and type of precipitation and the timing and rate of snowmelt (Fang et al., 2019; Qin et al., 2020) altered spatiotemporal changes in soil water availability. The profound effects of earlier snowmelts on SWY, especially in snow-dominated agricultural regions, have also been argued by Biemans et al. (2019). This indicates the significant role of hydrological processes in estimating soil water availability and therefore crop yield, especially in Canadian Prairies characterized by cold hydrology. Our hydrology model of the RDR

basin in Prairie Canada showed that while there is a substantial reduction in projected snowmelt from the historical time (Faramarzi et al., 2017; Zaremehrjardy et al., 2020), soil water availability has increased under future scenarios mainly due to earlier snowmelts and infiltration that increased soil water availability for the growing season.

We showed while increasing precipitation and early snowmelts, elevated CO_2 and warming may favor SWY in many ways, the yield potentials maybe limited due to the nitrogen deficiencies in the soil. Our results indicated considerable yield gains under RCP8.5 facilitated by increased N fertilizer application in some sub-basins. This aligns with the discussion by Kant et al. (2012), Schierhorn et al. (2015), Uddin et al. (2018), and Ngosong et al. (2019) that emphasized how additional N in the soil can escalate biomass production and close yield gaps, especially when elevated CO_2 force yield increases in the future. However, our results indicated that low transpiration and stomatal closure (i.e., RCP8.5) might limit N uptake by crops and trigger N_stress, making it a dominant SWY limiting factor especially under high CO_2 concentration in the future. Moreover, increased nitrogen application under RCP2.6 did not considerably influence yields, as atmospheric CO_2 which is a building block of the biomass assimilation and major driving force for crops did not considerably increase as compared to RCP2.8. This suggests, larger yield gains in the future, especially under larger elevated CO_2, may require substantial increases in N fertilizer applications only in some areas (see, for example, Figure 2.11f), which may also arise environmental concerns (Yu et al., 2019), but in other areas may not affect yields due to reduced N uptake.

Statistical analyses of the crop yield in global studies reveal important information on the warming effects and relationship between weather parameters and yields (Lesk et al., 2016; Lobell and Burke, 2010; Zhao et al., 2019). However, these studies lack dynamic feedback and non-

stationary behavior of cause-and-effect mechanisms under a wide range of hydro-climate and geophysical settings that affect crop yields and their response to future changes in temperature, atmospheric CO_2 concentration, water, and nutrient availability. Recent studies elaborated on the non-stationary behavior of feedbacks among climate, hydrology, and vegetation and their feedback (Milly et al., 2008). This implies that inference from historical observations and their trends alone cannot be implemented for future agricultural adaptation and management solutions (Ciscar et al., 2018). The majority of studies that utilized statistical analyses or used data-driven approaches for crop yield estimations only developed linear or nonlinear regression relationships between climate and observed crop data (Lesk et al., 2016; Lobell and Burke, 2010; Moore et al., 2017; Rayid et al., 2019; Zhao et al., 2019). Inference from these statistical models for future adaptations can be subjective. In such studies, the effects of CO_2 fertilization are typically neglected and they lack important process representations and non-stationary interactions between physical and biochemical processes related to crop growth, soil water hydrology, climate change, and management factors. Our study demonstrated crop yield variation is not a result of the changes in a single or a limited number of variables (e.g., temperature or precipitation). Different climatic and non-climatic variables related to the soil-plant-atmosphere system interact dynamically over time and space resulting in a heterogeneous response of SWY to future climate change in time and space (Lugoi et al., 2019). These effects bring the notion that analyses of crop response simulated by process-based crop models including hydrological, crop growth, and atmospheric processes may outperform statistical trend analyses, where the evolution of crop responses to interactive climate and non-climate changes are not quantified (Lobell and Asseng, 2017; Moore et al., 2017; Shi et al., 2013).

2.6 Limitation and future directions

The projected changes in the hydroclimatic and crop growth conditions derived from the agro-hydrological model in this study have some limitations. The model assumed the type of cultivars, crop varieties, and sowing dates under future scenarios to be the same as the historical period. Addressing these factors using socio-agro-hydrological modeling in future studies would be worthwhile. These approaches can examine tradeoffs and response of agricultural, hydrological, and socioeconomic factors to reflect a more accurate response of yields to management and human decisions.

Instrumental data (i.e., measured time series) for crop and hydrological modeling are not often available for long periods of time, which makes model verification and prediction of the state variables available only for a short period of time (e.g., 25 years historical period in our study). Prediction within a short period can increase the variance of the study variable (e.g., SWY), which requires additional investigation in future studies. However, for understanding the evolutions of agro-hydroclimatic conditions, non-overlapping periods (i.e., historical and future) can be simulated with the assumption of local stationarity within each period (Kavvas et al., 2017; Trinh et al., 2016).

Our model results showed negligible aeration stress in both historical and future scenarios. In other words, our simulated W_stress days were mainly due to water deficiency in the soil. Since the simulation of aeration stress is based on soil properties, the resolution and accuracy of soil data are crucial. Our soil data are supplied from available regional soil maps with rather a coarse resolution, which may have increased the uncertainty of the study results. It is suggested that more high-resolution soil data are used for W_stress and SWY simulations in the future. We highlight the necessity for environmental monitoring in various watersheds to establish baseline conditions.

This could include the collection of soil samples, which provide valuable data for identifying key physical and chemical properties and their changes that result from human activity, climate change, or any combination thereof.

The effect of the prevalence of pests, diseases, and weeds that are more probable in warmer and wetter conditions are of great importance to the projection of actual SWY (Oerke, 2006). As such, further studies are required to consider the effects of biotic stressors in future SWY in addition to the hydro-climate and crop phonological processes. Moreover, genetic improvement of crop varieties is another important component to be considered in future work, which can overshadow the adverse effects of abiotic stressors (i.e., drought) on SWY in the future.

2.7 Conclusions

Non-stationary response of the hydrological regime and crop yield to changes in climate variables and elevated CO_2 is one of the most trending topics in impact assessment studies. While earlier studies focused on the sole effects of elevated CO_2 compounded with higher annual mean temperature, and crop water productivity on crop yields, this paper showed that the magnitude of SWY variations differs depending on climate, location, management practices, soil types, and hydrologic regimes. We showed the time-varying behavior of SWY to the underlying cause-and-effect processes, which is very different in the future than historically. Our results revealed a similar or higher level of SWY under different agro-hydrological settings (e.g., N_stress dominated status) in the future than its historical conditions (e.g., W_stress dominated setting). This implies that cause-and-effect mechanisms, driving crop growth and yield development, may change over time, resulting in the non-stationary behavior of SWY.

Although it is widely discussed that elevated atmospheric CO_2 in the future may boost crop yields and therefore water productivity, our results showed that the response of crops to

atmospheric CO_2 is conditional and it depends not only on the aforementioned factors but also their non-linear interactions with other key parameters. In this study, the SWAT model along with ANOVA decomposition method was used for studying how and to what extent crop yields respond to GCMs, RCPs, DSs, 95PPUs, and N fertilizer application scenarios under different climatic conditions and agronomic management practices. Accordingly, the major conclusions of this study are as follows:

1- The largest share of variance in SWY results from RCPs followed by GCMs, DSs, and 95PPUs, respectively. This indicates the sensitivity of SWY to atmospheric CO_2 concentration followed by changes in precipitation and temperature projections and crop-hydrologic variables.

2- GCMs have a large contribution to the total share of SWY variance, especially in high W_stress regions, mainly because soil water stress is historically a main limiting factor to SWY. Alterations in soil moisture, which is stimulated by the agro-hydrologic model under various GCM- projections, stimulated SWYs, and their variations as compared to historical conditions.

3- The positive effects of atmospheric CO_2 fertilization on SWY are more evident in regions where there is less barrier from N deficiency (i.e., NS2). This implies increased N application may increase N uptake and benefit yield gains in some areas. On the other hand, the low transpiration due to the higher rates of stomatal closure under high atmospheric CO_2 concentration (RCP8.5) and inadequate water availability in the soil may reduce N uptake. The N uptake reduction may trigger N_stress and makes it a dominant SWY restraining factor in the future. Therefore, in some regions, N deficiency can highly limit the effects of soil water variation on SWY even under favorable climate. This denotes that increasing N fertilizer might be a potentially effective adaptation measure to cope with climate change especially under high

atmospheric CO_2 concentration. However, the impacts of N application on environmental land and water quality requires more studies.

4- The effects of elevated atmospheric CO_2 is not uniform across regions. In addition, a shift in the average and variability of SWY distribution was observed from the historical period to the future. This indicates that the experience and data may lack representation of the future as the spatial and temporal response of SWY to its cause-and-effect mechanisms is not stationary and is changing over time.

It is worth mentioning that the results have significant implications to water-food-climate change studies and global food security, as the study area is among key SWY producing areas in the Canadian Prairies, which is one of the most important bread baskets of the world. Therefore, our study provides valuable information to facilitate more informed adaptation measures for regional planning and policies of future agricultural production.

2.7 Acknowledgment

Funding for this study was primarily provided by the Natural Sciences and Engineering Research Council of Canada (Grant #RES0043463) and Campus Alberta Innovation Program Chair (Grant #RES0034497).

CHAPTER III – MANUSCRIPT 2

Assessment of blue water-green water interchange under extreme warm and dry events across different ecohydrological regions of western Canada

Pouya Khalili[1], Saman Razavi[2-3], Evan G.R. Davies[4], Daniel S. Alessi[5], Monireh Faramarzi[1*]

[1] *Watershed Science and Modeling Laboratory, Department of Earth and Atmospheric Sciences, Faculty of Science, University of Alberta, Edmonton, AB T6G 2R3, Canada*

[2] *Institute for Water Futures, Mathematical Science Institute, Australian National University, Canberra, Austrlaia*

[3] *Global Institute for Water Security, School of Envionment and Sustainability, and Department of Civil, Geological, and Environmental Enigeering, University of Saskatchewan*

[4] *Department of Civil and Environmental Engineering, University of Alberta, 9211, 116 Street NW, Edmonton, AB, T6G 2H5, Canada*

[5] *Department of Earth and Atmospheric Sciences, University of Alberta, Edmonton, Canada.*

[*]Corresponding author: faramarz@ualberta.ca

[*]Corresponding author: khalili@ualberta.ca

3.1 Abstract

As key drivers of terrestrial ecosystems and food production, green water (GW) and blue water (BW) are interlinked through natural and anthropogenic processes. Their relationship has reportedly been non-stationary, with an anticipated shift from BW to GW in the future. However, these potential shifts are poorly characterized, particularly in response to future extreme warm-dry events. To address this gap, we used a process-based agro-hydrological model to project GW-BW interlinkages and their potential shifts across three different ecohydrological regions – mountainous, crop, and natural lands – in the Nelson River Basin, the largest agricultural basin in Canada and a major breadbasket for the world. Our results indicate dissimilarity in the physical processes that link GW and BW across different ecohydrological regions, and therefore,

disproportional projected changes in BW and GW. In mountainous and natural lands, with projected decreases in precipitation in extreme warm-dry years of up to 56% and 46% under SSP126 and SSP585 scenarios, BW decreases by 64% and 42% while GW decreases only by 37% and 29%. The decline in GW is expected to be less because of the availability of evaporative water supplied by legacy soil moisture and groundwater contributions from earlier seasons. This available water to supply evaporative demand represents an overall shift of BW to GW. In crop lands, however, results show a significant decrease of precipitation (45%-55%), BW (up to 42%), and GW (up to 42%), with no remarkable shift of BW to GW in extreme warm-dry years in the future. The projected BW and GW declines in crop lands may impose severe water shortages on local and regional food production. Projected declines in BW from the mountains that serve as source water for downstream irrigation may exacerbate such possible shortages.

Keywords: CMIP6, SSP126 and SSP585, mountainous lands, natural lands, crop lands

3.2 Introduction

Green water (evapotranspiration, GW) and blue water (water yields, BW) are crucial for terrestrial ecosystems (Zang and Mao, 2019) and food production (Falkenmark and Rockström, 2006), especially in arid and semi-arid regions. Although most traditional water policy and development plans have focused on managing BW and its allocation to various economic sectors, GW forms the basis of most of the water consumption globally, with 70% of the agriculture sector relying on GW resources (Ringersma et al., 2003). Both GW and BW are limited in time and space in many regions (Schyns et al., 2019), and are interlinked through numerous biogeochemical and physical processes within the soil-plant-water-atmosphere system (Maxwell, 2020). Natural terrestrial processes and human activities can alter the availability and interlinkages of GW and BW resources. In addition, climate change and projected extreme climatic events are reported to

negatively impact the availability and distribution of GW and BW resources (Maxwell, 2020; Stenke, 2020). While most studies have focused on the assessment of the hydrological cycle or specific processes driving the water budget at a catchment to large watershed scale, a detailed assessment of GW and BW relationships across different ecological settings (i.e., mountainous lands, crop lands, and other natural lands) and their interlinkages under extreme climatic events (i.e., extreme warm-dry events) are limited at a regional scale.

The availability and variability of GW and BW are related to numerous factors such as precipitation, vegetation type, soil type and water infiltration (Destouni and Verrot, 2014), air and soil temperatures (Orth and Destouni, 2018), soil nutrients (Wang et al., 2018), and atmospheric CO_2 concentration (Ngosong et al., 2019). GW supply is the amount of soil moisture available for sustaining plant growth. Vegetation types and their growth conditions can significantly influence soil moisture and GW-BW relations due to root development and water uptake during the growing season. Vegetation can also affect surface water runoff through interception as canopy storage, a storage that can change over time with plant growth (Deb et al., 2019; Vicente-Serrano et al., 2021; Wasaya et al., 2018).

Some studies have focused on agricultural crop and water management and highlighted the role of soil nutrients and soil temperature in regulating soil water balance (Adimassu et al., 2017; Gao et al., 2018), which can impact the relationship between GW and BW. A reliable supply of soil nutrients can invigorate biomass development and plant growth, enhancing vegetation demand for soil moisture (Wang et al., 2019). As a result, more water can be used by plants, which can reduce the surface runoff over the long run, all of which can result in considerable change in the GW-BW relationship and its spatiotemporal variation. Further, vegetation growth is regulated by soil temperature, especially in mid-to-high latitude crop lands, where soil is frozen for several months

during cold season (Onwuka et al., 2016). In theory, warm soil induces plant growth processes such as water and nutrient uptake (Anderson and Markham, 2021), while lower soil temperatures inhibit water uptake due to lower water viscosity, thereby slowing photosynthesis and evapotranspiration (Zhang et al., 2020). In other words, low soil temperature can reduce nutrient and water uptake by plant roots, decreasing GW consumption rates and consequently altering GW-BW interlinkages.

Climate factors such as air temperature, relative humidity, wind speed, and atmospheric CO_2 also affect the GW-BW relationships by altering the potential and actual evapotranspiration (ET). Hereafter, the ET refers to transpiration by plants as well as evaporation from the soil. Generally, an increase in air temperature enhances the moisture holding capacity of the atmosphere and thus, intensifies the evaporative demand and accelerates the hydrological cycle (Massmann et al., 2019). Conversely, a higher relative humidity of the air can reduce ET rates, while a higher wind speed can trigger greater plant transpiration rates (Ackley, 2012). Plus, the alteration in the level of atmospheric CO_2 not only affects the climate change-induced water cycle but also affects plants' stomatal openings, thus altering their photosynthetic and transpirative rates (Manderscheid et al., 2018). Therefore, numerous terrestrial and atmospheric processes interplay to form a diverse range of GW-BW relations across regions and times.

Coinciding with the natural processes, the role of anthropogenic activities such as the construction of dams (Hogeboom et al., 2018), irrigation schemes (Nouri et al., 2020), and water transfer projects on changes in the BW regime are unavoidable. Disrupting soil structure through management practices such as agricultural tillage operations and early planting dates for improved crop yields have produced changes in surface runoff (i.e., BW) (da Luz et al., 2022) and ET rates (i.e., GW), possibly shifting GW-BW relationships (Masud et al., 2018).

While natural and anthropogenic processes directly affect GW-BW relationships, extreme climatic conditions, such as warm-dry events, are projected to significantly change the underlying processes that determine GW-BW relationships (Saft et al., 2015). The frequency and severity of warm-dry extremes will increase under global warming scenarios in the future (Gamelin et al., 2022). Recent studies have indicated a clear shift in recent decades from BW to GW within the hydrosphere-biosphere system in Alpine regions under warm and dry conditions (Orth & Destouni, 2018; Mastrotheodoros et al., 2020). They have also highlighted the continual and even potential intensification of that shift from BW to GW under future climate change scenarios (Mastrotheodoros et al., 2020). However, upscaling GW-BW relationships from a limited number of catchments to regional landscapes with heterogeneous ecological and climatological settings is challenging. The BW-to-GW shift depends on the cumulative effects of numerous ecohydrological processes that can spatially and temporally change under extreme climatic events (e.g., warm-dry events). Pre-drought aridity (Saft et al., 2016), characterized by reduced soil water infiltration, and the soil moisture carried from previous years (Klos et al., 2018; Rungee et al., 2019) can affect the amount of stored water available for plants during the dry season and thus GW-BW interlinkages. During the initial stages of a warm-dry event, multi-year legacy soil moisture from previous wet periods can partially compensate for missing precipitation input. This mechanism can offset ET deficit and support vegetation growth during warm-dry years (Massari et al., 2022). However, during a prolonged warm-dry event, a long-term precipitation deficit can ultimately cause vegetation mortality (Bales et al., 2018). Therefore, extreme changes in climate conditions, such as warm-dry events, can result in entirely dissimilar GW-BW relationships compared to average years.

The overarching goal of this study is to characterize changes in GW-BW relationships under future warm-dry events across different landscape and ecological settings such as mountainous lands, natural lands, and crop lands in large watersheds. To achieve this goal, our specific objectives are to (i) set up, calibrate, and validate a process-based agro-hydrological model at a watershed scale with heterogeneous ecohydrological conditions, using the best available input data; (ii) quantify spatiotemporal variations in the relationships between BW and GW under different ecological settings, including in mountains and foothills (i.e., mountainous lands), agricultural plains (i.e., crop lands), and other natural landscapes such as boreal forests and wetlands (i.e., natural lands); (iii) discuss the spatiotemporal variations of driving factors and how they affect changes in GW-BW relationships; and (iv) quantify GW-BW anomalies under possible future extreme warm-dry events from their historical averages. The insights gained through this study are relevant to other large river basins in mid-to-high latitude regions, which are typically centers for socioeconomic development and food production.

3.3 Materials and methods

3.3.1 Study area

The Nelson River Basin (NRB) covers a vast drainage area of approximately 1.2 million square kilometers, making it one of the largest watersheds in North America (Figure 3.1). With elevation of 3227 m, the NRB begins in the Rocky Mountains in the west and ends by discharging to Hudson Bay, which is the world's most immense inland sea (Joly, 2021) at sea level elevation (Figure 3.1A). The river basin extends as far south as South Dakota, United States to the middle of Saskatchewan and northern borders of Manitoba, Canada, and to near the Lake Superior in the east of the region. The entire NRB is delineated into six major river basins: Assiniboine River Basin (ARB), Red River Basin (RRB), Winnipeg River Basin (WRB), Lake Winnipeg Basin (LWB),

Saskatchewan River Basin (SRB), and Nelson River Local Basin (NRLB) (Keum et al., 2019) (Figure 3.1A). The RRB, ARB, WRB and SRB flow into the LWB, which drains into the NRLB.

With average annual precipitation levels of more than 800 mm, the western and eastern regions of the NRB are its wettest areas. In contrast, the central prairie region is dry, with an average annual precipitation of less than 400 mm. Annual average temperatures vary from -5 ˚C in the northern regions to 7 ˚C in the south. During winter, precipitation is generally in the form of snowfall. Based on Manitoba Hydro (2015) data for 1981-2010, the ARB has the smallest contribution to the NRB water supply, with annual average streamflow of about 45 m^3/s. NRLB carries the largest cumulative volume of water from the upstream basins, with an annual average streamflow of ~3200 m^3/s, which it discharges into Hudson Bay. The SRB, the largest river basin within NRB, and the WRB, which drains into Lake Winnipeg, have annual average streamflows of ~550 m^3/s and ~950 m^3/s at their outlets, respectively. LWB delivers annual average streamflow of ~2180 m^3/s at its outlet into the NRLB, which includes internal water yields and streamflow from upstream basins (Figure 3.1A). The RRB, which originates from the northern tributaries of the United States, discharges into Lake Winnipeg with average annual streamflow of ~250 m^3/s.

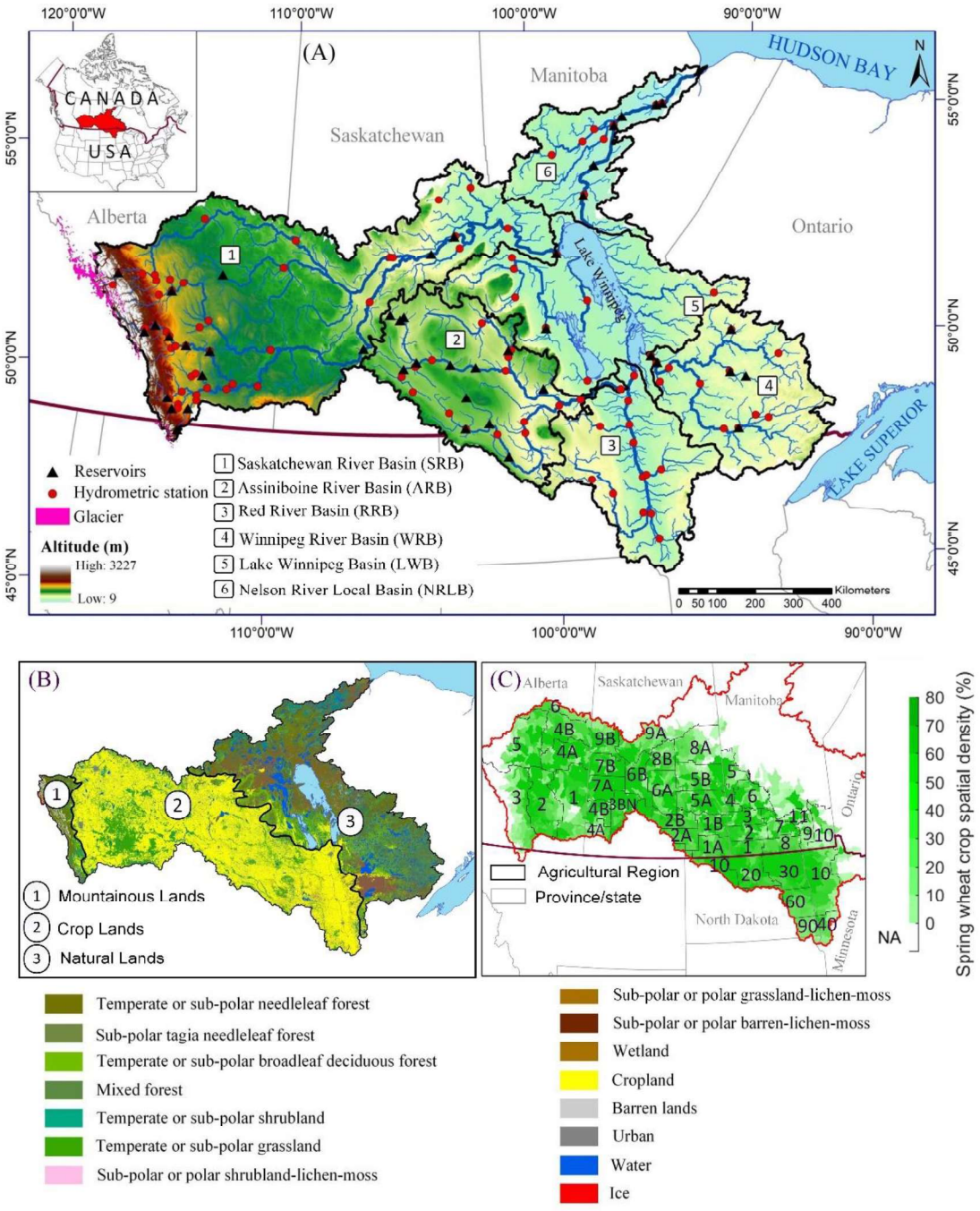

Figure 3.1. (A) Map of the Nelson River Basin including geographic extents, major watersheds, rivers, reservoirs, dams, lakes, hydrometric stations, (B) the land use map and land use classes considered in the model according to the Government of Canada (2019) classification, and the Census Agricultural Region (CAR), for which the agricultural management and crop yield time series are available from government of Canada for calibration and validation in this study.12

The land cover types in the NRB range from high mountains and mountain glaciers in the west to agricultural areas and pasture lands in the center to evergreen forests and wetlands in the

east and north (Figure 3.1B). The variation in topography, presence of glaciers and mountains, and heterogenous land covers such as forests, wetlands, and agricultural lands, have resulted in a wide range of ecohydrological processes governing GW-BW relationships in the region. Moreover, the central and southern regions of the NRB, which are also characterized as the Canadian Prairies (Figure 3.1B), are central to global grain production and a major breadbasket of the world (Khalili et al., 2021b). The Canadian Prairies account for roughly 80% of Canada's total cropland area (Statistics Canada, 2021) and play a vital role in the country's economy and national and global food security, with food exports to over 170 countries (Statistics Canada, 2021).

The soils in the crop lands of the NRB are key to the production of spring wheat (Figure 3.1C), which is a widely grown staple crop in the region (Statistics Canada, 2021). These soils are characterized as brown (Aridic Borolls), dark brown (Typic Borolls), black (Udic Borolls), and gray soils (Boralfs and Mollic Cryoboralfs) (Fuller, 2010). These are among the most fertile soils in the world and, together with management practices such as irrigation, fertilizer, and manure application, create a favourable land setting for crop production.

SRB supplies GW and BW for most of the crops in the prairies. Over 90% of water in SRB originates from the Rocky Mountains, which collectively make up only 12% of the area of the SRB, and where warming is a significant threat to freshwater resources (Halofsky et al., 2018). More than 70% of the natural lands in the eastern and north-eastern NRB are covered by forest and wetlands (Zubrycki et al., 2016). In these natural lands, seasonal temperature averages range from ~16 °C in July, August, and September to ~-12 °C in January, February, and March, and the annual mean temperature is 2.3 °C. Most precipitation in the natural lands occurs during the summer, and winters are dry and cold.

Historically, most areas of Canada have experienced periodic warm and dry events with different levels of severity, duration, and spatial extent (Bonsal et al., 2020). Particularly, the agricultural belt of the Canadian Prairies is highly susceptible to extreme warm and dry events in part because of its location in the lee of the Rocky Mountains and strong dependence on variable and unreliable rainfall (Khalili et al., 2021a; Masud et al., 2020, 2019). Canada has warmed at more than *twice* the rate of global warming (Bush and Lemmen, 2019), and this trend is projected to continue. Further, as the second largest country in the world and with diverse geospatial conditions (Bailey et al., 1997), significant changes in many other hydroclimatic processes in different parts of the country have accompanied this rapid warming, such as increases in precipitation (Ashraf Vaghefi et al., 2019; Vincent et al., 2018), decreases in the duration of snow cover (Vincent et al., 2018), and decreases in annual streamflow (Fang and W. Pomeroy, 2020). Climate projections also indicate that many regions of Canada are likely to experience increases in extreme warm and dry events by the end of the 21st century (Masud et al., 2017; Bonsal et al., 2013; Dibike et al., 2017).

3.3.2 Input data

To develop an agro-hydrological model of the NRB for simulation of streamflow and crop yields in the basin, the best available geospatial maps and times series were used (Table A.4). Digital Elevation Models (DEM) at 10m ×10m (AltaLIS, http://www.altalis.com) and 90m × 90m resolutions (SRTM, Jarvis et al., 2008) were used to delineate the NRB into 1988 sub-basins. The sub-basins were further characterized using a detailed land use-land cover (LULC) map and a processed soil map of the region. The LULC, obtained from the Government of Canada (2019), was available at 30m × 30m resolution and classified a total of 19 LULC classes for the NRB. The geospatial and physical parameters related to LULC and soil maps were obtained from the

Government of Canada (2019), FAO (1995), and Cordeiro et al. (2018). The soil map specified various soil classes for up to 10 soil layers for the root zone across the region (see Table A.4 for more details).

The WATCH Forcing Data ERA-Interim (WFDEI) historical climate dataset was used to force the hydrological model to obtain historical streamflow for the 1982-2016 period (Weedon et al., 2014a). This climate data product has produced superior results for Canadian studies (Wong et al., 2017) and successfully reproduces the historical trends and fluctuations of streamflow and crop yields in our model. The measured streamflow data at 86 hydrometric stations were obtained from the Water Survey Canada (WSC) and the National Water Information System (NWIS) database of the United States Geological Survey (USGS) to assess model performance for the 1982-2016 period. Daily operation data of 44 large reservoirs/dams across the basin were obtained from the Saskatchewan's Water Security Agency (WSA), Manitoba Hydro, Alberta Environment and Protected Areas (AEPA, formerly Alberta Environment and Parks), and the HydroLAKES database. The daily operation of these reservoirs/dams were aggregated to monthly and included in the model. This required assigning the geographic location of each reservoir/dam in its relevant sub-basin in the model and inputting its monthly operation for the study period. More details about model setup for dam outflow simulation is provided in Neitsch et al. (2011).

For calibration and validation of the simulated spring wheat yield (SWY), the crop yield time series (metric ton/ha) was obtained from Statistics Canada (2021) and the Alberta Financial Service Cooperation (AFSC) at the spatial resolution of Census Agricultural Regions (CAR), and from the 2021 Agricultural Census of the United States Department of Agriculture (USDA) at the county level, for the 1982-2016 period. For the simulation of SWY, the potential heat units, fertilizer application rates, and maximum amount of annual fertilizer application across 47

agricultural regions and four irrigated counties (Figure 3.1C) were adapted from Masud et al. (2019), the Government of Alberta (Alberta Fertilizer Guide, 2004), the Government of Manitoba (Heard, 2020), and the Government of Saskatchewan (2020).

3.3.3 Hydrology and crop model setup, calibration, validation, and uncertainty analysis

The Soil and Water Assessment Tool (SWAT) is a continuous-time, semi-distributed and process-based model, which simulates both landscape and instream processes related to hydrology, plant growth, sediment and nutrient loads and transport at a catchment scale on a daily time step (Arnold et al., 1998).

In this study, the SWAT model was calibrated and validated using monthly streamflow and annual crop yield data. The calibration and validation periods for the streamflow simulation was 1982-2006 and 2007-2016, respectively. For simulation of crop yield, the calibration and validation periods were 1992-2016 and 1982-1991, respectively. We considered 3 years as model warm-up years for all calibration and validation periods. Using the SWAT model, a basin is divided into several sub-basins based on topography, which are further subdivided into Hydrological Response Units (HRUs) based on soil, land use-land cover, and slope parameters. Hydrological processes are simulated at the HRU scale and then aggregated to sub-basin and basin levels. The hydrological, crop growth, and biogeochemical processes in each HRU are simulated in different soil layers at the root zone (1-2 m top soil layers) based on the soil map and soil data provided by the user.

The simulated processes in SWAT include but are not limited to actual and potential ET (Abiodun et al., 2018), runoff (Faramarzi et al., 2017, 2015), groundwater recharge (Chunn et al., 2019; Karamouz et al., 2021a), subsurface flows (lateral flow), return flow to streams based on

groundwater contribution (base flow), water balance of standing waterbodies (e.g., potholes and reservoirs) (Muhammad et al., 2018), crop growth and crop water consumption (Khalili et al., 2021; Masud et al., 2018), soil temperature (Qi et al., 2016), terrestrial and in-stream nutrient loads and transport, and erosion and sediment loads and transport (Dakhlalla and Parajuli, 2019). Furthermore, the snowfall and accumulation in SWAT are based on daily temperature and precipitation data. If the daily temperature falls below a specific threshold, precipitation is accounted as snow, which accumulates in the snowpack. The model further calculates the water equivalent of the snowpack. The snow cover module in the model allows non-uniform areal coverage of snow due to shading, drifting, topography, and land cover. Snowmelt is simulated based on snow temperature, melting factor, as well as areal coverage of snow, which is then further controlled by the atmospheric temperature and a snow temperature lag factor that represents the degree to which mean air temperature influences snowpack temperature. The melt factor allows simulation of alteration in melt rate due to compression of snow pack across regions as well as its seasonal variation throughout the year (Neitsch et al., 2011b). The meltwater from snow can infiltrate the soil if it is not frozen, or contribute to surface runoff if the soil is saturated or frozen. More details are provided in Neitsch et al. (2011). The term "return flow" or "base flow" refers to the volume of streamflow originating from groundwater. Specifically, in the SWAT model, the water percolating past the bottom of the root zone is partitioned into two fractions to feed two aquifer systems: a shallow unconfined aquifer which contributes return flow to streams delineated in each sub-basin, and a deep confined aquifer which can contribute return flow to streams outside the watershed (Arnold et al., 1993). In addition to return flow which occurs within the streams, water stored in the shallow aquifer can also supply moisture in the soil profile under dry conditions when evaporative demand is high.

The crop growth simulation in SWAT was initially adapted from the EPIC crop growth model (Williams et al., 1984) and further improved over the years (Neitsch et al., 2011). Plant growth is simulated using leaf area development, light interception, and conversion of intercepted light into biomass, assuming a plant species-specific radiation use efficiency at daily time step (Neitsch et al., 2011c). Above-ground and below-ground crop growth is simulated using crop-specific phenological and agricultural management data such as planting and harvesting dates, fertilizer and pesticide application, irrigation, tillage, and harvest and kill operations. Optimal biomass and potential yields are first simulated under ideal growing conditions consisting of adequate water and nutrient supply, and optimum temperature (Faramarzi et al., 2010). Actual yields are then simulated based on constraints induced by soil water deficiency (Uniyal and Dietrich, 2019), soil water surplus (Wang et al., 2016), soil nutrient availability (Haney et al., 2018b), and temperature stresses (Rai et al., 2021).

For simulation of GW, the modeled plant growth can facilitate simulation of ET. The ET is calculated based on potential evapotranspiration (PET), which is computed using Penman-Monteith method (Monteith, 1965), as well as the soil water balance, and plant growth. The SWAT model first allows the evaporation of any rainfall intercepted by the canopy. Then, the maximum amount of plant transpiration and sublimation/soil evaporation is calculated (Ritchie, 1972). The actual amount of sublimation, when snow is present, evaporation from the soil, and transpiration by plants are then calculated. Finally, for simulation of BW, the water yield (WYLD) is calculated as the sum of surface runoff, subsurface lateral flow, and groundwater (return flow) generated in each HRU, leaving the HRU, and entering the main channel in each sub-basin.

In our study, the simulated soil water is considered as the available water supply for consumptive water use of plants (Winchell et al., 2013; Veettil and Mishra, 2016; Rodrigues et al.,

2014). The consumptive water use by plants (ET) is considered as GW in our study, hereafter. The soil water is calculated based on the difference between the soil moisture within the root zone and the plants' wilting points, where the wilting point is defined as the minimum soil moisture accessible to plants below which the plants are permanently damaged or die (DeLiberty and Legates, 2003; Rodrigues et al., 2014). The green water flux (i.e., GW) is calculated as the summation of actual evaporation from the soil and transpiration by plants (Falkenmark and Rockström, 2006).

In order to validate the ET simulation, field-based measurements of the ET are required. However, these measurements are costly and the number of individual ET observations for model calibration is generally limited, making regional studies challenging. Moreover, the ET observations only represent local hydrological and crop growth processes at the data collection point and may not represent ET of their adjacent catchments. Given the limitations of measured ET data, calibration and validation against crop yields, in addition to the streamflow or other hydrological processes, are considered an effective means for verifying ET simulations (Faramarzi et al., 2009; Bennett and Harms, 2017). Earlier studies indicated a close relationship between crop yields and ET (Cordeiro et al., 2016; Masud et al., 2018). Therefore, the calibration of models against crop yields, in addition to the streamflow, increases model confidence for the simulation of ET (i.e., GW) (Faramarzi et al., 2009; Khalili et al., 2021; Masud et al., 2018).

Prior to calibration, we performed a sensitivity analysis (SA) using an approach similar to that of Faramarzi et al. (2017). SA in general has evolved into the hermeneutics of mathematical modelling (Saltelli et al,, 2021), which here help us to identify the key parameters related to hydrology and crop growth across different regions (see Table A.5, and Table A.6). These parameters are further regionalized to account for variations in the regions' geospatial, hydro-

climatic, and ecological conditions. This resulted in a total of 26 and 27 scaled parameters for each hydrological and agricultural region.

For model evaluation, we calibrated, validated, and performed uncertainty assessment of streamflow first (Table A.5) followed by crop yields (Table A.6) to ensure proper apportioning of soil water into the surface runoff, ET, and groundwater recharge. The calibration and uncertainty analyses were performed in an iterative procedure using: (1) the Latin Hypercube Sampling (LHS) of the input parameters (Ficklin et al., 2013), (2) SWAT model parameter updates, and model output comparison and uncertainty assessment using publicly available Sequential Uncertainty Fitting program (SUFI-2) (Abbaspour et al., 2007), and (3) parallel processing of the simulations in each calibration iteration (see Figure A.5). In the SUFI-2 algorithm, all uncertainties (parameter, conceptual model, input, and measured) are mapped onto the parameter ranges, which are calibrated to bracket most of the observed data within a 95 percent prediction uncertainty (95PPU) range of an output variable (e.g., streamflow and crop yield). The 95PPU has been calculated at the 2.5% and 97.5% levels of the cumulative distribution of output variables obtained through LHS of the input parameters (Abbaspour, 2015; Faramarzi et al., 2017; Ficklin et al., 2013).

For a cost-effective calibration, we used a similar approach to Gorgan et al. (2012) and developed a parallel processing program (PP-program) to calibrate, validate, and perform uncertainty assessment of our multi-variable SWAT model using a 200-core windows-based supercomputer. Based on a maximum physically meaningful range of each parameter, 1000 samples of parameter sets were created using LHS. Then each parameter set was fed into the SWAT model and the model was run in parallel using 200 cores to generate output variables (i.e., streamflow and crop yields) for comparison with measured data. If the comparison results were

unsuccessful, a new iteration was performed, and the procedure continued until satisfactory results were reached or no further improvements were obtained (see Figure A.5).

To compare the measured and simulated monthly streamflow during the calibration process, we employed bR^2 efficiency criterion introduced by Krause et al. (2005), with (Eq. 3.1) as the main objective function:

$$\Phi = \begin{cases} |b|R^2 & for \quad |b| \le 1 \\ |b|^{-1} R^2 & for \quad |b| > 1 \end{cases} \tag{3.1}$$

where R^2 is the coefficient of determination between the measured and simulated signals and b is the slope of the regression line. For multiple discharge stations, the objective function is an average of Φ for all stations within a region of interest (Eq. 3.2):

$$g = \frac{1}{n}\sum_{i=1}^{n} \Phi_i \,, \tag{3.2}$$

where n is the number of stations. The function Φ varies between 0 and 1. While bR^2 was considered as the primary objective function to direct our calibration iterations, several other objective functions were also used during this iterative procedure, including Nash-Sutcliffe (NS) efficiency (Nash and Sutcliffe, 1970), Coefficient of Determination (R^2), Percent Bias (PBIAS) (Gupta et al., 1999), and Kling-Gupta Efficiency (KGE) (Gupta et al., 2009).

To compare simulated crop yields with observed data, we used the Root Mean Squared Error (RMSE) for each of the regions where yield measurements were available as follows:

$$RMSE = \frac{1}{n}\sqrt{\sum_{i=1}^{n} (O_i - S_i)^2} \tag{3.3}$$

where n is the number of observed yields in each region, O is the observed yield, and S is the simulated yield for each measurement region. The crop yield was simulated at the sub-basin level, and further aggregated to the CAR scale to compare with the measurements that are available at a CAR level.

The objective functions (Eq. 3.1-3.3) in each iteration were used to provide direction to set the calibration and uncertainty analysis for the next iteration. Therefore, we revised the parameter ranges in each iteration to set a new parameter range for a new calibration-uncertainty iteration if the calibration and uncertainty performances of the current iteration were unacceptable. Overall, for calibration and uncertainty assessment of a given iteration, after objective functions were calculated two important indices were used to quantify the goodness of calibration-uncertainty performance, including the *p-factor*, which is the percentage of data bracketed by the 95PPU band (maximum value 100%), and the *r-factor*, which is the average width of the band divided by the standard deviation of the corresponding measured variable. In an ideal situation, most of the measured data (plus their uncertainties) are expected to be bracketed within the 95PPU band (*p-factor* $\rightarrow$ 1) with the narrowest band (*r-factor* $\rightarrow$ 0). In real-world regional studies, a *p-factor* of ~ 0.6 for streamflow and crop yield simulations and an *r-factor* of 1-2 and 3-5 for streamflow and crop yield simulations, respectively, are considered satisfactory (Faramarzi et al., 2010, 2015, 2017).

3.3.4 Calculation of extreme warm-dry events and historical averages for the growing season

Given the adverse effects of compound warm and dry events on agricultural production (Feng et al., 2019), we used monthly precipitation and temperature data during the growing season (i.e., May to September) for both historical and future periods. Although the calibration and

validation period spans from 1982 to 2016, we specifically selected 1987-2016, a 30-year period from model outputs, to compare with the future period (2070- 2099). We quantified the compound warm-dry years to study BW and GW variations and their relationships under extreme warm and dry conditions during the growing season. The compound warm-dry condition, defined as the simultaneous occurrence of extreme high temperature and low precipitation, is assessed using a Dry-Hot Magnitude Index (DHMI) developed by Wu et al. (2019). The DHMI requires two normalized indices to represent extreme warm and extreme dry conditions based on temperature and precipitation records. In the following, we explain the two normalized indices we developed to compute DHMI in our study region.

In the DHMI approach, the magnitude of an extreme warm is characterized by the temperature above a specific threshold (hereafter, denoted as ΔT). The threshold temperature is calculated based on the 90th percentile of daily temperature time series (see Alexander et al 2006, Perkins and Alexander 2013, Zampieri et al 2018). Later the ΔT time series are normalized by fitting to a cumulative density function to obtain its non-exceedance probability $P(\Delta T)$, which falls within [0, 1] (Russo et al., 2014). Through this procedure, the larger ΔT values correspond to higher non-exceedance probability $P(\Delta T)$ values and vice versa.

The magnitude of an extreme dry event is defined based on the difference between an extreme dry index and a threshold index (denoted as ΔDI), with a large departure from the threshold indicating a high magnitude of the extreme dry event. The extreme dry index in our study was calculated based on the commonly used Standardized Precipitation Index (SPI) (Naresh Kumar et al., 2009; Hayes et al., 2011). The SPI is calculated based on long-term daily precipitation records for a given geographic region for the desired period. This long-term record is fitted by a theoretical probability distribution (i.e., gamma distribution in this study), which is

then transformed by normalizing it so that the mean SPI equals zero and standard deviation equals one. McKee et al. (1993) and Edwards and McKee (1997) provide further details. It is worth noting that, due to the spatial variation of precipitation and hydrologic parameters and their skewness, we fitted independent gamma distributions (Martinez-Villalobos and Neelin, 2017) for each sub-basin to calculate spatially explicit SPI drought index. It is important to note that the appropriateness of the gamma distribution was tested using standard goodness-of-fit measures before the SPI computation. As such, two widely-used Kolmogorov-Smirnov (KS) and the Anderson-Darling (AD) tests (Ye et al., 2018; Jeong et al., 2014; Shin et al., 2012) were implemented and the appropriateness were evaluated based on their estimated p-values. Any p-values greater than 0.05 is typically interpreted as evidence that the data fit well with the assumed gamma distribution. For future projections, we used historical (1987-2016) simulation of each GCM as the reference period to fit the gamma distribution. This approach ensures that the SPI calculation is consistent and comparable between the historical and future periods, taking into account the sample size and distribution parameters. Our method is consistent with similar studies, such as Chen et al., (2022). Next, we arranged the data based on their probability of accumulation (CDF), with values ranging from 0 to 1. The CDF value of 1 indicates a very high SPI and a CDF value close to 0 indicates a very low SPI. Our study considered the normalized SPI value of -0.5 as the threshold index. This threshold was used in other similar studies to obtain a relatively large number of records of ΔDI used for the computation of compound warm-dry events (see Wu et al., 2019; Svoboda et al., 2002). With the threshold SPI of -0.5, the extreme dry events corresponded to SPI < -0.5 and were used to calculate ΔDI.

The *ΔDI*, *ΔT*, and the DHMI were computed using sub-basin-based area-weighted average precipitation and temperature time series for the entire NRB for the historical (1987-2016) and future (2070-2099) periods. The DHMI was calculated using Eq. 3.4 as follows:

$$DHMI = \sum_{m=1}^{M}\left[\left(P\left(\sum_{d_m=1}^{D_m}\Delta T_{d_m}\right)\right)\Delta DI_m\right] = \sum_{m=1}^{M}[P(\Delta T_m)\Delta DI_m] \quad (3.4)$$

where *M* is the timescale to investigate the persistence of extreme warm-dry conditions leading up to the month of interest. For example, the temporal evolution of an index for July at a 3-month timescale reflects the progress of warm-dry conditions over May, June, and July, and it provides a seasonal estimate of the warm-dry conditions. D_m is the number of days for the timescale m with the daily temperature higher than the threshold; ΔT_{d_m} is the difference between daily temperature and the threshold temperature for the day d_m (during which temperature is higher than the threshold). $P(\Delta T_m)$ is the distribution function of *ΔT* for each timescale m, and the ΔDI_m is the difference between normalized SPI and the corresponding threshold (SPI=-0.5) for the timescale m. ΔDI_m was computed as:

$$\Delta DI_m = \begin{cases} SPI_{thr} - SPI_m, & if\ SPI_m < SPI_{thr} \\ 0, & if\ SPI_m > SPI_{thr} \end{cases} \quad (3.5)$$

Overall, the DHMI index can be computed for different timescales (e.g., 1-month, 2-month, .. 12-month), and it ranges from 0 to the maximum value of *ΔDI* (i.e., 0-1 range in our study) with the larger values indicating the greater level of extreme dry-warm conditions. The regional DHMI in our study was computed based on a 9-month timescale window (January to September), which was selected based on some recent studies conducted in other regions with similar climatic and agro-hydrological conditions as NRB (Gurrapu et al., 2014; Kim et al., 2017). The 9-month timescale reflected the effects of the moisture condition for the crop growing season (i.e., May to

September) and the potential moisture carried over from earlier months. Based on the regional DHMI time series, we further performed sub-basin-based analyses to assess GW and BW relationships during the most extreme warm-dry years for both historical and future periods.

3.3.5 Climate projections from ensemble GCMs

For future projections of the hydrological cycle and crop growth, the climate data were incorporated from an ensemble of six Global Climate Models (GCMs) of the Coupled Model Intercomparison Project Phase 6 (CMIP6) (Eyring et al., 2016a). Most CMIP6 projected records indicate more critical global warming effects near the end of the 21st century, albeit subject to a greater spread of prediction uncertainty (Table 3.1) (O'Neill et al., 2016). Therefore, we performed our analyses for the 2070 to 2099 period.

We used the GCMs' simulated data based on two contrasting Shared Socio-economic Pathways, SSP126 and SSP585 (Table 3.1). The two selected SSPs represent the lowest (i.e., SSP126) and the highest (i.e., SSP585) radiative forcing levels projected for the year 2100 based on IPCC Assessment Report 6 scenarios (O'Neill et al., 2016). The former describes a world of sustainability-focused growth and equality (SSP-1) with a rising radiative forcing pathway of 2.6 W/m^2 in 2100, and the latter defines a world of rapid and unconstrained growth in economic output and energy use (SSP-5) with radiative forcing reaching 8.5 W/m^2 in 2100 (Mishra et al., 2020). For future hydrology and crop simulations in our study, we set the concentration of CO_2 to 350, 450, and 850 ppm for the historical, SSP126 future, and SSP585 future periods, respectively, based on IPCC data (Eyring et al., 2016a).

Based on an earlier study by Masud et al. (2021), the future climate data were statistically downscaled based on historical daily gridded climate data from WFDEI [GPCC] (Weedon et al.,

2014a) at roughly 0.5º grid resolution, resulting in 574 grids in the NRB. To ensure consistency with the WFDEI observation dataset and account for the varying grid projections of the CMIP6 GCMs (Table 3.1), we employed a reference grid with a horizontal resolution of approximately 6 km, following the methodology of Werner & Cannon (2016). To facilitate analysis, all model-simulated data were interpolated to this grid using the thin-plate spline interpolation algorithm (Masud et al., 2021). In the study by Masud et al., (2021), the 'ClimDown' R package (Hiebert et al., 2018) was used to downscale the GCM outputs to the specified spatial resolution. The package used multiple techniques, including Climate Imprint (CI) (Ahmed et al., 2013; Hunter and Meentemeyer, 2005), Quantile Delta Mapping (QDM) (Cannon et al., 2015), Constructed Analogues (CA) (Maurer et al., 2010), and Bias Correction/Constructed Analogues with Quantile mapping reordering (BCCAQ) (Werner and Cannon, 2016) to downscale the projected climate time series. For hydrological projections, the closest grid point of the downscaled data were assigned to the centroid of each sub-basin in the SWAT model.

Table 3.1. The climate change models information used in this study.

	GCM	Institution
A	EC-Earth3	27 research institutes from 10 European countries
B	MRI-ESM2.0	Meteorological Research Institute (MRI), Japan
C	BCC-CSM2-MR	Beijing Climate Center, China Meteorological Administration, China
D	CNRM-CM6-1	Center National de Recherches Météorologiques (CNRM), France European Earth System Model
E	EC-Earth3-veg	European Earth System Model by 27 research institutes from 10 European countries (with an additional vegetation component compared to EC-Earth3)
F	CanESM2	Canadian Centre for Climate Modeling and Analysis

3.4 Results and discussion

3.4.1 Model calibration, validation, and uncertainty analysis

Our sensitivity analysis indicated that streamflow was typically the most sensitive to snow parameters in high elevation regions and the Rocky Mountains, and to SCS runoff curve number and Manning's "n" value for the main channel in all other regions (i.e., crop lands, and natural lands) (See Table A.5 and A.6 for list of parameters and their descriptions). The hydrological model performance for streamflow simulation during the calibration (1982-2006) and validation (2007-2016) periods was robust, as evidenced by the bR^2 values ranging from 0.15 to 0.96 across hydrometric stations in small river tributaries (with NSE values ranging from 0.01 to 0.96), and from 0.5 to 0.95 in the main streams (with the NSE values ranging from 0.35 to 0.85) across the NRB (Tables A.7). Overall, for the entire calibration and validation period (1982-2016), 65% of the observed streamflow data were captured by the simulated 95PPU and the average r-factor was about 0.80 at the NRB scale. The average bR2 of the 86 stations was 0.70, and it varied from 0.2 to 0.95 for individual stations (Table A.7).

A total of 27 crop growth parameters were initially selected for each agricultural region based on the literature review and the authors' judgment (Table A.6). Sensitivity results of rainfed and irrigated SWY in 47 agricultural regions and four irrigated counties showed that SWY was sensitive to (1) crop and management-related parameters such as DAY, HEAT_UNITS, AUTO_NSTRS, AUTO_NYR, AUTO_EFF, and AUTO_WSTRS; (2) soil-related parameters such as SOL_CBN, SOL_K and SOL_AWC; and (3) hydrological parameters related to surface and sub-surface flows such as CN2, EPCO, and ESCO. The definition of the parameters is available in Table A.5.

Figure 3.2 shows SWY values for 47 agricultural regions (upper panels) and streamflow simulation values for 86 hydrometric stations (lower panels) for the entire calibration and validation period (1982-2016). The color in the heatmap counts the number of data points in the agricultural regions (upper panel) and hydrometric stations (lower panel) with their performance statistics (i.e., MSE, bR^2, *p-factor*, *r-factor* presented on the y-axis). Recall that ideally a greater *p-factor,* smaller *r-factor,* larger bR^2 and smaller *MSE* for a larger number of stations and agricultural regions are expected for satisfactory results. As shown in Figure 3.2, lighter colors indicate a greater number of data points associated with agricultural regions (or hydrometric stations). Lighter colors under lower values of MSE and *r-factor*, and higher values of bR^2 and *p-factor*, represents higher model performance. Overall, the NRB average *p-factor* was 0.89 and 0.79, with the *r-factor* of 2.09 and 2.22 for calibration and validation periods, respectively. Table A.8 gives detailed statistics of calibration, validation, and uncertainty analysis data for rainfed and irrigated spring wheat.

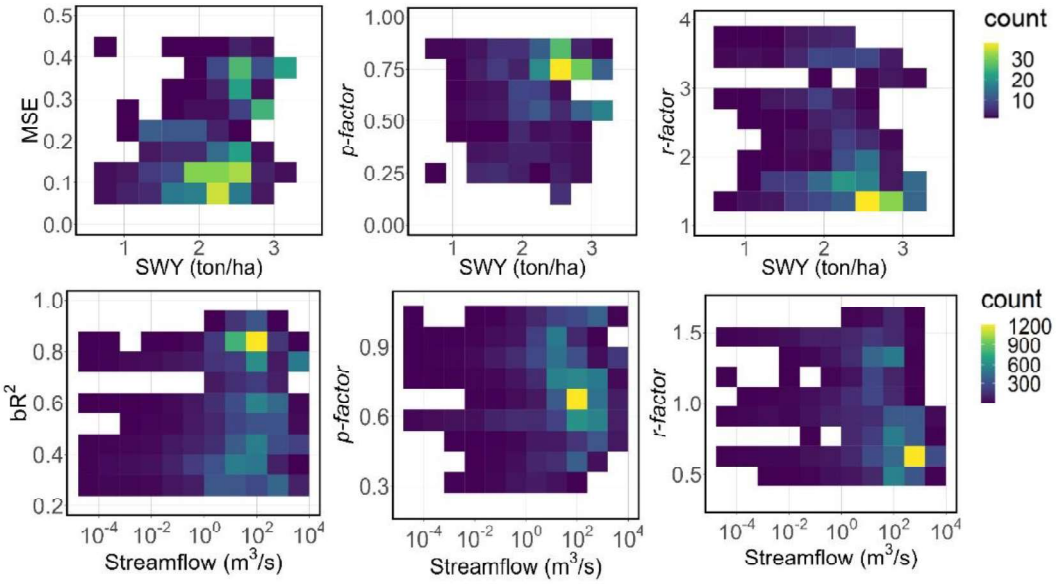

Figure 3.2. A color map demonstrating model performance for the entire calibration and validation period for spring wheat yield/SWY (upper row) and streamflow (lower row). The color cells (count

in the legend) represent the combination of the number of stations (or number of CARs) and number of times of occurrence during the study period, while whitespace denotes where no data exists.13

3.4.2 Status of growing-season BW and GW under average historical and future periods

In this section we report the variation and status of GW and BW under average historical and future conditions. Simulation results for growing season (May to September) during the historical period, including both warm-dry and normal years, indicated a slightly increasing trend for precipitation across all ecoregions (crop lands, mountainous lands, and natural lands), while temperature seems to have remained unchanged (Figure 3.3, Figure A.6, Figure A.7). The growing-season BW and GW for the same period followed a similar pattern as precipitation, with both indicating a slight increase over the historical period. The long-term average BW and GW during the growing season for the 1987-2016 period across the NRB were 15.9 mm/month and 67.5 mm/month, respectively (Figure 3.3). Based on linear trend lines fitted to precipitation and simulated BW and GW time series, we observed an increase of 0.20 mm per year in precipitation during the 1987-2016 period, which resulted in an increase of 0.11 mm per year BW and only a 0.06 mm per year increase in GW. With a coefficient of variation (CV) of 22%, the growing-season BW demonstrated a similar inter-annual variation to GW with a CV of 6% for the NRB. This is due to the larger mean GW, as compared to mean BW in the region (Figure 3.3).

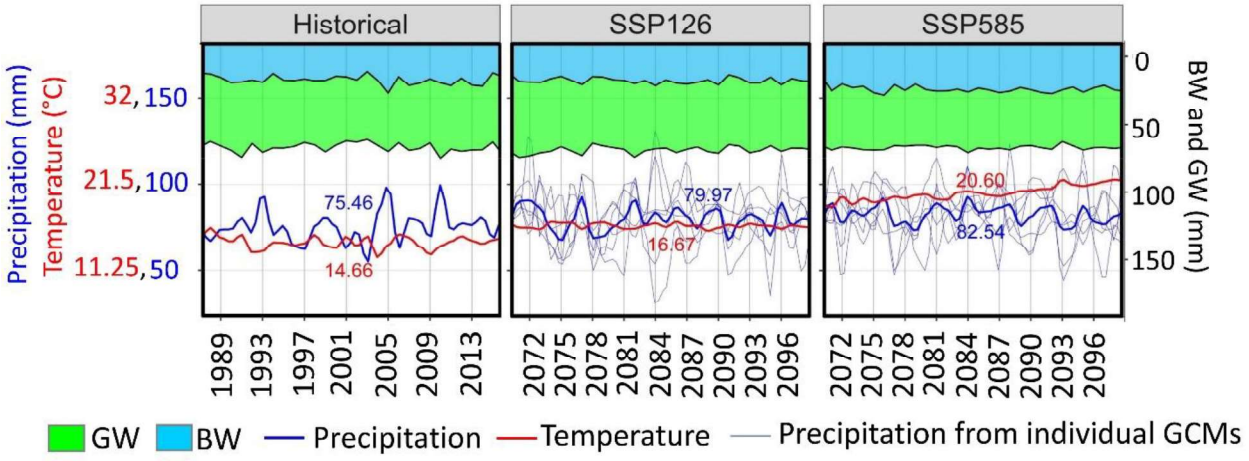

Figure 3.3. Historical (left panel) and multi-model ensemble mean (middle and right panels) annual precipitation, temperature, BW, and GW for NRB. The data are illustrated for the growing season (May-Sep). The BW and GW are shown with blue and green shades, which are overlaid along y axis. The blue and red lines illustrate the historical and multi-model ensemble mean annual precipitation and temperature with their long-term average values shown next to the lines.

Multi-model ensemble mean precipitation and temperature for the growing season in the future period were larger under SSP126 (i.e., 80.0 mm/month, and 16.7 ºC) and SSP585 (i.e., 82.5 mm/month, and 20.6 ºC) as compared to the historical period (i.e., 75.5 mm/month, and 14.7 ºC) (Figure 3.3). The projected results showed that annual average BW and GW for the growing season across the NRB were 16.5 mm/month and 69.5 mm/month for SSP126, and 23.1 mm/month and 67.5 mm/month for SSP585, respectively (Figure 3.3). The model ensemble mean CV values for BW and GW were 39.2% and 13% under SSP126, and 27.8% and 12.9% under SSP585, respectively. Overall, the average annual precipitation and temperature increased by 6.0% and 2.0 ºC under SSP126 and 9.4% and 5.9 ºC under SSP585 scenarios (Figure 3.3). This change in precipitation and temperature resulted in an increase of 3.3% in BW and an increase of 2.9% in GW under SSP126. For the SSP585, a significant increase of about 44.5% in BW and a slight decrease of about 0.1% in GW were observed. These contrasting values for projected BW and GW changes under SSP126 and SSP585 resulted from different underlying processes. The increase in

GW under SSP126 is linked to the projected warming, increased evaporation and vegetation water demand, and the increased soil moisture. Under this scenario the increase of BW results primarily from the increased volume of precipitation and surface runoff as compared to the historical period. In contrast, higher precipitation and more frequent wet years resulted in greater soil moisture storage under SSP585 than SSP126, and did not considerably increase GW as opposed to BW. Causes included increased plant water use efficiency as a result of greater atmospheric CO_2, which lead to reduced ET, and therefore, less GW under SSP585 than SSP126 (also reported by Fowler et al., 2019). Khalili et al., (2021), Masud et al., (2018), and Jasechko, (2018) also report on an improvement in plant water use efficiency due to the closure of plant stomata under higher levels of atmospheric CO_2 concentration under SSP 585 (i.e., 850 ppm) as compared with the historical period (i.e., 350 ppm). The reduced GW consumption leaves more water storage in the soil, triggering the larger runoff, groundwater recharge, and WYLD, all of which ultimately make substantial increase in BW (see also Lian et al. (2018)).

3.4.3 Assessment of extreme warm-dry events for the historical and future periods

The processing of precipitation data and the suitability test of the gamma distribution using KS and AD methods indicated that in 87% and 86% of the sub-basins, the p-values are greater than 0.1 in KS and AD approaches, respectively (Table A.9). In both methods, the p-values are ≥ 0.05 in 100% of the sub-basins. This is further shown in Figure A.8, where more detailed assessment of the suitability of gamma distribution is performed, and empirical precipitation time series against the theoretical gamma distribution are plotted for some selected sub-basins. The selection of sub-basins are based on their annual precipitation to represent a broad spectrum of precipitation values across the study watershed.

Figure 3.4 shows the results of ΔDI (i.e., using the SPI at a 9-month timescale), $P(\Delta T)$ and the DHMI obtained for the yearly growing seasons (i.e., May to September) during the selected historical period and future scenarios (i.e., SSP126, and SSP585). Overall, the DHMI was greater when both ΔDI and $P(\Delta T)$ were large. As shown in Figure 3.4, the value of DHMI was the largest under SSP126, followed by SSP585, and it was the smallest for the historic period. Out of six GCMs used in this study, the CNRM-CM6-1 climate model demonstrated the largest DHMI due to the largest dryness (ΔDI) that was projected under SSP126 (Figure 3.4). However, multi-model ensemble projections based on the six GCMs indicated that the DHMI ranged from 0 to 0.6 with the lowest values under the MRI-ESM2.0 GCM model, followed by EC-Earth3, BCC-CSM2-MR, EC-Earth3-veg, and CanESM2 GCM models, respectively.

For assessment of the GW-BW relationships under extreme warm-dry events, we chose the top 20% of simulated years with the highest DHMIs within each scenario, as the extreme warm-dry events for further analysis (Figure 3.4). The selected warm-dry years are demonstrated by red border lines in Figure 3.4. The simulated GW and BW data were selected and analyzed for historical (1987-2016) and future (2070-2099) periods under both SSP126 and SSP585 scenarios using climate data of all six GCMs.

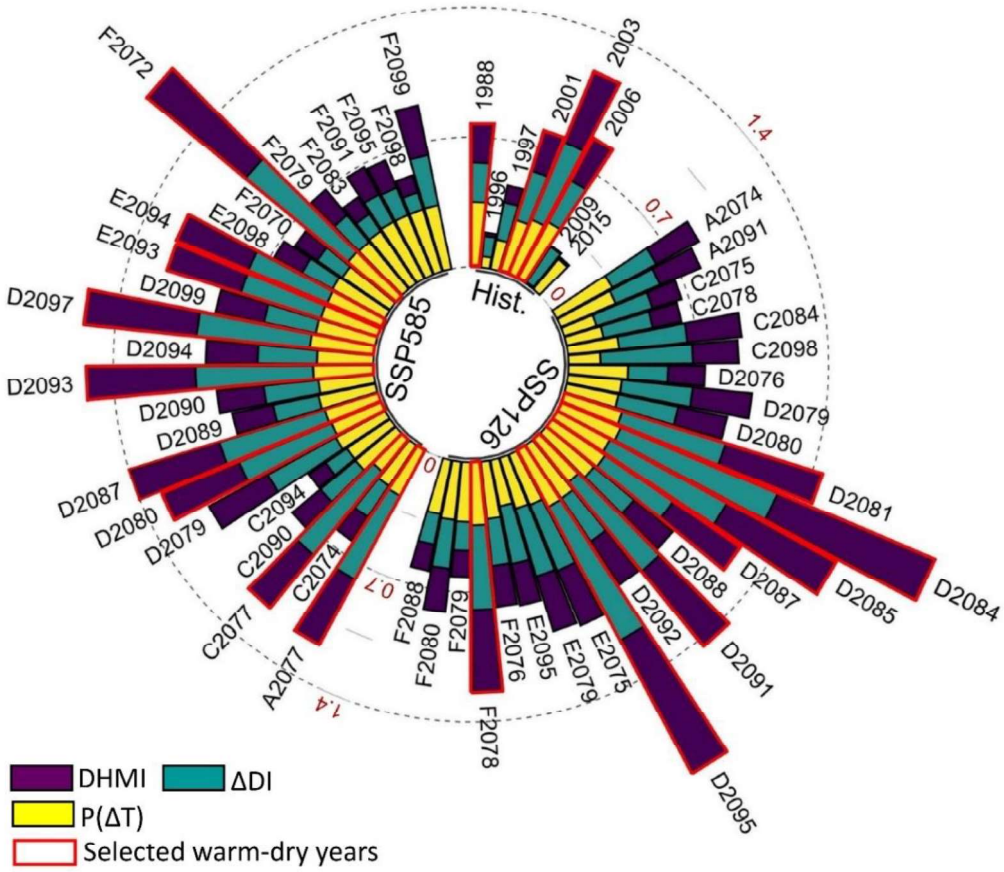

Figure 3.4. Temporal variation of the compound warm-dry events during the growing season (May to September) for the historical (1987-2016) and future (2070-2099) periods. A, B, C, D, E, and F represent the results that are derived based on the EC-Earth3, MRI-ESM2.0, BCC-CSM2-MR, CNRM-CM6-1, EC-Earth3-veg, and CanESM2 models, respectively. Note that warm-dry events are calculated for all years of the historical and future periods but for better visualization, only a limited number of warm-dry events are shown in the picture.14

3.4.4 Altitudinal variation of BW and GW during the growing season

Given the large variation in elevation in our study area, we opted to investigate how changes in GW and BW are affected by elevation. Therefore, we performed an elevation-based analyses to characterize GW and BW changes as a function of elevation. As previously mentioned in the watershed description, the mountains in the NRB have relatively high precipitation levels. Our analyses of the long-term Average Historical (AH) data across different elevation classes in the NRB (Figure 3.5a) support this trend, showing that the highest rates of BW and precipitation are

found at high altitudes, which make up only a small fraction (i.e., ~10%) of the NRB area. On the other hand, the lowest rates of precipitation and BW were observed in the elevation range of between 600 and 700 m above sea level (m.a.s.l), which make up 14% of the NRB area.

The analysis of extreme warm-dry years data in high altitude regions for historical period (EH, Extreme Historical) and their anomalies from the AH (Figure 3.5b) showed that precipitation was significantly less than that of average historical period and it could decline by up to 22.0% as compared to AH (Table 3.2). This 22.0% reduction in precipitation in high elevation regions resulted in a considerable reduction in BW availability (i.e., 42.0%), and decrease of GW by up to 12.2% under EH as compared to AH (Figure 3.5b, Table 3.2). Despite the decrease in GW, the high rate of GW consumption by plants due to the higher rates of evaporative demand under EH exacerbates the BW deficit in the hydrological cycle. This is demonstrated by the high rates of ET in Figure 3.6a. In lower elevation regions, the GW decreased by 15.4% in warm-dry years and, in combination with a 16.3% reduction in precipitation, it caused a reduction of 17.7% in BW. The reduction of GW in these low elevation regions is due to the low soil moisture availability resulting in water stress and reduced crop transpiration (Figure 3.6e).

We further assessed the effects of the projected extreme warm-dry events on BW and GW under SSP126 (i.e., EF126, Figure 3.5c) and SSP585 (i.e., EF585, Figure 3.5d) scenarios across different elevation zones. Similar to EH, under the EF126 and EF585 we calculated anomalies based on future and historical AH results. In other words, all extreme scenarios (i.e., EH, EF126, and EF585) present anomalies in the extreme warm-dry years from the average historical conditions (i.e., AH). Under EF126 and EF585, the BW and GW anomalies have shown contrasting results to the historical EH. Under EF126, which had the higher overall precipitation reduction as compared to AH (i.e., 38.0%, 50.2% reduction in high and low elevation areas), we

projected the largest BW reduction (i.e., 66.0%, 33.9% reduction in high and low elevation areas) and greatest GW decline (i.e., 26.2%, 39.6% in high and low elevation areas) among all extreme warm-dry scenarios (Table 3.2). With the higher rates of precipitation decline under EF585 compared to EH (i.e., 22.5%, 25.8% reduction in high and low elevation areas compared to EH), the BW decreased at a much lower pace in EF585 than EH (i.e., 25.3%, 6.8% reduction in high and low elevation areas compared to EH). The processes driving these contradictory results are described in section 3.5.

Table 3.2. Simulated climate and hydrologic variables for mountainous lands, natural lands, and crop lands under AH, EH, EF126, and EF585 scenarios. **AH:** average historical, **EH:** historical extreme warm-dry years, **EF126:** extreme warm-dry years under future SSP126, **EF585:** extreme warm-dry years under future SSP585. All extreme scenarios are anomalies from AH, and all future extreme scenarios are based on ensemble means. All data are monthly averages reported for the growing season.

Region	Scenario	Precipitation (mm)	Soil water (mm)	Runoff (mm)	Return flow (mm)	ET (mm)	Temperature (°C)
Mountainous lands (high elevation)	AH	75.2	69.6	19.7	4.4	58.1	12.2
	EH	59.0	55.9	14.2	2.8	51.0	12.8
	EF126	46.3	46.3	7.4	0.8	42.9	15.6
	EF585	45.7	60.1	10.0	2.7	43.4	20.4
Natural lands	AH	81.1	85.4	3.0	14.7	78.8	15.6
	EH	73.6	78.9	3.8	12.4	65.0	16.6
	EF126	44.5	68.6	2.0	10.1	49.1	18.8
	EF585	56.2	80.1	4.0	14.2	50.1	23.3
Crop lands (low elevation)	AH	70.1	41.2	2.7	2.3	65.8	16.2
	EH	53.0	37.6	2.5	3.2	57.1	17.4
	EF126	30.8	27.0	1.2	1.7	38.3	20.1
	EF585	37.7	44.9	1.6	3.7	42.8	24.6

Next, we assessed the growing-season data for AH, EH, EF126 and EF585 years across different elevation classes. The results showed that the areas falling within 1700 m.a.s.l and 1800 m.a.s.l range contributed proportionally the largest share of BW with a rate of 50 mm/month in

NRB under AH (Figure 3.5a). In addition, more than 35% of the BW under AH was found to be from the areas between 900 m.a.s.l and 2300 m.a.s.l, which corresponds to only 10% of the entire NRB area (Figure 3.5a). However, BW was substantially decreased in high elevation zones under extreme warm-dry events (i.e., EH, EF126, and EF585) (Figure 3.5b, 3.5c, and 3.5d). Despite the decrease, the maximum BW was still observed in elevations of 1400 m.a.s.l to 1500 m.a.s.l. The BW reduction in high elevation areas in EF126 (Figure 3.5c) and EF585 (Figure 3.5d) can be explained by a significant reduction in precipitation while retaining a similar level of GW consumption, which results in a severe BW deficit in these high altitude zones as compared to lower altitude areas.

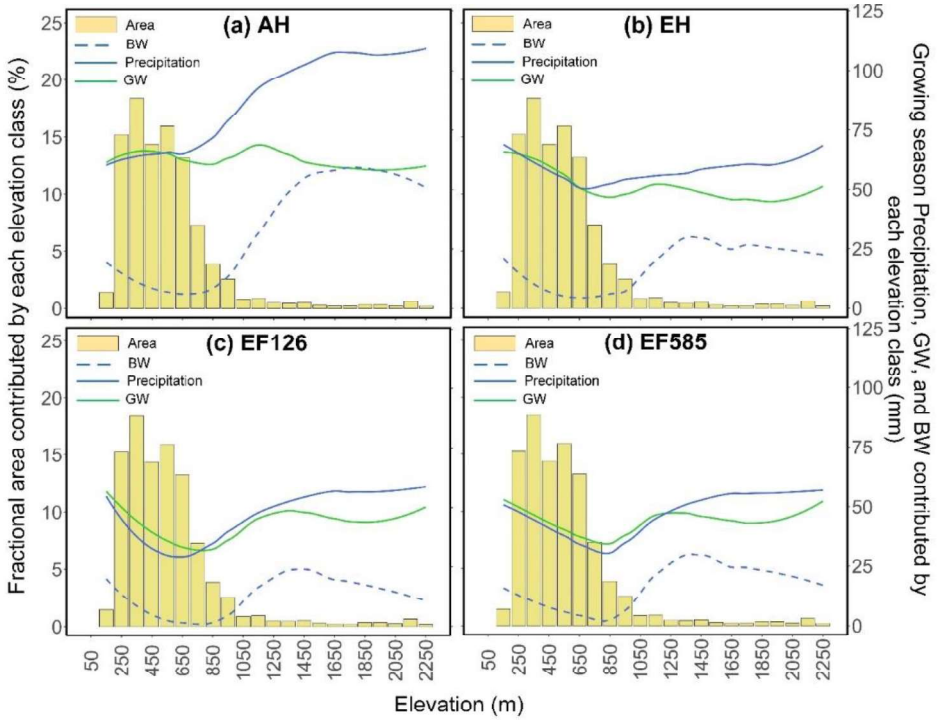

Figure 3.5. Fractional area of different elevation classes in simulated study area, and their percent contribution to GW, BW, and precipitation during the crop growing season (monthly averages

over the crop growing season). (a) average historical period (1987-2016), (b) historical warm-dry years, and future (2070-2099) warm-dry years under (c) SSP126 and (d) SSP585 scenarios.

3.4.5 Spatial variation of GW and BW under average historical and during extreme warm-dry seasons

3.4.5.1 GW and BW distribution across different ecohydrological regions

As previously shown in our analysis of long-term average historical data, crop lands in the NRB have the lowest rates of annual average precipitation and the highest average annual temperature (Figure A.6). These conditions, combined with high evaporative demand, result in high GW values and limited availability of BW (Figure 3.6d). Despite the highest precipitation CV (i.e., 37.2%) in crop lands, the highest rate of BW variation was observed in mountainous lands (i.e., CV of about 42.0%). The crop lands showed the highest variations of GW as compared to other regions in NRB (i.e., CV of about 20.9%). The larger GW variations in these lands are not only due to the high precipitation variations but the lower volume of precipitation and lower overall soil moisture in these regions, which can increase water stress and therefore crop sensitivity to small changes in precipitation and soil moisture conditions (Figure 3.6c). Other studies have also reported agricultural crops as among the most sensitive water users to even small changes in climate variables (Sadras et al., 2020; Jägermeyr et al., 2021).

The high rates of precipitation and snowmelt in mountainous lands contribute to relatively large volumes of soil water mainly in river valleys and lower altitude hill slopes (Figure 3.5, Figure 3.6c,f). Along with the low permeability of higher altitude soils, this results in higher rates of surface runoff generated in mountainous areas than other regions (Preston et al., 2014). As a consequence, the BW volumes are larger in these high-altitude regions than in other areas in NRB (Figure 3.6d). In contrast, natural lands present the highest soil water content among all of the regions (Figure 3.6c, Table 3.2), which is directly related to the large amount of precipitation and

greater rates of infiltration due to their permeable soils (Table 3.2), and therefore higher levels of return flow. During snowmelt and storm seasons, the near-saturated soils in these regions can increase return flow (base flow) and subsurface flow (lateral flow) to the streams. It can also lower infiltration rates, supporting runoff generation and forming a large volume of BW availability (Figure 3.6d).

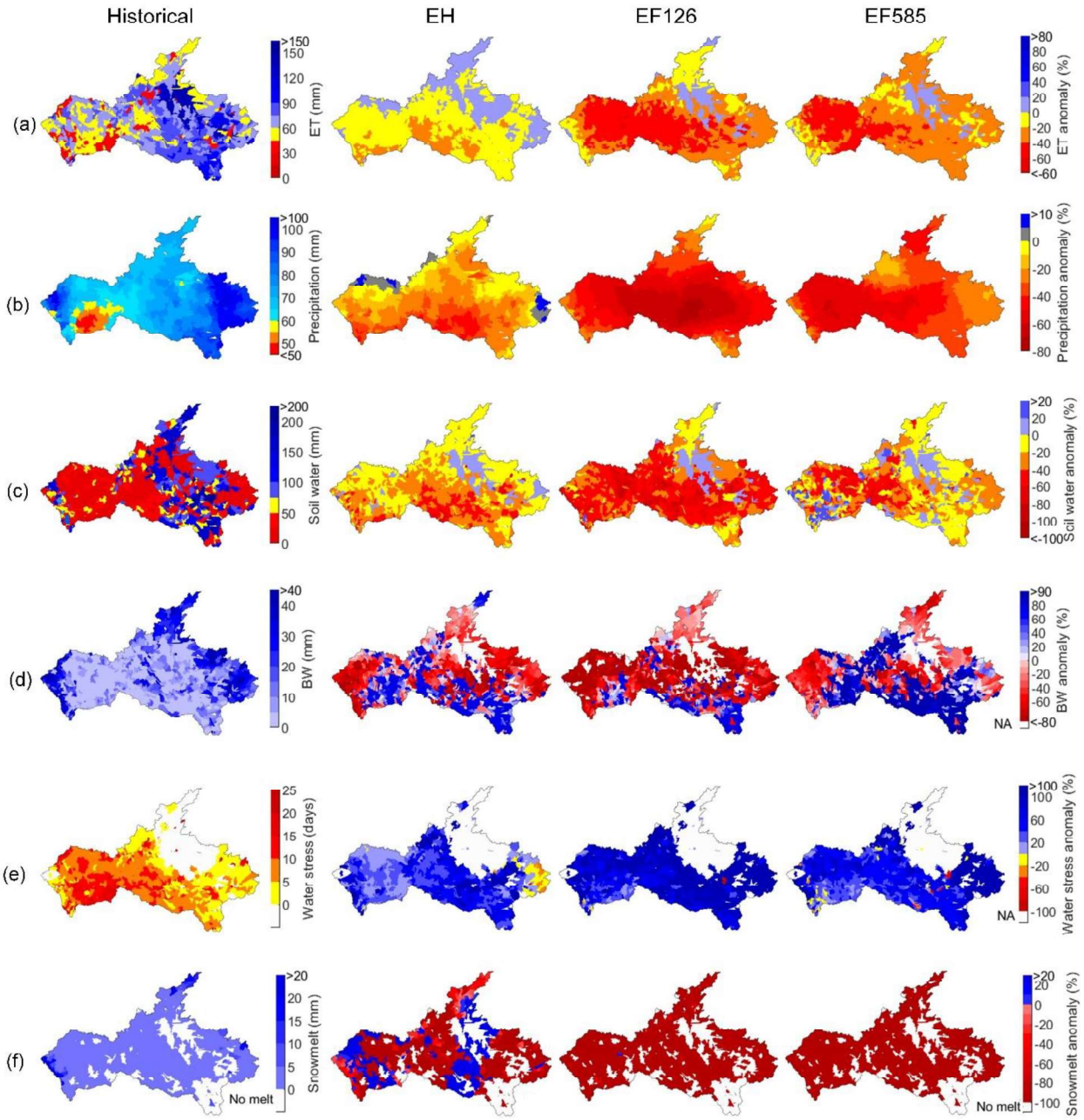

Figure 3.6. Simulated long-term average hydrologic water balance data during growing season (calculated as the averages over five months during the crop growing season) for historical period (left column), and their anomalies from AH under extreme dry-warm years (column 2-4 from the left). The maps in horizontal rows are: average GW (ET, mm/month), precipitation (mm/month), soil water (mm/month), BW (mm/month), water stress (days/month), and snowmelt (mm/month) during growing season.15

3.4.5.2 GW-BW relationships under historical and future extreme warm-dry years

To assess the GW and BW relationship during the growing season and under extreme warm-dry events across NRB, we calculated the sub-basin-based BW to GW ratio (BW/GW) for EH, EF126, and EF585 scenarios, as well as their anomalies from the AH scenario (Figure 3.7). Based on the underlying physical processes as explained in the following, the lower anomaly (warm colors in the figure) indicates a shift from BW to GW and the greater anomaly (cold colors in the figure) indicates no shift. As stated in Table 3.2, mountainous lands demonstrated relatively rich soil water (close to saturation) preventing further infiltration to the soil under AH (Figure 3.7a, Figure 3.8), which derived high volume of BW generation during flood seasons and therefore a large BW/GW ratio. However, less BW was predicted under extreme warm-dry years (EH) as compared to GW, which resulted in a decreasing BW/GW ratio as compared to AH scenario in these regions (Figure 3.7b). Three main physical processes were responsible for lower rates of BW/GW ratios during EH in these regions, which include: (1) low rates of precipitation reducing surface runoff and consequently the BW (Figure 3.6); (2) decreasing precipitation causing decreased soil water content and increasing soil dryness, which increased infiltration rates of precipitation and snowmelt in the following seasons and years. This ultimately reduced the fraction of the precipitation that flowed overland (i.e., surface runoff) (Figure 3.6, Figure 3.8); (3) greater soil water content (even under EH), which was carried over from earlier seasons and years, maintained ET (GW) which affected BW volume by reducing lateral and return flows (Figure 3.6, Figure 3.8).

In natural lands, despite a relatively small increase of annual average precipitation under EH as compared to AH, a higher evaporative demand under EH increased GW, causing lower soil moisture storage. Therefore, similar to mountainous lands, this resulted in an increase in infiltration rates of precipitation and snowmelt, which eventually reduced the proportion of the precipitation that could otherwise contribute to surface runoff and return flow (Figure 3.6, Figure 3.8). Consequently, a decreasing rate in the growing season BW/GW ratio is observed in this ecoregion under EH.

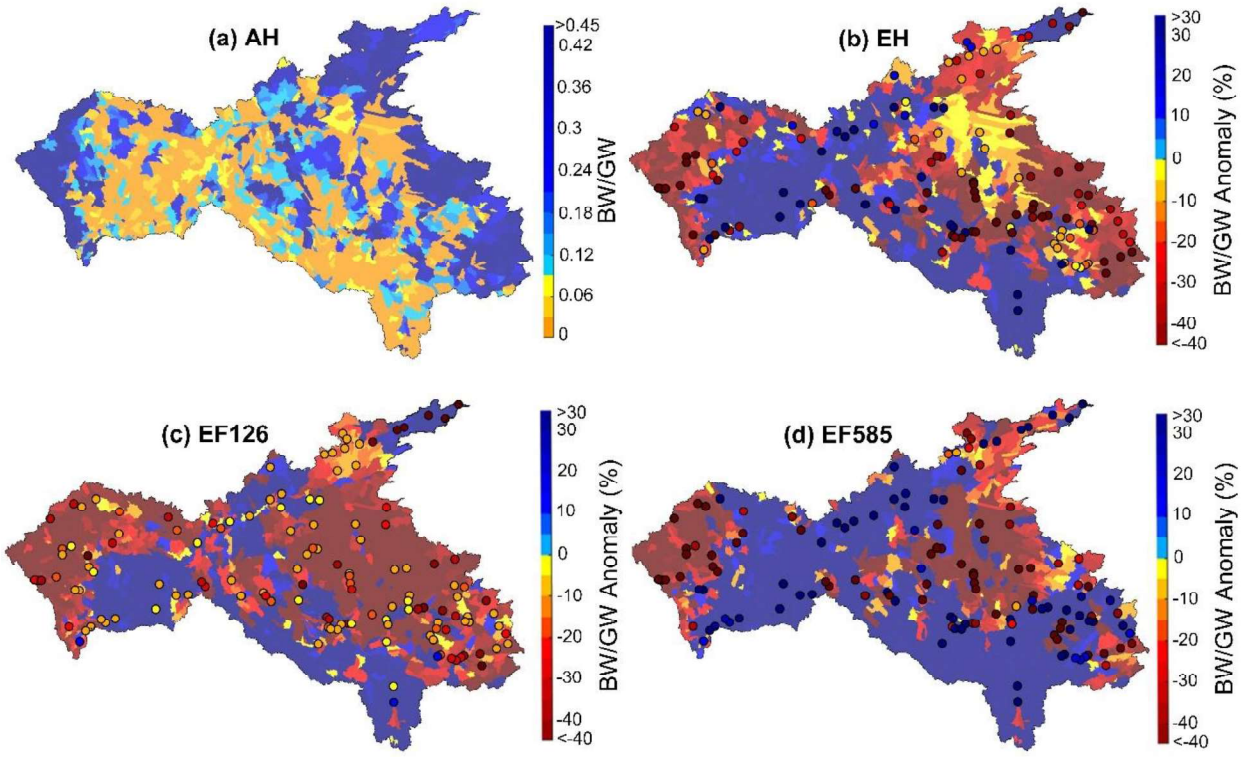

Figure 3.7. Sub-basin scale simulated blue to green water ratio (BW/GW) for the growing season. (a) long-term (1987-2016) average historical ratios (AH); (b) Anomalies of historical extreme warm-dry years ratios from those of AH; (c) Anomalies of future (2070-2099) extreme warm-dry years ratios under SSP126 from those of AH (EF126); (d) Anomalies of future (2070-2099) extreme warm-dry years ratios under SSP585 from those of AH (EF126) (EF585). The % anomalies in b, c, and d were calculated as: [(Extreme Scenario-AH)/AH]×100. Figures c and d are based on multi-model ensemble mean values. The circles represent streamflow anomalies in 150 select outlets (%). 16

Based on the anomaly map (% deviation from AH), a large BW/GW ratio was predicted for crop lands under EH (Figure 3.7b). This contrasts with the BW/GW ratio anomalies observed in mountainous lands and natural lands because of different underlying mechanisms. The simulated average historical GW rates in crop lands (Figure 3.7a) were greater than those of other regions under AH (i.e., 65.8 mm/month during the growing season, Figure 3.6a, Figure 3.8). The large historical GW rates in these areas were accompanied by the lowest rates of precipitation (i.e., 70.1 mm/month during the growing season) and the lowest soil water content (41.2 mm/month) as compared to the other regions (Figure 3.6b, c. Figure 3.8). The simulated extreme warm-dry years of the historical period (i.e., EH) had a ~8.8% reduction in soil water as compared with average conditions, creating a high water stress condition (Figure 3.6e, Figure 3.8c) for crops which lowered the GW by ~14% (Figure 3.7b, Figure 3.8c). Unlike the GW, the share of average historical BW in crop lands was small as compared to other ecoregions under AH: specifically, 63.8% and 55% less BW as compared to the mountainous lands and natural lands, respectively. This limited BW under AH showed a relatively small reduction under EH. In contrast, the insufficient soil water content under EH and a large number of water stress days (Figure 3.6e) ultimately resulted in a proportionally larger decline of GW than the corresponding decline in limited BW. Therefore, a larger BW/GW ratio was predicted under EH for the crop lands as compared to other ecoregions, mainly due to the larger decrease in GW (denominator) than BW (numerator) (Figure 3.7b).

The multi-model ensemble mean results for EF126 anomalies showed a decreasing BW/GW ratio for most of the NRB (Figure 3.7c). The regionally averaged growing-season precipitation for the future period (2070-2099) in EF126 scenario decreased by about 46.3% as compared to that of the historical period (1987-2016), which is the highest rate of decline among all scenarios (i.e.,

38.3% and 18.0% reduction under EF585 and EH, respectively). This decline in precipitation reduced BW by 50.4% and GW by 35.7% during the growing season at a regional scale. While both BW and GW decreased under EF126, the significant decline of the BW/GW ratio was because of a greater depletion of BW (in the numerator) than GW (in the denominator) at the regional scale.

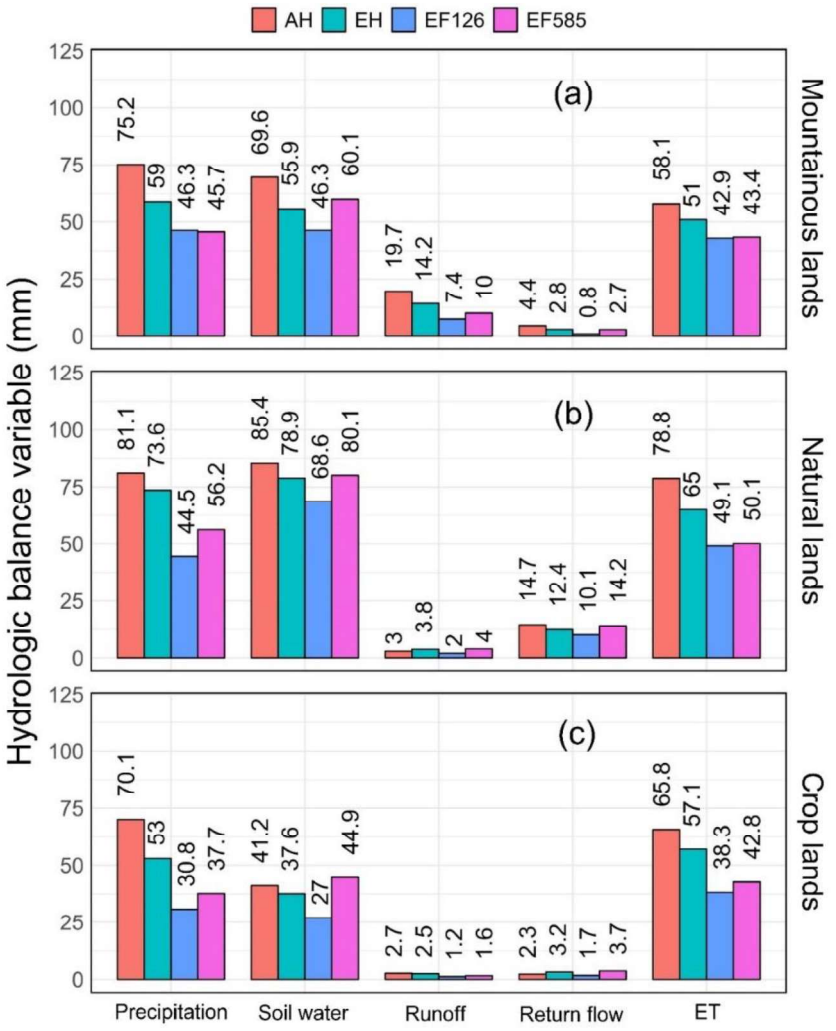

Figure 3.8. Comparison of simulated hydrologic variables for mountainous lands (a), natural lands (b), and crop lands (c) under AH, EH, EF126, and EF585 scenarios. AH is averaged over 30 years. EH, EF126 and EF585 are averaged over extreme warm-dry years. All extreme scenarios are anomalies from AH, and all future extreme scenarios are based on ensemble means. All data are reported for growing season.17

The declining trend in the BW/GW ratio was more pronounced in mountainous lands than natural lands in all scenarios (Figure 3.7b-d). Overall, In mountainous lands during extreme warm-dry years, the reduced precipitation compounded with higher atmospheric evaporative demand, as observed in Figure 3.8, resulted in reduced surface runoff more than soil water. Together, they resulted in low BW availability but a relatively high GW, because the carry over moisture from the non-growing season and cooler and wetter periods such as snowmelt infiltration in the soil can sustain soil water storage, which can support plant water demands during warm-dry years. This ability to sustain soil water storage can offset the negative impacts of limited precipitation during deficit periods for plant growth but at the expense of reduced BW (Bales et al., 2018), since a relatively larger share of precipitation increased GW levels through infiltration into drier soils. GW flow through soil moisture is a slower mechanism than surface runoff generation and it can be further exacerbated by increasing temperatures (Avanzi et al., 2019).

In most sub-basins of the natural lands, the average historical BW/GW rates were greater than those of other ecoregions (Figure 3.7a). However, this ratio decreased considerably in extreme warm-dry years under historical EF (Figure 3.7b) and under the future EF126 scenario (Figure 3.7c), where very low precipitation rates (see Figure 3.6b, Figure 3.8b) substantially lowered the surface runoff and the groundwater contribution to the streamflow via return flows, and therefore reduced the rates of BW (Figure 3.6d, Figure 3.8b). In contrast, the ensemble mean results indicated that unlike the limited BW rates under EF126, the projected GW remained high (Figure 3.8b) since sufficient soil water content was carried over from the normal years or previous wet seasons. Therefore, with the smaller BW and larger GW projections, the BW/GW ratio was considerably smaller than AH in these regions (Figure 3.7c).

Under EF126 a considerable decline of precipitation in the crop lands followed by large reduction of soil moisture (~28% reduction of soil moisture compared to AH, Figure 3.8c), resulted in the infiltration of a large share of the limited precipitation to the soil due to the lack of antecedent soil moisture and soil overall dry condition. The high rates of water entering to the soil, resulted in a considerable reduction of surface runoff and therefore a decline of ~ 51% in BW under EF126 (Figure 3.8c). This is much greater decrease than observed in the EH scenario, which showed only 16%, and 14.5% reduction in BW, and GW, respectively (Table 3.2, Figure 3.8). Further, it contrasts with conclusions from earlier studies, which generally related the increase of evaporation rates in warm-dry years to reduced streamflow, i.e., shift of BW to GW, without projections for future climate change scenarios (e.g., see Massari et al., (2022)). The very low soil moisture in crop lands resulted in increased water stress days during the crop growth season under EF126, which reduced GW consumption associated with plant growth in crop lands. Therefore, a substantial reduction of BW under EF126 (which was responsible for the BW/GW reduction), and the scarcity of soil moisture (which limited crop growth and GW), prevented the shift of BW to GW under EF126 conditions in crop lands. This was in contrast to the mountainous lands and natural lands, where deviation of BW from AH and its shift to GW was observed, albeit through the carry over moisture in the soil that resulted from infiltration of the BW generated in antecedent wet seasons and wet years.

The multi-model ensemble mean results for EF585 anomalies (Figure 3.7d) showed a similar spatial pattern of BW/GW alterations to EH and EF126, but resulted from a different set of underlying mechanisms. Although the surface runoff significantly decreased as compared to the AH (i.e., 40% reduction in runoff under EF585, Figure 3.8) with a relatively substantial decline of precipitation in EF585 (Figure 3.6b), the return flow increased by 3.6% (Table 3.2, Figure 3.8)

because of the reduction in stomatal conductance stemming from higher CO_2 emission under SSP585 (850 ppm) as compared to AH (350 ppm), EH (350 ppm), and EF126 (450 ppm). The higher atmospheric CO_2 concentration enhances plant water use efficiency and reduces transpiration (Masud et al., 2019), resulting in lower water consumption by plants. This allows more water to stored in the soil to further enter the groundwater and to support return flow, leading to an increase BW. However, these beneficial effects of atmospheric CO_2 concentration and water use efficiency could not counteract the significant runoff reduction compared to the AH and the extreme temperature rise in mountainous lands (Figure 3.7c, Figure 3.8a).

3.4.6 Streamflow during extreme warm-dry seasons for the historical and future periods

To understand the watershed response to the cumulative effects of changes in BW and GW, we further analyzed streamflow changes under EH, EF126, and EF585. Results for 150 selected sub-basin outlets (circles in Figure 3.7b-d) reveal declining growing-season streamflow under EH and EF126: 25% and 37% lower than the long-term historical mean streamflow (i.e., AH), respectively. These declining rates of streamflow were a maximum (37% and 49%) at the most downstream outlet of the NRB. Such reductions in the streamflow under EH and EF126 represent the amplified effect of low precipitation on BW during the warm-dry events as compared to average conditions under the historical period. In contrast, the growing-season streamflow under EF585 was, on average, 10% greater than the long-term historical mean. The higher level of atmospheric CO_2 concentration under EF585 and the resulting reduction of evapotranspiration are responsible for this increased streamflow, and outweigh the adverse effects of precipitation reduction on streamflow. Note that these are regionally averaged values and that the impacts of atmospheric CO_2 increases are spatially different across the region. Similar to GW and BW, the

compensation effects of increased atmospheric CO_2 were minimum on streamflow in upstream tributaries of mountainous lands under EF585. Together, the regional cumulative streamflow showed an increase of more than 30% at the most downstream outlet of the watershed as compared to AH (Figure 3.7d).

To better demonstrate the severity of streamflow changes for the EH, EF126, and EF585, we analyzed the simulated data for all 1988 sub-basins across the NRB. The results showed a reduction of 0-50% in growing-season streamflow in 65% of the outlets under EH (Figure 3.9a), with a slightly higher than average streamflow at some outlets in the crop land region (see Figure 3.7b). The decline in streamflow was intensified under EF126 where 75% of the outlets experienced a reduction of 0-50% in streamflow during the growing season (Figure 3.9b). In contrast, under EF585, only 40% of the outlets experienced reduced streamflow, while 60% of the outlets demonstrated an increase of 0-75% in their growing-season streamflow (Figure 3.9c). This increase was not identical across different ecoregions and demonstrated almost no increase in mountainous lands (Figure 3.6d). As seen in Figure 3.7c, only very small number of outlets demonstrated increase of 25%-75% in their streamflow under EF585. The primary underlying process is the larger soil moisture availability under EF585 because of low transpiration rates and earlier stomatal closure, as also reported by Jasechko (2018) and Fowler et al. (2019).

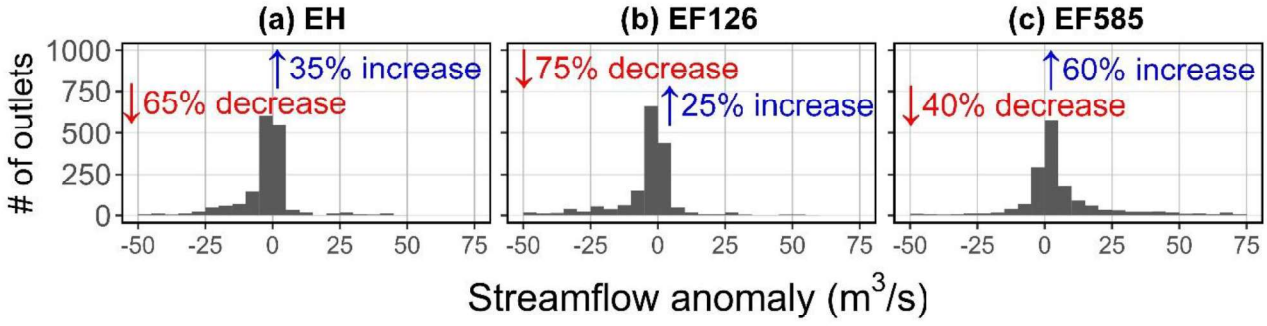

Figure 3.9. Histograms of streamflow anomalies during extreme warm-dry years in the historical period (EH) (a), SSP126 scenario (EF126) (b), and SSP585 scenario (EF585) (c), as compared to the historical average (AH) for 1988 modelled sub-basin outlets (m^3/s).

3.5 Discussion and implications of the BW and GW changes for future water and food security

Our results provide valuable information on BW and GW relationships and their changes during concurrent warm and dry extremes under historical and future climate change scenarios. Numerous global climate change studies projected an overall increase in mean precipitation and wet conditions in mid-to-high latitude regions under future global warming scenarios (O'Neill et al., 2016; Valentin et al., 2018). While increasing precipitation and warming temperatures can benefit crop production in agricultural watersheds of these cold regions (He et al., 2018; M. B. Masud et al., 2018), our study suggests a decreasing trend of precipitation, resulting in unfavorable hydrologic conditions during the growing season in the future extreme warm-dry years of mid-to-high latitude watersheds. In mountainous and natural lands, on the other hand, our results revealed a decrease in surface runoff and infiltration, but an increase in evapotranspiration due to the legacy soil moisture from earlier years and non-growing seasons. Given that the frequency, duration, and intensity of extreme warm-dry events are projected to increase under future global warming scenarios in western Canada (Tam et al., 2019; Yang et al., 2020), the availability of legacy soil moisture in dry years might severely decrease, triggering long-term soil water stress with severe effects for natural vegetation and ecosystems.

More recent studies suggested a shift of blue water to green water resources under historical warm and dry events (Mastrotheodoros et al., 2020; Orth and Destouni, 2018). These studies also suggested the likely amplification of the blue-to-green water shift under future global warming scenarios. Our study revealed a different pattern of BW and GW changes across different

ecohydrological regions. In mountainous and natural lands, a decrease in BW and an increase in GW were found. However, the cause was indirect, with overall increases in GW tied to the availability of legacy soil moisture from earlier seasons and/or earlier wet years, from snowmelt, groundwater contribution, and soil moisture stored. With the projected increase of more prolonged droughts in the future, the legacy soil moisture in these regions may not suffice to meet vegetation water needs. Further, wetlands are important natural features in western Canada, which play key role in regulating nutrients and their export to receiving water bodies (Colares et al., 2020; Greenwood and Eimers, 2022), maintaining biodiversity (Arya, 2021), and sequestering carbon (Moomaw et al., 2018) among others. Therefore, the availability of BW is key for their sustainability and healthy functioning (Cui et al., 2021), which can be affected by the decline of BW and spike of GW, as projected in our study.

The suggested shift of BW to GW in earlier studies (Mastrotheodoros et al., 2020; Orth and Destouni, 2018) did not match our results in the vast crop lands of Canadian Prairies. In crop lands, our results showed either no direct or an indirect shift of BW to GW. This is primarily due to the distinct ecohydrological and climatic conditions of our study area, which is often water-stressed and has limited soil water legacy (i.e., from earlier seasons or groundwater contribution) during droughts. Consequently, our results suggested a considerable reduction in both BW and GW in crop lands, which can seriously affect crop yields under warm-dry events in the future, with implications for their export to over 100 countries (Statistics Canada, 2022). Numerous studies have addressed the importance of irrigation as water supply for global crop production under the warming effects of future climate change in semi-arid regions (Ghoreishi et al., 2021; Wu et al., 2021) and the potential of water storage as an adaptation measure during drought spells (Avanzi et al., 2020). In most agricultural watersheds of mid-to-high latitude regions, snow precipitation

and snowmelt in upstream highland areas are key sources of freshwater for downstream irrigation purposes (Hrach, 2020). Our results suggested a significant reduction of BW during extreme warm-dry years in mountainous high-elevation areas, which can result in a severe water shortage for downstream irrigation during prolonged droughts. This underscores the importance of developing adaptation measures such as storage capacity for freshwater during the likely wet extremes in these regions, although environmental impacts of such strategies must be considered (Máté et al., 2020).

Natural lands provide numerous ecosystem services such as water resources for hydroelectricity (Hoffman, 2017) and forests for timber production, which can be heavily impacted by alteration of the hydrologic regime. For example, more than 98% of electricity generated in Manitoba is based on runoff from natural lands (Government of Manitoba, 2022). Electricity is an important economic resource for the province, which exports about half of its electricity (Government of Manitoba, 2022). More frequent and prolonged warm-dry events and exacerbated BW reduction, as shown in this study, may pose risks to energy production. Further, the forest industry is also one of the largest manufacturing sectors in NRB. Forest products are exported across provincial and international borders with an annual GDP contribution of about $900 million (Zubrycki et al., 2016). Depending on the SSP scenarios, our results suggest that limited BW from natural lands under future extreme warm-dry events during the growing season can impact forest growth and regeneration. Potential water shortages can also increase forest stress and thus effects of insects and diseases (Choat et al., 2018). Finally, stressed forests, and dry bush and trees face a higher risk of future wildfires (Halofsky et al., 2020).

Projected reductions in regional BW, particularly for long lasting and frequent events, can also alter the streamflow regime, changing perennial streams to intermittent ones (Fovet et al.,

2021), with significant implications for water quality (Addy et al., 2019), river ecosystems and fish survival (Lennox et al., 2019), and freshwater biodiversity (Datry et al., 2016) among other effects.

In glaciated basins, rising temperatures accelerate glacier melting. Recent studies have projected significant and rapid retreat of mountain glaciers all the way to complete loss (Clarke et al. 2015; Kotila et al., 2022). Our results predicted a significant decrease of BW and relatively high levels of GW across ecoregions under future extreme warm-dry years. Yet, our simulated results did not consider the effects of glacial melt and retreat in mountainous lands. More severe water shortage may occur under extreme-warm dry events in mountainous lands in the absence of glaciers, which can affect ecosystem services in upstream catchments and irrigation water storage for downstream users during potential prolonged drought years.

Therefore, a thorough understanding of GW-BW relations, particularly their shifts and alterations under extreme warm-dry events in different ecoregions, is essential for future planning and management. As a step towards such a comprehensive assessment, this study shows how warm-dry events, CO_2 enhancement, ecohydrological settings, and climate change can affect GW-BW relations and their changes under extreme events such as warm and dry years.

3.6 Limitations and future directions

The modelling framework in this study assumed the type and rate of fertilizer applications, crop varieties, sowing and harvesting dates under future scenarios to be the same as the historical period. In addition, the operation of 44 relatively large dams included in the historical simulation of the agro-hydrologic processes was assumed to be unchanged for future projections and under global warming scenarios. Addressing these factors using socio-agro-hydrological modelling and

examining the tradeoffs and response of agricultural, hydrological, and socioeconomic factors to changes in BW and GW fluxes and to management and human decisions would be beneficial for developing alternative adaptation measures.

Mountain glaciers are important freshwater resources and major climate change sentinels. Mountain glaciers have undergone significant changes in the last century, including relentless area and volume loss and increased contribution to streamflow in their downstream catchments (Kotila et al., 2022; Liu et al., 2022). Continued changes in their melt, mass balance, and evolution could result in their complete loss by the end of the century (Naz et al., 2014; Clarke et al. 2015). For the future projections in upstream mountainous lands, our model assumed similar glacial melt rates and runoff contributions to those of the historic period. In watersheds of the mid-to-high latitude regions, which rely on glacier melt runoff in their upstream catchments, simulation of the glacial runoff based on changes in their melt, mass balance, and evolution; and coupling with hydrological models can improve BW and GW projection results for future scenarios.

Large-scale disturbances (i.e., forest mortality), species changes and plant acclimation, which are not considered here, may partially offset the ET feedback during warmer years in the long term. Furthermore, in some areas of the NRB, vegetation management and past disturbances such as wildfires or forest logging may have influenced vegetation composition and function in ways that are not included in the model initialization.

Finally, our results might be affected by uncertainty stemming from different sources such as input data used for modelling (e.g., historical and future climate data, soil properties, agricultural land management data), model structure (e.g., hydrologic connectivity and explicit simulation of potholes and wetlands), and model parameters, as well as GCM model spread and downscaling approaches. An uncertainty prediction while incorporating more GCM projections can provide

important information on model confidence and projected results. Moreover, our drought assessment in this study is based on fitting a gamma distribution, which was verified using two widely used goodness-of-fit approaches. A more detailed analysis and comparison of other goodness-of-fit approaches, as well as comparison with other distribution models would reduce uncertainty inherent in the selection of a distribution model, thereby reducing uncertainty for the analysis of drought assessment.

3.7 Conclusions

In conclusion, this study explored the interlinkages between BW and GW and the potential shift of BW to GW under extreme warm-dry years of global warming scenarios in the future, by taking Nelson River Basin to represent agro-hydrological regions of mid-to-high latitude areas in arid and semi-arid regions. Using a process-based agro-hydrologic model, the study showed that the GW-BW relationship follows dissimilar patterns across different ecohydrological regions and under different global warming scenarios, which suggests different implications for various ecosystem services. The main conclusions of this study are that,

1. The multi-model ensemble mean projections for the entire basin indicated greater precipitation, BW, and GW during future growing seasons as compared to the historical period. However, the warmer scenario (SSP585) projected greater BW and less GW as compared to SSP126 scenario. These contrasting results were due to different behaviours of the underlying processes, which were also different across different ecohydrological regions and across different elevation ranges.
2. While multi-model ensemble mean data showed increasing precipitation, BW, and GW in the future, the averaged data for extreme warm-dry years indicated decreasing BW and GW rates for most of the region. The reduction of growing-season BW and GW during

extreme warm-dry periods under SSP126 was due to a significant decrease of precipitation. On the other hand, the magnitude of BW and GW under SSP585 was mainly influenced by the enhanced plant water use efficiency, which resulted from the reduction in stomatal conductance.

3. While the greatest historical average BW in growing season was observed in high altitude areas, which accounted for only 10% of the area, the future projected results indicated a greater reduction of precipitation, BW, and GW under future extreme warm-dry years in these regions. However the rates of BW and GW reductions were different across SSP scenarios.
4. The GW-BW relationships and their projected shifts under SSP scenarios were different across ecohydrological regions. Unlike significant decline of precipitation and BW under extreme warm-dry periods, the maintenance of GW consumption in mountainous and natural lands was related to the evapotranspiration supplied by the legacy soil moisture from earlier seasons and wet years in mountainous and natural lands. This implies a potential shift of BW to GW, although with a lag time and legacy moisture. There was no notable shift from BW to GW in crop lands under future global warming scenarios, and a significant decrease of precipitation, BW, and GW was projected in these lands.
5. Catchments are not equally susceptible to warm-dry events. In mountainous lands, the enhanced water use efficiency through CO_2-driven plant stomatal closure did not outweigh the significant runoff reduction and the temperature rise in extreme warm-dry years causing a significant shortage of BW in addition to GW in all extreme warm-dry scenarios. This projected shortage of BW in mountainous lands could exacerbate water challenges for local

and regional food production and their export potentials in crop lands, given that mountains are source water for downstream irrigation.

Overall, the three ecohydrological regions of this study provide various ecologic and economic services. Therefore, understanding GW-BW relationships, their potential shifts under global warming scenarios, and the processes driving them are important for future planning and management of the watersheds. Our results have significant implications for water-food-climate change studies and global food security, as the study area is among the key crop producing areas and is among the major breadbaskets of the world. Therefore, the findings of this study provide valuable information to facilitate more informed adaptation measures for regional planning and policies for future water resources management.

3.8 Acknowledgment

Funding for this study is primarily provided by the Natural Sciences and Engineering Research Council of Canada (Grant #RES0043463) and Campus Alberta Innovation Program Chair (Grant #RES0034497).

CHAPTER IV – MANUSCRIPT 3

Modelling the impacts of future droughts and post-droughts on hydrology, crop yields, and their linkages through assessing virtual water trade in agricultural watersheds of high latitude regions

Pouya Khalili[1*], Monireh Faramarzi[1*]

[1] *Watershed Science and Modeling Laboratory, Department of Earth and Atmospheric Sciences, Faculty of Science, University of Alberta, Edmonton, AB T6G 2R3, Canada*

[*]Corresponding authors: faramarz@ualberta.ca
khalili@ualberta.ca

4.1 Abstract

The unfolding climate change crisis poses a growing challenge to water and food security, and yet the reliability of the global breadbaskets and their relationship with water resources in the future are poorly understood. In the higher latitudes of the temperate zone, the global breadbaskets are projected to receive an overall increased precipitation and improved crop yields under the effects of global warming scenarios, which is often perceived as beneficial to crop production and export potentials in the future. However, the future projected extreme warm-dry events, can significantly affect the agro-hydrological processes, crop yields, and therefore export potential of the crops from these regions. Using a process-based agro-hydrologic model, this research examines the potential impacts of future droughts and post-droughts on water yield (WYLD), crop yield (Y), and their linkages through assessing the net virtual water export (NVWE), the water embodied in the production process of the crops that are exported to international countries. The study takes Nelson River Basin (NRB), a large agricultural watershed in western Canada that exports food to over 170 countries and plays part in global food security. The agro-hydrologic

model is forced using projected climate data and atmospheric CO_2 levels from an ensemble of six Global Climate Models (GCMs) of the Coupled Model Intercomparison Project Phase 6 (CMIP6) for the 2070-2099 period, based on two contrasting Shared Socio-economic Pathways (SSP126 and SSP585).

Contrary to prevalent long-term average projections of a wetter future for the higher latitudes of the temperate zone, our study results of the longest and the most severe drought (LMD), indicate a substantial reduction in precipitation, Y (rainfed wheat and canola in this study), as well as WYLD in the future. The reductions in these agro-hydrological variables are likely to be more severe under historical drought conditions and SSP126 than SSP585. The slight improvement under the SSP585 scenario due to the CO_2 effects on plant photosynthesis processes is not uniform across region and crop types.

Analysis of data for post-drought period, reveals variable recovery times for WYLD, Y, and NVWE in the future, with the WYLD demonstrating slower recovery time as compared to Y during the years after the longest and the most severe drought (LMD). Given the projected frequent droughts in the future, the slow recovery of the WYLD after droughts can be a limiting factor for sustainable production and export potentials as it can deteriorate environment and several economic sectors. Our study lays a strong basis for examination of a strategic crop selection and diversification, which can be considered as an adaptation measure for conservation of WYLD for an integrated water and food security in the future.

Keywords: Agro-hydrologic modelling, climate change projections, global climate models, water-food security, CMIP6, sustainable production

4.2 Introduction

Droughts are a common and recurring phenomenon with significant impacts on hydrology (Hasan et al., 2019) and crop production (Kuwayama et al., 2019), therefore, altering virtual water trade (VWT). The VWT is the flow of water embodied in the production process of food and other commodities which are traded between and within countries (Allan, 1998). Despite the well-documented negative effects of droughts on water resources and crop production, studies have less concentrated on the impacts of droughts on VWT. Moreover, most studies largely focused on the immediate impacts of droughts (Li et al., 2019; Zhao et al., 2020; Khalili et al., 2023) and have paid little attention to the long-term effects, such as post-drought impacts. For example, the post-drought precipitation may not contribute to runoff with a similar pattern as pre-drought condition, and instead the evapotranspiration (ET; also known as green water flow) rates can increase under post-drought condition (Deb et al., 2019; Saft et al., 2015). Such changes in the hydrological processes can cause hydrological or agricultural droughts to persist for a longer period after the occurrence of the initial droughts.

Sustained droughts can lead to significant and prolonged reductions in water yield (WYLD-net volume of freshwater, including surface runoff, lateral flow, and groundwater generated in a watershed), despite their termination (Y. Yang et al., 2017). The persistent reduction in WYLD following droughts is often attributed to factors such as increase in ET and shift in the annual rainfall-runoff relationship (Saft et al., 2016). It can also be related to changes in the seasonality of rainfall (Pepler et al., 2021), reductions in pre-drought precipitation (Wasko et al., 2020), increased soil moisture depletion (Filipović et al., 2018), and reductions in heavy rainfall frequency (Elliott et al., 2015). Furthermore, changes in soil physical properties (e.g., soil hydraulic conductivity, bulk density, available water capacity) due to drought (Van Loon and Van

Lanen, 2013), and soil conservation techniques, during and after drought can also contribute to reduced WYLD, which can exacerbate the adverse effects of post-droughts on hydrology (Cornish et al., 2020). In addition, plain areas with low slope and small topographic relief can generate less runoff as compared to highlands (Khalili et al., 2023), due to greater rates of infiltration and ET that may exacerbate the adverse effects of droughts on runoff generation after their termination. Increases in atmospheric evaporative demand, following a drought, and changes in vegetation growth pattern, and water use can also impact runoff generation and therefore streamflow (Mastrotheodoros et al., 2020). Moreover, reduced recharge to groundwater during the drought can also contribute to the decline in groundwater levels and further exacerbating the streamflow reduction after the drought termination (Khalili et al., 2023; Fowler et al., 2020). Therefore, the post-drought persistence of WYLD decline and streamflow reduction are complex processes, influenced by a wide range of factors. After a drought event, the altered terrestrial and atmospheric processes create a diverse range of variations in hydrological water components and environmental conditions. However, most studies have focused on short-term direct impact of droughts (Li et al., 2019; Zhao et al., 2020; Khalili et al., 2023), and the examination of long-term (multi-year) changes in hydrological processes in a post-drought period are limited.

The changes in hydrological processes following a drought event can impact crop yield (Y) and the time that takes for crops to recover from a given drought (Iqbal et al., 2020; Lesk et al., 2016). Understanding the effects of post-drought conditions on Y and its linkages with water (e.g, GW and WYLD) can inform sustainable water and food management strategies (Hamal et al., 2020; Krishnamurthy R et al., 2022; Srivastav et al., 2021). However, there is currently a limited understanding of the post-drought effects on Y due to the complexity of post-drought processes, lack of long-term data on spatiotemporal variability in recovery of hydrological regime and Y after

a drought event, and difficulty in controlling for other factors such as changes in land use, management practices. Studies have demonstrated that the recovery of Y from drought can be quicker than that of the watershed hydrology, leading to further stress on the hydrological balance (Orth and Destouni, 2018). This is attributed to the increased rate of infiltration after a drought, when the soil is dry, demanding a greater proportion of precipitation to infiltrate to the soil instead of contributing to surface runoff (Qiu et al., 2023). However, the infiltrated water can primarily replenish the topsoil moisture for crop use, leaving a limited soil water for groundwater recharge, which can result in a reduced groundwater levels (Khalili et al., 2023). The reduced groundwater level can ultimately lead to a reduced soil moisture for crop ET, which can be otherwise available from a high groundwater table through capillary fringe for root water uptake (Karamouz et al., 2011). The reduced groundwater levels can also decrease subsurface water contribution to streamflow, decreasing the return flow or base flow to the streams (Wossenyeleh et al., 2020) with potential impacts on irrigated Y (OECD, 2016). As a result, the recovery of Y under post-drought condition is highly related to the hydrological processes driving soil water and the feedback between crop growth and soil moisture availability.

The VWT (m^3/tonne) associated with the trade of crops is quantified based on the ratio of crop ET (m^3) to Y (tonne/ha) (Hoekstra, 2003), which can be variable depending on the geospatial, hydrological, climatological, and agricultural management practices where crops are produced. The VWT can also be dependent on the source of water used in the production process of the crops, including blue (i.e., WYLD in this study) and green (i.e., actual evapotranspiration) water resources. Given that all these factors can be considerably impacted by droughts, the VWT and the pattern of water transfer through the trade of crop products can also be affected by droughts. Despite the wide range of studies on VWT, a comprehensive assessment of the impacts of droughts

and post-drought condition on VWT is absent. Previous research on VWT has primarily concentrated on the role of VWT on water resource management, water savings, and socio-economic drivers of VWT and the VWT networks (Chapagain et al., 2006; Mekonnen and Hoekstra, 2020; Oki et al., 2017; Qu et al., 2018; Faramarzi et al., 2010; Zhang et al., 2016; Zhuo et al., 2016; Konar et al., 2011). However, these studies have largely overlooked the role of natural factors such as droughts and post-drought conditions in local hydrological processes driving VWT. Additionally, these studies have primarily focused on historical observations (Hoekstra and Mekonnen, 2016; Mekonnen and Hoekstra, 2020) and have not adequately addressed the changes under future extreme event conditions such as droughts and post-drought periods. The recent limited studies that addressed the impacts of climate change on VWT (Graham et al., 2020), elaborated on the food production and trade potentials under averaged future climate conditions. Overall, the ensemble mean model projections show a promising future with increases in precipitation, heat units, and Y for mid-to-high latitude regions (He et al., 2018; Khalili et al., 2021; IPCC, 2021; Masud et al., 2019). However, these assumptions lack assessment of the impacts under extreme dry events such as droughts and post-drought conditions on hydrological processes and blue-green water interchange that are key drivers of crop growth and VWT (Khalili et al., 2023; Marston and Konar, 2017). Therefore, to fully understand the combined and long-lasting impacts of droughts on hydrology, Y, and VWT, it is imperative to conduct a comprehensive analysis that considers the complex interactions and relationships among these factors. Such a study can help, inform, and guide sustainable water management and food production strategies in the face of global warming scenarios. More specifically, the agricultural watersheds of mid-to-high latitude regions, such as Canadian Prairies, are prone to frequent droughts, while they are also important breadbaskets of the world (Khalili et al., 2021b; Rubin and

Hurst, 2017). Given the potential adverse effects of post-droughts on water availability and crop production, it is crucial to assess the effects of droughts and post-droughts on VWT in crop producing watersheds of the mid-to-high latitude regions where droughts are frequent and their impact on hydrology, Y, and VWT can be substantial.

The primary goal of this study is to examine the impacts of droughts and post-droughts on hydrological processes, Y, and their linkages through assessment of VWT under global warming scenarios. To achieve this goal, the objectives of this study are to: (1) analyze the past and projected changes in WYLD under average, drought, and post drought conditions using Nelson River Basin (NRB) as a study region, which is the largest agricultural watershed (1.1 million km^2) in Canadian Prairies, covering various ecohydrological conditions; (2) assess the past and projected changes in Y, under average, drought, and post drought conditions in NRB; (3) evaluate the impacts of drought and post-drought conditions on VWT under historical and future scenarios in the NRB which is one of the important breadbaskets of the world and exports agricultural crops to over 170 countries around the world. The findings of this study are applicable to other large river basins in mid-to-high latitude regions, which often play a crucial role in socioeconomic development, food export, and global food security.

4.3 Materials and methods

4.3.1 Study region and data collection

4.3.1.1 Study region

The Nelson River Basin (NRB) is the largest agricultural watershed in western Canada NRB that supplies wheat crop and other agricultural commodities to over 170 countries around the world (Statistics Canada, 2021). While located in Canada and a small part of the northern US, known as

one of the most water-abundant regions in the world (World Bank, 2021), but crop production in NRB is highly reliant on variable hydrological processes (M. B. Masud et al., 2018) (Figure 4.1). Commencing in the Rocky Mountains at an altitude of 3,227 meters, the basin extends from South Dakota, USA, to the middle of Alberta, and the northern borders of Manitoba, Canada, to near Lake Superior in the eastern region. Covering an area of approximately 1.1 million square kilometers, the basin discharges about 2370 m^3/s into Hudson Bay, which is the most extensive inland sea globally (Figure 4.1A, 4.1B).

With over 40% agricultural lands, the NRB is recognized for its fertile soils and ideal for crop production. Wheat is one of the most extensively grown crops, with the prairie provinces of Alberta, Saskatchewan, and Manitoba producing about 25 million tonnes per year and contributing to over 85% of Canada's total wheat production (Figure 4.1C) (Statistics Canada, 2021). Although irrigation is practiced in certain areas of the Prairies to supplement precipitation and sustain crop growth, particularly in regions with scarce water resources, such as southern Alberta and Saskatchewan, the rainfed crop production is the primary approach in most of the region (Government of Canada, 2021). In addition to wheat, the region is also a major producer of canola (Figure 4.1D), with over 19 million tonnes of canola production per year, accounting for over 90% of the country's canola production (Statistics Canada, 2021). The NRB exports an average of 17 million tonnes of wheat and 10 million tonnes of canola to various countries worldwide, which counts for over 60% and 55% of Canada’s wheat and canola exports, respectively (Statistics Canada, 2021). This level of export scores the NRB at the 3rd rank after European Union and Russia, being the top most exporters of the wheat, globally; and making NRB as the leading region with 70% contribution to the global canola production and export (International Grains Council, 2021; Canola Council of Canada, 2021; Statistics Canada, 2021).

The mean temperature range for the growing season (i.e., May to September) across croplands of NRB is between 15°C and 25°C, with some areas experiencing higher temperatures. The average annual precipitation for the growing season in the agricultural region of NRB ranges from 200 mm to 500 mm, with some areas experiencing higher amounts of rainfall (Khalili et al., 2023). It is important to note that the prairies in the southern regions of the basin, such as southern Alberta and Saskatchewan, tend to be hotter and drier than the northern and eastern regions of the basin, such as northern Manitoba. This can affect crop production and the need for irrigation in these areas. Additionally, the prairies in the eastern region of the basin, near Lake Superior, tend to have greater precipitation amount than the western regions.

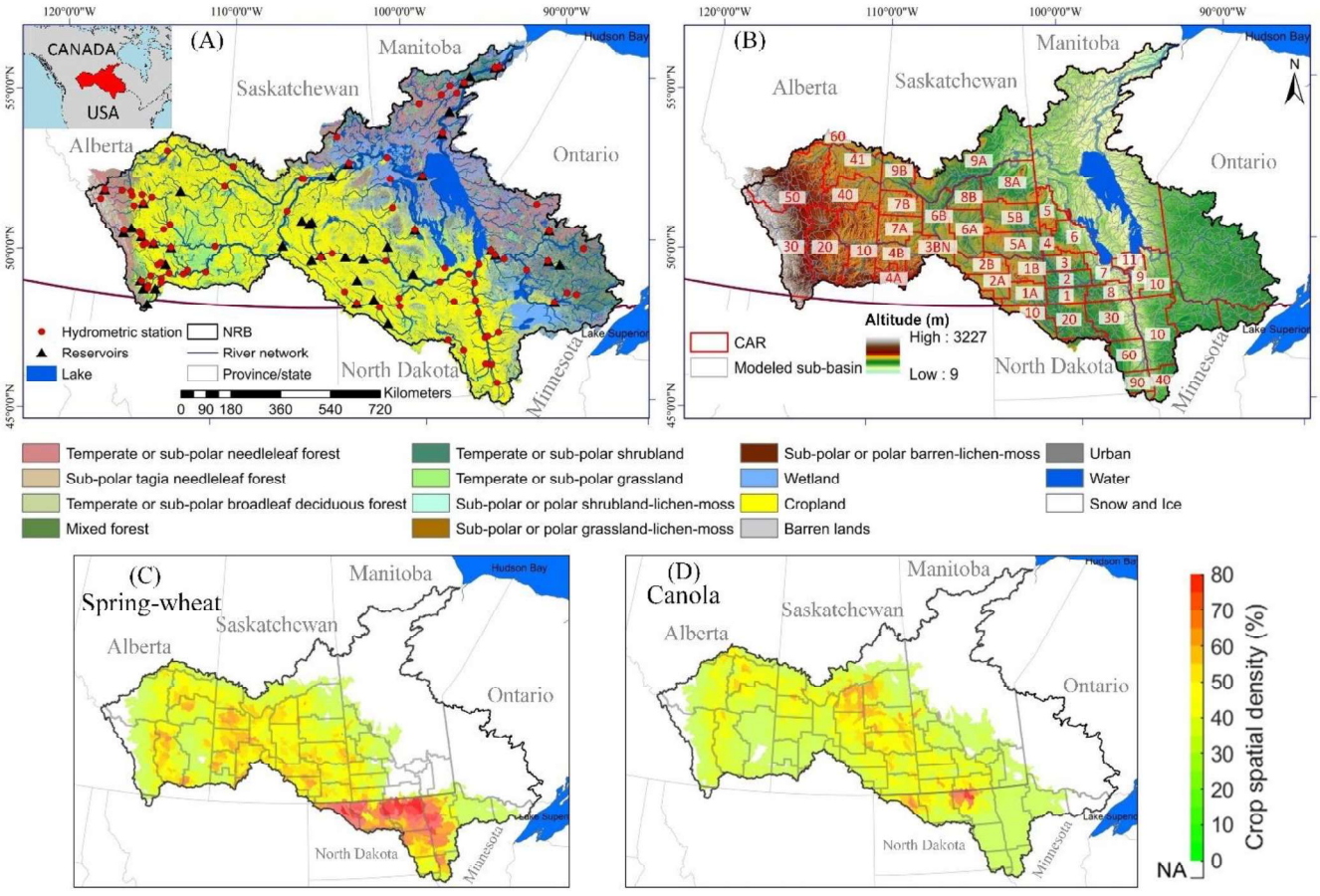

Figure 4.1. (A) Map of the NRB including the land use land cover classes considered in the model according to the Government of Canada (2019) classification, rivers, reservoirs, lakes, and

hydrometric stations; (B) geographic extent, and the Census Agricultural Region (CAR), for which crop yield time series are available from Government of Canada (2019) for calibration and validation in this study; (C) spring wheat and (D) canola crop spatial density maps (%) showing the density of cultivated lands in the study area.18

4.3.1.2 Data collection

The agro-hydrological model of NRB was developed utilizing a diverse range of geospatial maps and time series data, including Digital Elevation Models (DEM) (Jarvis et al., 2008), a detailed land use-land cover map (Government of Canada, 2019), and a processed soil map (Cordeiro et al., 2018; FAO, 1995). For model setup and calibration, the WATCH Forcing Data ERA-Interim (WFDEI) historical climate dataset (Weedon et al., 2014b), measured streamflow data from hydrometric stations, and daily operation data of 44 large reservoirs/dams were incorporated (Khalili et al., 2023). The simulation period (including calibration and validation) for this study was from 1987 to 2016. Additional information regarding the model's development can be found in Khalili et al. (2023). In order to develop rainfed crop models, an extensive amount of agricultural management data was collected, including planting and harvesting dates, volume and rate of fertilizer application, irrigation application, and crop-specific information such as plant growth parameters, phenological development stages, and potential heat units for spring wheat and canola (see Table A.10. Crop-specific fertilizer application rates (represented as N:P:K ratios), maximum annual fertilizer application (measured in kg/ha per year), and the potential heat units required for crops (degree days) were obtained from various sources such as Statistics Canada (2021) and the United States Department of Agriculture (2021) and earlier studies (Faramarzi et al., 2017; M. B. Masud et al., 2018; Masud et al., 2019). For the calibration purposes, the yearly time series of Y for rainfed spring wheat and canola were acquired at the CAR level from Statistics Canada (2021), Alberta Financial Service Cooperation (AFSC), as presented in Figure 4.1. The entire agricultural lands in the NRB encompass 37 Canadian census agricultural regions (CARs),

and 7 agricultural regions in the United States (collectively referred to as CARs, hereafter) (Figure 4.1B). Planting and harvesting dates were obtained from literature (Faramarzi et al., 2017; Mezbahuddin et al., 2020), and other available sources (see Alberta Agricultural and Rural Development, 2004; Government of Saskatchewan, 2020; Government of Manitoba, 2020), and they were further modified through calibration process.

The future climate data were incorporated from an ensemble of six Global Climate Models (GCMs) of the Coupled Model Intercomparison Project Phase 6 (CMIP6) for future projections of the hydrological processes and crop growth (see Table A.11). The future climate data are based on two contrasting Shared Socio-economic Pathways (SSP126 and SSP585) representing the lowest and highest radiative forcing levels projected for the year 2100. For future hydrology and crop simulations in the study, the concentration of CO_2 was set to 350, 450, and 850 ppm for the historical, SSP126, and SSP585 future periods, respectively (Eyring et al., 2016b). Most CMIP6 projected climate records indicate more critical global warming effects near the end of the 21st century, albeit subject to a greater spread of prediction uncertainty. Therefore, the analyses were performed for the 2070 to 2099 period using the two most extreme SSP scenarios. In an earlier study (Masud et al., 2021), the future climate data were statistically downscaled based on historical daily gridded climate data using multiple techniques, including Climate Imprint, Quantile Delta Mapping, Constructed Analogues, and Bias Correction/Constructed Analogues with Quantile mapping reordering. The downscaled climate data for future period were used to force agro-hydrologic model in this study. More detailed information can be found in Khalili et al., (2023) and Masud et al., (2021).

4.3.2 Model configuration and evaluation metrics

The Soil and Water Assessment Tool (SWAT) is a process-based semi distributed model that simulates various hydrological, plant growth, sediment, and nutrient cycling related processes (Neitsch et al., 2011b). The model has been used to simulate the impacts of climate change and management operations on hydrology, crop growth, sediment and nutrient transport and fate from catchment to large watersheds, and continental scales (Haney et al., 2018a; Karamouz et al., 2021b; Loiselle et al., 2020). It partitions a basin into sub-basins and Hydrological Response Units (HRUs) based on soil, land use-land cover, and slope parameters. Within each HRU, processes are simulated based on soil, vegetation, climate, and management data provided by the user, and then aggregated to sub-basin and basin levels. The model is capable of simulating a wide range of processes, including ET, surface runoff, snow accumulation and melt, groundwater recharge, subsurface flows, crop growth and crop water consumption, soil temperature, soil nutrient cycling, nutrient loads and transport, and erosion and sediment loads and transport among others (Neitsch et al., 2011b).

In this study, we utilized a calibrated hydrological model of the NRB (Khalili et al., 2023) to develop a crop growth model using the ArcSWAT 2012. The calibrated hydrological model of the NRB delineated the region into a total of 1988 sub-basins based on the DEM map (Khalili et al., 2023). Using the hydrologically calibrated model, the crop model in this study was developed and calibrated based on rainfed spring wheat and rainfed canola yields for the 1987-2016 period. The calibrated model was then used to project hydrology and Y for the 2070-2099 period. Heat unit requirements were optimized in the model through calibration procedure to represent different varieties of crops planted across the watershed, differing in their growing degree-days. The total fertilizer application per year in different sub-basins, and the rate of application were defined from

the available data, but fertilizer application frequency and timing was set to auto fertilizer option of the SWAT model, which was controlled by nutrient stress factor and plant-water-stress threshold simulated in the model.

Prior to conducting the calibration process, we performed a sensitivity analysis (SA) for model parameter selection using a methodology similar to Faramarzi et al. (2017). The SA can determine critical parameters that affect hydrology and crop growth in various regions. The selected parameters were scaled to simulate regional variations in geospatial, hydro-climatic, and ecological conditions (Faramarzi et al., 2017). We identified 26 and 27 scaled parameters for six major hydrological watersheds (Figure 4.1A) and 44 CARs (Figure 4.1B), respectively (Khalili et al., 2023).

To calibrate and evaluate the efficacy of our model, we followed an iterative procedure that involved the publicly available Sequential Uncertainty Fitting program (SUFI-2) (Abbaspour et al., 2015) and a parallel processing program scheme to utilize a 200-core advanced computer for parallel processing of the simulations (Khalili et al., 2023). The first iteration starts with assigning the largest physically meaningful range for each sensitive parameter and they are sampled using Latin Hypercube Sampling to create 1000 samples of parameter sets. Then, parameters are updated and model is forced based on each of the 1000 sample sets, for which 1000 sets of output variables, i.e., streamflow and Y, are generated and compared to the measured data. If the comparison results were unsuccessful, a new iteration is performed by revising the initial parameter ranges until satisfactory results are obtained. In this study, we used several objective functions to assess model performance for each of the 1000 times streamflow simulations. These objective functions include the coefficient of determination (R^2), the Nash-Sutcliffe efficiency (NSE), the percent bias (PBIAS), and the Kling-Gupta efficiency (KGE). To evaluate the agreement between the simulated

and observed Y, we used the mean square error (MSE). The simulated data at the sub-basin level were aggregated to the CAR level to maintain a consistent spatial resolution with the observed yield data. Given the large spatial extent of the study region, and various sources of uncertainty in the modeling (Khalili et al., 2021b), two significant measures were employed to evaluate the model calibration and uncertainty performance of a given iteration. The *p-factor*, which represents the percentage of data bracketed within the 95% prediction uncertainty (95PPU) band, and the *r-factor*, which measures the average width of the band relative to the standard deviation of the corresponding measured variable. At the scale of this study, the model is forced to capture the majority of the measured data within the simulated 95PPU band, indicating a high level of model accuracy (i.e., *p-factor* close to 1), and to result in a narrow uncertainty band (i.e., *r-factor* of 3-5 is an acceptable range for Y simulations). Additional information regarding the model calibration, validation, and uncertainty analysis can be found in Khalili et al. (2023).

4.4.3 Drought severity index calculation

To predict drought conditions, we used the widely-used Standardized Precipitation-Evapotranspiration Index (SPEI) approach (Vicente-Serrano et al., 2010). The SPEI is a multi-scalar drought index that considers both precipitation and potential evapotranspiration (PET) to evaluate the onset, duration, and severity of drought conditions. The calculation of the SPEI involves the analysis of precipitation (P) and PET times series data for a given time period (Vicente-Serrano et al., 2010). For instance, using a monthly time series, first a climatic water balance (WB) is calculated as the difference between P and PET for each month. To indicate whether for a certain period of time, the amount of WB is in deficit or surplus, the monthly WB data are then accumulated over a certain period (i.e., 1 month, 2 month, …, 12 month accumulated data). For example, to construct a 9-month times series data of WB, the first 9 months of data are

accumulated, then a times series of 9-month cumulative data are constructed by using a rolling-and-moving window of one month until time series data are constructed for the total number of years of study period. The accumulation period is any period of interest that quantifies the standardized surplus or deficit of WB (Vicente-Serrano et al., 2010). In this study, we opted to construct 9-month SPEI indices, to consider the legacy soil moisture from previous months that could potentially affect water availability for crop production during growing season in our study region. The selection of 9-month SPEI was verified by performing a correlation analysis between SPEI of different accumulation time (ranging from 1 to 12 months) and observed Y data for the 1987 to 2016 period. The highest correlation with Y was related to the 9-month time series (Figure A.9).

Overall, the SPEI approach quantifies WB as standardized departure from a selected probability distribution function that models the raw data (i.e., 9-month WB data in this study). The raw data are typically fitted to a best performing probability function distribution, and then transformed to a normal distribution to generate the SPEI indices. The constructed indices can be then interpreted as the number of standard deviations by which the observed anomaly deviates from the long-term mean (Vicente-Serrano et al., 2014). In this approach, negative index values indicate drought events and positive values indicate wet events.

The resulting SPEI indices are then employed to quantify drought severity, using a drought classification system, such as the one detailed by Svoboda et al., (2004) and employed by the U.S. Drought Monitor (USDM) (Svoboda et al., 2002). This classification approach interprets SPEI values to their corresponding degree of varying drought and wetness conditions and lists them from D0 (abnormal) to D4 (exceptional) droughts and from new normal to extreme wet conditions.

Table A.12 summarizes each drought and wet events with their corresponding SPEI values and their ecological implications (Svoboda et al., 2004).

Considering that precipitation and potential evapotranspiration (P and PET) data typically exhibit right-skewness due to the nature of rainfall patterns, a gamma distribution has been recommended as the most suitable fit (H. Wang et al., 2019). As such, in our study we fitted a gamma distribution to the constructed 9-month WB times series for each sub-basin. Using the gamma distribution, we further calculated the cumulative probability function (F(x)) for each WB value (x). Next, we constructed the standardized indices (SPEI) using the inverse of the standard normal distribution function (Φ^{-1}) as follows:

$$SPEI = \Phi^{-1}(F(x)) \quad (4.1)$$

Finally, we aggregated the sub-basin level SPEI time series to the NRB level to analyze the effects of regional droughts on Y, water yields, and virtual water trade, which are explained in the following sections. Next, using the regional SPEI times series, we calculated the regional drought duration for the NRB, based on the successive number of months experiencing a drought intensity of less than -0.5. This threshold delineates D0 or worse drought events, according to the U.S. Drought Monitor categories (see Table A.12). It is noteworthy that the use of regional SPEI times series for regional drought assessment, may result in non-drought condition for some sub-basins in the region.

4.3.4 WYLD, Y, and VWT accounting

4.3.4.1 WYLD and Y calculation

In SWAT model, the WYLD in each day and for a given sub-basin is calculated as follows:

$$Q_{WYLD} = Q_{Surf} + Q_{Lat} + Q_{GW} - Q_{TLoss} \quad (4.2)$$

Where Q_{WYLD} is WYLD (mm), Q_{Surf} is surface runoff (mm), Q_{Lat} is lateral flow, which is the volume of water that moves laterally within the soil profile and enters the main channel in each sub-basin (mm), Q_{GW} is the water from the shallow aquifer that enters the main channel when the groundwater level is high (mm), Q_{TLoss} is water loss due to transmission through the streambed (mm).

Y is also determined by various factors, such as leaf area development, light interception, and conversion of intercepted light into biomass, using a plant species-specific radiation use efficiency at a daily time step. The model simulates above ground and below ground biomass using 40 crop-specific phonological parameters (such as, potential heat units, base temperature, optimum temperature, maximum leaf area index, radiation use efficiency, etc.), and agricultural management data (such as, crop planting areas, planting and harvesting dates, fertilizer and pesticide application, irrigation, tillage, and harvest and kill operations). First, optimal biomass and potential yields are simulated under ideal growing conditions, which include adequate water and nutrient supply and a favorable climate, such as optimum temperature. Then, actual yields are simulated based on constraints induced by deficiency or surpluses in soil water availability, soil nutrient availability, and temperature stresses, which are simulated on daily time step across different soil layers introduced by the modeler in each sub-basin. Biomass development begins when the temperature exceeds the plant-specific base temperature from planting to harvest date, or until it reaches the crop-specific maximum heat units. Actual water uptake by the crop is simulated based on potential ET, biomass development (above ground and below ground), and water availability in the soil layers on a daily basis (Neitsch et al., 2011b).

4.3.4.2 Virtual water content (VWC) and VWT accounting

The virtual water content (VWC) is a measure of the amount of water required for crop production, expressed as volume of water per unit of mass produced (Hoekstra, 2003). The VWC (m^3/tonne) in our study was calculated as follows:

$$VWC = \frac{ET}{Y} \times 10 \quad (4.3)$$

Where, ET is the simulated crop water consumption (mm) during the crop growing period, Y is the simulated Y (tonne/ha). To convert the simulated ET (mm) into m^3/ha, a factor of 10 is used in the calculation. A higher VWC indicates a greater amount of water used per tonne of crop production, resulting in a lower water use efficiency. The VWC of wheat and canola was calculated for historical (1987-2016) and future (2070-2099) periods for each sub-basin using simulated Y and ET data. We further calculated the net virtual water trade (NVWT, m^3) from the NRB to assess the effects of drought and post-drought on regional water resources in relation to crop productions and their potential exports. The NVWT is the volume of water that is associated with the export of crops (Hoekstra and Chapagain, 2007; Mekonnen and Hoekstra, 2011). As the total volume of crop exports are not known for the future scenarios, we assumed the crop surplus that is not consumed domestically, would be available for export. As such, we excluded the water embedded in the production of crops that are consumed domestically in the NRB. Therefore, we estimated both the domestic crop requirement (P_r, tonne) and the total crop production (P_a, tonne) in the NRB. We calculated domestic crop consumption using the approach proposed by Ercin and Hoekstra, (2014) as follows:

$$P_r = 1.2 \times per\ capita\ crop\ consumption\ \times Total\ population \quad (4.4)$$

For the purpose of this study, the per capita consumption rates of wheat and canola were obtained from the FAOSTAT Commodity Balance Sheets (FAOSTAT, 2021). The per capita crop consumption was assumed to be constant for both past and future scenarios. This assumption was based on the relatively stable trends observed in crop consumption patterns in the historical data. For future scenarios, total population was estimated based on the historical growth rate observed over the last 30 years, data sourced from the U.S. Census Bureau and Statistics Canada. This projection assumes that the historical growth rate will remain consistent over the years. However, given potential future changes in fertility, mortality, and migration trends, this carries inherent uncertainty. Then, total crop production in the region was calculated as follows:

$$P_a = Y \times A \tag{4.5}$$

Where, Y is simulated Y (tonne/ha), A is the area under cultivation (ha) for each crop type, derived from crop inventory maps (Government of Canada, 2021). The crop inventory maps, have a grid resolution of 30 m × 30 m, and provide annual area under cultivation for various crops. It is important to note that not all grid cells have a 100% cultivated area for a given crop. In our analyses, we considered any grid cells with the cultivated area of ≥ 10%. Finally, we summed the product of P_a for all crop types (rainfed spring wheat and canola in this study) to obtain the total crop production in the NRB.

The NVWT (m^3) for the future period was calculated as follows:

$$NVWT = \Sigma((P_a - P_r)_c \times (VWC_c)) \tag{4.6}$$

$(P_a - P_r)_c$ is the surplus of a given crop that is not consumed domestically and potentially available for export (tonne), $(VWC)_c$ is the virtual water content of a given crop (m^3/tonne). Overall, the positive NVWT in Eq. 4.6 indicates a net virtual water that flows outside of the region

(NVWE) and the negative values indicate, otherwise. It is worth noting that, in the current state of affairs, a substantial portion of crop surplus in the NRB is indirectly exported through the production and export of meat, live animals, dairy products, and beverages (AAFC, 2021). However, in this study, we did not explicitly determine the VWC and VWT associated with these commodities. Instead, we assumed that all crop surplus could be directly exported as grain without any further processing.

4.3.5 Drought and post-drought analysis of WYLD, Y, and VWT

To address the prolonged effects of droughts on Y, WYL, and VWC after a given drought event terminates, it is crucial to establish a clear definition of the end of a given drought. The definition of the end of a drought can vary depending on the drought index employed and the research objectives. In this study, we defined the end of a drought as the time when the SPEI value is greater than -0.5, based on USDA drought classification approach. Theoretically, an SPEI value greater than -0.5 indicates a reduced deficit between precipitation and PET, which implies the agro-hydrological conditions improvement to a state of relative normalcy (Nam et al., 2015).

To assess the response of Y, WYLD, and VWT to post-drought condition, we analyzed the data for the five years following the cessation of the longest and most severe droughts (LMD) at a regional scale, as predicted by each of the six GCMs. We selected a five-year post-drought period based on our observation that the impacts of the drought were undetectable beyond this period in all the regions in this study. Our results are reported as the ensemble mean values for the five-year post-drought periods. The most severe drought for each GCM and for each SSP scenario was calculated based on the lowest SPEI values from the regional averaged time series (see section 4.4.3), as a lower value indicates greater severity. The longest drought was determined by the

highest count of consecutive months where the regional SPEI value was less than -0.5, indicating sustained periods of at least D0 event or worse.

For the years after the selected extreme droughts, we simulated Y, WYLD, and VWT using our calibrated model (*D* Scenario), and compared the results with a 'theoretical scenario' where we assumed there was no extreme drought events in our model (*ND* scenario). To simulate ND scenario, the model input climate data (e.g., daily precipitation, maximum and minimum temperature, solar radiation, wind speed, and relative humidity of the air) were modified. Specifically, we replaced climate data from the years identified as non-drought years. With this approach, we ensured the sequence of years in the ND scenario reflected a continuous, uninterrupted series of non-drought conditions.

Since the Y model was calibrated based on CAR-based observed yield data, our simulated results were aggregated from sub-basin to CAR and presented at CAR spatial resolution. Next, we evaluated the differences between the *D* and *ND* scenarios to explore the post-drought recovery of the Y, WYLD, and VWT in different ecohydrological regions and under different SSP scenarios in the future.

4.4 Results and discussion

4.4.1 Model configuration and evaluation metrics

The calibration and validation processes were conducted across 44 CARs, encompassing both canola and spring wheat crops. For the sake of conciseness, we present the results of our analysis at the average watershed level for both crops in Table 4.1. A detailed information on the crop model calibration and validation results can be found in Tables A.13 and A.14. Overall, the two Y models for simulation of rainfed wheat and canola growth were built upon a hydrology

model developed and calibrated in an earlier study by Khalili et al. (2023), which provided the foundation for the crop growth simulation. The hydrology model and the calibration and validation of the spring wheat crop are discussed in greater details in Khalili et al. (2023). In the present study, we constructed a canola yield simulation model. The model successfully reproduced observed annual rainfed canola yields for calibration period (1992-2016). The average *p-factor* for the calibration period consistently exceeded 87%, indicating that the observed yield data was adequately captured within the simulated 95PPU. The average *r-factor* values were 2.05 and 2.41 for wheat (Khalili et al., 2023) and canola, respectively (Table 4.1). The average mean squared error (MSE) values across the study region for wheat and canola yields were 0.16 and 0.10, respectively. A similar performance was observed during the validation period (Table 4.1). The minimum and maximum statistics for all CARs demonstrated overall satisfactory performance for both rainfed crops for the calibration and validation periods. It should be noted that improvements in *p-factor* were occasionally achieved at the cost of increased *r-factor* and higher MSE values in certain regions. Consequently, a judicious balance between the *p-factor* and *r-factor* must be established throughout the calibration process. Inherent uncertainties are present in large-scale models due to errors in input data, process simplification, and variations in historical management practices. Nevertheless, the model performance was deemed satisfactory for the majority of regions and time periods within the study area.

Table 4.1. Minimum, maximum, and average values for p-factor, r-factor, and MSE in the calibration and validation periods for spring wheat and canola using the CAR-based approach.

Spring wheat						
	Calibration			Validation		
	p-factor	*r-factor*	MSE	*p-factor*	*r-factor*	MSE
Minimum	0.50	1.15	0.01	0.26	0.93	0.02
Maximum	1.00	4.57	0.48	1.00	6.33	0.54
Average	0.89	2.05	0.16	0.78	2.20	0.18
Canola						
	Calibration			Validation		
	p-factor	*r-factor*	MSE	*p-factor*	*r-factor*	MSE
Minimum	0.60	1.55	0.05	0.65	1.11	0.07
Maximum	1.00	3.61	0.22	1.00	3.44	0.19
Average	0.87	2.41	0.10	0.83	2.28	0.11

4.4.2 Historical and future variation of WYLD, Y, and VWT under long-term average conditions for growing season

4.4.2.1 Precipitation patterns and WYLD

The analysis of historical data and projections for the growing season (May-September) under the SSP126 and SSP585 scenarios revealed noteworthy changes in precipitation (Figure 4.2a). Across the study area, monthly precipitation during the growing season varies considerably, ranging from 45 mm/month in the agricultural watersheds of southern Alberta and Saskatchewan to 100 mm/month in the southeastern region of our study area, which covers parts of both the Canadian and U.S. agricultural lands. The ensemble mean precipitation data from the six downscaled future climate data for the 2070-2099 period indicated that the majority of the study area will likely experience a precipitation increase of 6% and 10% per month for the growing season under SSP126 and SSP585 scenarios, respectively. Furthermore, the projected future scenarios demonstrated an increase in WYLD compared to the historical period. In particular, the monthly WYLD projections during the growing season showed an increase of 30% (i.e., 1.5 mm)

under SSP126 and more than 200% (i.e., 10 mm) under SSP585 relative to the historical period (Figure 4.2b).

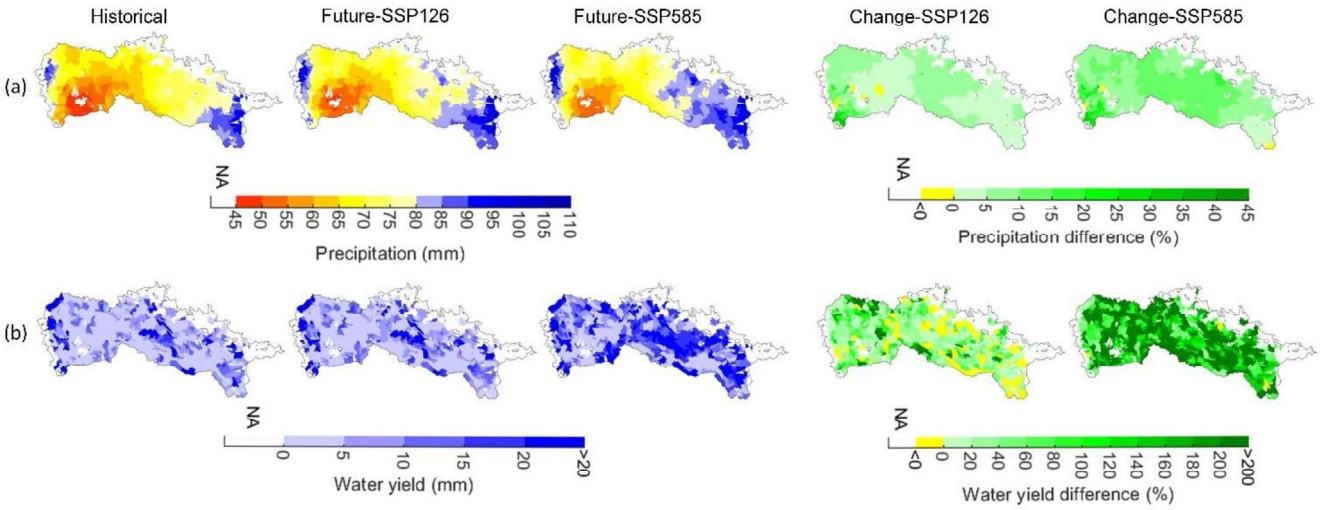

Figure 4.2. Simulated long-term average monthly WYLD (mm) and precipitation (mm) during the crop growing season (monthly averages during May-Sept): historical (first column), future SSP126 scenario (second column), future SSP585 scenario (third column), and the anomalies from the historical baseline for both future SSP126 (fourth column) and SSP585 (fifth column) scenarios.19

4.4.2.2 Rainfed wheat and canola yields

The simulated results for historical period indicated that the average spring wheat yields (2.3 tonne/ha) was higher than that of canola (1.4 tonne/ha) (Figure 4.3). For the historical period, simulated Y for both crops were higher in the eastern and western sub-basins of the study area, ranging between 2-5 tonne/ha for spring wheat and 1-3 tonne/ha for canola. Lower yields were observed in the central regions with approximately 0.5-3 tonne/ha for spring wheat and 0-2 tonne/ha for canola. The long-term average projected data showed that Y will likely increase under both SSP scenarios (SSP126 and SSP585). On average, the ensemble mean projected data showed that wheat and canola yields are likely to increase by 9% (2.3-2.6 tonne/ha) and 8% (1.3-1.5 tonne/ha) under SSP126, and by 26% (up to 2.9 tonne/ha) and 29% (up to 1.7 tonne/ha) under SSP585, respectively.

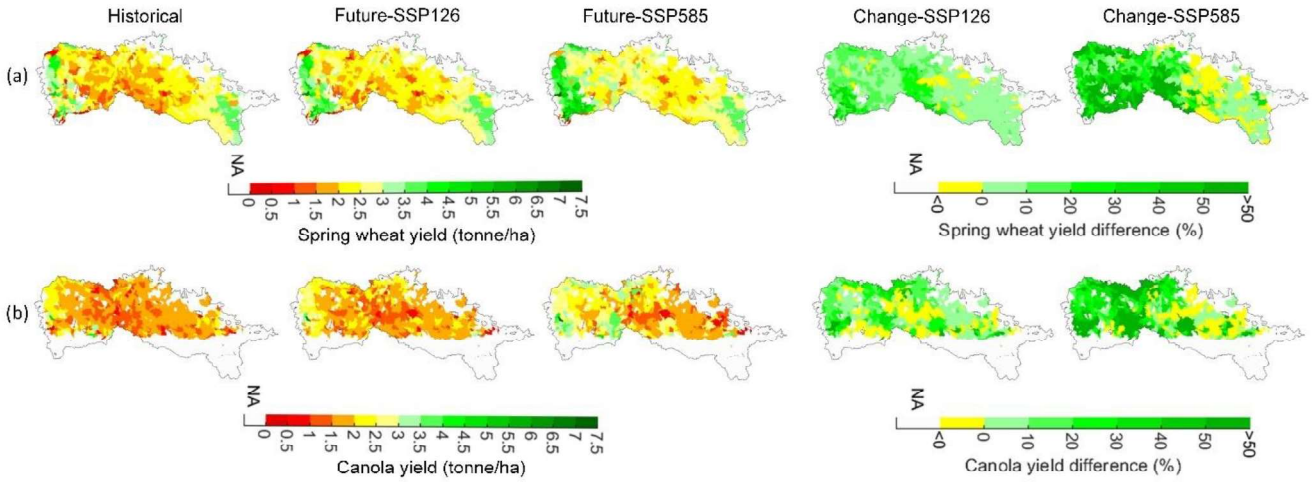

Figure 4.3. Simulated long-term average annual (1987-2016) crop yields for spring wheat and canola (tonne/ha) during crop growing seasons: historical baseline (first column from left), future SSP126 scenario (second column), future SSP585 scenario (third column), and anomalies from the historical baseline for both future SSP126 (fourth column) and SSP585 (fifth column) scenarios.20

4.4.2.3 VWC and VWT

Our simulated VWC for the rainfed wheat and canola crops during the historical period indicated that canola exhibits higher VWC (1000-2000 m^3/tonne) than spring wheat (700-1700 m^3/tonne), suggesting a greater water requirement for producing a tonne of canola compared to spring wheat (Figure 4.3a and 4.3c). VWC analysis of the western and eastern regions revealed that these regions are characterized by higher precipitation, greater ET, and lower VWC as compared to the central regions of the study area. Future VWC projections displayed a reduction from the SSP126 to SSP585 scenarios. The reduced VWC is attributed to the lower projected ET under the SSP585 scenario, where elevated CO_2 concentrations result in reduced stomatal closure in crops, decreasing plant transpiration (Deryng et al., 2016; Masud et al., 2019).

The analysis of modeled data indicated that, of the total net NVWE resulting from both spring wheat and canola, spring wheat accounts for an average of 66%, while canola constitutes the remaining 33%. This means that the spring wheat contributes two-thirds of the total NVWE,

with canola contributing one-third. The average annual NVWE were 41.4 billion m^3 and 20.9 billion m^3 for spring wheat and canola, respectively, totaling 62.3 billion m^3 per year for historical period. This was associated with the potential export of surplus crop grains that are not consumed, domestically. However, a considerable share of surplus crops is consumed in food industry and indirectly exported from the NRB. Some examples are the export of meat (e.g., beef), live animals (e.g., cattle, calves), dairy products, and beverages (StatCan, 2021). While this study did not explicitly calculate the VWC and VWT of these commodities, we assumed that all crop surplus could be directly exported in the form of grain.

Future export potential of wheat and canola crops under SSP126 scenario indicated likely export of 41.1 billion m^3 and 20.1 billion m^3 per year of virtual water, respectively, representing a relatively similar volume of NVWE to their historical volumes. This amount decreased to 38.5 billion m^3 and 19.5 billion m^3 under SSP585 scenario. It is important to note that we assumed future cropping areas remain the same as historical coverage. Overall, using the simulated Y for the future period, and based on historical crop area inventory maps, the projected annual export potential for wheat and canola are likely to increase from 35.1 and 12.6 million tonnes during historical period to 37.9 and 13.2 million tonnes under SSP126, respectively, with further increases up to 42.1 and 13.7 million tonnes under SSP585. Again, it should be emphasized that the projected increases in crop production and potential exports are based on the assumption that all of the projected crops are exported in the form of grain and they are not consumed by livestock and in meat production, which are normally exported from the region. However, the volume of crop production and export potentials and their associated NVWE can be different under drought and post-drought events, which are discussed in the following sections.

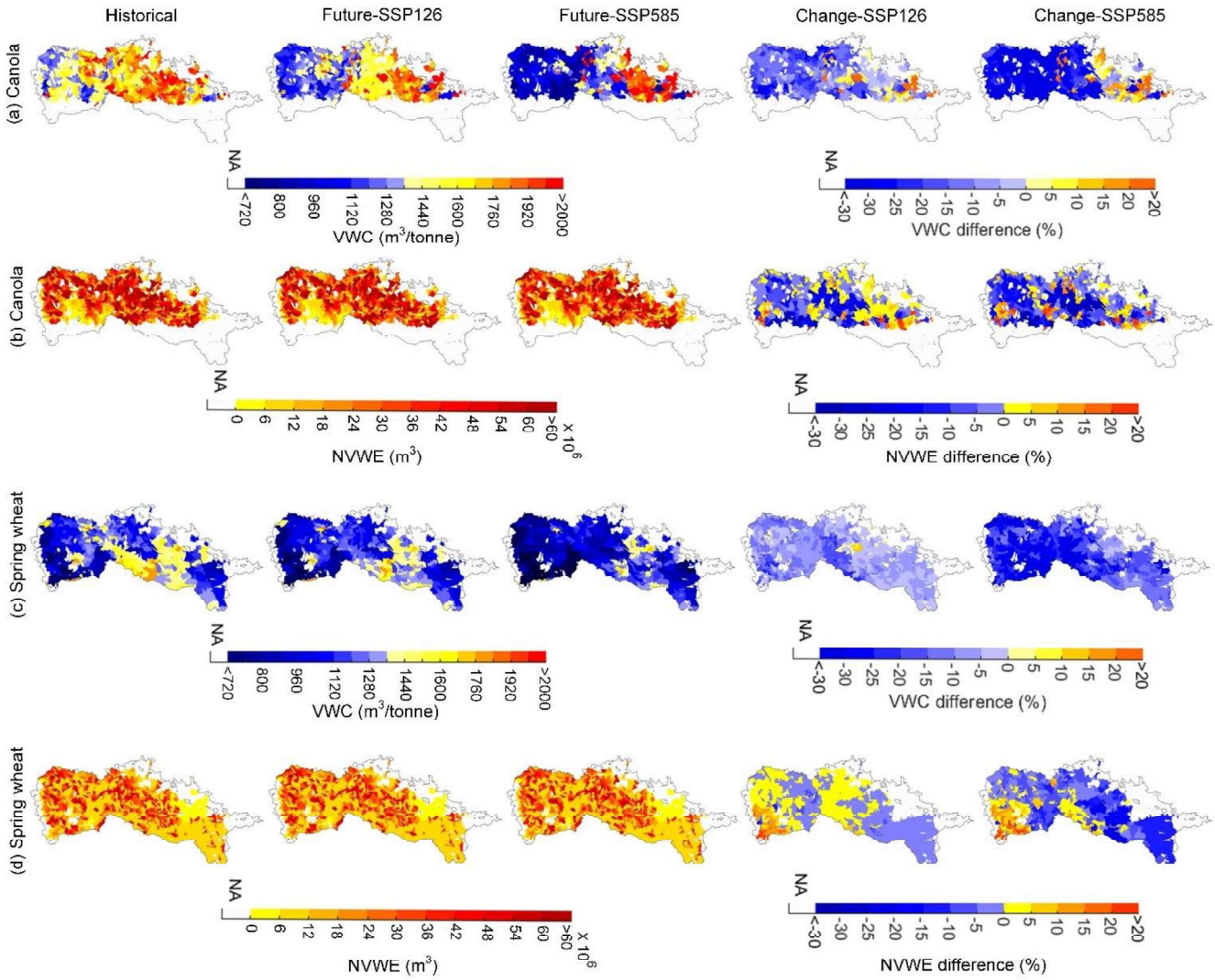

Figure 4.4. Long-term average simulated virtual water content (VWC; m³/tonne) and net virtual water export (NVWE; m³) for spring wheat and canola under historical and future scenarios (SSP126 and SSP585), accompanied by their projected anomalies as compared to the historical values (%) (right two columns).21

4.4.3 Impacts of drought and post-drought conditions on WYLD, Y, and VWT

4.4.3.1 WYLD, Y, and VWC response to droughts

The ensemble mean simulated duration of the LMDs for the historical period was 11 months, while it was 18.5 months for the SSP126 scenario, and 16.8 months for the SSP585 scenario. The average SPEI, representing different drought severities, followed a similar trend, being 1.1

(representing D1 drought) for the historical period, 1.7 (representing D3 drought) for the SSP126 scenario, and 1.5 (representing D2 drought) for the SSP585 scenario.

Under LMD events, the ensemble mean precipitation decreased in all scenarios (historical and future) for most of the NRB (Figure 4.5a). During historical period, the LMD events resulted in precipitation reduction of up to 17% as compared to historical average condition (Figure 4.5a). The projected precipitation during future LMDs indicated a reduction of up to 27% under the SSP126, and as high as 35% under the SSP585 as compared to the historical average condition (Figure 4.5a). This suggests a likely drier LMDs for the region in the future as compared to historical period. Unlike the long-term average projections which indicate a wetter overall future (Bush and Lemmen, 2019), with the SSP585 as the wettest scenario (Figure 4.2a), the projections under LMD indicates a drier conditions in the future as compared to average historical conditions. The LMD results also demonstrated a drier SSP585 than SSP126 as shown by reduced precipitating during the LMD years.

Despite the less magnitude of precipitation occurring under the LMD events of SSP585 scenario as compared to SSP126 and historical period, the WYLD increased by up to 80% in some areas under the projected LMD events of the SSP585 compared to the average historical period (Figure 4.5b). However, the 80% anomaly is particularly evident in the areas where WYLD is not substantial (e.g, of 0-5 mm) under historical average conditions (Figure 4.5b), resulting in a meager amount of water yields generated under the SSP585 scenario in the future. The 80% increase under the SSP585 scenario is also related to the elevated atmospheric CO_2 concentration, which leads to reduced crop water use, resulting in a greater proportion of precipitation contributing to water yield. In contrast, under LMD conditions of the SSP126 and historical years, we observed up to 55% and 50% reductions in water yield compared to the average historical period. This also

highlights the complex interplay between precipitation, CO_2 concentration, and water yield under various climate change scenarios (Khalili et al., 2021).The analysis of the spring wheat yields indicated a 32% reduction during historical LMD years as compared to the historical average condition (Figure 4.5c). However, under the SSP126 scenario, there was a 10% improvement with only a 22% reduction during LMD years, and almost no change during LMD years of the SSP585 scenario as compared to the historical average condition (Figure 4.5c). In contrast, canola yield showed only a 9% reduction during historical LMD years (Figure 4.5d), while SSP126 and SSP585 scenarios displayed up to a 29% and 6% decline, respectively, as compared to historical average condition (Figure 4.5d). The difference in percentage reductions between spring wheat and canola during historical droughts can be attributed to the fact that most precipitation decline occurs in the southeastern regions (Figure 4.5a), where canola is not extensively cultivated (Figure 4.1). The analysis of VWC, indicated increase of 0-50% across the NRB under the SSP126 and historical LMD years as compared to the historical average condition (Figure 4.5g, and 4.5h). This suggests a likely decrease of water use efficiency by crops (or increase of VWC), indicating a greater consumption of water to produce a tonne of wheat or canola during LMD events under both historical and SSP126 scenarios as compared to average conditions. The increase of VWC is attributed to either reduced Y (Figure 4.5c, and 4.5d), necessitating more water to produce a tonne of crop; or droughts are often accompanied by high temperatures and low humidity, both of which can increase soil water evaporation and ET (Trenberth et al., 2013; see Eq. 4.3). The SSP585 scenario showed an improvement of up to 30% in VWC under future LMDs (i.e., reduction in VWC) as compared to historical conditions (Figure 4.5g and Figure 4.5h), but yet in most areas where historical VWC was relatively low.

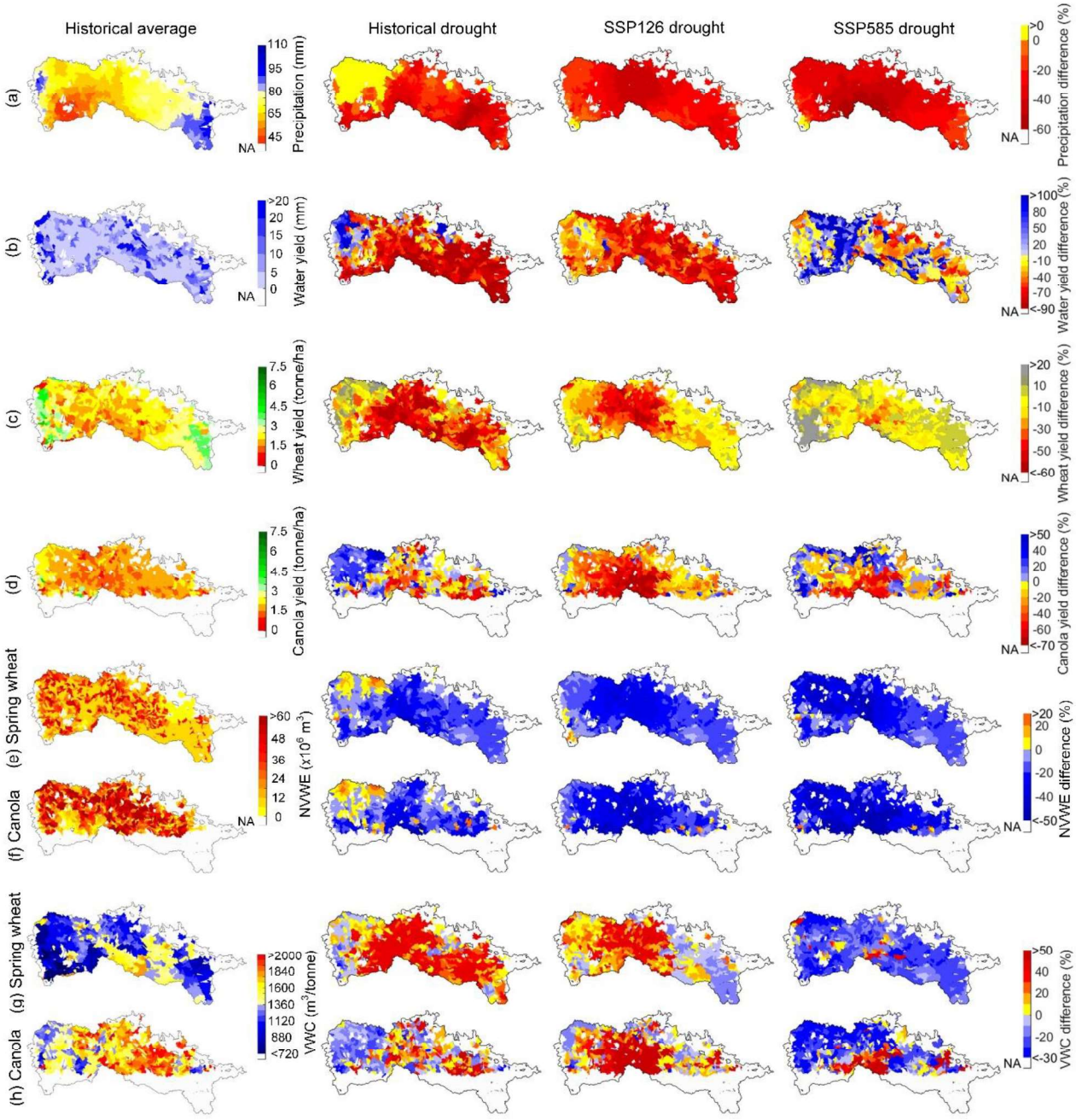

Figure 4.5. Simulated long-term average precipitation, WYLD, spring wheat yield, canola yield, NVWE, and VWC for historical (1987-2016) period (column 1, left), and their projected anomalies (% change) under extreme drought conditions (column 2 to 4, left). The anomalies are calculated based on ensemble mean simulated data under extreme droughts of historical, SSP126, and SSP585 scenarios from the average historical conditions, respectively.

4.4.3.2 Post-drought recovery of WYLD and Y and variations among regions

Analysis of data for post-drought period (D and ND scenarios, see Section 4.3.5), revealed variable recovery times for WYLD, Y, and VWT across different agricultural and ecohydrological regions as compared to non-drought conditions (Figure 4.6 and Figure 4.7). Under SSP 126, in some CARs (e.g., MA1, Figure 4.6d), it appears that even after five years following the drought; the WYLD does not fully recover. This is evident as the red line (representing the D scenario) consistently remains in a far proximity to the blue line (representing the ND scenario). Conversely, some other CARs, such as AB10 (Figure 4.6a), exhibit a rapid recovery, approximately after a year in the post-drought condition. This is attributed to the topographical characteristics, specifically, the steeper land gradients found in this region, as compared to other regions; lead to reduced infiltration of water. Instead, a larger proportion of precipitation contributes to surface runoff, leading to a faster recovery of WYLD after LMD events. As shown in Figure 4.6, in most of the CARs, the WYLD is not recovered immediately or after a few years from the termination of the LMD events (i.e., shown by red and blue lines remaining in distant proximity over the first few years). In most of the CARs, the two lines ultimately overlap after the first few years elapse, indicating that it takes approximately 3-5 years for the WYLD to recover from the LMD.

In contrast to WYLD results, no significant differences were found for Y under D and ND scenarios, especially for spring wheat (Figure 4.7, A.10, and A.12). This resilience of Y, despite the elapsed LMD, can be attributed to several factors. Primarily, the sustained Y during post-drought periods is related to the availability of soil moisture. After a drought event, the soil moisture is replenished by post-drought precipitation, making the soil water available for crop use and evapotranspiration (ET) rather than generating excess saturation for surface runoff and WYLD.

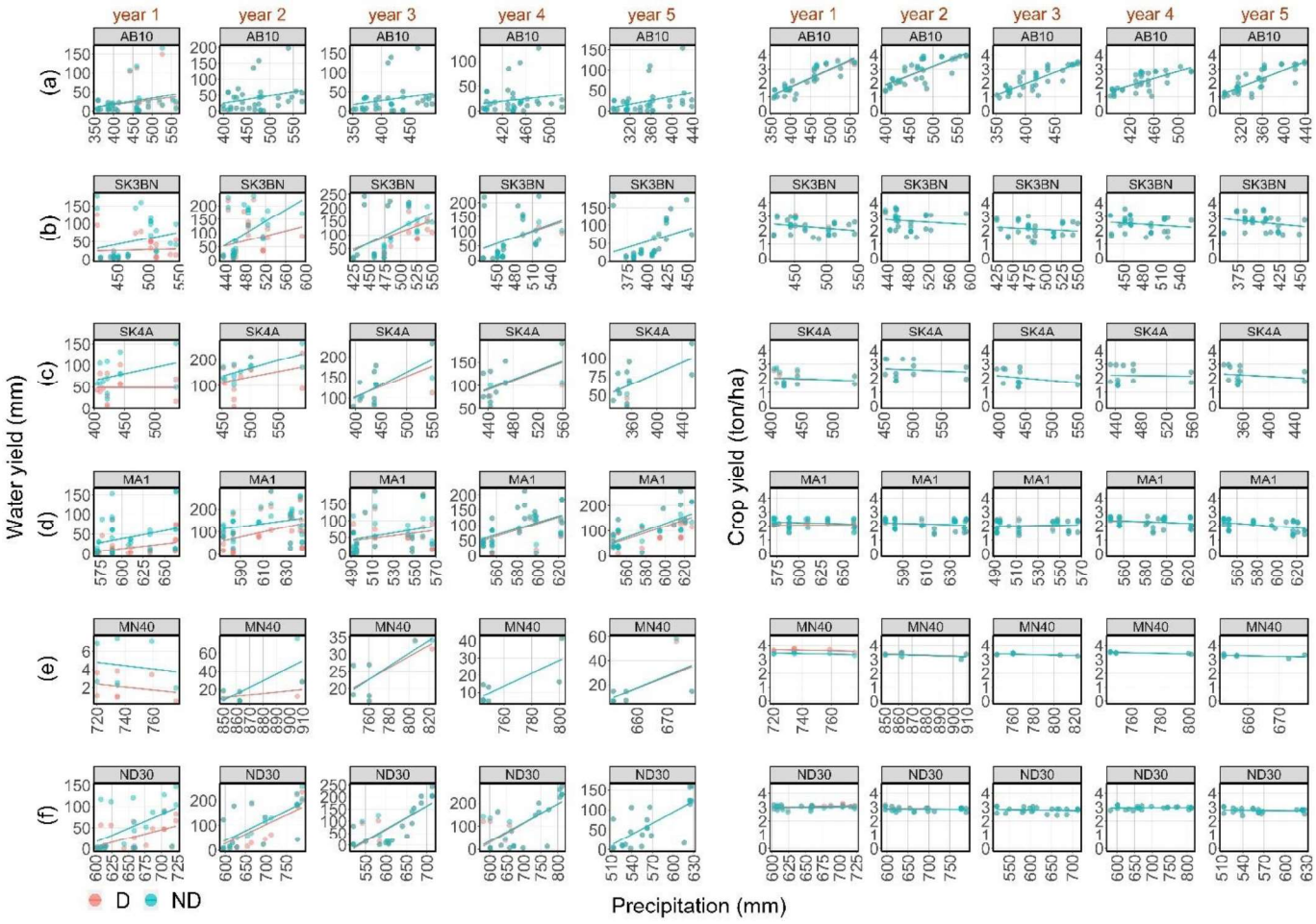

Figure 4.6. Simulated WYLD (left) and Y (right) versus cumulative precipitation in six selected CARs across the basin. The data are presented for the five consecutive post-drought years (D scenario, red) and the same years assuming no prior drought (ND scenario, blue) under the SSP126 future scenario. Only spring wheat Y is presented due to its prevalence in the basin. Each dot represents a sub-basin within a CAR.22

This is reflected in the WYLD results during post-drought periods, where recovery is not achieved shortly after the drought events (Figure 4.6). This suggests a greater or sustained wheat yields following the droughts are likely to occur in the future but at the expense of reduced WYLD in these regions. While several studies project promising Y for mid-to-high latitude areas in the future and following drought events (Challinor et al., 2014; He et al., 2018; M. B. Masud et al., 2018), these projections should be treated with caution. Our results illustrate that hydrological and water balance processes are closely connected with vegetation growth and crop types, emphasizing

the need for a multi-disciplinary approach for management of agricultural cropping patterns, land use changes, and watershed hydrology.

Another reason for Y resilience during a post-drought period is attributed to the potential accumulation of soil nutrients during drought years. During a LMD event, under rainfed condition, Y declines (Figure 4.5c, and 4.5d), implying that less nutrients are extracted from the soil (Rattalino Edreira et al., 2018). This can result in soil nutrient accumulation, which can be carried over to post-drought years creating a short-term positive 'legacy' effect for crops, resulting in an increase in their yields (Siebert et al., 2019; Bista et al., 2018). This process is more pronounced under future scenarios (i.e., SSP126 and SSP585), because with increasing atmospheric CO_2 concentrations, the water use efficiency and VWC can improve (Figure 4.4a, and 4.4c), resulting in improvement of Y under a reduced soil water conditions (Deryng et al., 2016; Khalili et al., 2021b; Masud et al., 2019). However, the availability and deficiency of nutrients in the soil can be a controlling factor, because elevated CO_2 concentrations can enhance potential crop growth, thereby increasing the nutrient demand from the soil as discussed by Khalili et al., (2021b).

It is noteworthy that similar to SSP126, wheat Y showed speedy recovery after the LMD events under the SSP585 and historical periods (Figure A.10, A.11). Overall, the regional average decrease of wheat Y immediately after the LMD (year 1) was only 0.9 tonne/ha for the historical period (Figure A.10), which was relatively similar for the SSP126 (i.e., 0.9 tonne/ha, Figure 4.7) and SSP585 (i.e., 1.2 tonne/ha, Figure A.11). The reduced Y was rapidly recovered in the following years until no difference was observed between the D and ND scenarios (i.e., Figure A.10j).

4.4.3.3 VWT recovery and differences under future scenarios

The analysis of our modeled data under SSP126 scenario indicated that the NVWE associated with the potential export of surplus wheat (presented as an example dominant crop) will

likely decrease by up to 4.7% (corresponding to 12.8 km^3) under the D as compared to the ND scenario in the first year after the LMD termination (Figure 4.7, Year 1). The reduction in NVWE in the first year after LMD was 2.4% (corresponding to 5.4 km^3) and 3.4% (corresponding to 8.5 km^3) under the historical (Figure A.12) and SSP585 (Figure A.13) scenarios, respectively. As shown in the figures, the reduction of NVWE in all scenarios is greater immediately after the LMD termination (i.e., positive anomalies in y-axis) and it diminishes by time reaching to near zero decline (i.e., a full recovery from drought, illustrated with zero anomalies in y-axis) during the later years (e.g., year 5). The SSP585 demonstrates the fastest recovery (Figure A.13), followed by SSP126 (Figure 4.7), and then the historical scenario (Figure A.12). As shown in Figure A.13, two years after the drought (i.e., in year 2) in SSP585 scenario, the NVWE under the D scenario exceeds that of the ND scenario, which is a different trend as compared to historical and SSP126 scenarios. This is because during post-drought period, soil water is replenished more rapidly under SSP585 than under other scenarios (Figure 4.2b, and 4.5b), which can aid dissolution of remaining soil nutrients from drought years (Bista et al., 2018), making them readily available for plant use. The availability of water and nutrients in the soil under D scenario drives plant growth and increases total volume of plant transpiration and ET (Liu et al. 2017). The increased volume of ET results in a greater NVWE under the D scenario compared to the ND scenario.

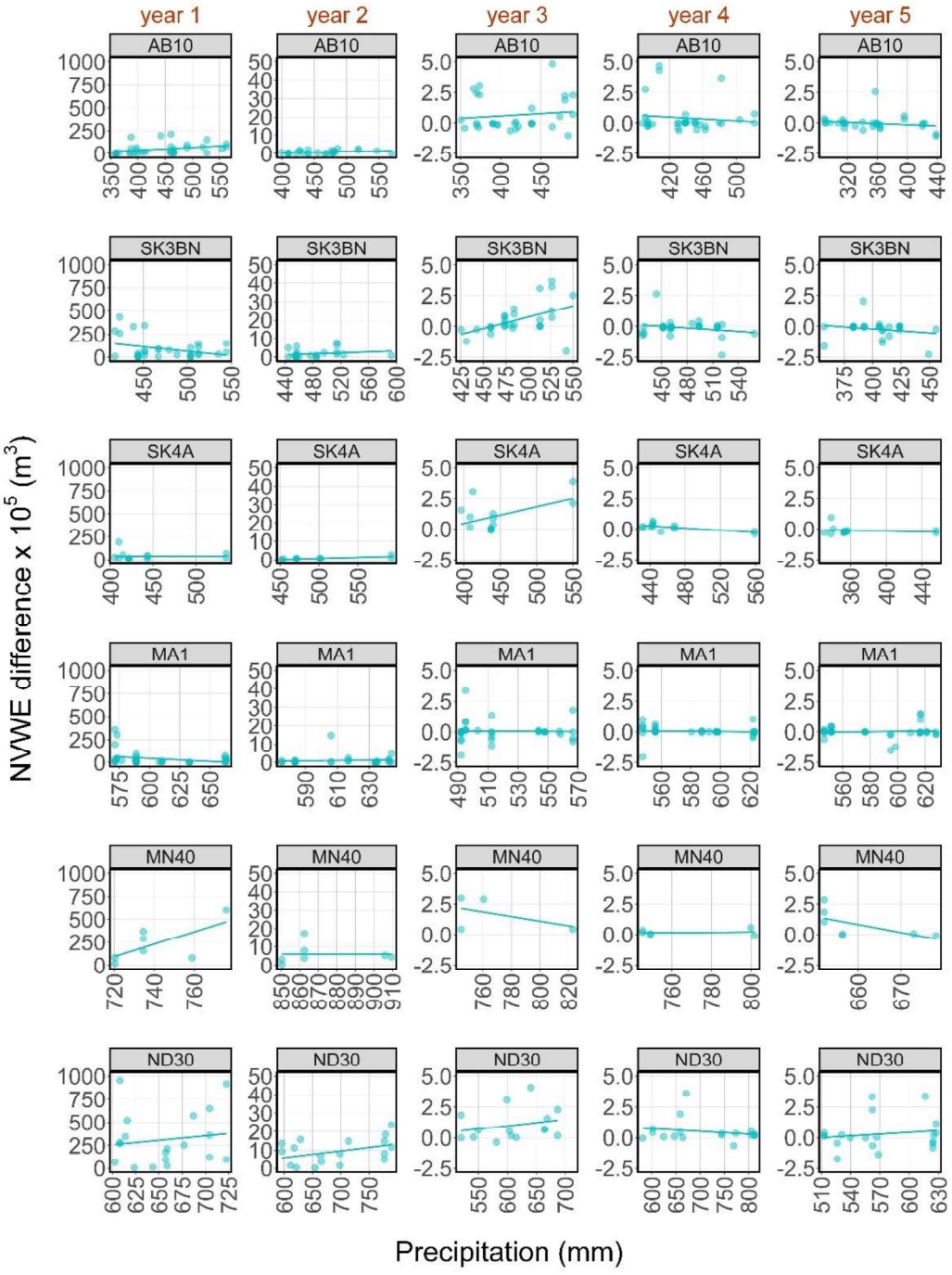

Figure 4.7. Simulated net virtual water export (NVWE) anomalies between D and ND scenarios (i.e., calculated as NVWE (D) - NVWE (ND)) in six selected CARs across the basin. The data are presented for five consecutive post-drought years under the SSP126 future scenario. Only spring wheat NVWE anomalies ($\times 10^5$ m³) is presented due to its prevalence in the basin. Each dot represents a sub-basin within a CAR.23

4.5 Global and regional implications

The results of this study have compelling implications for the agricultural watersheds of mid-to-high latitude regions, particularly concerning VWT for post-drought periods. As one of the major global agricultural exporters in the mid-to-high latitude regions, the Nelson River Basin covering most of Canadian Prairies, plays a crucial role in global food security (Bajracharya et al., 2020). Unlike the long-term average projections from the global studies, which often suggest a wetter overall future (Bush and Lemmen, 2019; Collins et al., 2013; IPCC, 2021) in the mid-to-high latitude regions, our study projections under extreme drought events indicate a reduced precipitation and drier condition in the future as compared to the past.

While agricultural watersheds of the mid-to-high latitude areas, especially the Canadian Parries, are susceptible to extreme drought conditions, often resulting in a significant yield loss (Lesk et al., 2016), the results of this and other studies demonstrated that the Y will likely improve in the future depending on the global warming scenarios (Rosenzweig et al., 2014). However, our results revealed that the improvement of Y under extreme droughts will likely be compounded by increases in their VWC, meaning that more water will be consumptively used by crops to produce a tonne of the same crop as compared to the historical conditions. This will likely cost a substantial depletion of the net annual freshwater generated in hydrologic catchments and, therefore, reduction in water yields as shown in this research. The reduced water yield may have serious implications for economic sectors and ecosystem (Vörösmarty et al., 2010), including also the irrigated crop production and export potentials during extreme drought conditions in these regions (Deryng et al., 2014).

During post-droughts, our results indicated a decrease in NVWE, with a stable rainfed Y following drought events in the future. However, the reduced NVWE and sustained yields

following drought events in the future are associated with a substantial decline in water yield in both historical and future scenarios. The continued decline of water yield during and after droughts as shown in this study can exacerbate the impacts of droughts on various economic sectors (Rosa et al., 2020) and the environment (Gleeson et al., 2020). The aquatic environment, for instance, is highly sensitive to the concentration of nutrients and organic material (Moe et al., 2016). The decline of water yield during and after severe droughts as shown in this study can reduce streamflow, especially in upstream tributaries and in low flow seasons, which can then increase concentration of chemicals and nutrients, triggering aquatic health. Therefore, an integrated assessment and management of agricultural Y, virtual water export associated with potential export of crops, and the linkages with hydrological water balance (e.g., WYLD) is crucial for sustainable management of water and food and for adaptation to climate change extremes.

Our study showed considerable differences in Y, VWC, and WYLD between wheat and canola crops during drought periods. For instance, wheat crop exhibited lower VWC during drought events compared to the canola crop. Therefore, changes in cropping pattern, e.g., selection of optimum crop types during and after extreme droughts, can be a promising strategy for improved WYLD and integrated management of water and food under extreme climate conditions in the agricultural watersheds of mid-to-high latitude regions. However, more crops (e.g., drought-tolerant crop varieties) should be examined using the approach and the framework we have developed in this study.

Another approach to conserve WYLD while maintaining Y during and after droughts, could be implementing soil conservation practices and enhancing water retention capacity, such as conservation tillage, cover cropping, and mulching (Powlson et al., 2011). These practices help maintain adequate soil moisture for rainfed crops during and after droughts, which can help

conserving WYLD and hydrologic water balance (Zhang et al., 2020). However, the tradeoffs and the effects of such practices should be systematically examined in a modelling framework similar to this study.

Our study indicated that NVWE of wheat is different from that of canola under extreme drought conditions. Given that the VWC of the corps vary spatiotemporally and among crops, too, diversification in NVWE could be another strategy to improve soil water and, therefore, WYLD under extreme droughts in the future. Optimizing crop structure pattern corresponding to virtual water trade strategy has been suggested in a limited number of studies (Antonelli and Sartori, 2015; Faramarzi et al., 2010; Huang et al., 2023) and more in the context of water scarce countries. However, a modelling framework similar to this study provides the basis for examining how the optimum cropping pattern strategy and NVWE can conserve WYLD under the future extreme droughts and how it helps a sustainable agricultural production and global food supply in crop exporting watersheds of mid-to-high latitude regions.

Overall, this study underscores the importance of addressing global and regional implications of drought and post-drought periods in crop exporting regions, such as in Canadian Prairies. The projected reduced NVWE, stable rainfed Y, and reduced water yield observed in our study present both challenges and opportunities for the region. By adopting strategies that optimize Y while also conserving water yield and minimizing net virtual water export, can foster a more sustainable and resilient economy, environment, and agricultural system. Development of interdisciplinary research studies are key for examining and incorporating these factors into regional and global agricultural policies and water management strategies for adaptation to global food crisis, especially under extreme climate events.

4.6 Conclusions

This research provides insights into the linkages between WYLD and crop Y, and it projects NVWE as a measure to investigate the production and export potentials of an agricultural watershed in high latitude temperate zone under future global warming scenarios. The study illuminates the often-counterintuitive impacts of future drought and post-drought conditions on reliability of global breadbaskets, by modelling WYLD, Y, and NVWE in NRB, a large agricultural watershed in western Canada that supplies food to over 170 countries globally.

The study results reveals a wetter overall future with larger precipitation, greater WYLD, and improved Y under SSP126 and SSP585 scenarios as compared to the historical period, only when the modelled data are averaged over the study period (35 years in this study). Under both SSP scenarios, the long-term average data shows a reduction of NVWE associated with the export of greater volume of rainfed wheat and canola from the NRB as compared to the average historical period. However, the inter-related response of agro-hydrological variables (i.e., crop Y, WYLD, VWC, NVWE) to future droughts and post-droughts, are considerably different from those of average historical conditions.

Contrary to the long-term average projected results, suggesting an improved future for Y, WYLD, and NVWE, the results of regional LMD drought indicate a substantial reduction in precipitation, Y (rainfed wheat and canola in this study), as well as WYLD in the future. Under SSP126, the reduction of precipitation, WYLD, Y, and NVWE during future droughts remain the same or become more severe than historical droughts, specifically in the central regions, which are prominent for grain production in the NRB.

A deeper investigation of the modelled data, under future LMD conditions, reveals that agro-hydrological variables slightly improve under the SSP585 scenario due to the CO_2 effects on plant

photosynthesis processes. However, the improvement of Y is not uniform across the region and crop types, with canola Y demonstrating less improvement as compared to the wheat Y, which is compounded with a greater VWC of canola than wheat. The larger VWC of canola in central areas, suggests larger crop water consumption in production of a tonne of crop, resulting in a considerable reduction of WYLD as compared to wheat crop and relative to the other regions across NRB. Overall, the regional scale WYLD, Y, and VWC show improvement during SSP585 droughts as compared to those of SSP126; however, they remain considerably lower than the average historical conditions regardless of crop type and the geographic location.

Analysis of data for post-drought period, reveals variable recovery times for WYLD, Y, and NVWE in the future, with the WYLD demonstrating slower recovery time as compared to Y during the years after an LMD. The study results show a decrease in NVWE during post-drought years, with a stable rainfed Y following the years after the drought termination in the future. However, the reduced NVWE with sustained Y following the drought events in the future are associated with a substantial decline in WYLD. The continued reduction in WYLD during the years following droughts can significantly affect not only environment ecosystem and several economic sectors, but also consequently crop production and export potential from these regions. Given the differences in VWC of crops, such as rainfed wheat and canola in this study, a strategic crop selection and diversification can be considered as an adaptation measure for conservation of WYLD for an integrated water and food security.

4.7 Acknowledgment

Funding for this study is primarily provided by the Natural Sciences and Engineering Research Council of Canada (Grant #RES0043463) and Campus Alberta Innovation Program Chair (Grant #RES0034497).

4.8 Credit author statement

Pouya Khalili: Data curation, Formal analysis, Methodology, Software, Validation, Visualization, Writing - original draft, Writing - review & editing. **Monireh Faramarzi:** Supervision, Conceptualization, Writing - review & editing, Project administration, Funding acquisition.

CHAPTER V – CONCLUSION

5.1 Research Summary

The unfolding climate change crisis poses a growing challenge to water and food security, and yet the reliability of the global breadbaskets and their relation with water resources in the future is poorly understood. The global breadbaskets are defined as key production regions for food grains and recognized for their vital contribution to global food security. In the high latitude watersheds of the temperate zone, the global breadbaskets are projected to receive an overall increased precipitation and improved crop yields under the effects of global warming scenarios, which is often perceived as beneficial to crop production and export potentials in the future (Myers et al., 2017; IPCC, 2021). However, the extreme warm-dry events, anticipated as a consequence of global warming, can significantly affect the agro-hydrological processes, crop yields, and therefore export potential of the crops from these regions. This research examines the potential impacts of future droughts and post-droughts on hydrology, crop yields, and their linkages through assessing NVWE, the water embodied in the production process of the crops that are exported to international countries. The study examines NRB a large agricultural watershed in western Canada, which is one of the high latitude breadbaskets of the temperate zone, and provides insights for future planning and informed decisions for water and food security.

To understand the hydrological processes affecting crop yield and soil nutrients (i.e., nitrogen in this study) and their relation with changes in climate, this study employs a semi-distributed process-based agro-hydrologic model to an agricultural catchment in the NRB, i.e., RDRB, in the province of Alberta, Canada. Specifically, the research explores the effects of climate change and availability of soil water, as well as nitrogen fertilizer application scenarios on

crop yields. The study examines the impacts on rainfed spring wheat, which is a dominant crop grown in most of NRB and in the RDRB. The results indicate that nitrogen stress may dominate other stress factors in producing rainfed wheat yields in the future as compared to the historical conditions that water-stress has been a dominant factor in the region. This is likely due to the overall increase in soil moisture expected in the future that when compounded with a warmer temperature, triggers crop growth and potential yields, demanding more nitrogen in the soil. However, a regional assessment of the soil water availability, which affects nutrient and water uptakes by crops and their evapotranspiration rates (ET, green water), and the effects on hydrological water balance under extreme climatic events such as droughts in the future, is required.

In a closed hydrological system, i.e., a watershed, the blue water (BW, or net annual freshwater generated in a catchment) and green water (GW, or actual evapotranspiration) are interlinked through numerous climate, soil, and plant processes. Their relationship has reportedly been non-stationary, with an anticipated shift from BW to GW in the future. Importantly, GW represents a significant portion of water consumption in global food production, with agricultural water withdrawals accounting for 70% globally. Further research in this study scrutinizes the interlinkages between BW and GW and their potential shifts, primarily in response to future extreme warm-dry events. The results indicate dissimilarity in the physical processes that link GW and BW across different ecohydrological regions, and therefore, disproportional projected changes in BW and GW. Mountainous and natural lands exhibit a shift from BW to GW, due to legacy soil moisture from earlier seasons and groundwater contributions. Conversely, in crop lands, there is a significant decrease in both BW and GW with no notable shift from BW to GW, posing severe threats to local and regional food production.

Lastly, the research evaluates the effects of drought and subsequent post-drought conditions on crop production and its relation to watershed hydrology (i.e., water yield in this study) through assessment of NVWE. Contrary to prevalent long-term average projections of a wetter future for high latitude regions of temperate zone, this research suggests a potentially drier future due to reduced precipitation and water yield under extreme drought scenarios in the future. The study suggests improvement of crop yields under future droughts of SSP585 scenario as compared to historical drought conditions, yet lower than historical average yields. The crop yield improvement is compounded by an increase in VWC, suggesting likely increase in crop water consumption in production of a tonne of crop, resulting in a considerable reduction of water yield as compared to historical conditions.

During post-drought conditions, the study results indicate a decrease in NVWE, along with a stable yield of rainfed crops in the future. However, the reduced NVWE and sustained yields following drought events in the future are associated with a substantial decline in water yield in both historical and future scenarios. The continued reduction in water yields during the years following droughts can significantly impact not only environment and several economic sectors but consequently crop production and export potential from these regions.

5.2 Study Conclusions and Implications

With the overarching goal of understanding the GW-BW linkages and their relation to crop yields and NVWE under average historical and future conditions, and their anomalies under future extreme climatic events—especially warm and dry spells—and their post-drought recovery, each chapter has made specific conclusions that contribute to this grand understanding:

Objective 1 (chapter 2): *Provide an improved understanding of non-stationary crop yield response to climate change-induced agro-hydrological processes and management factors at a regional scale.*

In **chapter 2**, the primary conclusion drawn revolves around the non-stationary response of spring wheat yield (SWY) to climatic changes and elevated CO_2 levels. This response is complex, influenced by a variety of factors such as soil type, hydrological regime, location, and management practices. The study explores that nitrogen (N) stress may dominate other stress factors in producing rainfed wheat yields in the future as compared to the current conditions that water-stress is a dominant factor. It argues that the future N stress might be due to (1) reduced evapotranspiration and earlier stomatal closure in response to saturated atmospheric CO_2, (2) insufficient N availability in the soil, and (3) insufficient moisture in the soil to produce soluble N for plants to uptake. The study concludes that a higher N application with supplement irrigation might be a potential measure to enhance yields under a changing climate. However, water availability for irrigation (i.e. BW), its connection with changes in GW, as well as land and water quality concerns due to a higher rate of fertilizer application can raise environmental issues and limit the sustainability goals of agricultural practices in the region. These results bear important implications for water-food-climate change studies and global food security, which guides the current research study to the following objective-chapter for examination of GW-BW interchange at the large NRB scale, which is a critical SWY producing area and a global breadbasket in the northern latitudes of the global temperate zone.

Objective 2 (chapter 3): *Characterize changes in GW-BW relationships under future warm-dry events across different landscape and ecohydrological settings.*

In **chapter 3**, the study delves into the interlinkages between BW and GW and potential shifts from BW to GW under extreme warm-dry years of global warming scenarios. The research demonstrates that the GW-BW relationship varies across different ecohydrological regions and under different global warming scenarios, with implications for various ecosystem services. Under future extreme warm-dry events, the study suggests dissimilarity in the physical processes that link GW and BW across different ecohydrological regions, and therefore, disproportional projected changes in BW and GW, and their linkages across regions. Mountainous and natural lands exhibit a shift from BW to GW, due to legacy soil moisture from earlier seasons and groundwater contributions. Conversely, in crop lands, there is a significant decrease in both BW and GW with no notable shift from BW to GW. The projected BW and GW declines in crop lands may impose severe water shortages on local and regional food production. Projected declines of BW in the mountains that serve as source water for downstream irrigation may exacerbate such possible shortages. The findings and the study framework in this chapter, lays the basis for a deeper evaluation of the linkages between GW-BW resources, crop yields, and NVWE in chapter 4.

Objective 3 (chapter 4): *Examine the impacts of future droughts and post-droughts on crop yields, crop production and NVWE, and their effects and relations to water resources.*

In **chapter 4**, the research further investigates the interplay between climate extremes, particularly drought and post-drought conditions, and the hydrological and agricultural processes in the NRB, one of the breadbaskets located at the high latitudes of temperate zone. The research provides insights into the linkages between WYLD and crop Y, through assessment of NVWE. The study results reveals a wetter overall future with larger precipitation, greater WYLD, and improved Y under SSP126 and SSP585 scenarios as compared to the historical period, only when the modelled data are averaged over the study period (35 years in this study). Under both SSP

scenarios, the long-term average data shows a reduction of NVWE associated with the export of greater volume of rainfed wheat and canola from the NRB as compared to the average historical period. However, the inter-related response of agro-hydrological variables (i.e., crop Y, WYLD, VWC, NVWE) to future droughts and post-droughts, are considerably different from those of average historical conditions.

Contrary to the long-term average projected results, suggesting an improved future for Y, WYLD, and NVWE, the results of regional LMD drought indicate a substantial reduction in precipitation, Y (rainfed wheat and canola in this study), as well as WYLD in the future. Under SSP126, the reduction of precipitation, WYLD, Y, and NVWE during future droughts remain the same or become more severe than historical droughts, specifically in the central regions, which are prominent for grain production in the NRB.

A detailed investigation of the modelled data, under future LMD conditions, reveals that agro-hydrological variables slightly improve under the SSP585 scenario due to the CO2 effects on plant photosynthesis processes. However, the improvement of Y is not uniform across the region and crop types, with canola Y demonstrating less improvement as compared to the wheat Y, which is compounded with a greater VWC of canola than wheat. The larger VWC of canola in central areas, suggests larger crop water consumption in production of a tonne of crop, resulting in a considerable reduction of WYLD as compared to wheat crop and relative to the other regions across NRB. Overall, the regional scale WYLD, Y, and VWC show improvement during SSP585 droughts as compared to those of SSP126; however, they remain considerably lower than the average historical conditions regardless of crop type and the geographic location.

Analysis of data for post-drought period, reveals variable recovery times for WYLD, Y, and NVWE in the future, with the WYLD demonstrating slower recovery time as compared to crop

yields during the years after an LMD. The study results show a decrease in NVWE during post-drought years, with a stable rainfed Y following the years after the drought termination in the future. However, the reduced NVWE with sustained Y following the drought events in the future are associated with a substantial decline in WYLD. The continued reduction in WYLD during the years following droughts can significantly affect not only environment ecosystem and several economic sectors, but also consequently crop production and export potential from these regions. Given the differences in VWC of crops, such as VWC of rainfed wheat and canola in this study, a strategic crop selection and diversification can be considered as an adaptation measure for conservation of WYLD for an integrated water and food security.

5.3 Study Limitations and Future Directions

While this research provides a thorough examination of the impacts of climate change on agricultural productivity and water resources, it acknowledges several limitations, reflecting the inherent uncertainty that is common in regional modeling efforts. It should be noted that large-scale models suffer from various sources of uncertainty including input data, model conceptualization, observed data used for calibration, and model parameters (Abbaspour et al., 2015).

One of the assumptions made in this study was related to the use of cultivars, crop varieties, and sowing dates under future scenarios, which remained the same as historical period. Similarly, the operation of large dams included in the historical simulation remained unchanged for future projections. However, given that the focus of this research was on assessment of water yield (the amount of fresh water generated in each sub-basin) rather than prediction of of future stream flows for water allocation and managements, flood projections, or similar studies, the conclusions of this study remain reliable.

Other assumptions in the current research extend to large-scale disturbances such as forest mortality, species changes, and plant acclimation. These factors may influence the GW-BW accounting in natural lands or foothills, where natural disturbances such as wildfires or anthropogenic factors such as forest logging, have potentially influenced vegetation composition and hydrologic water balance. However, given that the focus of this research was on regional scale water-food relationship and mainly agricultural production and NVWE, the conclusions still remain valid. A further analysis of the effects of such land disturbances, using socio-hydrological modelling, can improve reliability in the future studies.

Assumptions made about mountainous regions, specifically the contribution of glacial melt runoff to upstream tributaries. The current research used modelled glacier data from an earlier study for the historical period, and assumed they remain similar in the future. However, changes in glacier melt and their evolution could alter streamflow, especially in headwater catchments, warranting closer attention in future studies.

Data used in our research, such as soil properties, climate data, and land management data, were derived from various sources, each carrying specific resolution and accuracy. Some of our soil data came from regional soil maps with coarse resolution, which could possibly contribute to uncertainty. A limitation associated with data collection was the unavailability of instrumental data for extended periods, resulting in a short prediction period. This increases the variance of study variables, requiring further investigation in future studies. To address these limitations, availability of higher-resolution datasets is fundamental, which encourages a more extensive environmental monitoring.

This research did not explicitly examine the effect of biotic stressors, including pests, diseases, and weeds. In light of their probable increase under warmer and wetter conditions, future

studies should consider their impacts on crop yield projections. Additionally, the genetic improvement of crops, an important aspect not considered, could counteract adverse effects of abiotic stressors like drought, on future crop yields.

This study also did not account for the influence of economic activities on water use. A substantial portion of crop surplus in the NRB is indirectly exported through meat, live animals, dairy products, and beverages. However, the study did not explicitly calculate the VWC and NVWE associated with these commodities, but assumed all crop surplus is directly exported in the form of grain. Future research could reduce uncertainty by including the commodity-specific export of virtual water from the region. Moreover, consideration of socio-economic factors influencing spatiotemporal volume of trade of commodities, e.g., food prices, land availability, labor cost, subsidies, taxes, domestic and international markets, and transportation can reduce uncertainty in projection of future NVWE from the region.

In summary, improved monitoring and measurement of important data, as explored and explained in this study, can provide opportunities for a more comprehensive assessment of water-food relationships and it provides a robust basis for adaptation to future extreme events such as those studied in this research.

BIBLIOGRAPHY

Abbaspour, K., 2015. SWAT-Calibration and uncertainty programs (CUP), Neprashtechnology.Ca. https://doi.org/10.1007/s00402-009-1032-4

Abbaspour, K.C., Rouholahnejad, E., Vaghefi, S., Srinivasan, R., Yang, H., Kløve, B., 2015. A continental-scale hydrology and water quality model for Europe: Calibration and uncertainty of a high-resolution large-scale SWAT model. https://doi.org/10.1016/j.jhydrol.2015.03.027

Abbaspour, K.C., Yang, J., Maximov, I., Siber, R., Bogner, K., Mieleitner, J., Zobrist, J., Srinivasan, R., 2007. Modelling hydrology and water quality in the pre-alpine/alpine Thur watershed using SWAT. J. Hydrol. 333, 413–430. https://doi.org/10.1016/j.jhydrol.2006.09.014

Abedinpour, M., Sarangi, A., Rajput, T.B.S., Singh, M., Pathak, H., Ahmad, T., 2012. Performance evaluation of AquaCrop model for maize crop in a semi-arid environment. Agric. Water Manag. 110, 55–66. https://doi.org/10.1016/j.agwat.2012.04.001

Abiodun, O.O., Guan, H., Post, V.E.A., Batelaan, O., 2018. Comparison of MODIS and SWAT evapotranspiration over a complex terrain at different spatial scales. Hydrol. Earth Syst. Sci 22, 2775–2794. https://doi.org/10.5194/hess-22-2775-2018

Ackley, S.F., 2012. The Global Cryosphere, Past, Present and Future. By Roger Barry and Thian Yew Gan [WWW Document]. Arctic, Antarct. Alp. Res. https://doi.org/10.1657/1938-4246-44.4.520a

Addy, K., Gold, A.J., Welsh, M.K., August, P. V., Stolt, M.H., Arango, C.P., Groffman, P.M., 2019. Connectivity and nitrate uptake potential of intermittent streams in the Northeast USA. Front. Ecol. Evol. 7, 225. https://doi.org/10.3389/fevo.2019.00225

Adimassu, Z., Langan, S., Johnston, R., Mekuria, W., Amede, • Tilahun, 2017. Impacts of Soil and Water Conservation Practices on Crop Yield, Run-off, Soil Loss and Nutrient Loss in Ethiopia: Review and Synthesis. Environ. Manage. 59, 87–101. https://doi.org/10.1007/s00267-016-0776-1

Ahmed, K.F., Wang, G., Silander, J., Wilson, A.M., Allen, J.M., Horton, R., Anyah, R., 2013. Statistical downscaling and bias correction of climate model outputs for climate change impact assessment in the U.S. northeast. Glob. Planet. Change 100, 320–332. https://doi.org/10.1016/j.gloplacha.2012.11.003

Ahmed, M., Stöckle, C.O., Nelson, R., Higgins, S., Ahmad, S., Raza, M.A., 2019. Novel multimodel ensemble approach to evaluate the sole effect of elevated CO2 on winter wheat productivity. Sci. Rep. 9. https://doi.org/10.1038/s41598-019-44251-x

Alberta Agricultural and Rural Development, 2004. Alberta Fertilizer Guide [WWW Document]. URL https://www1.agric.gov.ab.ca/$department/deptdocs.nsf/all/agdex3894/$file/541-1.pdf?OpenElement (accessed 7.3.19).

Allan, J.A., 1998. Virtual water: a strategic resource. Ground Water 36, 545–547.

Allan, J.A., 1993. Fortunately there are substitutes for water otherwise our hydro-political futures would be impossible, Priorities for Water Resources Allocation and Management; ODA: London, UK.

Ammar, M.E., Gharib, A., Islam, Z., Davies, E.G.R., Seneka, M., Faramarzi, M., 2020. Future floods using hydroclimatic simulations and peaks over threshold: An alternative to nonstationary analysis inferred from trend tests. Adv. Water Resour. 136, 103463. https://doi.org/10.1016/j.advwatres.2019.103463

Anderson, P., Markham, J., 2021. Soil temperature limits nitrogen fixation, photosynthesis, and growth in a boreal actinorhizal shrub. Plant Soil 468, 411–421. https://doi.org/10.1007/S11104-021-05127-0/TABLES/2

Angulo, C., Rötter, R., Lock, R., Enders, A., Fronzek, S., Ewert, F., 2013. Implication of crop model calibration strategies for assessing regional impacts of climate change in Europe. Agric. For. Meteorol. 170, 32–46. https://doi.org/10.1016/j.agrformet.2012.11.017

Anjum, S.A., Ashraf, U., Zohaib, A., Tanveer, M., Naeem, M., Ali, I., Tabassum, T., Nazir, U., 2017. Growth and developmental responses of crop plants under drought stress: a review. Zemdirbyste-Agriculture 104, 267–276. https://doi.org/10.13080/z-a.2017.104.034

Antonelli, M., Sartori, M., 2015. Unfolding the potential of the virtual water concept. What is still under debate? Environ. Sci. Policy 50, 240–251. https://doi.org/10.1016/J.ENVSCI.2015.02.011

Arnell, N.W., Gosling, S.N., 2013. The impacts of climate change on river flow regimes at the global scale. J. Hydrol. 486, 351–364. https://doi.org/10.1016/j.jhydrol.2013.02.010

Arnold, J.G., Allen, P.M., Bernhardt, G., 1993. A comprehensive surface-groundwater flow model. J. Hydrol. 142, 47–69. https://doi.org/10.1016/0022-1694(93)90004-S

Arnold, J.G., Srinivasan, R., Muttiah, R.S., Williams, J.R., 1998. LARGE AREA HYDROLOGIC MODELING AND ASSESSMENT PART I: MODEL DEVELOPMENT. J. Am. Water Resour. Assoc. 34, 73–89. https://doi.org/10.1111/j.1752-1688.1998.tb05961.x

Arora, G., Feng, H., Anderson, C.J., Hennessy, D.A., 2020. Evidence of climate change impacts on crop comparative advantage and land use. Agric. Econ. 51, 221–236. https://doi.org/10.1111/agec.12551

Arya, S., 2021. Freshwater Biodiversity and Conservation Challenges: a Review. Int. J. Biol. Innov. 03, 75–78. https://doi.org/10.46505/ijbi.2021.3106

Aryal, A., Shrestha, S., Babel, M.S., 2019. Quantifying the sources of uncertainty in an ensemble of hydrological climate-impact projections. Theor. Appl. Climatol. 135, 193–209. https://doi.org/10.1007/s00704-017-2359-3

Ashraf Vaghefi, S., Iravani, M., Sauchyn, D., Andreichuk, Y., Goss, G., Faramarzi, M., 2019. Regionalization and parameterization of a hydrologic model significantly affect the cascade of uncertainty in climate-impact projections. Clim. Dyn. 1–26. https://doi.org/10.1007/s00382-019-04664-w

Avanzi, F., Rungee, J., Maurer, T., Bales, R., Ma, Q., Glaser, S., Conklin, M., 2020. Climate elasticity of evapotranspiration shifts the water balance of Mediterranean climates during multi-year droughts. Hydrol. Earth Syst. Sci. 24, 4317–4337. https://doi.org/10.5194/hess-24-4317-2020

Avanzi, F., Rungee, J., Maurer, T., Bales, R., Ma, Q., Glaser, S., Conklin, M., 2019. Evapotranspiration feedbacks shift annual precipitation-runoff relationships during multi-year droughts in a Mediterranean mixed rain-snow climate. Hydrol. Earth Syst. Sci. Discuss. 1–35. https://doi.org/10.5194/hess-2019-377

Bailey, W.G., Oke, T.R., Wayne, R.R., 1997. Climates of Canada. Int. J. Climatol. 369.

Bajracharya, A., Awoye, H., Stadnyk, T., Asadzadeh, M., 2020. Time Variant Sensitivity Analysis of Hydrological Model Parameters in a Cold Region Using Flow Signatures. Water 12, 961. https://doi.org/10.3390/w12040961

Bales, R.C., Goulden, M.L., Hunsaker, C.T., Conklin, M.H., Hartsough, P.C., O'Geen, A.T., Hopmans, J.W., Safeeq, M., 2018. Mechanisms controlling the impact of multi-year drought on mountain hydrology. Sci. Rep. 8, 1–8. https://doi.org/10.1038/s41598-017-19007-0

Bentley, C.F., Peters, T.W., Henning, A.M.F., Walker, D.R., 1971. Gray wooded soils and their management.

Beven, K., 1979. A sensitivity analysis of the Penman-Monteith actual evapotranspiration estimates. J. Hydrol. 44, 169–190. https://doi.org/10.1016/0022-1694(79)90130-6

Biemans, H., Siderius, C., Lutz, A.F., Nepal, S., Ahmad, B., Hassan, T., von Bloh, W., Wijngaard, R.R., Wester, P., Shrestha, A.B., Immerzeel, W.W., 2019. Importance of snow and glacier meltwater for agriculture on the Indo-Gangetic Plain. Nat. Sustain. 2, 594–601. https://doi.org/10.1038/s41893-019-0305-3

Bonsal, B., Liu, Z., Wheaton, E., Stewart, R., 2020. Historical and projected changes to the stages and other characteristics of severe canadian prairie droughts. Water (Switzerland) 12, 3370. https://doi.org/10.3390/w12123370

Bouman, B.A.M., Van Keulen, H., Van Laar, H.H., Rabbinge, R., 1996. The "School of de Wit" crop growth simulation models: A pedigree and historical overview. Agric. Syst. https://doi.org/10.1016/0308-521X(96)00011-X

Bower, K.E., 2008. RELATIONSHIP BETWEEN TRANSPIRATION AND NITROGEN UPTAKE BY PEPPER (CAPSICUM ANNUUM) AS MEDIATED BY VAPOR PRESSURE DEFICIT.

Brisson, N. (INRA (France). U. 0409 U. de B., Mary, B. (INRA (France). U. 0471 U. d'Agronomie de L.-P., Ripoche, D. (INRA (France). U. 0409 U. de B., Jeuffroy, M.H. (INRA (France). 0211 U. associée I.-P. d'Agronomie), Ruget, F. (INRA (France). U. 0409 U. de B., Nicoullaud, B. (INRA (France). U. 0272 U. de recherche S. du S., Gate, P. (Institut T. des C. et des F.., Devienne-Barret, F. (INRA (France). U. 0471 U. d'Agronomie de L.-P., Antonioletti, R. (INRA (France). U. 0409 U. de B., Durr, C. (INRA (France). U. 0471 U. d'Agronomie de L.-P., Richard, G. (INRA (France). U. 0471 U. d'Agronomie de

L.-P., Beaudoin, N. (INRA (France). U. 0471 U. d'Agronomie de L.-P., Recous, S. (INRA (France). U. 0471 U. d'Agronomie de L.-P., Tayot, X. (Institut N. de la R.A.., Plenet, D. (INRA (France). U. 0417 U. d'Agronomie), Cellier, P. (INRA (France). U. 0253 U. de recherches en B., Machet, J.M. (INRA (France). U. 0471 U. d'Agronomie de L.-P., Meynard, J.M. (INRA (France). 0211 U. associée I.-P. d'Agronomie), Delécolle, R. (INRA (France). U. 0409 U. de B., 1998. STICS: a generic model for the simulation of crops and their water and nitrogen balances. I. Theory and parameterization applied to wheat and corn.

Broberg, M.C., Högy, P., Feng, Z., Pleijel, H., 2019. Effects of Elevated CO2 on Wheat Yield: Non-Linear Response and Relation to Site Productivity. Agronomy 9, 243. https://doi.org/10.3390/agronomy9050243

Burek, P., Satoh, Y., Fischer, G., Taher Kahil, M., Scherzer, A., Tramberend, S., Fabiola Nava, L., Wada, Y., Eisner Martina Flörke Naota Hanasaki Piotr Magnuszewski, S., Wiberg, D., Cosgrove, B., 2016. Water Futures and Solution Fast Track Initiative-Final Report.

Bush, E., Lemmen, D.., 2019. Canada's Changing Climate Report [WWW Document]. Environ. Clim. Chang. Canada, Gov. Canada. URL www.ChangingClimate.ca/CCCR2019 (accessed 1.16.23).

Canadian Fertilizer Institute, 1998. Nutrient uptake and removal by field crops—western Canada 1998.

Cannon, A.J., Sobie, S.R., Murdock, T.Q., 2015. Bias Correction of GCM Precipitation by Quantile Mapping: How Well Do Methods Preserve Changes in Quantiles and Extremes? J. Clim. 28, 6938–6959. https://doi.org/10.1175/JCLI-D-14-00754.1

Ceglar, A., van der Wijngaart, R., de Wit, A., Lecerf, R., Boogaard, H., Seguini, L., van den Berg, M., Toreti, A., Zampieri, M., Fumagalli, D., Baruth, B., 2019. Improving WOFOST model to simulate winter wheat phenology in Europe: Evaluation and effects on yield. Agric. Syst. 168, 168–180. https://doi.org/10.1016/j.agsy.2018.05.002

Challinor, A.J., Simelton, E.S., Fraser, E.D.G., Hemming, D., Collins, M., 2010. Increased crop failure due to climate change: Assessing adaptation options using models and socio-economic data for wheat in China. Environ. Res. Lett. 5, 034012. https://doi.org/10.1088/1748-9326/5/3/034012

Challinor, A.J., Watson, J., Lobell, D.B., Howden, S.M., Smith, D.R., Chhetri, N., 2014. A meta-analysis of crop yield under climate change and adaptation. Nat. Clim. Chang. 4, 287–291. https://doi.org/10.1038/nclimate2153

Chapagain, A.K., Hoekstra, A.Y., Savenije, H.H.G., 2006. Water saving through international trade of agricultural products. Hydrol. Earth Syst. Sci. 10, 455–468. https://doi.org/10.5194/hess-10-455-2006

Chen, J., Brissette, F.P., Leconte, R., 2011. Uncertainty of downscaling method in quantifying the impact of climate change on hydrology. J. Hydrol. 401, 190–202. https://doi.org/10.1016/J.JHYDROL.2011.02.020

Chen, L., Climatology, T.F.-I.J. of, 2023, undefined, 2022. Future changes in the transitions of monthly-to-seasonal precipitation extremes over the Midwest in Coupled Model

Intercomparison Project Phase 6 models. Wiley Online Libr. 43, 255–274. https://doi.org/10.1002/joc.7756

Chen, Y., Marek, G.W., Marek, T.H., Moorhead, J.E., Heflin, K.R., Brauer, D.K., Gowda, P.H., Srinivasan, R., 2019. Simulating the impacts of climate change on hydrology and crop production in the Northern High Plains of Texas using an improved SWAT model. Agric. Water Manag. 221, 13–24. https://doi.org/10.1016/j.agwat.2019.04.021

Choat, B., Brodribb, T.J., Brodersen, C.R., Duursma, R.A., López, R., Medlyn, B.E., 2018. Triggers of tree mortality under drought. Nat. 2018 5587711 558, 531–539. https://doi.org/10.1038/s41586-018-0240-x

Chunn, D., Faramarzi, M., Smerdon, B., Alessi, D., 2019. Application of an Integrated SWAT–MODFLOW Model to Evaluate Potential Impacts of Climate Change and Water Withdrawals on Groundwater–Surface Water Interactions in West-Central Alberta. Water 11, 110. https://doi.org/10.3390/w11010110

Ciscar, J.C., Fisher-Vanden, K., Lobell, D.B., 2018. Synthesis and review: An inter-method comparison of climate change impacts on agriculture. Environ. Res. Lett. https://doi.org/10.1088/1748-9326/aac7cb

Clarke, G.K.C., Naz, B.S., Frans, C.D., Lettenmaier, D.P., Burns, P., 2014. Modeling the effect of glacier recession on streamflow response using a coupled glacio-hydrological model. Hydrol. Earth Syst. Sci. 18, 787–802. https://doi.org/10.5194/hess-18-787-2014

Collins, M., Knutti, R., Arblaster, J., Dufresne, J., Fichefet, T., 2013. Long-term climate change: projections, commitments and irreversibility.

Corbeels, M., Berre, D., Rusinamhodzi, L., Lopez-Ridaura, S., 2018. Can we use crop modelling for identifying climate change adaptation options? Agric. For. Meteorol. https://doi.org/10.1016/j.agrformet.2018.02.026

Cordeiro, M., Krahn, V., … R.R.-C.B., 2015, undefined, 2016. Water table contribution and diurnal water redistribution within the corn root zone. researchgate.net. https://doi.org/10.7451/CBE.2015.57.1.39

Cordeiro, M.R.C., Lelyk, G., Kröbel, R., Legesse, G., Faramarzi, M., Masud, M.B., McAllister, T., 2018a. Deriving a dataset for agriculturally relevant soils from the Soil Landscapes of Canada (SLC) database for use in Soil and Water Assessment Tool (SWAT) simulations. Earth Syst. Sci. Data 10, 1673–1686. https://doi.org/10.5194/essd-10-1673-2018

Cordeiro, M.R.C., Lelyk, G., Kröbel, R., Legesse, G., Faramarzi, M., Masud, M.B., McAllister, T., 2018b. Deriving a dataset for agriculturally relevant soils from the Soil Landscapes of Canada (SLC) database for use in Soil and Water Assessment Tool (SWAT) simulations. Earth Syst. Sci. Data 10, 1673–1686. https://doi.org/10.5194/essd-10-1673-2018

Cornish, Peter S, Tullberg, Jeff N, Lemerle, Deirdre, Flower, Ken, Cornish, P S, Tullberg, J N, Lemerle, D, Flower, K, 2020. No-Till Farming Systems in Australia. No-till Farming Syst. Sustain. Agric. 511–531. https://doi.org/10.1007/978-3-030-46409-7_29

Cui, Q., Ammar, M.E., Iravani, M., Kariyeva, J., Faramarzi, M., 2021. Regional wetland water storage changes: The influence of future climate on geographically isolated wetlands. Ecol.

Indic. 120, 106941. https://doi.org/10.1016/j.ecolind.2020.106941

D'Odorico, P., Carr, J., Dalin, C., Dell'Angelo, J., Konar, M., Laio, F., Ridolfi, L., Rosa, L., Suweis, S., Tamea, S., Tuninetti, M., 2019. Global virtual water trade and the hydrological cycle: Patterns, drivers, and socio-environmental impacts. Environ. Res. Lett. https://doi.org/10.1088/1748-9326/ab05f4

da Luz, F.B., Carvalho, M.L., Castioni, G.A.F., de Oliveira Bordonal, R., Cooper, M., Carvalho, J.L.N., Cherubin, M.R., 2022. Soil structure changes induced by tillage and reduction of machinery traffic on sugarcane – A diversity of assessment scales. Soil Tillage Res. 223, 105469. https://doi.org/10.1016/J.STILL.2022.105469

Dakhlalla, A.O., Parajuli, P.B., 2019. Assessing model parameters sensitivity and uncertainty of streamflow, sediment, and nutrient transport using SWAT. Inf. Process. Agric. 6, 61–72. https://doi.org/10.1016/J.INPA.2018.08.007

Datry, T., Fritz, K., Leigh, C., 2016. Challenges, developments and perspectives in intermittent river ecology. Freshw. Biol. 61, 1171–1180. https://doi.org/10.1111/fwb.12789

Deb, P., Kiem, A.S., Willgoose, G., 2019. Mechanisms influencing non-stationarity in rainfall-runoff relationships in southeast Australia. J. Hydrol. 571, 749–764. https://doi.org/10.1016/j.jhydrol.2019.02.025

Deryng, D., Conway, D., Ramankutty, N., Price, J., Warren, R., 2014. Global crop yield response to extreme heat stress under multiple climate change futures. Environ. Res. Lett. 9, 034011. https://doi.org/10.1088/1748-9326/9/3/034011

Deryng, D., Elliott, J., Folberth, C., Müller, C., Pugh, T.A.M., Boote, K.J., Conway, D., Ruane, A.C., Gerten, D., Jones, J.W., Khabarov, N., Olin, S., Schaphoo, S., Schmid, E., Yang, H., Rosenzweig, C., 2016. Regional disparities in the beneficial eeects of rising CO 2 concentrations on crop water productivity. https://doi.org/10.1038/NCLIMATE2995

Destouni, G., Verrot, L., 2014. Screening long-term variability and change of soil moisture in a changing climate. J. Hydrol. 516, 131–139. https://doi.org/10.1016/J.JHYDROL.2014.01.059

Diepen, C.A., Wolf, J., Keulen, H., Rappoldt, C., 1989. WOFOST: a simulation model of crop production. Soil Use Manag. 5, 16–24. https://doi.org/10.1111/j.1475-2743.1989.tb00755.x

Du, X., Loiselle, D., Alessi, D.S., Faramarzi, M., 2020. Hydro-climate and biogeochemical processes control watershed organic carbon inflows: Development of an in-stream organic carbon module coupled with a process-based hydrologic model. Sci. Total Environ. 718, 137281. https://doi.org/10.1016/j.scitotenv.2020.137281

Elliott, K.J., Miniat, C.F., Pederson, N., Laseter, S.H., 2015. Forest tree growth response to hydroclimate variability in the southern Appalachians. Glob. Chang. Biol. 21, 4627–4641. https://doi.org/10.1111/gcb.13045

Ercin, A.E., Hoekstra, A.Y., 2014. Water footprint scenarios for 2050: A global analysis. Environ. Int. 64, 71–82. https://doi.org/10.1016/J.ENVINT.2013.11.019

Eyring, V., Bony, S., Meehl, G.A., Senior, C.A., Stevens, B., Stouffer, R.J., Taylor, K.E., 2016a.

Overview of the Coupled Model Intercomparison Project Phase 6 (CMIP6) experimental design and organization. Geosci. Model Dev. 9, 1937–1958. https://doi.org/10.5194/GMD-9-1937-2016

Eyring, V., Bony, S., Meehl, G.A., Senior, C.A., Stevens, B., Stouffer, R.J., Taylor, K.E., 2016b. Overview of the Coupled Model Intercomparison Project Phase 6 (CMIP6) experimental design and organization. Geosci. Model Dev. 9, 1937–1958. https://doi.org/10.5194/gmd-9-1937-2016

Falkenmark, M., Rockström, J., 2006. The New Blue and Green Water Paradigm: Breaking New Ground for Water Resources Planning and Management. J. Water Resour. Plan. Manag. 132, 129–132. https://doi.org/10.1061/(asce)0733-9496(2006)132:3(129)

Fang, G., Yang, J., Chen, Y., Li, Z., De Maeyer, P., 2018. Impact of GCM structure uncertainty on hydrological processes in an arid area of China. Hydrol. Res. 49, 893–907. https://doi.org/10.2166/nh.2017.227

Fang, X., W. Pomeroy, J., 2020. Diagnosis of future changes in hydrology for a Canadian Rockies headwater basin. Hydrol. Earth Syst. Sci. 24, 2731–2754. https://doi.org/10.5194/hess-24-2731-2020

FAOSTAT, 2021. FAOSTAT commodity balance sheets. Rome, Italy: Food and Agriculture Organization of the United Nations.

Faramarzi, M., Abbaspour, K.C., Adamowicz, W.L. (Vic), Lu, W., Fennell, J., Zehnder, A.J.B., Goss, G.G., 2017. Uncertainty based assessment of dynamic freshwater scarcity in semi-arid watersheds of Alberta, Canada. J. Hydrol. Reg. Stud. 9, 48–68. https://doi.org/10.1016/J.EJRH.2016.11.003

Faramarzi, M., Abbaspour, K.C., Schulin, R., Yang, H., 2009. Modelling blue and green water resources availability in Iran. Hydrol. Process. 23, 486–501. https://doi.org/10.1002/hyp.7160

Faramarzi, M., Khalili, P., Zaremehrjardy, M., Silwal, G., Masud, M.B., 2019. The cascade of uncertainties in agro-hydrological model projections: implications for future water-food nexus in snow-dominated regions. Agufm 2019, H31M-1919.

Faramarzi, M., Srinivasan, R., Iravani, M., Bladon, K.D., Abbaspour, K.C., Zehnder, A.J.B., Goss, G.G., 2015. Setting up a hydrological model of Alberta: Data discrimination analyses prior to calibration. Environ. Model. Softw. 74, 48–65. https://doi.org/10.1016/J.ENVSOFT.2015.09.006

Faramarzi, M., Yang, H., Schulin, R., Abbaspour, K.C., 2010. Modeling wheat yield and crop water productivity in Iran: Implications of agricultural water management for wheat production. Agric. Water Manag. 97, 1861–1875. https://doi.org/10.1016/j.agwat.2010.07.002

Feng, X., Thompson, S.E., Woods, R., Porporato, A., 2019. Quantifying Asynchronicity of Precipitation and Potential Evapotranspiration in Mediterranean Climates. Geophys. Res. Lett. 46, 14692–14701. https://doi.org/10.1029/2019GL085653

Fezzi, C., Bateman, I., 2015. The impact of climate change on agriculture: Nonlinear effects and

aggregation bias in ricardian models of farmland values. J. Assoc. Environ. Resour. Econ. 2, 57–92. https://doi.org/10.1086/680257

Ficklin, D.L., Luo, Y., Zhang, M., 2013. Climate change sensitivity assessment of streamflow and agricultural pollutant transport in California's Central Valley using Latin hypercube sampling. Hydrol. Process. 27, 2666–2675. https://doi.org/10.1002/HYP.9386

Filipović, V., Weninger, T., Filipović, L., Schwen, A., Bristow, K.L., Zechmeister-Boltenstern, S., Leitner, S., 2018. Inverse estimation of soil hydraulic properties and water repellency following artificially induced drought stress. sciendo.com 66, 170–180. https://doi.org/10.2478/johh-2018-0002

Folberth, C., Skalský, R., Moltchanova, E., Balkovič, J., Azevedo, L.B., Obersteiner, M., van der Velde, M., 2016. Uncertainty in soil data can outweigh climate impact signals in global crop yield simulations. Nat. Commun. 7, 11872. https://doi.org/10.1038/ncomms11872

Fovet, O., Belemtougri, A., Boithias, L., Braud, I., Charlier, J.B., Cottet, M., Daudin, K., Dramais, G., Ducharne, A., Folton, N., Grippa, M., Hector, B., Kuppel, S., Le Coz, J., Legal, L., Martin, P., Moatar, F., Molénat, J., Probst, A., Riotte, J., Vidal, J.P., Vinatier, F., Datry, T., 2021. Intermittent rivers and ephemeral streams: Perspectives for critical zone science and research on socio-ecosystems. Wiley Interdiscip. Rev. Water 8, e1523. https://doi.org/10.1002/wat2.1523

Fowler, K., Knoben, W., Peel, M., Peterson, T., Ryu, D., Saft, M., Seo, K.W., Western, A., 2020. Many Commonly Used Rainfall-Runoff Models Lack Long, Slow Dynamics: Implications for Runoff Projections. Water Resour. Res. 56, e2019WR025286. https://doi.org/10.1029/2019WR025286

Fowler, M.D., Kooperman, G.J., Randerson, J.T., Pritchard, M.S., 2019. The effect of plant physiological responses to rising CO2 on global streamflow. Nat. Clim. Chang. 9, 873–879. https://doi.org/10.1038/s41558-019-0602-x

Frieler, K., Schauberger, B., Arneth, A., Balkovič, J., Chryssanthacopoulos, J., Deryng, D., Elliott, J., Folberth, C., Khabarov, N., Müller, C., Olin, S., Pugh, T.A.M., Schaphoff, S., Schewe, J., Schmid, E., Warszawski, L., Levermann, A., 2017. Understanding the weather signal in national crop-yield variability. Earth's Futur. 5, 605–616. https://doi.org/10.1002/2016EF000525@10.1002/(ISSN)2328-4277.HAZARDS1

Fuller, W.H., 2010. My Pilgrimage in Mission. Int. Bull. Mission. Res. 34, 37–40. https://doi.org/10.1177/239693931003400110

Gamelin, B.L., Feinstein, J., Wang, J., Bessac, J., Yan, E., Kotamarthi, V.R., 2022. Projected U.S. drought extremes through the twenty-first century with vapor pressure deficit. Sci. Rep. 12, 1–15. https://doi.org/10.1038/s41598-022-12516-7

Gao, B., Yang, D., Qin, Y., Wang, Y., Li, H., Zhang, Y., Zhang, T., 2018. Change in frozen soils and its effect on regional hydrology, upper Heihe basin, northeastern Qinghai-Tibetan Plateau. Cryosphere 12, 657–673. https://doi.org/10.5194/TC-12-657-2018

Garcia-Vila, M., Morillo-Velarde, R., Fereres, E., 2019. Modeling Sugar Beet Responses to Irrigation with AquaCrop for Optimizing Water Allocation. Water 11, 1918.

https://doi.org/10.3390/w11091918

Geng, X., Wang, F., Ren, W., Hao, Z., 2019. Climate Change Impacts on Winter Wheat Yield in Northern China. Adv. Meteorol. 2019. https://doi.org/10.1155/2019/2767018

Ghoreishi, M., Razavi, S., Elshorbagy, A., 2021. Understanding human adaptation to drought: agent-based agricultural water demand modeling in the Bow River Basin, Canada. https://doi.org/10.1080/02626667.2021.1873344 66, 389–407. https://doi.org/10.1080/02626667.2021.1873344

Gorgan, D., Bacu, V., Mihon, D., Rodila, D., Abbaspour, K., Rouholahnejad, E., 2012. Grid based calibration of SWAT hydrological models. Nat. Hazards Earth Syst. Sci. 12, 2411–2423. https://doi.org/10.5194/NHESS-12-2411-2012

Graham, N.T., Hejazi, M.I., Kim, S.H., Davies, E.G.R., Edmonds, J.A., Miralles-Wilhelm, F., 2020. Future changes in the trading of virtual water. Nat. Commun. 11, 1–7. https://doi.org/10.1038/s41467-020-17400-4

Greve, P., Orlowsky, B., Mueller, B., Sheffield, J., Reichstein, M., Seneviratne, S.I., 2014. Global assessment of trends in wetting and drying over land. Nat. Geosci. 7, 716–721. https://doi.org/10.1038/NGEO2247

Guan, K., Sultan, B., Biasutti, M., Baron, C., Lobell, D.B., 2017. Assessing climate adaptation options and uncertainties for cereal systems in West Africa. Agric. For. Meteorol. 232, 291–305. https://doi.org/10.1016/j.agrformet.2016.07.021

Guidelines for Safe Rates of Fertilizer Applied With the Seed | Soils, Fertility and Nutrients | Government of Saskatchewan [WWW Document], n.d. URL https://www.saskatchewan.ca/business/agriculture-natural-resources-and-industry/agribusiness-farmers-and-ranchers/crops-and-irrigation/soils-fertility-and-nutrients/guidelines-for-safe-rates-of-fertilizer-applied-with-the-seed (accessed 3.9.21).

Gupta, H.V., Sorooshian, S., Yapo, P.O., 1999. Status of Automatic Calibration for Hydrologic Models: Comparison with Multilevel Expert Calibration. J. Hydrol. Eng. 4, 135–143. https://doi.org/10.1061/(asce)1084-0699(1999)4:2(135)

Gupta, H. V., Kling, H., Yilmaz, K.K., Martinez, G.F., 2009. Decomposition of the mean squared error and NSE performance criteria: Implications for improving hydrological modelling. J. Hydrol. 377, 80–91. https://doi.org/10.1016/J.JHYDROL.2009.08.003

Gurrapu, S., Chipanshi, A.C., Sauchyn, D., Howard, A., 2014. Comparison of the SPI and SPEI on Predicting Drought Conditions and. Proc. 28th Conf. Hydrol. - 94th Am. Meteorol. Soc. Annu. Meet. Atlanta (GA, USA), Febrary 2-6. Am. Meteorol. Soc. Boston, MA, USA.

Halofsky, J.E., Peterson, D.L., Harvey, B.J., 2020. Changing wildfire, changing forests: the effects of climate change on fire regimes and vegetation in the Pacific Northwest, USA. Fire Ecol. 16, 1–26. https://doi.org/10.1186/S42408-019-0062-8/FIGURES/4

Halofsky, J.E., Peterson, D.L., Ho, J.J., Little, N., Joyce, L.A., 2018. Climate Change Vulnerability and Adaptation in the Intermountain Region. Gen. Tech. Rep. RMRS-GTR-375. Fort Collins, CO U.S. Dep. Agric. For. Serv. Rocky Mt. Res. Station. Part 1. 374, 1–197. https://doi.org/10.2737/RMRS-GTR-374PART1

Hamal, K., Sharma, S., Khadka, N., Haile, G.G., Joshi, B.B., Xu, T., Dawadi, B., 2020. Assessment of drought impacts on crop yields across Nepal during 1987–2017. Meteorol. Appl. 27, e1950. https://doi.org/10.1002/MET.1950

Haney, E.B., Haney, R.L., White, M.J., Arnold, J.G., 2018a. Comparison of Wheat Yield Simulated Using Three N Cycling Options in the SWAT Model. Open J. Soil Sci. 08, 197–211. https://doi.org/10.4236/ojss.2018.88016

Haney, Elizabeth Brooke, Haney, R.L., White, M.J., Arnold, J.G., Haney, E B, 2018b. Comparison of Wheat Yield Simulated Using Three N Cycling Options in the SWAT Model. Open J. Soil Sci. 8, 197–211. https://doi.org/10.4236/ojss.2018.88016

Harris, I., Jones, P.D., Osborn, T.J., Lister, D.H., 2014. Updated high-resolution grids of monthly climatic observations - the CRU TS3.10 Dataset. Int. J. Climatol. 34, 623–642. https://doi.org/10.1002/joc.3711

Hasan, H.H., Razali, S.F.M., Muhammad, N.S., Ahmad, A., 2019. Research Trends of Hydrological Drought: A Systematic Review. Water 2019, Vol. 11, Page 2252 11, 2252. https://doi.org/10.3390/W11112252

Hayes, M., Svoboda, M., Wall, N., Widhalm, M., 2011. The lincoln declaration on drought indices: Universal meteorological drought index recommended. Bull. Am. Meteorol. Soc. 92, 485–488. https://doi.org/10.1175/2010BAMS3103.1

He, W., Yang, J.Y., Drury, C.F., Smith, W.N., Grant, B.B., He, P., Qian, B., Zhou, W., Hoogenboom, G., 2018. Estimating the impacts of climate change on crop yields and N2O emissions for conventional and no-tillage in Southwestern Ontario, Canada. Agric. Syst. 159, 187–198. https://doi.org/10.1016/j.agsy.2017.01.025

Heard, J., 2020. 2020 View of Fertilizer Guidelines for Manitoba.

Hiebert, J., Cannon, A.J., Murdock, T., Sobie, S., Werner, A., 2018. ClimDown: Climate Downscaling in R Software • Review • Repository • Archive. https://doi.org/10.21105/joss.00360

Hoekstra, A.Y., 2003. Virtual Water Trade. Proceedings of the internacional expert meeting on virtual water trade. Int. Expert Meet. Virtual Water Trade 12, 1–244.

Hoekstra, A.Y., Chapagain, A.K., 2007. Water footprints of nations: Water use by people as a function of their consumption pattern. Integr. Assess. Water Resour. Glob. Chang. A North-South Anal. 21, 35–48. https://doi.org/10.1007/978-1-4020-5591-1-3

Hoekstra, A.Y., Mekonnen, M.M., 2016. Imported water risk: The case of the UK. Environ. Res. Lett. 11, 055002. https://doi.org/10.1088/1748-9326/11/5/055002

Hoffman, S.M., 2017. Powering Injustice: Hydroelectric Development in Northern Manitoba. Environ. Justice 147–170. https://doi.org/10.4324/9781351311687-7

Hogeboom, R.J., Knook, L., Hoekstra, A.Y., 2018. The blue water footprint of the world's artificial reservoirs for hydroelectricity, irrigation, residential and industrial water supply, flood protection, fishing and recreation. Adv. Water Resour. 113, 285–294. https://doi.org/10.1016/J.ADVWATRES.2018.01.028

Högy, P., Wieser, H., Köhler, P., Schwadorf, K., Breuer, J., Franzaring, J., Muntifering, R., Fangmeier, A., 2009. Effects of elevated CO2 on grain yield and quality of wheat: Results from a 3-year free-air CO2 enrichment experiment. Plant Biol. 11, 60–69. https://doi.org/10.1111/j.1438-8677.2009.00230.x

Hopkinson, R.F., McKenney, D.W., Milewska, E.J., Hutchinson, M.F., Papadopol, P., Vincent, L.A., Hopkinson, R.F., McKenney, D.W., Milewska, E.J., Hutchinson, M.F., Papadopol, P., Vincent, L.A., 2011. Impact of Aligning Climatological Day on Gridding Daily Maximum–Minimum Temperature and Precipitation over Canada. J. Appl. Meteorol. Climatol. 50, 1654–1665. https://doi.org/10.1175/2011JAMC2684.1

Houshmandfar, A., Fitzgerald, G.J., O'Leary, G., Tausz-Posch, S., Fletcher, A., Tausz, M., 2018. The relationship between transpiration and nutrient uptake in wheat changes under elevated atmospheric CO2. Physiol. Plant. 163, 516–529. https://doi.org/10.1111/ppl.12676

Hrach, D.M., 2020. Quantifying the role of shade on microclimate conditions and water use efficiency of a subalpine wetland in the Canadian Rocky Mountains, Kananaskis, Alberta.

Huang, H., Xie, P., Duan, Y., Wu, P., Zhuo, L., 2023. Cropping pattern optimization considering water shadow price and virtual water flows: A case study of Yellow River Basin in China. Agric. Water Manag. 284, 108339. https://doi.org/10.1016/J.AGWAT.2023.108339

Hunter, R.D., Meentemeyer, R.K., 2005. Climatologically Aided Mapping of Daily Precipitation and Temperature. J. Appl. Meteorol. Climatol. 44, 1501–1510. https://doi.org/10.1175/JAM2295.1

Hydro, M., n.d. CLIMATE CHANGE REPORT.

Iqbal, M.S., Singh, A.K., Ansari, M.I., 2020. Effect of drought stress on crop production. New Front. Stress Manag. Durable Agric. 35–47. https://doi.org/10.1007/978-981-15-1322-0_3/FIGURES/3

J. R. Williams, C. A. Jones, J. R. Kiniry, D. A. Spanel, 1989. The EPIC Crop Growth Model. Trans. ASAE 32, 0497–0511. https://doi.org/10.13031/2013.31032

J. R. Williams, J.R., C. A. Jones, C.A., P. T. Dyke, P.T., 1984. A Modeling Approach to Determining the Relationship Between Erosion and Soil Productivity. Trans. ASAE 27, 0129–0144. https://doi.org/10.13031/2013.32748

Jablonski, L.M., Wang, X., Curtis, P.S., 2002. Plant reproduction under elevated CO2 conditions: a meta-analysis of reports on 79 crop and wild species. New Phytol. 156, 9–26. https://doi.org/10.1046/j.1469-8137.2002.00494.x

Jabran, K., Florentine, S., Chauhan, B.S., 2020. Impacts of Climate Change on Weeds, Insect Pests, Plant Diseases and Crop Yields: Synthesis, in: Crop Protection Under Changing Climate. Springer International Publishing, pp. 189–195. https://doi.org/10.1007/978-3-030-46111-9_8

Jägermeyr, J., Müller, C., Ruane, A.C., Elliott, J., Balkovic, J., Castillo, O., Faye, B., Foster, I., Folberth, C., Franke, J.A., Fuchs, K., Guarin, J.R., Heinke, J., Hoogenboom, G., Iizumi, T., Jain, A.K., Kelly, D., Khabarov, N., Lange, S., Lin, T.S., Liu, W., Mialyk, O., Minoli, S., Moyer, E.J., Okada, M., Phillips, M., Porter, C., Rabin, S.S., Scheer, C., Schneider, J.M.,

Schyns, J.F., Skalsky, R., Smerald, A., Stella, T., Stephens, H., Webber, H., Zabel, F., Rosenzweig, C., 2021. Climate impacts on global agriculture emerge earlier in new generation of climate and crop models. Nat. Food 2, 873–885. https://doi.org/10.1038/s43016-021-00400-y

Jarvis, A., Guevara, E., Reuter, H.I., Nelson, A.D., 2008. Hole-filled SRTM for the globe : version 4 : data grid.

Jasechko, S., 2018. Plants turn on the tap. Nat. Clim. Chang. 8, 562–563. https://doi.org/10.1038/s41558-018-0212-z

Jin, Z., Zhuang, Q., Tan, Z., Dukes, J.S., Zheng, B., Melillo, J.M., 2016. Do maize models capture the impacts of heat and drought stresses on yield? Using algorithm ensembles to identify successful approaches. Glob. Chang. Biol. 22, 3112–3126. https://doi.org/10.1111/gcb.13376

Joly, F., 2021. Water Falling onto Soil and the Effects It Produces. Mank. Deserts 2 1–38. https://doi.org/10.1002/9781119808275.ch1

Kanda, E.K., Mabhaudhi, T., Senzanje, A., 2018. Coupling hydrological and crop models for improved agricultural water management-A review VLIR-UOS Moi Unversity CSE project View project Development of WEF nexus sustainability indicators View project.

Kang, H., Sridhar, V., 2018. Assessment of Future Drought Conditions in the Chesapeake Bay Watershed. JAWRA J. Am. Water Resour. Assoc. 54, 160–183. https://doi.org/10.1111/1752-1688.12600

Kant, S., Seneweera, S., Rodin, J., Materne, M., Burch, D., Rothstein, S.J., Spangenberg, G., 2012. Improving yield potential in crops under elevated CO2: Integrating the photosynthetic and nitrogen utilization efficiencies. Front. Plant Sci. https://doi.org/10.3389/fpls.2012.00162

Karamouz, M., Ahmadi, A., Akhbari, M., 2011. Groundwater hydrology: Engineering, planning, and management. Groundw. Hydrol. Eng. Planning, Manag. 1–634.

Karamouz, M., Taheri, M., Khalili, P., Chen, X., 2019. Building Infrastructure Resilience in Coastal Flood Risk Management. J. Water Resour. Plan. Manag. 145. https://doi.org/10.1061/(asce)wr.1943-5452.0001043

Karamouz, M., Teymoori, J., Olyaei, M.A., 2021a. A Spatial Non-Stationary Based Site Selection of Artificial Groundwater Recharge: a Case Study for Semi-Arid Regions. Water Resour. Manag. 35, 963–978. https://doi.org/10.1007/S11269-020-02762-7/FIGURES/4

Karamouz, M., Teymoori, J., Olyaei, M.A., 2021b. A Spatial Non-Stationary Based Site Selection of Artificial Groundwater Recharge: a Case Study for Semi-Arid Regions. Water Resour. Manag. 35, 963–978. https://doi.org/10.1007/S11269-020-02762-7/FIGURES/4

Keum, J., Awol, F.S., Ursulak, J., Coulibaly, P., 2019. Introducing the Ensemble-Based Dual Entropy and Multiobjective Optimization for Hydrometric Network Design Problems: EnDEMO. Entropy 21, 947. https://doi.org/10.3390/e21100947

Khalili, P., Faramarzi, M., Khalili, P., Faramarzi, M., 2021a. Setting up a hydrologic model of

Canadian Prairies: A framework to assess crop production under uncertain blue and green water resources availability. AGUFM 2021, H45U-1446.

Khalili, P., Masud, B., Qian, B., Mezbahuddin, S., Dyck, M., Faramarzi, M., 2021b. Non-stationary response of rain-fed spring wheat yield to future climate change in northern latitudes. Sci. Total Environ. 772, 145474. https://doi.org/10.1016/j.scitotenv.2021.145474

Kim, K., Wang, M. cheng, Ranjitkar, S., Liu, S. hong, Xu, J. chu, Zomer, R.J., 2017. Using leaf area index (LAI) to assess vegetation response to drought in Yunnan province of China. J. Mt. Sci. 2017 149 14, 1863–1872. https://doi.org/10.1007/S11629-016-3971-X

Kimball, B.A., 2016. Crop responses to elevated CO2 and interactions with H2O, N, and temperature. Curr. Opin. Plant Biol. https://doi.org/10.1016/j.pbi.2016.03.006

Klos, P.Z., Goulden, M.L., Riebe, C.S., Tague, C.L., O'Geen, A.T., Flinchum, B.A., Safeeq, M., Conklin, M.H., Hart, S.C., Berhe, A.A., Hartsough, P.C., Holbrook, W.S., Bales, R.C., 2018. Subsurface plant-accessible water in mountain ecosystems with a Mediterranean climate. WIREs Water 5, e1277. https://doi.org/10.1002/wat2.1277

Krause, P., Boyle, D.P., Bäse, F., 2005. Comparison of different efficiency criteria for hydrological model assessment. Adv. Geosci. 5, 89–97. https://doi.org/10.5194/adgeo-5-89-2005

Krishnamurthy R, P.K., Fisher, J.B., Choularton, R.J., Kareiva, P.M., 2022. Anticipating drought-related food security changes. Nat. Sustain. 2022 511 5, 956–964. https://doi.org/10.1038/s41893-022-00962-0

Kukal, M.S., Irmak, S., 2020. Light interactions, use and efficiency in row crop canopies under optimal growth conditions. Agric. For. Meteorol. 284, 107887. https://doi.org/10.1016/j.agrformet.2019.107887

Kuwayama, Y., Thompson, A., Bernknopf, R., Zaitchik, B., Vail, P., 2019. Estimating the impact of drought on agriculture using the U.S. Drought Monitor. Am. J. Agric. Econ. 101, 193–210. https://doi.org/10.1093/AJAE/AAY037

Lambers, H., Chapin III, F.S., Pons, T.L., 2008. Plant Physiological Ecology.

Leakey, A.D.B., Ainsworth, E.A., Bernacchi, C.J., Rogers, A., Long, S.P., Ort, D.R., 2009. Elevated CO2 effects on plant carbon, nitrogen, and water relations: Six important lessons from FACE, in: Journal of Experimental Botany. pp. 2859–2876. https://doi.org/10.1093/jxb/erp096

Lennox, R.J., Crook, D.A., Moyle, P.B., Struthers, D.P., Cooke, S.J., 2019. Toward a better understanding of freshwater fish responses to an increasingly drought-stricken world. Rev. Fish Biol. Fish. 29, 71–92. https://doi.org/10.1007/s11160-018-09545-9

Lesk, C., Rowhani, P., Ramankutty, N., 2016. Influence of extreme weather disasters on global crop production. Nature 529, 84–87. https://doi.org/10.1038/nature16467

Li, X., Dong, J., Gruda, N.S., Chu, W., Duan, Z., 2020. Interactive Effects of the CO2 Enrichment and Nitrogen Supply on the Biomass Accumulation, Gas Exchange Properties, and Mineral Elements Concentrations in Cucumber Plants at Different Growth Stages.

Agronomy 10, 139. https://doi.org/10.3390/agronomy10010139

Li, Y., Guan, K., Schnitkey, G.D., DeLucia, E., Peng, B., 2019. Excessive rainfall leads to maize yield loss of a comparable magnitude to extreme drought in the United States. Glob. Chang. Biol. 25, gcb.14628. https://doi.org/10.1111/gcb.14628

Lian, X., Piao, S., Huntingford, C., Li, Y., Zeng, Z., Wang, X., Ciais, P., Mcvicar, T.R., Peng, S., Ottlé, C., Yang, H., Yang, Y., Zhang, Y., Wang, T., 2018. Partitioning global land evapotranspiration using CMIP5 models constrained by observations. Nat. Clim. Chang. https://doi.org/10.1038/s41558-018-0207-9

Lobell, D.B., Asseng, S., 2017. Comparing estimates of climate change impacts from process-based and statistical crop models. Environ. Res. Lett. 12, 015001. https://doi.org/10.1088/1748-9326/aa518a

Lobell, D.B., Burke, M.B., 2010. On the use of statistical models to predict crop yield responses to climate change. Agric. For. Meteorol. 150, 1443–1452. https://doi.org/10.1016/j.agrformet.2010.07.008

Loiselle, D., Du, X., Alessi, D.S., Bladon, K.D., Faramarzi, M., 2020. Projecting impacts of wildfire and climate change on streamflow, sediment, and organic carbon yields in a forested watershed. J. Hydrol. 590. https://doi.org/10.1016/j.jhydrol.2020.125403

Long, S.P., Ainsworth, E.A., Rogers, A., Ort, D.R., 2004. RISING ATMOSPHERIC CARBON DIOXIDE: Plants FACE the Future. Annu. Rev. Plant Biol. 55, 591–628. https://doi.org/10.1146/annurev.arplant.55.031903.141610

Lugoi, L.P., Bamutaze, Y., Martinsen, V., Dick, B., Almås, R., 2019. Ecosystem productivity response to environmental forcing, prospect for improved rain-fed cropping productivity in lake Kyoga Basin. Appl. Geogr. 102, 1–11. https://doi.org/10.1016/j.apgeog.2018.11.001

Manderscheid, R., Dier, M., Erbs, M., Sickora, J., Weigel, H.J., 2018. Nitrogen supply – A determinant in water use efficiency of winter wheat grown under free air CO2 enrichment. Agric. Water Manag. 210, 70–77. https://doi.org/10.1016/j.agwat.2018.07.034

Marston, L., Konar, M., 2017. Drought impacts to water footprints and virtual water transfers of the Central Valley of California. Water Resour. Res. 53, 5756–5773. https://doi.org/10.1002/2016WR020251

Massari, C., Avanzi, F., Bruno, G., Gabellani, S., Penna, D., Camici, S., 2022. Evaporation enhancement drives the European water-budget deficit during multi-year droughts. Hydrol. Earth Syst. Sci 26, 1527–1543. https://doi.org/10.5194/hess-26-1527-2022

Massmann, A., Gentine, P., Lin, C., 2019. When Does Vapor Pressure Deficit Drive or Reduce Evapotranspiration? J. Adv. Model. Earth Syst. 11, 3305–3320. https://doi.org/10.1029/2019MS001790

Masson-Delmotte, V., Zhai, P., Chen, Y., Goldfarb, L., Gomis, M.I., Matthews, J.B.R., Berger, S., Huang, M., Yelekçi, O., Yu, R., Zhou, B., Lonnoy, E., Maycock, T.K., Waterfield, T., Leitzell, K., Caud, N., 2021. Climate change 2021: the physical science basis. ipcc.ch. https://doi.org/10.1017/9781009157896

Mastrotheodoros, T., Pappas, C., Molnar, P., Burlando, P., Manoli, G., Parajka, J., Rigon, R., Szeles, B., Bottazzi, M., Hadjidoukas, P., Fatichi, S., 2020. More green and less blue water in the Alps during warmer summers. Nat. Clim. Chang. 10, 155–161. https://doi.org/10.1038/s41558-019-0676-5

Masud, B., Cui, Q., Ammar, M.E., Bonsal, B.R., Islam, Z., Faramarzi, M., 2021. Means and Extremes: Evaluation of a CMIP6 Multi-Model Ensemble in Reproducing Historical Climate Characteristics across Alberta, Canada. Water 2021, Vol. 13, Page 737 13, 737. https://doi.org/10.3390/W13050737

Masud, M., Ferdous, J., Faramarzi, M., 2018. Projected Changes in Hydrological Variables in the Agricultural Region of Alberta, Canada. Water 10, 1810. https://doi.org/10.3390/w10121810

Masud, M.B., McAllister, T., Cordeiro, M.R.C., Faramarzi, M., 2018. Modeling future water footprint of barley production in Alberta, Canada: Implications for water use and yields to 2064. Sci. Total Environ. 616–617, 208–222. https://doi.org/10.1016/j.scitotenv.2017.11.004

Masud, M.B., Qian, B., Faramarzi, M., 2020. Performance of multivariate and multiscalar drought indices in identifying impacts on crop production. Int. J. Climatol. 40, 292–307. https://doi.org/10.1002/JOC.6210

Masud, M.B., Wada, Y., Goss, G., Faramarzi, M., 2019. Global implications of regional grain production through virtual water trade. Sci. Total Environ. 659, 807–820. https://doi.org/10.1016/j.scitotenv.2018.12.392

Máté, D., Rabbi, M.F., Novotny, A., Kovács, S., 2020. Grand challenges in Central Europe: The relationship of food security, climate change, and energy use. Energies 13, 5422. https://doi.org/10.3390/en13205422

Maurer, E.P., Hidalgo, H.G., Das, T., Dettinger, M.D., Cayan, D.R., 2010. The utility of daily large-scale climate data in the assessment of climate change impacts on daily streamflow in California. Hydrol. Earth Syst. Sci. 14, 1125–1138. https://doi.org/10.5194/HESS-14-1125-2010

Maxwell, R.M., 2020. Water colour and climate. Nat. Clim. Chang. https://doi.org/10.1038/s41558-019-0683-6

McCarl, B.A., Villavicencio, X., Wu, X., 2008. Climate Change and Future Analysis: Is Stationarity Dying? Am. J. Agric. Econ. 90, 1241–1247. https://doi.org/10.1111/j.1467-8276.2008.01211.x

McKenney, D.W., Hutchinson, M.F., Papadopol, P., Lawrence, K., Pedlar, J., Campbell, K., Milewska, E., Hopkinson, R.F., Price, D., Owen, T., McKenney, D.W., Hutchinson, M.F., Papadopol, P., Lawrence, K., Pedlar, J., Campbell, K., Milewska, E., Hopkinson, R.F., Price, D., Owen, T., 2011. Customized Spatial Climate Models for North America. Bull. Am. Meteorol. Soc. 92, 1611–1622. https://doi.org/10.1175/2011BAMS3132.1

Mekonnen, M.M., Hoekstra, A.Y., 2020. Blue water footprint linked to national consumption and international trade is unsustainable. Nat. Food 1, 792–800.

https://doi.org/10.1038/s43016-020-00198-1

Mekonnen, M.M., Hoekstra, A.Y., 2016. Sustainability: Four billion people facing severe water scarcity. Sci. Adv. 2. https://doi.org/10.1126/SCIADV.1500323

Mekonnen, M.M., Hoekstra, A.Y., 2011. The green, blue and grey water footprint of crops and derived crop products. Hydrol. Earth Syst. Sci. 15, 1577–1600. https://doi.org/10.5194/hess-15-1577-2011

Mezbahuddin, S., Spiess, D., Hildebrand, D., Kryzanowski, L., Itenfisu, D., Goddard, T., Iqbal, J., Grant, R., 2020. Assessing Effects of Agronomic Nitrogen Management on Crop Nitrogen Use and Nitrogen Losses in the Western Canadian Prairies. Front. Sustain. Food Syst. 4, 512292. https://doi.org/10.3389/fsufs.2020.512292

Milly, P., Betancourt, J., Falkenmark, M., Earth, R.H.-, 2008, U., 2008. Stationarity is dead: Whither water management? Earth 4. https://doi.org/10.1126/science.1151915

Milly, P.C.D., Betancourt, J., Falkenmark, M., Hirsch, R.M., Kundzewicz, Z.W., Lettenmaier, D.P., Stouffer, R.J., Dettinger, M.D., Krysanova, V., 2015. On Critiques of "Stationarity is Dead: Whither Water Management?" Water Resour. Res. 51, 7785–7789. https://doi.org/10.1002/2015WR017408@10.1002/(ISSN)1944-9208.COMHES1

Mishra, V., Bhatia, U., Tiwari, A.D., 2020. Bias-corrected climate projections for South Asia from Coupled Model Intercomparison Project-6. Sci. Data 7. https://doi.org/10.1038/s41597-020-00681-1

Montanari, A., Koutsoyiannis, D., 2014. Modeling and mitigating natural hazards: Stationarity is immortal! Water Resour. Res. 50, 9748–9756. https://doi.org/10.1002/2014WR016092

Monteith, J.L., 1965. Evaporation and environment. Symp. Soc. Exp. Biol. 19, 205–234.

Monteith, J.L., Moss, C.J., 1977. Climate and the Efficiency of Crop Production in Britain [and Discussion]. Philos. Trans. R. Soc. B Biol. Sci. 281, 277–294. https://doi.org/10.1098/rstb.1977.0140

Moore, F.C., Baldos, U.L.C., Hertel, T., 2017. Economic impacts of climate change on agriculture: a comparison of process-based and statistical yield models. Environ. Res. Lett. 12, 065008. https://doi.org/10.1088/1748-9326/aa6eb2

Muhammad, A., Evenson, G., Stadnyk, T., Boluwade, A., Jha, S., Coulibaly, P., 2018. Assessing the Importance of Potholes in the Canadian Prairie Region under Future Climate Change Scenarios. Water 10, 1657. https://doi.org/10.3390/w10111657

Myers, S.S., Smith, M.R., Guth, S., Golden, C.D., Vaitla, B., Mueller, N.D., Dangour, A.D., Huybers, P., 2017. Climate Change and Global Food Systems: Potential Impacts on Food Security and Undernutrition. Annu. Rev. Public Health 38, 259–277. https://doi.org/10.1146/annurev-publhealth-031816-044356

Nam, W.H., Hayes, M.J., Svoboda, M.D., Tadesse, T., Wilhite, D.A., 2015. Drought hazard assessment in the context of climate change for South Korea. Agric. Water Manag. 160, 106–117. https://doi.org/10.1016/J.AGWAT.2015.06.029

Naresh Kumar, M., Murthy, C.S., Sesha sai, M.V.R., Roy, P.S., 2009. On the use of Standardized Precipitation Index (SPI) for drought intensity assessment. Meteorol. Appl. 16, 381–389. https://doi.org/10.1002/met.136

Nash, J.E., Sutcliffe, J. V., 1970. River flow forecasting through conceptual models part I — A discussion of principles. J. Hydrol. 10, 282–290. https://doi.org/10.1016/0022-1694(70)90255-6

Neitsch, S.L., Arnold, J.G., Kiniry, J.R., Williams, J.R., 2011a. COLLEGE OF AGRICULTURE AND LIFE SCIENCES Soil and Water Assessment Tool Theoretical Documentation Version 2009.

Neitsch, S.L., Arnold, J.G., Kiniry, J.R., Williams, J.R., 2011b. Soil and water assessment tool theoretical documentation version 2009.

Neitsch, S.L., Arnold, J.G., Kiniry, J.R., Williams, J.R., 2011c. COLLEGE OF AGRICULTURE AND LIFE SCIENCES Soil and Water Assessment Tool Theoretical Documentation Version 2009.

Ngosong, C., Bongkisheri, V., Tanyi, C.B., Nanganoa, L.T., Tening, A.S., 2019. Optimizing Nitrogen Fertilization Regimes for Sustainable Maize (Zea mays L.) Production on the Volcanic Soils of Buea Cameroon . Adv. Agric. 2019, 1–8. https://doi.org/10.1155/2019/4681825

Nouri, H., Stokvis, B., Chavoshi Borujeni, S., Galindo, A., Brugnach, M., Blatchford, M.L., Alaghmand, S., Hoekstra, A.Y., 2020. Reduce blue water scarcity and increase nutritional and economic water productivity through changing the cropping pattern in a catchment. J. Hydrol. 588, 125086. https://doi.org/10.1016/J.JHYDROL.2020.125086

Nowak, R.S., Ellsworth, D.S., Smith, S.D., 2004. Functional responses of plants to elevated atmospheric CO 2 - Do photosynthetic and productivity data from FACE experiments support early predictions? New Phytol. https://doi.org/10.1111/j.1469-8137.2004.01033.x

O'Neill, B.C., Tebaldi, C., Van Vuuren, D.P., Eyring, V., Friedlingstein, P., Hurtt, G., Knutti, R., Kriegler, E., Lamarque, J.F., Lowe, J., Meehl, G.A., Moss, R., Riahi, K., Sanderson, B.M., 2016. The Scenario Model Intercomparison Project (ScenarioMIP) for CMIP6. Geosci. Model Dev. 9, 3461–3482. https://doi.org/10.5194/gmd-9-3461-2016

OECD, 2016. Tackling the challenges of agricultural groundwater use. Trade Agric. Dir. https://doi.org/10.1787/9789264238701-en

Oerke, E.C., 2006. Crop losses to pests. J. Agric. Sci. https://doi.org/10.1017/S0021859605005708

Oki, T., Kanae, S., 2006. Global hydrological cycles and world water resources. Science (80-.). 313, 1068–1072. https://doi.org/10.1126/SCIENCE.1128845

Oki, T., Yano, S., Hanasaki, N., 2017. Economic aspects of virtual water trade. Environ. Res. Lett. 12, 044002. https://doi.org/10.1088/1748-9326/AA625F

Onwuka, Brown M, Cusack, D., Lydon, S., Karpman, J., Onwuka, B M, 2016. Effects of soil temperature on Some Soil properties and plant growth. Sch. J. Agric. Sci. 6, 89–93.

Orth, R., Destouni, G., 2018. Drought reduces blue-water fluxes more strongly than green-water fluxes in Europe. Nat. Commun. 9. https://doi.org/10.1038/s41467-018-06013-7

Pepler, A.S., Dowdy, A.J., Hope, P., 2021. The differing role of weather systems in southern Australian rainfall between 1979–1996 and 1997–2015. Clim. Dyn. 56, 2289–2302. https://doi.org/10.1007/S00382-020-05588-6

Pomeroy, J.W., Gray, D.M., Brown, T., Hedstrom, N.R., Quinton, W.L., Granger, R.J., Carey, S.K., 2007. The cold regions hydrological model: a platform for basing process representation and model structure on physical evidence. Hydrol. Process. 21, 2650–2667. https://doi.org/10.1002/hyp

Porter, J.R., Semenov, M.A., 2005. Crop responses to climatic variation. Philos. Trans. R. Soc. B Biol. Sci. 360, 2021–2035. https://doi.org/10.1098/rstb.2005.1752

Preston, S.D., Alexander, R.B., Schwarz, G.E., Smith, R.A., 2014. Spatially Explicit Modeling to Evaluate Regional Stream Water Quality. Compr. Water Qual. Purif. 1, 221–244. https://doi.org/10.1016/B978-0-12-382182-9.00013-X

Qi, J., Li, S., Li, Q., Xing, Z., P-A Bourque, C., Meng, F.-R., 2016. A new soil-temperature module for SWAT application in regions with seasonal snow cover. https://doi.org/10.1016/j.jhydrol.2016.05.003

Qin, Y., Abatzoglou, J.T., Siebert, S., Huning, L.S., AghaKouchak, A., Mankin, J.S., Hong, C., Tong, D., Davis, S.J., Mueller, N.D., 2020. Agricultural risks from changing snowmelt. Nat. Clim. Chang. 10, 459–465. https://doi.org/10.1038/s41558-020-0746-8

Qiu, J., Shen, Z., Xie, H., 2023. Drought impacts on hydrology and water quality under climate change. Sci. Total Environ. 858, 159854. https://doi.org/10.1016/j.scitotenv.2022.159854

Qu, S., Liang, S., Konar, M., Zhu, Z., Chiu, A.S.F., Jia, X., Xu, M., 2018. Virtual Water Scarcity Risk to the Global Trade System. Environ. Sci. Technol. 52, 673–683. https://doi.org/10.1021/ACS.EST.7B04309/ASSET/IMAGES/LARGE/ES-2017-04309V_0004.JPEG

Quilbé, R., Rousseau, A.N., Moquet, J.S., Trinh, N.B., Dibike, Y., Gachon, P., Chaumont, D., 2008. Assessing the effect of climate change on river flow using general circulation models and hydrological modelling - Application to the chaudière River, Québec, Canada. Can. Water Resour. J. 33, 73–94.

Raes, D., Steduto, P., Hsiao, T.C., Fereres, E., 2018. Chapter 3 Calculation procedures AquaCrop Reference manual.

Rai, R.K., Gosain, A.K., Singh, P., Dixit, S., 2021. Farm Advisory Services for Farmers Using SWAT and APEX Model. Springer, Cham, pp. 444–458. https://doi.org/10.1007/978-3-030-67654-4_47

Rayid, D.K., West, P.C., Clark, M., Gerber, J.S., Prishchepov, A. V, Chatterjee, S., 2019. Climate change has likely already affected global food production. https://doi.org/10.1371/journal.pone.0217148

Reich, P.B., Hobbie, S.E., Lee, T.D., 2014. Plant growth enhancement by elevated CO 2

eliminated by joint water and nitrogen limitation. https://doi.org/10.1038/NGEO2284

Ringersma, J., Batjes, N., Dent, D., 2003. Green Water: definitions and data for assessment. ISRIC – World Soil Inf. 83.

Ritchie, J.T., 1972. Model for predicting evaporation from a row crop with incomplete cover. Water Resour. Res. 8, 1204–1213. https://doi.org/10.1029/WR008i005p01204

Rockström, J., 2003. Water for food and nature in droughtprone tropics: vapour shift in rainfed agriculture. Philos. Trans. R. Soc. London. Ser. B Biol. Sci. 358, 1997–2009. https://doi.org/10.1098/RSTB.2003.1400

Rosenzweig, C., Elliott, J., Deryng, D., Ruane, A.C., Müller, C., Arneth, A., Boote, K.J., Folberth, C., Glotter, M., Khabarov, N., Neumann, K., Piontek, F., Pugh, T.A.M., Schmid, E., Stehfest, E., Yang, H., Jones, J.W., 2014. Assessing agricultural risks of climate change in the 21st century in a global gridded crop model intercomparison. Proc. Natl. Acad. Sci. U. S. A. 111, 3268–3273. https://doi.org/10.1073/PNAS.1222463110/SUPPL_FILE/SAPP.PDF

Roudier, P., Sultan, B., Quirion, P., Berg, A., 2011. The impact of future climate change on West African crop yields: What does the recent literature say? Glob. Environ. Chang. 21, 1073–1083. https://doi.org/10.1016/j.gloenvcha.2011.04.007

Rouholahnejad, E., Abbaspour, K.C., Srinivasan, R., Bacu, V., Lehmann, A., 2014. Water resources of the Black Sea Basin at high spatial and temporal resolution. Water Resour. Res. 50, 5866–5885. https://doi.org/10.1002/2013WR014132

Rubin, J., Hurst, C., 2017. C. Hurst and; Company Report Part Title: A High-latitude Breadbasket in a Warming Climate Report Title: Economic Opportunities from a Changing Climate.

Rungee, J., Bales, R., Goulden, M., 2019. Evapotranspiration response to multiyear dry periods in the semiarid western United States. Hydrol. Process. 33, 182–194. https://doi.org/10.1002/hyp.13322

Sadras, V., Alston, J., Aphalo, P., Connor, D., Denison, R.F., Fischer, T., Gray, R., Hayman, P., Kirkegaard, J., Kirchmann, H., Kropff, M., Lafitte, H.R., Langridge, P., Lenne, J., Mínguez, M.I., Passioura, J., Porter, J.R., Reeves, T., Rodriguez, D., Ryan, M., Villalobos, F.J., Wood, D., 2020. Making science more effective for agriculture. Adv. Agron. 163, 153–177. https://doi.org/10.1016/bs.agron.2020.05.003

Saft, M., Peel, M.C., Western, A.W., Zhang, L., 2016. Predicting shifts in rainfall-runoff partitioning during multiyear drought: Roles of dry period and catchment characteristics. Water Resour. Res. 52, 9290–9305. https://doi.org/10.1002/2016WR019525

Saft, M., Western, A.W., Zhang, L., Peel, M.C., Potter, N.J., 2015. The influence of multiyear drought on the annual rainfall-runoff relationship: An Australian perspective. Water Resour. Res. 51, 2444–2463. https://doi.org/10.1002/2014WR015348

Saltelli, A., Jakeman, A., Razavi, S., Wu, Q., 2021. Sensitivity analysis: A discipline coming of age. Environ. Model. Softw. 146, 105226. https://doi.org/10.1016/J.ENVSOFT.2021.105226

Schewe, J., Heinke, J., Gerten, D., Haddeland, I., Arnell, N.W., Clark, D.B., Dankers, R., Eisner, S., Fekete, B.M., Colón-González, F.J., Gosling, S.N., Kim, H., Liu, X., Masaki, Y., Portmann, F.T., Satoh, Y., Stacke, T., Tang, Q., Wada, Y., Wisser, D., Albrecht, T., Frieler, K., Piontek, F., Warszawski, L., Kabat, P., 2014. Multimodel assessment of water scarcity under climate change. Proc. Natl. Acad. Sci. U. S. A. 111, 3245–3250. https://doi.org/10.1073/PNAS.1222460110/-/DCSUPPLEMENTAL/SAPP.PDF

Schyns, J.F., Hoekstra, A.Y., Booij, M.J., Hogeboom, R.J., Mekonnen, M.M., 2019. Limits to the world's green water resources for food, feed, fiber, timber, and bioenergy. Proc. Natl. Acad. Sci. U. S. A. 116, 4893–4898. https://doi.org/10.1073/PNAS.1817380116/SUPPL_FILE/PNAS.1817380116.SAPP.PDF

Shahvari, N., Khalilian, S., Mosavi, S.H., Mortazavi, S.A., 2019. Assessing climate change impacts on water resources and crop yield: a case study of Varamin plain basin, Iran. Environ. Monit. Assess. 191, 134. https://doi.org/10.1007/s10661-019-7266-x

Sharma, L.K., Bali, S.K., 2017. A review of methods to improve nitrogen use efficiency in agriculture. Sustain. https://doi.org/10.3390/su10010051

Shi, W., Tao, F., Zhang, Z., 2013. A review on statistical models for identifying climate contributions to crop yields. J. Geogr. Sci. 23, 567–576. https://doi.org/10.1007/s11442-013-1029-3

Smith, C.J., Hunt, J.R., Wang, E., Macdonald, B.C.T., Xing, H., Denmead, O.T., Zeglin, S., Zhao, Z., 2019. Using fertiliser to maintain soil inorganic nitrogen can increase dryland wheat yield with little environmental cost. Agric. Ecosyst. Environ. 286, 106644. https://doi.org/10.1016/j.agee.2019.106644

Srivastav, A.L., Dhyani, R., Ranjan, M., Madhav, S., Sillanpää, M., 2021. Climate-resilient strategies for sustainable management of water resources and agriculture. Environ. Sci. Pollut. Res. 2021 2831 28, 41576–41595. https://doi.org/10.1007/S11356-021-14332-4

Starr, M., Deng, B., Helenius, J., 2020. AquaCrop-Simulated Response of Sorghum Biomass and Grain Yield to Biochar Amendment in South Sudan. Agronomy 10, 67. https://doi.org/10.3390/agronomy10010067

Steduto, P., 2003. Biomass Water-Productivity Comparing the Growth-Engines of Crop Models-Faculty of Agriculture, Bologna Biomass Water-Productivity Pasquale Steduto.

Steduto, P., Hsiao, T.C., Raes, D., Fereres, E., 2009. Aquacrop-the FAO crop model to simulate yield response to water: I. concepts and underlying principles. Agron. J. 101, 426–437. https://doi.org/10.2134/agronj2008.0139s

Stenke, A., 2020. Natural control on ozone pollution. Nat. Clim. Chang. 10, 101–102. https://doi.org/10.1038/s41558-019-0686-3

Stocker, T.F., Qin, D., Plattner, G.-K., Tignor, M.M.B., Allen, S.K., Boschung, J., Nauels, A., Xia, Y., Bex, V., Midgley, P.M., 2013. Climate Change 2013 The Physical Science Basis Working Group I Contribution to the Fifth Assessment Report of the Intergovernmental Panel on Climate Change Edited by.

Stöckle, C.O., Donatelli, M., Nelson, R., 2003. CropSyst, a cropping systems simulation model,

in: European Journal of Agronomy. Elsevier, pp. 289–307. https://doi.org/10.1016/S1161-0301(02)00109-0

Svoboda, M., LeComte, D., Hayes, M., Heim, R., Gleason, K., Angel, J., Rippey, B., Tinker, R., Palecki, M., Stooksbury, D., Miskus, D., Stephens, S., 2002. the Drought Monitor. Bull. Am. Meteorol. Soc. 83, 1181–1190. https://doi.org/10.1175/1520-0477-83.8.1181

Svoboda, M.D., Hayes, M.J., Wilhite, D.A., Tadesse, T., 2004. Recent advances in drought monitoring. Bull. Am. Meteorol. Soc. 5237–5240.

Swann, A.L.S., Hoffman, F.M., Koven, C.D., Randerson, J.T., 2016. Plant responses to increasing CO2 reduce estimates of climate impacts on drought severity. Proc. Natl. Acad. Sci. U. S. A. 113, 10019–10024. https://doi.org/10.1073/pnas.1604581113

Tam, B.Y., Szeto, K., Bonsal, B., Flato, G., Cannon, A.J., Rong, R., 2019. CMIP5 drought projections in Canada based on the Standardized Precipitation Evapotranspiration Index. Can. Water Resour. J. 44, 90–107. https://doi.org/10.1080/07011784.2018.1537812

Tao, F., Yokozawa, M., Zhang, Z., 2009. Modelling the impacts of weather and climate variability on crop productivity over a large area: A new process-based model development, optimization, and uncertainties analysis. Agric. For. Meteorol. 149, 831–850. https://doi.org/10.1016/j.agrformet.2008.11.004

Trenberth, K.E., Dai, A., Van Der Schrier, G., Jones, P.D., Barichivich, J., Briffa, K.R., Sheffield, J., 2013. Global warming and changes in drought. Nat. Clim. Chang. 2014 41 4, 17–22. https://doi.org/10.1038/nclimate2067

Tubiello, F.N., Amthor, J.S., Boote, K.J., Donatelli, M., Easterling, W., Fischer, G., Gifford, R.M., Howden, M., Reilly, J., Rosenzweig, C., 2007. Crop response to elevated CO2 and world food supply. A comment on "Food for Thought..." by Long et al., Science 312:1918-1921, 2006. Eur. J. Agron. 26, 215–223. https://doi.org/10.1016/j.eja.2006.10.002

Uddin, S., Löw, M., Parvin, S., Fitzgerald, G., Bahrami, H., Tausz-Posch, S., Armstrong, R., O'Leary, G., Tausz, M., 2018. Water use and growth responses of dryland wheat grown under elevated [CO2] are associated with root length in deeper, but not upper soil layer. F. Crop. Res. 224, 170–181. https://doi.org/10.1016/j.fcr.2018.05.014

Uniyal, B., Dietrich, J., 2019. Modifying Automatic Irrigation in SWAT for Plant Water Stress scheduling. Agric. Water Manag. 223, 105714. https://doi.org/10.1016/j.agwat.2019.105714

Urban, J., Ingwers, M., McGuire, M.A., Teskey, R.O., 2017. Stomatal conductance increases with rising temperature. Plant Signal. Behav. 12, e1356534. https://doi.org/10.1080/15592324.2017.1356534

Valentin, M.M., Hogue, T.S., Hay, L.E., 2018. Hydrologic regime changes in a high-latitude glacierizedwatershed under future climate conditions. Water (Switzerland) 10, 128. https://doi.org/10.3390/w10020128

Van Dam, J.C., Huygen, J., Wesseling, J.G., Feddes, R.A., Kabat, P., Van, P.E. V, Groenendijk, W.P., Van, C.A., Report, D., 1979. Theory of SWAP version 2.0 Simulation of water flow, solute transport and plant growth in the Soil-Water-Atmosphere-Plant environment.

Van Ittersum, M.K., Leffelaar, P.A., Van Keulen, H., Kropff, M.J., Bastiaans, L., Goudriaan, J., 2003. On approaches and applications of the Wageningen crop models, in: European Journal of Agronomy. Elsevier, pp. 201–234. https://doi.org/10.1016/S1161-0301(02)00106-5

Van Loon, A.F., Van Lanen, H.A.J., 2013. Making the distinction between water scarcity and drought using an observation-modeling framework. Water Resour. Res. 49, 1483–1502. https://doi.org/10.1002/WRCR.20147

Vetter, T., Reinhardt, J., Flörke, M., van Griensven, A., Hattermann, F., Huang, S., Koch, H., Pechlivanidis, I.G., Plötner, S., Seidou, O., Su, B., Vervoort, R.W., Krysanova, V., 2017. Evaluation of sources of uncertainty in projected hydrological changes under climate change in 12 large-scale river basins. Clim. Change 141, 419–433. https://doi.org/10.1007/s10584-016-1794-y

Vicente-Serrano, S.M., Beguería, S., López-Moreno, J.I., 2010. A Multiscalar Drought Index Sensitive to Global Warming: The Standardized Precipitation Evapotranspiration Index. J. Clim. 23, 1696–1718. https://doi.org/10.1175/2009JCLI2909.1

Vicente-Serrano, S.M., Domínguez-Castro, F., Murphy, C., Peña-Angulo, D., Tomas-Burguera, M., Noguera, I., López-Moreno, J.I., Juez, C., Grainger, S., Eklundh, L., Conradt, T., Azorin-Molina, C., El Kenawy, A., 2021. Increased Vegetation in Mountainous Headwaters Amplifies Water Stress During Dry Periods. Geophys. Res. Lett. 48, e2021GL094672. https://doi.org/10.1029/2021GL094672

Vicente-Serrano, S.M., Van Der Schrier, G., Beguería, S., Azorin-Molina, C., Lopez-Moreno, J.-I., 2014. Contribution of precipitation and reference evapotranspiration to drought indices under different climates. https://doi.org/10.1016/j.jhydrol.2014.11.025

Vincent, L.A., Zhang, X., Mekis, Wan, H., Bush, E.J., 2018. Changes in Canada's Climate: Trends in Indices Based on Daily Temperature and Precipitation Data. Atmos. - Ocean 56, 332–349. https://doi.org/10.1080/07055900.2018.1514579

Vörösmarty, C.J., McIntyre, P.B., Gessner, M.O., Dudgeon, D., Prusevich, A., Green, P., Glidden, S., Bunn, S.E., Sullivan, C.A., Liermann, C.R., Davies, P.M., 2010. Global threats to human water security and river biodiversity. Nat. 2010 4677315 467, 555–561. https://doi.org/10.1038/nature09440

Wang, B., Liu, D.L., Waters, C., Yu, Q., 2018. Quantifying sources of uncertainty in projected wheat yield changes under climate change in eastern Australia. Clim. Change 151, 259–273. https://doi.org/10.1007/s10584-018-2306-z

Wang, E., Xu, J., Jiang, Q., Austin, J., 2009. Assessing the spatial impact of climate on wheat productivity and the potential value of climate forecasts at a regional level. Theor. Appl. Climatol. 95, 311–330. https://doi.org/10.1007/s00704-008-0009-5

Wang, H., Chen, Y., Pan, Y., Chen, Z., Ren, Z., 2019. Assessment of candidate distributions for SPI/SPEI and sensitivity of drought to climatic variables in China. Int. J. Climatol. 39, 4392–4412. https://doi.org/10.1002/JOC.6081

Wang, R., Bowling, L.C., Cherkauer, K.A., 2016. Estimation of the effects of climate variability

on crop yield in the Midwest USA. Agric. For. Meteorol. 216, 141–156. https://doi.org/10.1016/j.agrformet.2015.10.001

Wang, S.W., Lee, W.K., Son, Y., 2017. An assessment of climate change impacts and adaptation in South Asian agriculture. Int. J. Clim. Chang. Strateg. Manag. 9, 517–534. https://doi.org/10.1108/IJCCSM-05-2016-0069

Wang, X., Fan, J., Xing, Y., Xu, G., Wang, H., Deng, J., Wang, Y., Zhang, F., Li, P., Li, Z., 2019. The Effects of Mulch and Nitrogen Fertilizer on the Soil Environment of Crop Plants. Adv. Agron. 153, 121–173. https://doi.org/10.1016/bs.agron.2018.08.003

Wasaya, A., Zhang, X., Fang, Q., Yan, Z., 2018. Root Phenotyping for Drought Tolerance: A Review. Agron. 2018, Vol. 8, Page 241 8, 241. https://doi.org/10.3390/AGRONOMY8110241

Wasko, C., Nathan, R., Peel, M.C., 2020. Changes in Antecedent Soil Moisture Modulate Flood Seasonality in a Changing Climate. Water Resour. Res. 56, no. https://doi.org/10.1029/2019WR026300

Weedon, G.P., Balsamo, G., Bellouin, N., Gomes, S., Best, M.J., Viterbo, P., 2014a. The WFDEI meteorological forcing data set: WATCH Forcing Data methodology applied to ERA-Interim reanalysis data. Water Resour. Res. 50, 7505–7514. https://doi.org/10.1002/2014WR015638

Weedon, G.P., Balsamo, G., Bellouin, N., Gomes, S., Best, M.J., Viterbo, P., 2014b. The WFDEI meteorological forcing data set: WATCH Forcing Data methodology applied to ERA-Interim reanalysis data. Water Resour. Res. 50, 7505–7514. https://doi.org/10.1002/2014WR015638

Werner, A.T., Cannon, A.J., 2016. Hydrologic extremes - An intercomparison of multiple gridded statistical downscaling methods. Hydrol. Earth Syst. Sci. 20, 1483–1508. https://doi.org/10.5194/hess-20-1483-2016

Wong, J.S., Razavi, S., Bonsal, B.R., Wheater, H.S., Asong, Z.E., 2017. Inter-comparison of daily precipitation products for large-scale hydro-climatic applications over Canada. Hydrol. Earth Syst. Sci. 21, 2163–2185. https://doi.org/10.5194/hess-21-2163-2017

Wossenyeleh, B.K., Verbeiren, B., Diels, J., Huysmans, M., 2020. Vadose Zone Lag Time Effect on Groundwater Drought in a Temperate Climate. Water 2020, Vol. 12, Page 2123 12, 2123. https://doi.org/10.3390/W12082123

Wu, L., Elshorbagy, A., Pande, S., Zhuo, L., 2021. Trade-offs and synergies in the water-energy-food nexus: The case of Saskatchewan, Canada. Resour. Conserv. Recycl. 164. https://doi.org/10.1016/J.RESCONREC.2020.105192

Wu, X., Hao, Z., Hao, F., Singh, V.P., Zhang, X., 2019. Dry-hot magnitude index: a joint indicator for compound event analysis. Environ. Res. Lett. 14, 064017. https://doi.org/10.1088/1748-9326/AB1EC7

Yang, C., Fraga, H., Ieperen, W. Van, Santos, J.A., 2017. Assessment of irrigated maize yield response to climate change scenarios in Portugal. Agric. Water Manag. 184, 178–190. https://doi.org/10.1016/j.agwat.2017.02.004

Yang, X., Tian, Z., Sun, L., Chen, B., Tubiello, F.N., Xu, Y., 2017. The impacts of increased heat stress events on wheat yield under climate change in China. Clim. Change 140, 605–620. https://doi.org/10.1007/s10584-016-1866-z

Yang, Y., Gan, T.Y., Tan, X., 2020. Spatiotemporal changes of drought characteristics and their dynamic drivers in Canada. Atmos. Res. 232. https://doi.org/10.1016/J.ATMOSRES.2019.104695

Yang, Y., McVicar, T.R., Donohue, R.J., Zhang, Y., Roderick, M.L., Chiew, F.H.S., Zhang, L., Zhang, J., 2017. Lags in hydrologic recovery following an extreme drought: Assessing the roles of climate and catchment characteristics. Water Resour. Res. 53, 4821–4837. https://doi.org/10.1002/2017WR020683

Zang, C., Mao, G., 2019. A Spatial and Temporal Study of the Green and Blue Water Flow Distribution in Typical Ecosystems and its Ecosystem Services Function in an Arid Basin. Water 2019, Vol. 11, Page 97 11, 97. https://doi.org/10.3390/W11010097

Zaremehrjardy, M., Razavi, S., Faramarzi, M., 2020. Assessment of the cascade of uncertainty in future snow depth projections across watersheds of mountainous, foothill, and plain areas in northern latitudes. J. Hydrol. 125735. https://doi.org/10.1016/j.jhydrol.2020.125735

Zhang, F., Lu, K., Gu, Y., Zhang, L., Li, W., Li, Z., 2020. Effects of Low-Temperature Stress and Brassinolide Application on the Photosynthesis and Leaf Structure of Tung Tree Seedlings. Front. Plant Sci. 10, 1767. https://doi.org/10.3389/FPLS.2019.01767/XML/NLM

Zhang, S., Tao, F., Zhang, Z., 2016. Changes in extreme temperatures and their impacts on rice yields in southern China from 1981 to 2009. F. Crop. Res. 189, 43–50. https://doi.org/10.1016/j.fcr.2016.02.008

Zhang, Y., Zhang, J., Tang, G., Chen, M., Wang, L., 2016. Virtual water flows in the international trade of agricultural products of China. Sci. Total Environ. 557–558, 1–11. https://doi.org/10.1016/j.scitotenv.2016.02.166

Zhao, C., Brissette, F., Chen, J., Martel, J.L., 2020. Frequency change of future extreme summer meteorological and hydrological droughts over North America. J. Hydrol. 584, 124316. https://doi.org/10.1016/j.jhydrol.2019.124316

Zhao, Y., Wang, C., Zhang, Y., 2019. Uncertainties in the Effects of Climate Change on Maize Yield Simulation in Jilin Province: A Case Study. J. Meteorol. Res. 33, 777–783. https://doi.org/10.1007/s13351-019-8143-9

Zhuo, L., Mekonnen, M.M., Hoekstra, A.Y., 2016. The effect of inter-annual variability of consumption, production, trade and climate on crop-related green and blue water footprints and inter-regional virtual water trade: A study for China (1978-2008). Water Res. 94, 73–85. https://doi.org/10.1016/j.watres.2016.02.037

Zubrycki, K., Roy, D., Osman, H., Lewtas, K., Gunn, G., Grosshans, R., 2016. Large Area Planning in the Nelson-Churchill River Basin (NCRB): Laying a foundation in northern Manitoba.

APPENDICES

Table A.1. Data sources used in this study (Adapted from Faramarzi *et al.*, (2015)).

Input variable type	dataset	Resolution	Reference
Climate data	Meteorological stations	-	Government of Canada; http://climate.weather.gc.ca/
	CFSR	0.3° grid	http://globalweather.tamu.edu/
	CRU	0.5° grid	Harris *et al.*, (2014)
	NRCAN	10 km × 10 km	McKenney *et al.*, (2011)
Land use map	USGS Landuse/land cover map	1 km × 1 km	USGS Global Land Use Land Cover Characterization (GLCC) database; https://www.usgs.gov/
Soil map	Soil Landscapes of Canada	250 meter	Cordeiro *et al.*, (2018)
DEM map	Shuttle Radar Topography Mission	90 meter	http://srtm.csi.cgiar.org

Table A.2. The climate change models information used in this study.

GCM	Modeling center	Institution	Scenario
CanESM2	CCCma	Canadian Centre for Climate Modeling and Analysis	RCP 2.6, 8.5
CCSM4	NCAR	National Center for Atmospheric Research	RCP 2.6, 8.5
CNRM-CM5	CNRM-CERFACS	Centre National de Recherches Meteorologiques/Centre Europeen de Recherche et Formation Avancees en Calcul Scientifique	RCP 2.6, 8.5
CSIRO-MK3.6.0	CSIRO-QCCCE	Commonwealth Scientific and Industrial Research Organization in collaboration with the Queensland Climate Change Centre of Excellence	RCP 2.6, 8.5
GFDL-ESM2G	NOAA GFDL	Geophysical Fluid Dynamics Laboratory	RCP 2.6, 8.5
HadGEM2	MOHC	Met Office Hadley Centre (additional HadGEM2-ES runs by Instituto Nacional de Pesquisas Espaciais)	RCP 2.6, 8.5
MIROC5	MIROC	Meteorological Research Institute	RCP 2.6, 8.5
MPI-ESM-LR	MPI-M	Max Planck Institute for Meteorology	RCP 2.6, 8.5
MRI-CGCM3	MRI	Meteorological Research Institute	RCP 2.6, 8.5

Table A.3. Model performance statistics for streamflow simulation during the entire calibration and validation period for individual hydrometric stations (1986-2007).

Station Number	p-factor	r-factor	bR^2	NSE
1	0.76	1.51	0.19	0.38
2	0.94	1.85	0.43	0.08
3	0.89	1.93	0.35	0.18
4	0.56	1.65	0.36	0.14
5	0.58	0.63	0.47	0.57
6	0.59	0.77	0.43	0.59
7	0.27	1.20	0.01	0.02
8	0.74	0.92	0.56	0.46
9	0.22	0.51	0.06	0.19
10	0.62	0.78	0.44	0.61
11	0.66	0.75	0.55	0.47
12	0.73	3.74	0.01	0.18
13	0.80	1.37	0.64	0.64

Table A.4. List of available data and their specifications.

Input data		Time Span	Resolution	Time step	Region	Nr. Of stations/grids in study area	References
DEM		2008	10 m × 10 m and 90 m × 90 m	-	Global	100% coverage	AltaLIS, http://www.altalis.com; SRTM, Jarvis et al., (2008)
Land use/Land cover		2015	30 m × 30 m	-	Regional/Canadian	100% coverage	Government of Canada (2019)
Soil map	FAO	2005	10 km × 10 km	-	Global	100% coverage	FAO, (1995)
	SLC V3.2	2018	1 km × 1 km	-	Regional/Canadian	Covers the agricultural lands in Canada	Cordeiro et al., (2018)
Climate	WFDEI	1979-2016	0.5° grid	3 hr	Global	574	Weedon et al., (2014)
Potholes		Delineated for each sub-basin	100% coverage	-	Regional/Canadian	100% coverage	Messager et al., (2016)
Reservoir		1982-2016	100% coverage	monthly	Local	44 main reservoirs-lakes	Alberta Environment and Parks; Water Security Agency (WSA) in Saskatchewan; Manitoba Hydro; and HydroLAKES database
Date of planting and harvesting, volume and rate of fertilizer and irrigation application		1982-2016	100% coverage	-	Local	Covers the agricultural lands in Canada	Government of Alberta (Alberta Fertilizer Guide, 2004); Government of Manitoba (Heard, 2020); and Government of Saskatchewan, (2020)
Crop yield		1982-2016	Census Agricultural Region level	yearly	Local	Covers the agricultural lands in Canada	Alberta Financial Service Cooperation (AFSC); Statistics Canada (2021); Manitoba Agricultural Services Corporation; Government of Saskatchewan

Table A.5. Selected parameters for sensitivity analysis and calibration of crop yields.

No.	Parameter	Underlying SWAT parameter
1	v__DAY{[],1}.mgt	Plant growing season date
2	v__DAY{[],5}.mgt	Day harvest takes place
3	v__HEAT_UNITS{[],1}.mgt	Total heat units for plant to reach maturity
4	v__HI_TARG{[],1}.mgt	Harvest index target ((kg/ha)/(kg/ha))
5	v__AUTO_NSTRS{[],11}.mgt	N-stress factor of plant that triggers fertilization
6	v__AUTO_NAPP{[],11}.mgt	Maximum amount of mineral N allowed in any one application (kg N/ha)
7	v__AUTO_NYR{[],11}.mgt	Maximum amount of mineral N allowed to be applied in any one year (kg N/ha)
8	v__AUTO_EFF{[],11}.mgt	Application efficiency
9	v__AUTO_WSTRS{[],10}.mgt	Water stress threshold that triggers irrigation
10	v__AFRT_SURFACE{[],11}.mgt	Fraction of fertilizer applied to top 10 mm of soil
11	r__CN2.mgt	SCS runoff curve number for moisture condition II
12	v__ESCO.hru	Soil evaporation factor
13	v__EPCO.hru	Plant uptake compensation factor
14	v__OV_N.hru	Manning's n value for overland flow
15	v__LAT_TTIME.hru	Lateral flow travel time (days)
16	r__CANMX.hru	Maximum canopy storage (mm H2O)
17	r__HRU_SLP.hru	Average slope steepness (m/m)
18	r__SOL_BD(1).sol	Soil bulk density in layer 1 of soil profile (g/cm3)
19	r__SOL_ALB(1).sol	Moist soil albedo in layer 1 of soil profile
20	r__SOL_K(1).sol	Saturated hydraulic conductivity in layer 1 of soil profile (mm/h)
21	r__SOL_CRK.sol	Potential or maximum crack volume of the soil profile
22	r__SOL_AWC().sol	Available water capacity of the soil layer (mm H2O/mm soil)
23	v__SHALLST.gw	Initial depth of water in the shallow aquifer (mm H2O)
24	v__ALPHA_BF.gw	Baseflow alpha factor (1/days)
25	v__SHALLST_N.gw	Initial concentration of nitrate in shallow aquifer (mg N/L or ppm)
26	v__GW_SPYLD.gw	Specific yield of the shallow aquifer (m3/m3)
27	v__HLIFE_NGW.gw	Half-life of nitrate in the shallow aquifer (days)

Table A.6. Selected parameters for sensitivity analysis and calibration of streamflow.

No.	Parameter	Underlying SWAT parameter
1	v__TLAPS.sub	Temperature lapse rate (°C/km)
2	v__PLAPS.sub	Precipitation lapse rate (mm H_2O/km)
3	v__SUB_SFTMP().sno	Snowfall temperature (°C)
4	v__SUB_SMTMP().sno	Snowmelt base temperature (°C)
5	v__SUB_SMFMX().sno	Melt factor for snow on June 21 (mm H_2O/°C-day)
6	v__SUB_SMFMN().sno	Melt factor for snow on Dec. 21 (mmH_2O/°C-day)
7	v__SUB_TIMP().sno	Snow pack temperature lag factor
8	r__HRU_SLP.hru	Average slope steepness (m/m)
9	r__SLSUBBSN.hru	Average slope length (m)
10	r__CN2.mgt	SCS runoff curve number for moisture condition II
11	v__ESCO.hru	Soil evaporation factor
12	v__EPCO.hru	Plant uptake compensation factor
13	v__OV_N.hru	Manning's n value for overland flow
14	r__ALPHA_BF.gw	Baseflow alpha factor (1/days)
15	r__SOL_ALB().sol	Soil albedo
16	r__SOL_AWC().sol	Available water capacity of the soil layer (mm H_2O/mm soil)
17	r__SOL_K().sol	Saturated hydraulic conductivity (mm/h)
18	r__SOL_BD().sol	Soil bulk density (g/cm^3)
19	v__GW_DELAY.gw	Groundwater delay time (days)
20	v__GW_REVAP.gw	Groundwater “revap” coefficient
21	v__GWQMN.gw	Threshold depth of water in the shallow aquifer required for return flow to occur
22	r__RCHRG_DP.gw	Deep aquifer percolation factor
23	r__REVAPMN.gw	Threshold depth of water in the shallow aquifer for “revap” or percolation to the deep aquifer to occur
24	v__SURLAG.hru	Surface runoff lag coefficient
25	r__POT_FR.hru	Fraction of HRU area that drains into pothole
26	r__POT_VOLX.hru	Maximum volume of water stored in the pothole over the entire HRU

Table A.7. Summary statistics during calibration and validation of discharge.

Basin	bR^2							
	Average of small tributaries			Basin outlet				
	Nr. of calibrated stations	Calibration (1982-2006)	Validation (2007-2016)	Outlet Gauge ID	Calibration (1982-2006)	Validation (2007-2016)	p-factor	r-factor
SRB	43	0.61	0.57	05KJ001	0.60	0.53	0.8	0.85
ARB	9	0.35	0.42	05NG001	0.60	0.70	0.55	0.7
RRB	12	0.55	0.45	05OC012	0.51	0.40	0.67	0.82
WRB	8	0.55	0.5	05PF069	0.61	0.56	0.64	0.65
LWB	7	0.45	0.35	05UB009	0.95	0.96	1	0.01
NRLB	7	0.6	0.6	05UF007	0.82	0.74	0.89	0.4
Basin	NSE							
	Average of small tributaries			Basin outlet				
	Nr. Of calibrated stations	Calibration (1982-2006)	Validation	Outlet Gauge ID	Calibration (1982-2006)	Validation (2007-2016)	p-factor	r-factor
SRB	43	0.4	0.35	05KJ001	0.75	0.67	0.8	0.85
ARB	9	0.3	0.2	05NG001	0.70	0.80	0.55	0.7
RRB	12	0.3	0.3	05OC012	0.65	0.56	0.67	0.82
WRB	8	0.45	0.37	05PF069	0.72	0.65	0.64	0.65
LWB	7	0.3	0.22	05UB009	0.99	0.97	1	0.01
NRLB	7	0.5	0.6	05UF007	0.90	0.88	0.89	0.4

Table A.8. Model performance statistics in each agricultural region during calibration and validation for rainfed and irrigated spring wheat.

			Calibration (1992-2016)			Validation (1982-1991)		
	Province/State	Agricultural region #	p-factor	r-factor	MSE	p-factor	r-factor	MSE
1	Alberta	AB_1	0.95	1.60	0.05	0.80	1.31	0.20
2		AB_1 (irrigated)	0.85	1.80	0.08	0.70	0.93	0.41
3		AB_2	1.00	2.67	0.08	0.90	3.43	0.19
4		AB_2 (irrigated)	0.90	1.84	0.03	0.70	1.55	0.20
5		AB_3	1.00	2.61	0.16	0.70	3.94	0.39
6		AB_3 (irrigated)	1.00	3.70	0.04	0.60	1.55	0.20
7		AB_4A	0.90	1.15	0.10	0.75	2.12	0.16
8		AB_4B	1.00	1.25	0.10	0.76	2.46	0.08
9		AB_5	1.00	2.39	0.11	0.92	3.28	0.14
10		AB_6	0.95	1.57	0.10	0.60	3.13	0.54
11	Manitoba	MA_1	0.95	2.14	0.19	0.60	2.82	0.11
12		MA_2	0.95	1.78	0.14	0.75	1.55	0.13
13		MA-3	0.95	1.88	0.13	0.75	1.96	0.10
14		MA_4	1.00	2.23	0.01	0.94	1.69	0.07
15		MA_5	1.00	2.02	0.05	0.81	1.49	0.15
16		MA_6	0.82	1.54	0.09	0.78	1.51	0.14
17		MA_7	0.89	2.73	0.26	0.84	1.39	0.25
18		MA_8	1.00	2.25	0.23	0.85	2.19	0.15
19		MA_9	0.90	2.34	0.46	0.85	3.43	0.12
20		MA_11	0.80	1.69	0.31	0.82	1.25	0.33
21		MA_12	0.71	1.34	0.20	0.70	1.24	0.23
22	Saskatchewan	SK_1A	0.90	3.41	0.17	1.00	3.40	0.09
23		SK_1B	0.95	1.46	0.10	0.60	1.72	0.16
24		SK_2A	0.90	3.35	0.18	1.00	3.32	0.06
25		SK_2B	0.50	1.51	0.33	0.80	1.77	0.11
26		SK_3AN	0.95	1.99	0.08	0.90	1.28	0.08
27		SK_3BN	1.00	4.57	0.03	0.90	3.69	0.11
28		SK_3BS	1.00	1.67	0.03	0.85	1.20	0.17
29		SK_4A	0.94	2.63	0.07	1.00	2.78	0.06
30		SK_4B	0.82	1.56	0.12	0.70	0.95	0.20
31		SK_5A	1.00	2.43	0.08	0.75	3.74	0.09
32		SK_5B	1.00	4.51	0.09	1.00	6.33	0.13
33		SK_6A	0.90	2.76	0.22	1.00	2.97	0.02
34		SK_6B	0.90	1.43	0.09	0.90	1.47	0.04
35		SK_7A	0.78	1.57	0.17	0.80	1.34	0.07
36		SK_7B	0.80	1.72	0.18	0.80	2.30	0.05
37		SK_8A	0.94	1.24	0.08	0.60	1.31	0.25
38		SK_8B	0.85	1.73	0.10	0.95	1.94	0.12
39		SK_9A	0.84	1.18	0.12	0.95	1.76	0.10
40		SK_9B	0.89	1.62	0.15	0.75	3.34	0.07
41	Minnesota	MN_10	0.90	1.85	0.34	0.70	1.32	0.53
42		MN_40	0.95	1.60	0.18	0.77	1.51	0.36
43	North Dakota	ND_10	0.90	2.77	0.20	1.00	2.45	0.12
44		ND_20	0.75	1.14	0.23	0.26	3.58	0.40
45		ND_30	0.65	3.25	0.38	0.85	1.36	0.30
46		ND_60	0.75	1.67	0.48	0.43	1.20	0.50
47		ND_90	0.60	1.29	0.33	0.87	1.89	0.36

Table A.9. Goodness-of-fit test results of gamma distribution used for all sub-basins. The table presents p-values from KS and AD tests, supporting the gamma distribution model's suitability across all sub-basins. Note that all data are sorted based on SK method.

Subbasin	KS_p_value	AD_p_value	Subbasin	KS_p_value	AD_p_value	Subbasin	KS_p_value	AD_p_value	Subbasin	KS_p_value	AD_p_value	Subbasin	KS_p_value	AD_p_value	Subbasin	KS_p_value	AD_p_value	Subbasin	KS_p_value	AD_p_value	Subbasin	KS_p_value	AD_p_value	Subbasin	KS_p_value	AD_p_value
1	0.996	0.978	1816	0.82	0.936	291	0.623	0.59	1209	0.473	0.365	1968	0.358	0.466	562	0.267	0.159	872	0.192	0.478	945	0.14	0.215	607	0.091	0.074
1807	0.996	0.959	807	0.82	0.711	1934	0.623	0.517	1243	0.472	0.731	1729	0.358	0.298	63	0.267	0.061	1486	0.192	0.468	261	0.14	0.125	1410	0.091	0.055
579	0.995	0.991	1457	0.82	0.701	1004	0.623	0.416	1160	0.472	0.56	783	0.358	0.094	796	0.266	0.215	536	0.192	0.198	1910	0.139	0.292	1321	0.09	0.469
1824	0.995	0.959	1675	0.817	0.806	24	0.623	0.4	1670	0.472	0.392	1174	0.357	0.558	949	0.266	0.172	1030	0.192	0.177	1909	0.139	0.224	1325	0.09	0.469
195	0.995	0.955	30	0.817	0.4	3	0.622	0.965	1435	0.471	0.61	1386	0.357	0.463	1626	0.266	0.141	340	0.192	0.078	994	0.139	0.22	1797	0.09	0.254
1778	0.991	0.959	1874	0.816	0.936	1579	0.622	0.957	1901	0.471	0.072	424	0.356	0.433	1592	0.265	0.46	958	0.191	0.35	343	0.139	0.158	660	0.09	0.102
1945	0.991	0.957	883	0.816	0.711	1086	0.622	0.717	1207	0.47	0.56	1175	0.356	0.265	531	0.265	0.375	1043	0.191	0.21	350	0.139	0.081	1164	0.09	0.09
187	0.99	0.975	388	0.814	0.81	977	0.622	0.365	959	0.47	0.558	1359	0.356	0.22	1741	0.265	0.354	1707	0.191	0.208	1530	0.138	0.468	671	0.09	0.053
1447	0.989	0.946	1883	0.813	0.919	1827	0.621	0.901	459	0.468	0.913	182	0.355	0.259	922	0.265	0.325	612	0.191	0.155	1776	0.138	0.243	1328	0.089	0.206
1932	0.988	0.994	1908	0.813	0.818	1088	0.621	0.823	1363	0.468	0.094	644	0.355	0.15	92	0.265	0.272	1521	0.191	0.123	138	0.138	0.121	613	0.089	0.196
1809	0.988	0.959	552	0.813	0.604	371	0.619	0.676	716	0.467	0.853	516	0.355	0.116	861	0.264	0.426	54	0.191	0.052	1182	0.138	0.104	1696	0.089	0.093
201	0.988	0.929	1582	0.812	0.957	1480	0.618	0.47	1607	0.467	0.505	45	0.354	0.052	1158	0.264	0.252	176	0.19	0.308	85	0.138	0.066	1324	0.088	0.469
208	0.987	0.964	771	0.812	0.358	1058	0.617	0.97	1806	0.467	0.272	1898	0.352	0.756	405	0.264	0.198	1343	0.189	0.469	1889	0.138	0.063	1737	0.088	0.17
489	0.984	0.998	1145	0.811	0.735	1922	0.614	0.774	951	0.467	0.099	1692	0.352	0.066	692	0.264	0.198	1775	0.189	0.243	841	0.137	0.491	1083	0.088	0.124
540	0.983	0.998	1099	0.809	0.735	250	0.614	0.75	1320	0.463	0.823	998	0.352	0.053	966	0.264	0.052	358	0.189	0.209	1727	0.137	0.208	460	0.088	0.114
941	0.982	0.934	1346	0.807	0.895	1531	0.613	0.501	1823	0.463	0.461	747	0.351	0.454	284	0.263	0.545	767	0.189	0.168	1370	0.137	0.166	1159	0.088	0.094
404	0.98	0.99	1766	0.806	0.945	227	0.611	0.53	526	0.463	0.215	97	0.351	0.334	186	0.263	0.259	1255	0.189	0.131	1505	0.137	0.123	435	0.087	0.4
324	0.98	0.975	170	0.805	0.562	1195	0.611	0.394	211	0.463	0.056	200	0.351	0.259	1685	0.263	0.138	276	0.188	0.365	1774	0.137	0.053	1525	0.087	0.384
1344	0.979	0.656	1185	0.804	0.859	505	0.61	0.782	1716	0.462	0.649	225	0.35	0.53	1552	0.263	0.123	1573	0.188	0.238	86	0.137	0.052	384	0.087	0.372
10	0.977	0.815	229	0.804	0.726	1598	0.609	0.614	277	0.461	0.682	1469	0.35	0.47	1588	0.263	0.123	920	0.188	0.215	1925	0.136	0.678	283	0.087	0.285
591	0.976	0.982	1921	0.801	0.916	541	0.609	0.464	4	0.46	0.81	192	0.35	0.452	880	0.262	0.295	364	0.188	0.209	563	0.136	0.397	179	0.087	0.283
194	0.976	0.955	1402	0.801	0.815	1790	0.609	0.33	214	0.46	0.259	96	0.35	0.443	1193	0.262	0.252	1109	0.188	0.186	1033	0.136	0.21	70	0.087	0.066
1655	0.976	0.868	1856	0.801	0.803	281	0.608	0.556	1449	0.459	0.459	1882	0.35	0.433	64	0.262	0.186	503	0.188	0.159	689	0.136	0.168	1892	0.087	0.063
1076	0.975	0.934	1558	0.801	0.501	1453	0.608	0.497	1699	0.459	0.383	1698	0.35	0.178	657	0.261	0.259	1024	0.188	0.107	1326	0.136	0.156	765	0.086	0.293
1280	0.975	0.886	496	0.8	0.929	240	0.607	0.8	866	0.457	0.636	1197	0.35	0.166	761	0.261	0.2	707	0.187	0.198	377	0.136	0.114	642	0.086	0.275

13	0.974	0.963	1171	0.8	0.735	409	0.606	0.829	53	0.457	0.11	640	0.35	0.102	90	0.26	0.447	1702	0.187	0.17	805	0.136	0.069	237	0.086	0.272
1976	0.973	0.912	835	0.8	0.685	1580	0.604	0.85	1888	0.457	0.056	763	0.349	0.2	792	0.26	0.215	148	0.186	0.308	777	0.136	0.053	634	0.086	0.251
592	0.972	0.982	842	0.798	0.711	1466	0.604	0.61	206	0.456	0.232	35	0.349	0.115	1307	0.259	0.339	608	0.186	0.15	1756	0.135	0.384	1002	0.086	0.143
518	0.971	0.976	1972	0.797	0.726	1498	0.604	0.472	122	0.455	0.35	1023	0.348	0.138	584	0.259	0.224	755	0.186	0.126	1738	0.135	0.243	651	0.086	0.137
1954	0.971	0.957	1885	0.793	0.857	1459	0.604	0.468	714	0.453	0.155	641	0.347	0.106	1748	0.259	0.178	398	0.186	0.095	1834	0.135	0.072	205	0.085	0.313
1571	0.971	0.896	1731	0.793	0.73	947	0.603	0.711	1688	0.453	0.056	558	0.347	0.065	40	0.259	0.103	935	0.186	0.079	1759	0.135	0.056	1074	0.085	0.147
1373	0.97	0.905	1616	0.792	0.896	1331	0.603	0.546	1191	0.452	0.339	81	0.346	0.443	860	0.258	0.426	69	0.186	0.052	397	0.134	0.078	382	0.085	0.095
1425	0.97	0.895	1411	0.79	0.815	1563	0.602	0.957	539	0.451	0.782	27	0.346	0.4	1474	0.257	0.468	1912	0.185	0.577	1677	0.133	0.425	770	0.085	0.095
735	0.968	0.839	1820	0.789	0.901	544	0.602	0.68	731	0.451	0.685	448	0.346	0.255	666	0.257	0.428	1497	0.185	0.472	37	0.133	0.103	1112	0.085	0.086
1526	0.968	0.546	1583	0.789	0.656	1858	0.601	0.901	997	0.451	0.08	1965	0.346	0.241	1138	0.257	0.124	565	0.185	0.176	44	0.132	0.195	1819	0.085	0.075
9	0.967	0.815	1595	0.787	0.879	1785	0.601	0.429	1859	0.45	0.343	1206	0.346	0.174	506	0.256	0.281	1010	0.185	0.128	1399	0.132	0.165	167	0.084	0.232
582	0.965	0.967	1577	0.785	0.701	1564	0.598	0.573	190	0.45	0.304	77	0.344	0.286	1090	0.256	0.271	480	0.185	0.095	1478	0.132	0.123	1334	0.083	0.37
1815	0.965	0.959	1313	0.784	0.815	481	0.597	0.676	1152	0.446	0.339	1637	0.343	0.531	923	0.256	0.199	775	0.185	0.094	1042	0.132	0.085	226	0.083	0.232
1635	0.965	0.946	230	0.782	0.674	1668	0.595	0.392	635	0.446	0.281	1747	0.343	0.461	1267	0.256	0.186	1919	0.185	0.063	1105	0.131	0.286	42	0.083	0.195
181	0.964	0.9	1843	0.781	0.833	1309	0.594	0.269	525	0.445	0.433	51	0.343	0.072	1566	0.256	0.138	1352	0.184	0.469	1094	0.131	0.22	1798	0.083	0.17
1360	0.964	0.895	1215	0.78	0.735	256	0.591	0.685	1273	0.443	0.56	1705	0.343	0.053	845	0.256	0.072	956	0.184	0.293	1950	0.131	0.188	1262	0.083	0.156
1463	0.963	0.895	1368	0.779	0.724	218	0.591	0.53	918	0.443	0.474	113	0.34	0.066	610	0.255	0.106	1708	0.184	0.243	1832	0.131	0.179	383	0.083	0.116
1008	0.962	0.95	228	0.778	0.644	1051	0.591	0.365	198	0.443	0.271	1757	0.339	0.649	1914	0.254	0.188	1316	0.183	0.469	1391	0.13	0.339	630	0.083	0.095
639	0.96	0.854	1581	0.777	0.85	680	0.59	0.772	1854	0.443	0.21	1603	0.339	0.46	375	0.253	0.48	1294	0.183	0.265	828	0.13	0.215	794	0.082	0.293
928	0.958	0.732	1584	0.777	0.656	234	0.589	0.674	932	0.442	0.325	1381	0.339	0.449	1541	0.253	0.322	1609	0.183	0.238	158	0.13	0.121	436	0.082	0.166
488	0.956	0.998	1948	0.777	0.517	819	0.588	0.636	899	0.441	0.069	111	0.338	0.446	1390	0.252	0.061	1355	0.183	0.166	1725	0.13	0.093	209	0.082	0.154
734	0.956	0.854	751	0.777	0.485	1274	0.587	0.823	826	0.44	0.319	1128	0.338	0.339	1133	0.251	0.359	1300	0.182	0.469	1585	0.129	0.305	1284	0.082	0.098
537	0.955	0.977	1554	0.775	0.879	1726	0.587	0.774	670	0.44	0.224	292	0.338	0.16	978	0.251	0.325	1261	0.182	0.271	1935	0.129	0.251	1127	0.082	0.086
1864	0.954	0.936	1569	0.774	0.701	426	0.586	0.79	726	0.439	0.421	1365	0.337	0.468	795	0.251	0.293	1791	0.182	0.17	1821	0.129	0.054	370	0.082	0.053
221	0.954	0.934	337	0.773	0.947	1067	0.584	0.745	609	0.439	0.126	1489	0.337	0.33	887	0.251	0.081	838	0.182	0.143	511	0.128	0.4	837	0.081	0.094
1440	0.953	0.895	1873	0.77	0.818	1364	0.584	0.589	522	0.438	0.308	1287	0.337	0.272	831	0.251	0.071	1593	0.182	0.111	499	0.128	0.397	1170	0.081	0.086
363	0.952	0.931	1904	0.77	0.818	1289	0.584	0.459	57	0.437	0.11	1226	0.337	0.269	169	0.25	0.344	1125	0.182	0.086	1475	0.128	0.222	1642	0.081	0.075
133	0.952	0.884	235	0.77	0.581	255	0.583	0.75	891	0.436	0.636	1258	0.337	0.269	241	0.25	0.272	898	0.181	0.285	270	0.128	0.168	1204	0.081	0.061
191	0.951	0.929	1970	0.768	0.669	550	0.583	0.28	678	0.436	0.478	1869	0.336	0.461	1266	0.25	0.098	67	0.181	0.052	1048	0.128	0.085	1542	0.08	0.174
262	0.951	0.685	16	0.767	0.846	249	0.581	0.726	1115	0.435	0.147	1487	0.336	0.46	600	0.249	0.106	762	0.18	0.224	471	0.128	0.065	858	0.08	0.164
1814	0.95	0.959	1984	0.765	0.912	335	0.58	0.676	896	0.435	0.069	1032	0.336	0.416	1509	0.248	0.37	1423	0.18	0.222	1718	0.127	0.354	1643	0.08	0.075

1926	0.949	0.97	1649	0.765	0.392	32	0.58	0.3	571	0.434	0.224	1518	0.335	0.322	934	0.248	0.168	1427	0.18	0.203	781	0.127	0.215	1664	0.08	0.075
874	0.949	0.941	434	0.764	0.811	39	0.58	0.3	1650	0.433	0.392	1442	0.335	0.298	178	0.247	0.283	139	0.18	0.145	41	0.127	0.195	71	0.08	0.052
1398	0.949	0.546	1143	0.764	0.735	266	0.579	0.59	1056	0.433	0.359	1706	0.335	0.056	1744	0.247	0.178	875	0.179	0.293	1101	0.126	0.398	780	0.079	0.473
673	0.948	0.854	1022	0.763	0.732	1479	0.579	0.589	1139	0.433	0.094	1596	0.334	0.46	821	0.247	0.133	1872	0.179	0.292	513	0.126	0.275	1940	0.079	0.177
739	0.947	0.967	1292	0.763	0.731	1855	0.579	0.33	625	0.432	0.198	1470	0.334	0.33	1617	0.246	0.472	1944	0.179	0.188	1927	0.126	0.177	1559	0.079	0.164
581	0.946	0.967	365	0.763	0.676	948	0.578	0.717	1746	0.431	0.21	713	0.334	0.2	857	0.246	0.072	1228	0.179	0.146	147	0.126	0.145	1049	0.079	0.085
1608	0.944	0.879	667	0.762	0.454	1597	0.577	0.85	766	0.431	0.168	285	0.334	0.073	359	0.245	0.48	1758	0.179	0.056	394	0.126	0.074	1663	0.079	0.075
1063	0.942	0.973	449	0.761	0.929	34	0.577	0.3	960	0.431	0.059	1574	0.333	0.472	710	0.245	0.251	862	0.178	0.491	878	0.125	0.176	1594	0.078	0.279
1742	0.942	0.959	1224	0.761	0.735	5	0.576	0.965	921	0.43	0.474	1244	0.333	0.375	1495	0.244	0.472	1538	0.178	0.123	1107	0.125	0.131	907	0.078	0.215
1890	0.942	0.919	1960	0.761	0.517	912	0.576	0.711	1374	0.429	0.449	1717	0.333	0.354	813	0.244	0.211	1568	0.178	0.123	207	0.125	0.056	128	0.078	0.159
1860	0.941	0.803	273	0.76	0.752	1270	0.576	0.459	439	0.428	0.54	1045	0.333	0.199	1893	0.244	0.063	876	0.178	0.099	711	0.124	0.478	254	0.078	0.088
224	0.939	0.975	856	0.758	0.867	1847	0.572	0.857	1939	0.428	0.503	1069	0.333	0.172	797	0.243	0.454	605	0.177	0.375	677	0.124	0.259	995	0.078	0.08
1239	0.939	0.735	1561	0.758	0.573	29	0.57	0.4	510	0.428	0.464	303	0.332	0.545	332	0.243	0.088	1786	0.177	0.243	1633	0.124	0.238	477	0.077	0.4
1524	0.938	0.946	1496	0.758	0.546	232	0.569	0.675	1241	0.428	0.375	94	0.331	0.334	1451	0.242	0.449	931	0.177	0.137	1529	0.124	0.123	140	0.077	0.261
143	0.938	0.821	1007	0.757	0.859	7	0.568	0.81	1975	0.427	0.466	964	0.331	0.22	325	0.242	0.392	768	0.177	0.133	633	0.123	0.463	1630	0.077	0.123
599	0.937	0.977	738	0.757	0.839	494	0.566	0.464	490	0.427	0.267	576	0.331	0.081	1915	0.242	0.188	1291	0.176	0.265	1404	0.123	0.16	1126	0.077	0.086
231	0.937	0.675	1800	0.757	0.773	1896	0.565	0.711	1930	0.427	0.177	457	0.331	0.078	693	0.242	0.15	1721	0.176	0.093	1179	0.123	0.154	663	0.076	0.259
1611	0.936	0.946	1177	0.754	0.905	1208	0.565	0.56	1659	0.427	0.075	62	0.331	0.061	704	0.242	0.127	1701	0.175	0.351	430	0.123	0.055	1714	0.076	0.243
1416	0.936	0.868	362	0.754	0.847	177	0.564	0.289	36	0.426	0.137	1669	0.33	0.573	1517	0.241	0.165	849	0.175	0.231	1053	0.122	0.379	1947	0.076	0.177
1122	0.935	0.964	474	0.751	0.782	1793	0.563	0.21	529	0.426	0.082	1222	0.329	0.724	1342	0.241	0.12	703	0.175	0.198	1268	0.122	0.186	215	0.076	0.167
1064	0.935	0.735	132	0.751	0.69	244	0.562	0.726	385	0.426	0.053	1540	0.329	0.463	52	0.241	0.11	443	0.175	0.196	265	0.121	0.404	352	0.076	0.16
597	0.934	0.998	1253	0.751	0.676	524	0.561	0.487	219	0.424	0.48	107	0.329	0.272	561	0.24	0.28	299	0.175	0.168	543	0.121	0.397	986	0.076	0.136
1276	0.934	0.734	236	0.75	0.726	1618	0.561	0.392	1624	0.423	0.46	1773	0.328	0.461	653	0.24	0.259	79	0.175	0.108	453	0.121	0.196	719	0.076	0.089
1089	0.933	0.735	418	0.75	0.684	1534	0.56	0.449	1200	0.423	0.174	685	0.328	0.112	1353	0.24	0.166	700	0.174	0.168	1187	0.121	0.185	1322	0.075	0.469
1091	0.933	0.735	171	0.747	0.741	1548	0.56	0.449	745	0.422	0.485	1653	0.327	0.384	56	0.239	0.055	360	0.174	0.158	423	0.121	0.174	1681	0.075	0.22
403	0.931	0.99	1301	0.747	0.731	372	0.559	0.682	553	0.422	0.28	1232	0.326	0.51	1782	0.239	0.053	1504	0.174	0.123	1314	0.121	0.111	1641	0.075	0.187
1788	0.931	0.959	1471	0.747	0.589	1290	0.559	0.59	1740	0.422	0.145	546	0.326	0.463	1507	0.238	0.328	790	0.174	0.094	645	0.121	0.102	1111	0.075	0.124
624	0.929	0.998	1464	0.745	0.815	1438	0.559	0.47	1850	0.421	0.56	88	0.326	0.443	1553	0.238	0.061	116	0.174	0.077	1779	0.121	0.093	428	0.075	0.116
331	0.929	0.931	1848	0.745	0.622	203	0.556	0.751	746	0.421	0.487	1613	0.325	0.298	1421	0.237	0.322	1192	0.173	0.252	1176	0.121	0.086	643	0.075	0.095
1327	0.929	0.905	2	0.744	0.978	551	0.556	0.423	1974	0.421	0.466	939	0.325	0.215	199	0.235	0.452	1172	0.173	0.216	1679	0.121	0.066	924	0.075	0.071
1092	0.928	0.95	1006	0.744	0.867	652	0.555	0.485	1003	0.42	0.339	743	0.324	0.079	1623	0.234	0.46	1140	0.173	0.203	279	0.12	0.226	395	0.075	0.062

1132	0.928	0.95	1503	0.743	0.505	1431	0.553	0.449	1458	0.42	0.33	675	0.323	0.102	1895	0.234	0.251	1958	0.173	0.184	1676	0.12	0.164	1394	0.075	0.061
1329	0.927	0.546	1155	0.742	0.745	622	0.553	0.358	1293	0.42	0.265	1988	0.322	0.191	594	0.233	0.602	817	0.173	0.133	391	0.12	0.053	162	0.075	0.056
1000	0.926	0.941	1647	0.741	0.911	1863	0.552	0.787	919	0.42	0.261	348	0.322	0.167	338	0.233	0.16	574	0.173	0.106	903	0.119	0.131	507	0.074	0.308
1813	0.925	0.959	748	0.741	0.727	1205	0.552	0.56	1350	0.42	0.252	1450	0.32	0.288	135	0.233	0.143	387	0.172	0.48	1903	0.119	0.063	1697	0.074	0.208
890	0.925	0.772	1870	0.74	0.806	1877	0.552	0.374	1441	0.42	0.16	1913	0.319	0.601	288	0.233	0.125	1229	0.172	0.275	953	0.119	0.057	1361	0.074	0.185
1615	0.924	0.957	1180	0.739	0.745	165	0.552	0.318	787	0.419	0.727	466	0.319	0.4	46	0.233	0.052	1021	0.172	0.232	239	0.118	0.282	760	0.074	0.164
1781	0.924	0.429	389	0.738	0.626	815	0.55	0.543	784	0.419	0.485	1118	0.319	0.339	476	0.232	0.375	1345	0.172	0.187	251	0.118	0.209	105	0.074	0.077
589	0.923	0.977	425	0.737	0.676	975	0.549	0.365	1539	0.419	0.384	1011	0.319	0.128	1719	0.232	0.243	1444	0.172	0.16	1648	0.118	0.187	741	0.074	0.077
15	0.923	0.963	1771	0.737	0.602	1371	0.548	0.589	112	0.417	0.771	60	0.319	0.061	996	0.232	0.22	1156	0.172	0.156	1311	0.118	0.166	732	0.074	0.061
1936	0.923	0.852	1784	0.737	0.602	260	0.548	0.51	1084	0.417	0.339	1437	0.318	0.16	750	0.231	0.478	649	0.172	0.089	316	0.117	0.365	259	0.074	0.059
694	0.922	0.967	1512	0.737	0.472	1656	0.548	0.392	1764	0.416	0.461	882	0.318	0.069	1383	0.231	0.298	141	0.171	0.116	1136	0.117	0.286	172	0.073	0.283
1157	0.921	0.905	14	0.736	0.963	1544	0.548	0.322	1183	0.415	0.272	1037	0.316	0.136	791	0.231	0.285	1046	0.171	0.069	1792	0.117	0.17	623	0.073	0.255
1018	0.92	0.973	1920	0.735	0.787	1052	0.547	0.97	980	0.415	0.084	144	0.315	0.159	196	0.231	0.154	1602	0.17	0.279	1599	0.117	0.123	802	0.073	0.081
1085	0.92	0.95	1254	0.735	0.269	1260	0.547	0.56	101	0.415	0.066	1384	0.314	0.326	547	0.231	0.106	1967	0.17	0.208	1338	0.117	0.109	1906	0.073	0.072
972	0.92	0.854	1306	0.732	0.886	1124	0.546	0.653	1644	0.414	0.46	1586	0.314	0.305	1041	0.23	0.181	1780	0.17	0.179	785	0.117	0.069	782	0.073	0.068
145	0.92	0.562	1805	0.732	0.857	946	0.546	0.319	1098	0.414	0.269	136	0.314	0.148	1078	0.23	0.124	528	0.169	0.421	1587	0.116	0.164	758	0.072	0.473
193	0.919	0.929	538	0.732	0.782	560	0.546	0.28	406	0.414	0.062	1900	0.314	0.072	168	0.229	0.48	829	0.169	0.215	267	0.116	0.106	329	0.072	0.392
1802	0.919	0.429	1979	0.73	0.912	1842	0.545	0.833	468	0.414	0.062	1297	0.313	0.272	242	0.229	0.272	864	0.169	0.112	973	0.116	0.085	1886	0.072	0.224
304	0.917	0.931	1712	0.729	0.957	1418	0.545	0.59	1514	0.413	0.322	1059	0.313	0.147	123	0.229	0.14	309	0.169	0.106	1050	0.116	0.085	354	0.072	0.205
1372	0.917	0.905	43	0.729	0.225	149	0.545	0.562	479	0.413	0.142	1236	0.313	0.107	905	0.229	0.079	690	0.168	0.491	1040	0.116	0.084	127	0.072	0.135
1436	0.917	0.886	877	0.728	0.772	264	0.543	0.675	521	0.413	0.082	369	0.313	0.053	691	0.228	0.428	1347	0.168	0.288	1905	0.116	0.063	1629	0.072	0.075
1720	0.916	0.896	1281	0.724	0.886	83	0.543	0.636	472	0.412	0.065	1426	0.312	0.51	290	0.228	0.392	590	0.168	0.198	853	0.115	0.215	238	0.072	0.066
1269	0.916	0.886	416	0.723	0.829	1079	0.541	0.408	1638	0.41	0.531	1476	0.312	0.268	1951	0.228	0.341	1472	0.168	0.174	1013	0.115	0.199	515	0.072	0.055
648	0.915	0.772	121	0.722	0.718	115	0.54	0.624	1330	0.41	0.272	1987	0.311	0.44	1349	0.228	0.328	91	0.168	0.152	1277	0.115	0.156	1388	0.071	0.469
895	0.915	0.732	1982	0.722	0.339	1614	0.539	0.957	1963	0.409	0.341	568	0.311	0.397	495	0.228	0.137	125	0.168	0.145	676	0.114	0.259	74	0.071	0.447
1378	0.915	0.656	1730	0.721	0.73	1351	0.536	0.895	965	0.409	0.22	257	0.31	0.751	1448	0.227	0.468	462	0.168	0.053	1691	0.114	0.208	487	0.071	0.367
1985	0.914	0.601	1557	0.72	0.946	1257	0.536	0.731	1891	0.409	0.056	1902	0.31	0.601	1550	0.227	0.468	1104	0.167	0.286	757	0.114	0.198	1969	0.071	0.208
20	0.913	0.846	17	0.719	0.963	1194	0.536	0.394	983	0.408	0.463	446	0.309	0.509	1876	0.227	0.447	799	0.166	0.463	705	0.114	0.068	298	0.071	0.113
1028	0.911	0.973	1080	0.719	0.823	1862	0.535	0.916	1783	0.408	0.325	1481	0.309	0.472	1165	0.227	0.272	1646	0.166	0.187	1100	0.114	0.052	938	0.071	0.099
1884	0.909	0.857	22	0.719	0.549	1163	0.534	0.735	161	0.406	0.082	1223	0.309	0.166	1220	0.227	0.086	1789	0.166	0.17	78	0.112	0.447	969	0.071	0.099
806	0.909	0.854	1844	0.719	0.429	1446	0.534	0.278	970	0.405	0.474	504	0.309	0.082	1341	0.226	0.326	1818	0.166	0.17	1694	0.112	0.178	1315	0.07	0.37

1203	0.908	0.734	1560	0.719	0.268	1683	0.532	0.56	1955	0.405	0.341	498	0.309	0.055	598	0.226	0.304	823	0.166	0.127	863	0.112	0.136	461	0.07	0.319
150	0.907	0.9	1333	0.717	0.589	596	0.532	0.485	50	0.405	0.137	793	0.308	0.455	1029	0.226	0.136	454	0.165	0.4	1543	0.112	0.123	621	0.07	0.251
1751	0.905	0.429	942	0.716	0.717	1852	0.532	0.21	1308	0.404	0.823	850	0.307	0.231	1238	0.225	0.269	545	0.165	0.254	810	0.112	0.101	632	0.07	0.185
847	0.903	0.941	595	0.716	0.602	108	0.531	0.272	119	0.404	0.109	1012	0.307	0.22	730	0.224	0.454	1035	0.165	0.22	846	0.112	0.094	727	0.069	0.421
1841	0.901	0.945	1419	0.716	0.579	1097	0.529	0.265	475	0.403	0.782	1660	0.306	0.33	456	0.224	0.392	1490	0.165	0.123	1938	0.111	0.577	699	0.069	0.416
1093	0.898	0.95	1851	0.716	0.56	1385	0.528	0.546	940	0.403	0.558	1407	0.305	0.51	1894	0.224	0.224	1142	0.165	0.079	1219	0.111	0.275	967	0.069	0.398
248	0.898	0.757	1380	0.715	0.815	18	0.527	0.4	1429	0.401	0.305	1519	0.304	0.472	1502	0.224	0.16	183	0.164	0.452	1825	0.111	0.272	575	0.069	0.275
585	0.898	0.604	361	0.715	0.757	1754	0.527	0.21	688	0.399	0.428	1547	0.304	0.468	614	0.223	0.089	1651	0.164	0.279	698	0.111	0.168	392	0.069	0.205
1811	0.894	0.936	1493	0.715	0.546	1619	0.526	0.392	353	0.399	0.404	1533	0.304	0.179	1369	0.222	0.468	1937	0.164	0.188	1812	0.11	0.272	1071	0.069	0.147
1871	0.894	0.922	1510	0.714	0.858	1977	0.526	0.339	1546	0.399	0.174	702	0.303	0.455	1015	0.222	0.325	327	0.164	0.117	1733	0.11	0.141	517	0.069	0.137
1591	0.893	0.946	1237	0.712	0.886	1395	0.526	0.326	422	0.398	0.48	210	0.303	0.167	586	0.222	0.176	809	0.164	0.071	137	0.11	0.106	412	0.069	0.116
1610	0.893	0.896	1777	0.712	0.21	289	0.524	0.669	153	0.398	0.318	120	0.302	0.624	725	0.222	0.15	1461	0.163	0.51	620	0.11	0.081	929	0.069	0.068
1070	0.892	0.973	1565	0.711	0.701	1073	0.524	0.352	606	0.398	0.074	1249	0.302	0.21	89	0.222	0.066	1488	0.163	0.468	1971	0.109	0.258	1826	0.068	0.272
1186	0.891	0.964	1916	0.709	0.711	1387	0.523	0.328	1787	0.397	0.21	1667	0.301	0.383	1420	0.221	0.449	566	0.163	0.159	1745	0.109	0.243	984	0.068	0.052
820	0.891	0.636	1482	0.709	0.573	467	0.521	0.684	1639	0.396	0.573	1680	0.301	0.178	103	0.221	0.272	626	0.163	0.095	679	0.109	0.102	1396	0.067	0.339
1214	0.89	0.735	1072	0.708	0.352	508	0.52	0.464	943	0.396	0.35	909	0.301	0.176	1686	0.221	0.138	788	0.162	0.2	911	0.109	0.079	1695	0.067	0.208
1060	0.89	0.727	1964	0.707	0.669	557	0.52	0.28	95	0.396	0.061	1147	0.301	0.094	1739	0.22	0.649	1120	0.162	0.124	1150	0.109	0.079	1201	0.067	0.147
1286	0.889	0.886	889	0.705	0.474	1674	0.517	0.46	1684	0.394	0.305	1443	0.3	0.449	482	0.22	0.281	993	0.162	0.053	438	0.109	0.065	1189	0.067	0.146
1918	0.888	0.97	295	0.704	0.904	944	0.517	0.35	554	0.394	0.176	478	0.3	0.114	1312	0.22	0.166	1728	0.161	0.208	1654	0.108	0.22	402	0.067	0.142
1424	0.888	0.573	1704	0.703	0.957	1625	0.516	0.806	1375	0.392	0.449	80	0.299	0.286	1693	0.219	0.472	834	0.161	0.133	1750	0.108	0.179	1167	0.067	0.12
1736	0.886	0.957	1861	0.703	0.833	825	0.516	0.636	164	0.392	0.318	213	0.299	0.259	1652	0.219	0.279	1432	0.16	0.222	587	0.107	0.198	1923	0.066	0.577
1600	0.886	0.879	1857	0.702	0.916	1956	0.516	0.517	682	0.392	0.224	1500	0.298	0.472	1225	0.219	0.269	469	0.16	0.164	937	0.107	0.128	302	0.066	0.16
142	0.885	0.562	1456	0.702	0.701	729	0.516	0.485	904	0.392	0.069	1966	0.298	0.179	59	0.219	0.186	955	0.16	0.099	687	0.107	0.126	601	0.066	0.065
1961	0.884	0.517	282	0.702	0.661	410	0.515	0.676	82	0.391	0.334	233	0.298	0.166	1516	0.219	0.123	61	0.16	0.072	1657	0.106	0.425	886	0.066	0.059
580	0.882	0.982	1672	0.702	0.392	1465	0.513	0.573	156	0.391	0.318	1570	0.297	0.383	458	0.219	0.065	55	0.16	0.055	772	0.106	0.293	1887	0.065	0.447
1302	0.882	0.731	1973	0.701	0.726	754	0.513	0.485	1810	0.391	0.272	1116	0.297	0.099	1804	0.218	0.354	789	0.159	0.2	1943	0.106	0.177	1627	0.065	0.257
274	0.882	0.661	421	0.7	0.811	308	0.512	0.167	204	0.39	0.341	867	0.296	0.215	855	0.218	0.285	263	0.159	0.158	305	0.106	0.168	1605	0.065	0.141
709	0.881	0.772	753	0.7	0.485	1899	0.511	0.756	1555	0.39	0.322	1879	0.295	0.461	859	0.218	0.072	1151	0.159	0.086	1227	0.106	0.086	217	0.065	0.106
1251	0.881	0.676	1799	0.7	0.21	1835	0.51	0.429	1551	0.39	0.066	1413	0.295	0.206	720	0.217	0.168	1141	0.159	0.07	1433	0.105	0.222	979	0.065	0.057
926	0.88	0.727	1082	0.698	0.352	954	0.508	0.474	1129	0.389	0.352	833	0.295	0.133	801	0.217	0.133	1406	0.158	0.37	1622	0.105	0.164	1767	0.065	0.053
484	0.879	0.977	314	0.696	0.847	798	0.507	0.485	564	0.389	0.123	1483	0.293	0.472	76	0.217	0.072	701	0.158	0.285	1492	0.105	0.123	1337	0.064	0.206

189	0.878	0.929	1304	0.696	0.823	6	0.506	0.81	1403	0.387	0.823	413	0.293	0.464	697	0.216	0.229	756	0.158	0.221	124	0.105	0.107	712	0.064	0.174
1400	0.878	0.656	1066	0.694	0.964	728	0.505	0.543	1305	0.387	0.724	962	0.293	0.2	1468	0.216	0.174	892	0.158	0.137	519	0.105	0.082	300	0.064	0.168
1867	0.877	0.936	1520	0.694	0.701	1621	0.505	0.438	1687	0.387	0.383	306	0.293	0.158	985	0.216	0.147	1356	0.158	0.109	900	0.105	0.069	1801	0.063	0.254
1357	0.877	0.815	915	0.693	0.87	1537	0.503	0.305	357	0.387	0.078	803	0.293	0.133	1068	0.215	0.232	1455	0.157	0.51	1711	0.104	0.305	339	0.063	0.168
884	0.876	0.87	618	0.693	0.786	1259	0.502	0.61	246	0.386	0.751	326	0.293	0.117	602	0.215	0.159	588	0.157	0.275	1452	0.104	0.222	1264	0.063	0.07
501	0.876	0.782	534	0.692	0.913	1181	0.502	0.416	1840	0.385	0.833	1494	0.292	0.33	1135	0.215	0.126	1027	0.157	0.21	293	0.104	0.106	473	0.063	0.062
1549	0.876	0.546	1831	0.692	0.901	1303	0.5	0.459	933	0.385	0.325	93	0.292	0.272	1392	0.215	0.098	570	0.157	0.106	1628	0.104	0.066	839	0.062	0.2
1836	0.875	0.949	1114	0.688	0.735	1102	0.5	0.206	779	0.385	0.293	1666	0.292	0.164	619	0.215	0.089	1017	0.157	0.104	683	0.103	0.304	952	0.062	0.081
415	0.875	0.829	1640	0.688	0.573	1575	0.498	0.701	419	0.385	0.267	1700	0.292	0.164	197	0.214	0.452	313	0.156	0.404	216	0.103	0.155	1803	0.062	0.053
1604	0.872	0.946	1233	0.687	0.745	555	0.498	0.397	1942	0.384	0.274	1202	0.292	0.147	616	0.214	0.421	848	0.156	0.176	65	0.103	0.108	989	0.062	0.052
1134	0.872	0.895	1980	0.687	0.601	902	0.498	0.379	431	0.383	0.684	916	0.292	0.071	437	0.214	0.104	1047	0.155	0.408	252	0.103	0.066	1408	0.061	0.463
131	0.87	0.69	1515	0.685	0.546	1245	0.498	0.375	1235	0.383	0.51	1445	0.291	0.449	1833	0.213	0.272	1941	0.155	0.292	870	0.102	0.285	1845	0.061	0.158
420	0.869	0.947	1039	0.684	0.973	1299	0.497	0.468	1031	0.383	0.416	1354	0.291	0.339	345	0.213	0.16	1218	0.155	0.265	1121	0.102	0.177	615	0.061	0.154
1054	0.869	0.859	1634	0.683	0.93	1678	0.497	0.257	665	0.383	0.055	881	0.29	0.295	654	0.213	0.133	968	0.155	0.128	1166	0.102	0.177	1055	0.061	0.138
146	0.867	0.884	465	0.682	0.509	1578	0.496	0.701	1196	0.382	0.497	73	0.29	0.072	500	0.213	0.059	184	0.155	0.088	1075	0.102	0.147	366	0.061	0.113
223	0.867	0.75	1319	0.679	0.546	1952	0.496	0.517	1978	0.382	0.339	1796	0.289	0.622	185	0.212	0.344	1296	0.154	0.469	974	0.102	0.079	1026	0.061	0.081
390	0.866	0.931	1511	0.679	0.505	1131	0.496	0.259	888	0.382	0.231	1034	0.289	0.194	1632	0.212	0.187	971	0.154	0.185	1703	0.102	0.066	583	0.061	0.078
1077	0.865	0.732	1749	0.679	0.21	523	0.495	0.423	87	0.381	0.527	721	0.288	0.228	155	0.212	0.1	319	0.154	0.117	659	0.101	0.428	452	0.061	0.055
1933	0.865	0.711	1817	0.676	0.945	114	0.494	0.718	323	0.381	0.476	1828	0.288	0.158	1484	0.211	0.339	318	0.153	0.545	869	0.101	0.426	681	0.06	0.478
533	0.864	0.991	491	0.676	0.54	684	0.494	0.174	23	0.381	0.3	104	0.287	0.446	617	0.211	0.065	1661	0.153	0.33	744	0.101	0.164	990	0.06	0.463
1636	0.864	0.896	1210	0.673	0.269	400	0.493	0.484	628	0.381	0.251	1248	0.287	0.271	737	0.21	0.251	706	0.152	0.198	774	0.101	0.079	749	0.06	0.428
1119	0.861	0.734	695	0.672	0.786	1231	0.493	0.269	1271	0.381	0.181	655	0.287	0.102	1499	0.209	0.472	342	0.152	0.073	930	0.101	0.068	502	0.059	0.397
188	0.859	0.929	1173	0.669	0.579	75	0.493	0.108	1506	0.38	0.472	1005	0.286	0.261	527	0.209	0.215	593	0.152	0.065	1061	0.1	0.379	222	0.059	0.304
629	0.859	0.839	752	0.669	0.358	927	0.492	0.727	118	0.38	0.35	1589	0.286	0.169	1168	0.209	0.194	1199	0.151	0.286	1732	0.1	0.243	662	0.059	0.255
1907	0.859	0.818	12	0.668	0.815	1658	0.492	0.243	98	0.38	0.334	336	0.286	0.074	1662	0.208	0.179	1606	0.151	0.141	1722	0.1	0.178	1772	0.059	0.053
1282	0.857	0.886	180	0.666	0.833	8	0.491	0.754	1462	0.378	0.51	1234	0.286	0.055	386	0.207	0.463	297	0.151	0.113	102	0.1	0.152	1822	0.058	0.301
910	0.856	0.934	19	0.664	0.846	106	0.491	0.446	486	0.378	0.375	49	0.285	0.306	47	0.207	0.055	294	0.151	0.073	159	0.1	0.121	1108	0.058	0.166
1501	0.856	0.815	368	0.663	0.8	808	0.491	0.293	28	0.378	0.3	1188	0.285	0.252	202	0.206	0.452	1340	0.15	0.22	950	0.1	0.099	569	0.058	0.137
1853	0.856	0.803	723	0.662	0.485	399	0.491	0.164	1897	0.378	0.224	1735	0.284	0.461	1417	0.206	0.339	1917	0.15	0.188	638	0.1	0.055	393	0.058	0.078
556	0.855	0.92	21	0.661	0.4	535	0.49	0.913	1473	0.377	0.472	280	0.284	0.16	894	0.206	0.295	220	0.15	0.154	559	0.1	0.053	163	0.057	0.348
604	0.854	0.839	33	0.661	0.4	110	0.489	0.771	31	0.376	0.3	470	0.284	0.142	1285	0.206	0.098	573	0.15	0.106	1837	0.099	0.272	631	0.057	0.251

836	0.854	0.543	307	0.66	0.904	287	0.489	0.751	1001	0.376	0.22	1422	0.283	0.322	160	0.206	0.082	1162	0.149	0.261	577	0.099	0.229	1009	0.057	0.2
311	0.853	0.86	532	0.658	0.945	1339	0.489	0.326	1881	0.375	0.678	450	0.283	0.166	1110	0.205	0.286	1508	0.149	0.222	1428	0.099	0.185	656	0.057	0.15
724	0.853	0.685	433	0.658	0.509	1567	0.488	0.47	1986	0.375	0.44	100	0.282	0.334	1198	0.205	0.269	275	0.149	0.209	567	0.099	0.15	109	0.057	0.082
999	0.851	0.727	130	0.651	0.718	1240	0.488	0.375	520	0.374	0.433	1527	0.281	0.288	987	0.205	0.194	427	0.149	0.104	578	0.098	0.275	152	0.057	0.082
447	0.85	0.684	647	0.649	0.604	1454	0.488	0.326	603	0.373	0.375	1536	0.281	0.169	68	0.205	0.061	286	0.149	0.088	1513	0.098	0.222	1755	0.056	0.301
1770	0.85	0.614	1838	0.648	0.429	686	0.486	0.68	906	0.373	0.072	1769	0.279	0.145	992	0.204	0.177	1358	0.148	0.469	1389	0.098	0.185	328	0.056	0.205
1144	0.848	0.735	1576	0.646	0.868	982	0.486	0.352	493	0.371	0.602	374	0.278	0.48	840	0.204	0.071	1590	0.148	0.305	1265	0.098	0.16	669	0.056	0.155
1562	0.847	0.868	717	0.646	0.853	1278	0.486	0.185	157	0.371	0.318	84	0.278	0.272	497	0.203	0.059	1263	0.148	0.271	1335	0.098	0.12	355	0.056	0.073
1283	0.846	0.815	1230	0.646	0.56	1620	0.486	0.141	1709	0.371	0.298	1535	0.277	0.328	38	0.203	0.055	812	0.148	0.176	822	0.097	0.231	1405	0.055	0.469
865	0.846	0.636	278	0.644	0.59	26	0.485	0.4	429	0.371	0.104	868	0.277	0.319	1414	0.202	0.288	1025	0.148	0.138	1153	0.097	0.126	440	0.055	0.397
800	0.844	0.941	843	0.642	0.87	715	0.485	0.319	1753	0.369	0.145	786	0.277	0.215	1957	0.202	0.184	1184	0.147	0.359	151	0.097	0.1	1362	0.055	0.206
1036	0.844	0.717	367	0.641	0.757	627	0.485	0.123	1190	0.368	0.359	1409	0.277	0.16	72	0.202	0.079	1715	0.147	0.243	742	0.096	0.428	1682	0.055	0.164
664	0.844	0.224	1117	0.64	0.717	417	0.485	0.104	893	0.368	0.094	873	0.277	0.055	1830	0.202	0.072	1734	0.147	0.243	1762	0.096	0.22	346	0.055	0.16
824	0.843	0.636	1415	0.639	0.653	778	0.485	0.061	1376	0.367	0.653	672	0.276	0.428	708	0.202	0.069	1723	0.147	0.075	271	0.096	0.209	1665	0.055	0.123
776	0.842	0.727	1981	0.638	0.442	1288	0.484	0.272	247	0.367	0.581	1467	0.276	0.33	722	0.201	0.164	166	0.146	0.283	253	0.096	0.154	871	0.055	0.101
1434	0.842	0.676	1761	0.637	0.392	1323	0.483	0.724	1601	0.367	0.46	1743	0.276	0.21	830	0.201	0.055	1760	0.146	0.22	963	0.096	0.128	1829	0.055	0.072
1763	0.841	0.93	411	0.636	0.464	315	0.483	0.476	885	0.367	0.319	378	0.276	0.142	1279	0.201	0.052	1430	0.146	0.169	1865	0.096	0.054	740	0.054	0.416
1310	0.841	0.815	492	0.636	0.464	1808	0.483	0.429	1081	0.367	0.252	1332	0.275	0.469	134	0.2	0.159	483	0.146	0.164	1645	0.095	0.279	1256	0.054	0.37
1397	0.841	0.815	1868	0.635	0.833	1959	0.481	0.517	380	0.367	0.123	1765	0.275	0.461	129	0.2	0.145	341	0.146	0.078	1252	0.095	0.271	1393	0.054	0.37
373	0.84	0.847	1924	0.635	0.711	512	0.481	0.4	321	0.366	0.345	1839	0.275	0.461	988	0.2	0.124	572	0.145	0.15	1710	0.095	0.093	514	0.054	0.275
245	0.84	0.8	58	0.635	0.225	832	0.481	0.215	1016	0.366	0.325	718	0.275	0.319	1250	0.199	0.275	317	0.145	0.117	269	0.094	0.282	1044	0.054	0.086
611	0.839	0.982	333	0.632	0.51	908	0.48	0.059	981	0.366	0.124	1213	0.275	0.269	1123	0.198	0.359	769	0.145	0.072	901	0.094	0.215	310	0.054	0.081
432	0.838	0.947	11	0.63	0.832	301	0.479	0.669	1880	0.366	0.056	1178	0.275	0.126	1096	0.198	0.286	854	0.145	0.072	414	0.093	0.281	1673	0.054	0.066
1439	0.838	0.815	509	0.629	0.464	636	0.478	0.358	548	0.364	0.215	668	0.274	0.224	99	0.198	0.152	407	0.145	0.062	957	0.093	0.224	914	0.054	0.057
1522	0.837	0.656	1928	0.628	0.994	347	0.478	0.319	1246	0.363	0.468	66	0.273	0.061	451	0.197	0.463	1317	0.144	0.469	851	0.093	0.164	463	0.054	0.055
1379	0.835	0.656	243	0.628	0.752	816	0.478	0.102	1983	0.363	0.339	1689	0.272	0.178	1929	0.197	0.184	1911	0.144	0.292	117	0.093	0.143	312	0.053	0.404
1336	0.835	0.546	1953	0.628	0.517	1713	0.477	0.243	1148	0.363	0.126	542	0.272	0.102	917	0.196	0.069	1103	0.144	0.177	1137	0.093	0.086	212	0.053	0.259
1367	0.834	0.905	658	0.627	0.684	1878	0.477	0.224	1095	0.362	0.97	1217	0.272	0.061	936	0.196	0.069	1295	0.144	0.12	330	0.093	0.081	1412	0.053	0.206
1212	0.833	0.676	1221	0.627	0.653	1946	0.477	0.177	1485	0.362	0.46	1795	0.271	0.243	764	0.195	0.176	442	0.143	0.196	1690	0.093	0.075	464	0.053	0.142
441	0.832	0.829	1962	0.627	0.466	379	0.477	0.166	1113	0.362	0.359	1724	0.271	0.208	396	0.195	0.164	1572	0.143	0.169	733	0.093	0.061	1130	0.053	0.136
736	0.831	0.839	1161	0.627	0.394	1216	0.477	0.07	1318	0.362	0.326	1866	0.271	0.054	1298	0.195	0.098	1491	0.143	0.123	322	0.092	0.484	173	0.052	0.348

1377	0.831	0.546	1272	0.626	0.653	759	0.476	0.215	1846	0.361	0.433	549	0.27	0.215	1065	0.195	0.084	1523	0.143	0.123	485	0.092	0.397	1528	0.052	0.164
1949	0.829	0.852	1154	0.626	0.339	1794	0.476	0.21	455	0.361	0.4	1752	0.27	0.178	1477	0.194	0.288	445	0.143	0.065	334	0.092	0.205	1087	0.052	0.147
1062	0.828	0.973	174	0.626	0.318	991	0.476	0.124	1382	0.361	0.216	811	0.27	0.176	268	0.194	0.209	1348	0.142	0.469	1401	0.092	0.185	1057	0.052	0.138
925	0.827	0.636	1671	0.625	0.392	1020	0.475	0.126	351	0.361	0.168	401	0.27	0.142	1931	0.194	0.188	344	0.142	0.392	376	0.092	0.095	1038	0.052	0.136
1612	0.826	0.863	661	0.625	0.358	818	0.474	0.636	827	0.361	0.168	48	0.27	0.11	1275	0.194	0.166	773	0.142	0.068	1169	0.092	0.086	320	0.052	0.117
1211	0.826	0.676	1849	0.624	0.803	296	0.474	0.545	637	0.36	0.73	381	0.269	0.73	1146	0.194	0.124	272	0.141	0.209	897	0.091	0.426	126	0.052	0.104
408	0.824	0.929	814	0.624	0.636	650	0.474	0.101	1014	0.36	0.325	1242	0.269	0.054	1247	0.193	0.271	154	0.141	0.159	1545	0.091	0.279	1149	0.052	0.079
1556	0.824	0.546	25	0.624	0.4	1875	0.473	0.756	879	0.36	0.133	258	0.268	0.389	1019	0.193	0.22	1768	0.141	0.145	696	0.091	0.168	530	0.051	0.304
674	0.822	0.839	1631	0.623	0.858	913	0.473	0.474	1532	0.358	0.531	976	0.267	0.224	1366	0.193	0.185	961	0.141	0.131	646	0.091	0.102	175	0.051	0.259

Table A.10. Overview and specifications of the data utilized in this study, adapted from Khalili et al., (2023).

Input data		Time Span	Resolution	Time step	Region	Nr. Of stations/grids in study area	References
DEM		2008	10 m × 10 m and 90 m × 90 m	-	Global	100% coverage	AltaLIS, http://www.altalis.com; SRTM, Jarvis et al., (2008)
Land use/Land cover		2015	30 m × 30 m	-	Regional/Canadian	100% coverage	Government of Canada (2019)
Soil map	FAO	2005	10 km × 10 km	-	Global	100% coverage	FAO, (1995)
	SLC V3.2	2018	1 km × 1 km	-	Regional/Canadian	Covers the agricultural lands in Canada	Cordeiro et al., (2018)
Climate	WFDEI	1979-2016	0.5° grid	3 hr	Global	574	Weedon et al., (2014)
Potholes		Delineated for each sub-basin	100% coverage	-	Regional/Canadian	100% coverage	Messager et al., (2016)
Reservoir		1982-2016	100% coverage	monthly	Local	44 main reservoirs-lakes	Alberta Environment and Parks; Water Security Agency (WSA) in Saskatchewan; Manitoba Hydro; and HydroLAKES database
Date of planting and harvesting, volume and rate of fertilizer and irrigation application		1982-2016	100% coverage	-	Local	Covers the agricultural lands in Canada	Government of Alberta (Alberta Fertilizer Guide, 2004); Government of Manitoba (Heard, 2020); and Government of Saskatchewan, (2020)
Crop yield		1982-2016	Census Agricultural Region level	yearly	Local	Covers the agricultural lands in Canada	Alberta Financial Service Cooperation (AFSC); Statistics Canada (2021); Manitoba Agricultural Services Corporation; Government of Saskatchewan

Table A.11. Information on the Global Climate Models (GCMs) used in this study to simulate future climate scenarios.

GCM	Institution	Country	Resolution	Forcing scenario
EC-Earth3	27 research institutes from 10 European countries	Europe	1.0° x 1.0°	SSP126, SSP585
MRI-ESM2.0	Meteorological Research Institute (MRI)	Japan	1.4° x 1.4°	SSP126, SSP585
BCC-CSM2-MR	Beijing Climate Center, China Meteorological Administration	China	1.1° x 1.1°	SSP126, SSP585
CNRM-CM6-1	Center National de Recherches Météorologiques (CNRM), France European Earth System Model	France	1.3° x 1.3°	SSP126, SSP585
EC-Earth3-veg	European Earth System Model by 27 research institutes from 10 European countries	Europe	1.0° x 1.0°	SSP126, SSP585
CanESM2	Canadian Centre for Climate Modeling and Analysis	Canada	2.8° x 2.8°	SSP126, SSP585

Table A.12. Classification and Impacts of Drought Severity According to U.S. Drought Monitor Categories and Corresponding SPEI Ranges.

Drought category	SPEI range (intensity)	Impacts
D0 – Abnormally dry	-0.5 to -0.8	Potential stress on some sensitive ecosystems; heightened fire risk. Short-term water deficits can affect planting and growth of crops. Potential for lingering water deficits.
D1 – Moderate drought	-0.8 to -1.3	Stress on more drought-sensitive species; potential for reduced growth rates. Damage to crops and pastures; lowered yield. Some water shortages occurring; voluntary water-use restrictions may be in place.
D2 – Severe drought	-1.3 to -1.5	Widespread stress on many species; increased susceptibility to disease and pests. Likely crop and pasture losses; potential for increased livestock mortality. Water shortages common; mandatory water-use restrictions may be in place.

D3 – Extreme drought	-1.5 to -2.0	Major risk of widespread die-offs and long-term ecosystem change; heightened fire risk. Major crop and pasture losses; risk of financial ruin for farmers. Widespread water shortages; emergency water-use measures may be in effect.
D4 – Exceptional drought	< -2.0	Potential for large-scale and irreversible changes; extreme fire danger. Exceptional and widespread crop and pasture losses; livestock culling. Extreme water shortages creating water emergencies; reservoirs and wells running dry.

Table A.13. Model performance statistics in each agricultural region during calibration and validation for rainfed spring wheat. Adapted from Khalili et al., (2023).

			Calibration (1992-2016)			Validation (1982-1991)		
	Province/State	Agricultural region #	p-factor	r-factor	MSE	p-factor	r-factor	MSE
1	Alberta	AB_1	0.95	1.60	0.05	0.80	1.31	0.20
2		AB_2	1.00	2.67	0.08	0.90	3.43	0.19
3		AB_3	1.00	2.61	0.16	0.70	3.94	0.39
4		AB_4A	0.90	1.15	0.10	0.75	2.12	0.16
5		AB_4B	1.00	1.25	0.10	0.76	2.46	0.08
6		AB_5	1.00	2.39	0.11	0.92	3.28	0.14
7		AB_6	0.95	1.57	0.10	0.60	3.13	0.54
8	Manitoba	MA_1	0.95	2.14	0.19	0.60	2.82	0.11
9		MA_2	0.95	1.78	0.14	0.75	1.55	0.13
10		MA-3	0.95	1.88	0.13	0.75	1.96	0.10
11		MA_4	1.00	2.23	0.01	0.94	1.69	0.07
12		MA_5	1.00	2.02	0.05	0.81	1.49	0.15
13		MA_6	0.82	1.54	0.09	0.78	1.51	0.14
14		MA_7	0.89	2.73	0.26	0.84	1.39	0.25
15		MA_8	1.00	2.25	0.23	0.85	2.19	0.15
16		MA_9	0.90	2.34	0.46	0.85	3.43	0.12
17		MA_11	0.80	1.69	0.31	0.82	1.25	0.33
18		MA_12	0.71	1.34	0.20	0.70	1.24	0.23
19	Saskatchewan	SK_1A	0.90	3.41	0.17	1.00	3.40	0.09
20		SK_1B	0.95	1.46	0.10	0.60	1.72	0.16
21		SK_2A	0.90	3.35	0.18	1.00	3.32	0.06
22		SK_2B	0.50	1.51	0.33	0.80	1.77	0.11
23		SK_3AN	0.95	1.99	0.08	0.90	1.28	0.08
24		SK_3BN	1.00	4.57	0.03	0.90	3.69	0.11
25		SK_3BS	1.00	1.67	0.03	0.85	1.20	0.17
26		SK_4A	0.94	2.63	0.07	1.00	2.78	0.06
27		SK_4B	0.82	1.56	0.12	0.70	0.95	0.20
28		SK_5A	1.00	2.43	0.08	0.75	3.74	0.09
29		SK_5B	1.00	4.51	0.09	1.00	6.33	0.13
30		SK_6A	0.90	2.76	0.22	1.00	2.97	0.02
31		SK_6B	0.90	1.43	0.09	0.90	1.47	0.04
32		SK_7A	0.78	1.57	0.17	0.80	1.34	0.07
33		SK_7B	0.80	1.72	0.18	0.80	2.30	0.05
34		SK_8A	0.94	1.24	0.08	0.60	1.31	0.25
35		SK_8B	0.85	1.73	0.10	0.95	1.94	0.12
36		SK_9A	0.84	1.18	0.12	0.95	1.76	0.10
37		SK_9B	0.89	1.62	0.15	0.75	3.34	0.07
38	Minnesota	MN_10	0.90	1.85	0.34	0.70	1.32	0.53
39		MN_40	0.95	1.60	0.18	0.77	1.51	0.36
40	North Dakota	ND_10	0.90	2.77	0.20	1.00	2.45	0.12
41		ND_20	0.75	1.14	0.23	0.26	3.58	0.40
42		ND_30	0.65	3.25	0.38	0.85	1.36	0.30
43		ND_60	0.75	1.67	0.48	0.43	1.20	0.50
44		ND_90	0.60	1.29	0.33	0.87	1.89	0.36

Table A.14. Model performance statistics in each agricultural region during calibration and validation for rainfed canola.

			Calibration (1992-2016)			Validation (1982-1991)		
	Province/State	Agricultural region #	p-factor	r-factor	MSE	p-factor	r-factor	MSE
1	Alberta	AB_1	0.90	2.00	0.08	0.85	1.94	0.09
2		AB_2	0.95	1.55	0.07	0.90	1.64	0.07
3		AB_3	0.60	2.25	0.08	0.65	2.34	0.10
4		AB_4A	0.80	1.56	0.08	0.80	1.69	0.07
5		AB_4B	0.90	2.42	0.07	0.95	2.56	0.08
6		AB_5	1.00	2.73	0.07	1.00	2.61	0.08
7		AB_6	1.00	3.37	0.10	1.00	3.10	0.11
8	Manitoba	MA_1	0.70	2.58	0.08	0.75	2.63	0.07
9		MA_2	0.95	2.57	0.08	0.90	3.11	0.07
10		MA-3	0.90	2.37	0.10	0.85	2.11	0.12
11		MA_4	0.85	2.09	0.13	0.85	2.20	0.12
12		MA_5	0.95	3.09	0.13	0.90	2.95	0.14
13		MA_6	0.95	2.92	0.09	0.95	3.01	0.09
14		MA_7	0.80	3.36	0.22	0.70	3.44	0.17
15		MA_8	0.95	3.61	0.11	0.90	3.37	0.12
16		MA_9	0.85	2.25	0.19	0.80	2.47	0.18
17		MA_11	0.80	1.89	0.14	0.80	2.01	0.15
18		MA_12	0.95	3.06	0.07	0.90	3.12	0.09
19	Saskatchewan	SK_1A	0.90	3.25	0.08	0.95	3.27	0.09
20		SK_1B	0.85	2.52	0.08	0.85	2.60	0.08
21		SK_2A	0.80	1.82	0.15	0.70	2.12	0.13
22		SK_2B	0.80	2.58	0.16	0.70	2.96	0.13
23		SK_3AN	1.00	2.56	0.08	0.95	2.43	0.09
24		SK_3BN	0.70	1.84	0.17	0.70	1.11	0.19
25		SK_3BS	0.85	1.95	0.13	0.80	2.01	0.15
26		SK_4A	0.84	1.82	0.13	0.79	1.56	0.14
27		SK_4B	0.79	2.24	0.13	0.74	2.39	0.11
28		SK_5A	1.00	3.18	0.05	1.00	2.68	0.07
29		SK_5B	0.95	2.69	0.09	0.85	2.42	0.09
30		SK_6A	0.95	2.69	0.08	0.80	2.38	0.10
31		SK_6B	0.85	1.67	0.06	0.70	1.23	0.08
32		SK_7A	0.85	2.18	0.18	0.75	1.52	0.15
33		SK_7B	0.75	1.63	0.14	0.65	1.22	0.16
34		SK_8A	1.00	2.60	0.06	0.95	2.45	0.07
35		SK_8B	0.90	1.70	0.05	0.80	1.88	0.07
36		SK_9A	0.85	2.02	0.10	0.80	2.16	0.11
37		SK_9B	0.95	2.29	0.12	0.90	2.55	0.13

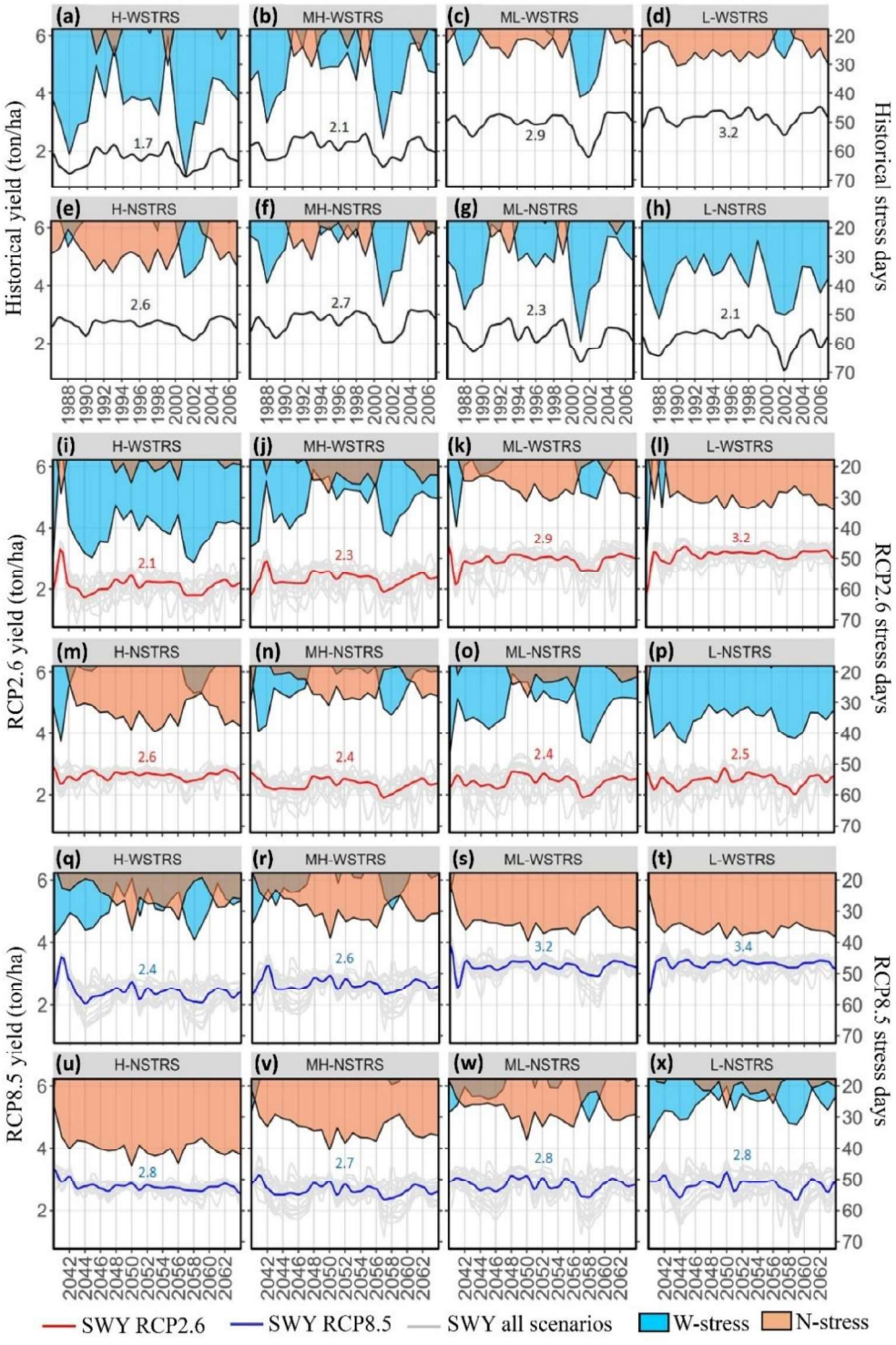

Figure A.1. Comparison of historical SWY and projected SWY in high, mid-high, mid-low, and low W/N-stress regions and each region's respective W-N-stress days. Black, red and blue lines illustrate average of historical and 36 projected SWY scenarios under RCP2.6 and RCP8.5, respectively. The number inside each sub-figure shows the average SWY during the respective time span. Grey signals in each panel are simulated SWY under the 36 scenarios.

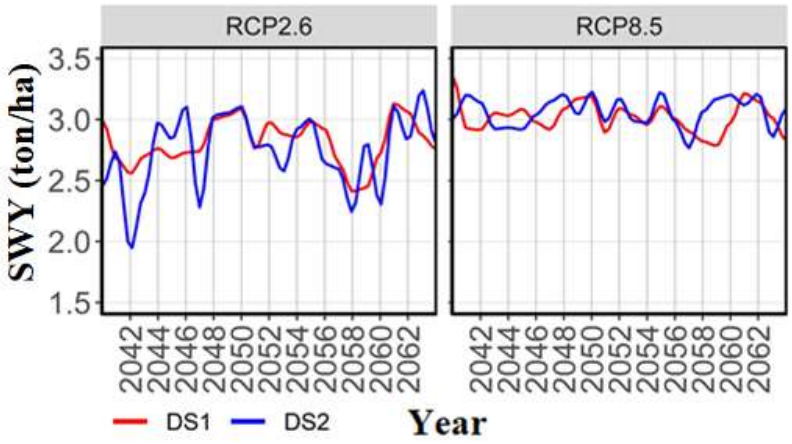

Figure A.2. Comparison of DS1 and DS2 simulated SWY scenarios under RCP2.6, and RCP8.5. DS1 and DS2 denotes ensemble mean of simulated SWY under nine GCMs.

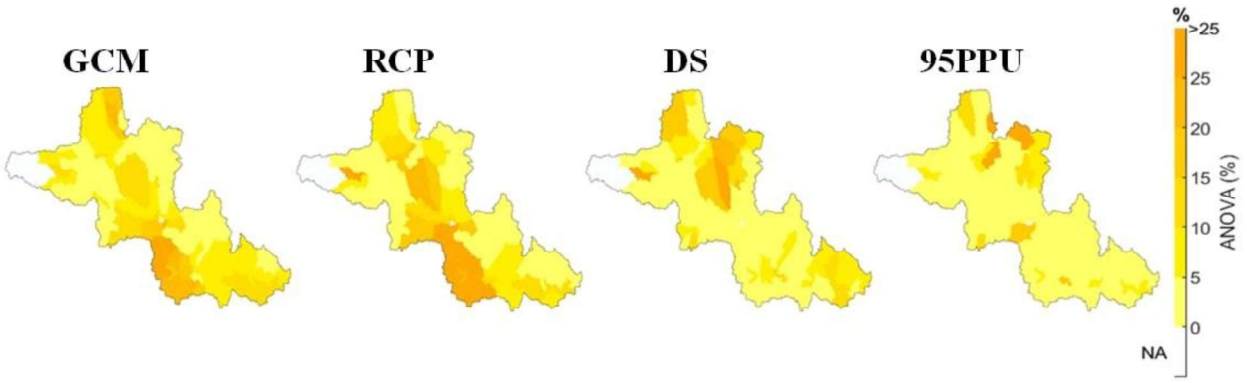

Figure A.3. Spatial distribution of the share of variance under different GCMs, RCPs, DSs, and 95PPUs in RDR basin for future (2040-2064) yield projections.

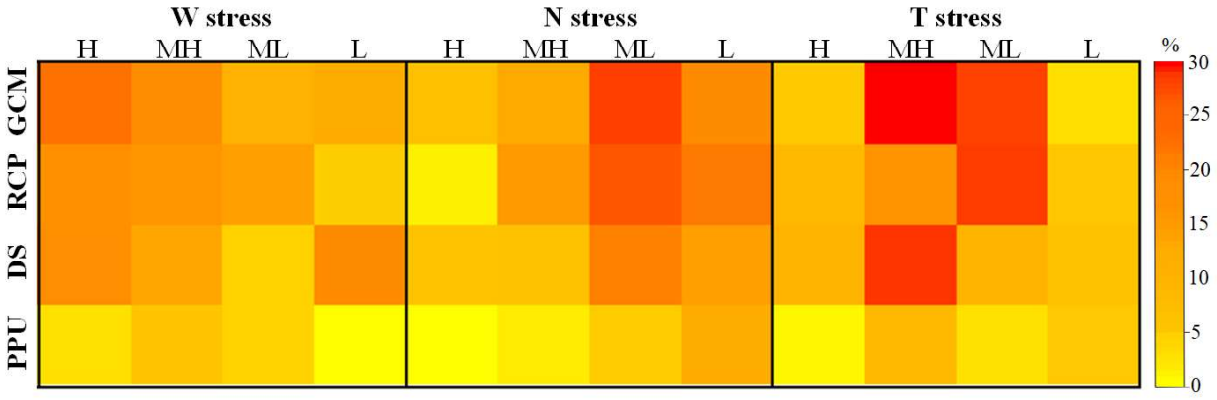

Figure A.4. Share of variance (mean % ANOVA) related to GCM, RCP, DS, and PPU in high (H), mid-high (MH), mid-low (ML), and low (L) W/N/T stress regions for future (2040-2064) yield projections.

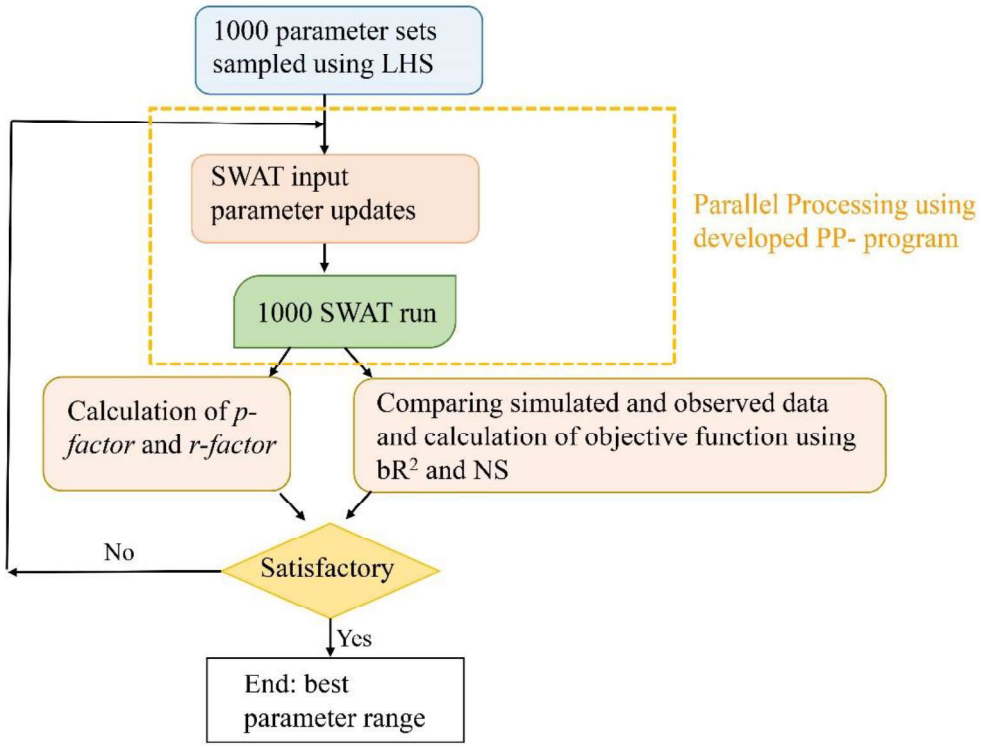

Figure A.5. Main steps of the SWAT, SUFI-2, and PP-program parallel processing used in this study.

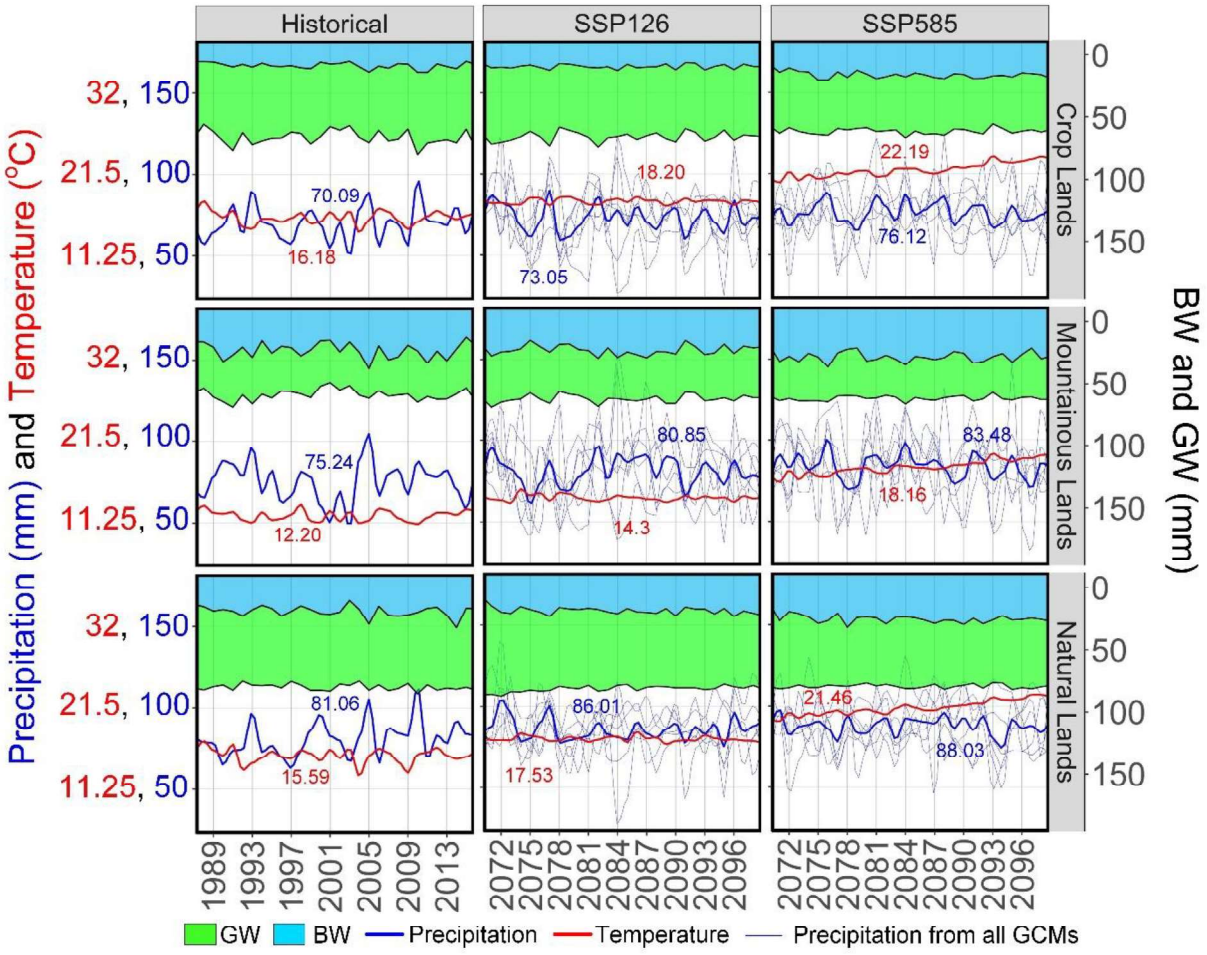

Figure A.6. Comparison of historical precipitation and temperature (left column) and their projected values (middle and right columns) based on six downscaled GCMs used from CMIP6 collection. The data are illustrated for Crop Lands, Mountainous Lands, and Natural Lands during the growing season (May-Sep), and each region's respective BW and GW are shown with blue and green shades. The blue and red lines illustrate the historical and multi-model ensemble mean annual precipitation and temperature with their long-term average values shown next to the lines.

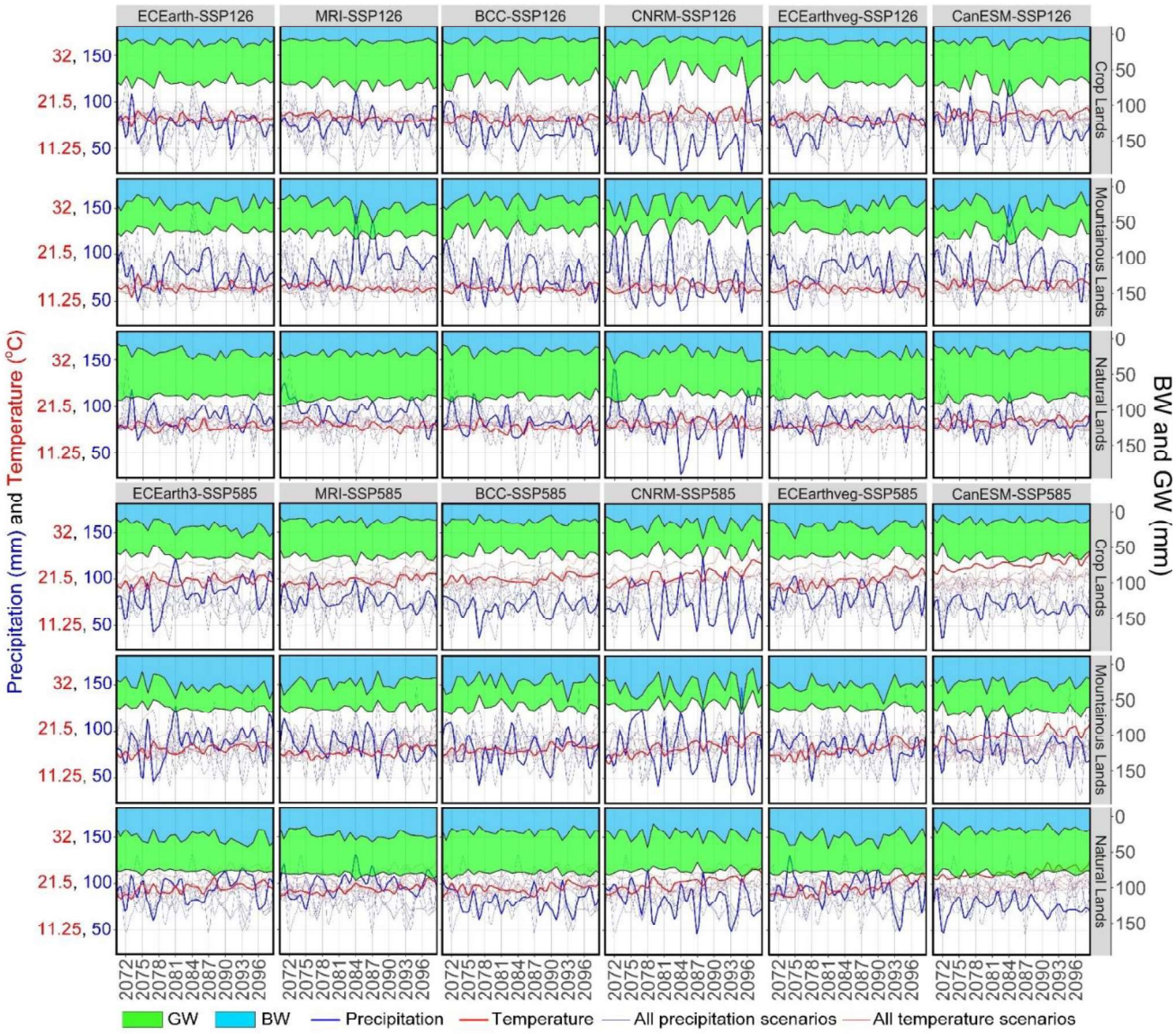

Figure A.7. Comparison of projected precipitation and temperature under ECEEarth3, MRI, BCC, CNRM, ECEarthveg, and CanESM2 GCMs and SSP126, and SSP585 scenarios in crop lands, mountainous lands, and natural lands during the growing season and each region's respective BW and GW. Thick blue and red lines illustrate yearly average projected precipitation and temperature.

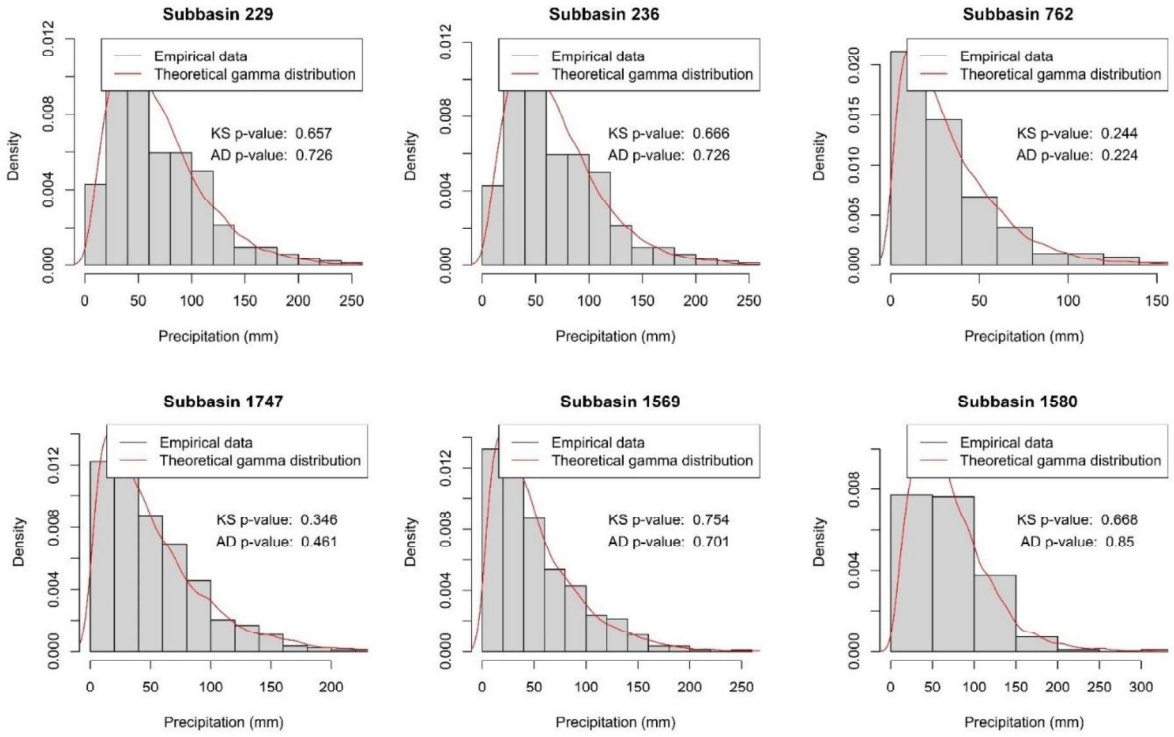

Figure A.8. Empirical versus theoretical Gamma Distribution for selected sub-basins. In sub-figures, a comparison of observed data and gamma distribution model is demonstrated and the p-values are presented for both KS and AD methods. NOTE: the annual precipitation in the selected sub-basins ranges from 391 mm (in sub-basin 762) to 845 mm (in sub-basin 1580), with sub-basins 1569 and 1747 receiving annual precipitations of 612 mm and 620 mm, respectively.

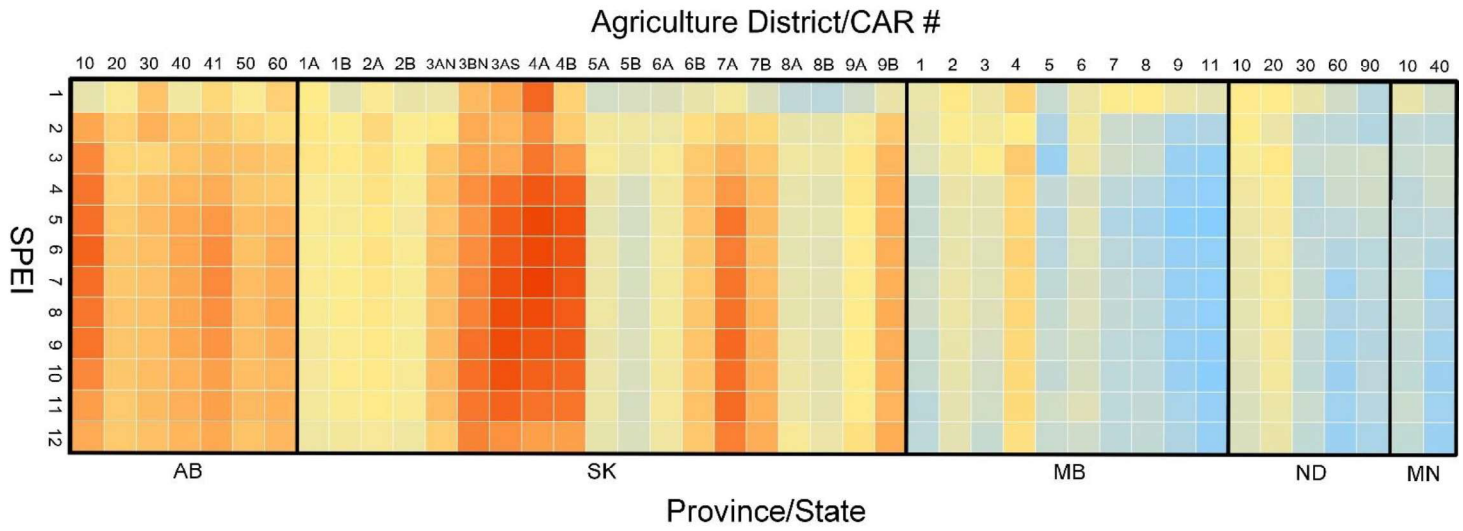

Figure A.9. Pearson correlation coefficient between monthly detrended Standardized Precipitation Evapotranspiration Index (SPEI) and spring wheat yield for different CARs. The horizontal axis represents the various regions. The vertical axis displays different SPEI time scales ranging from 1 to 12 months. A gradient color scale is employed to indicate the strength of the correlation, with a more intense red color signifying a correlation close to 1 (strong positive correlation) and a more prominent blueish color representing weaker correlations.

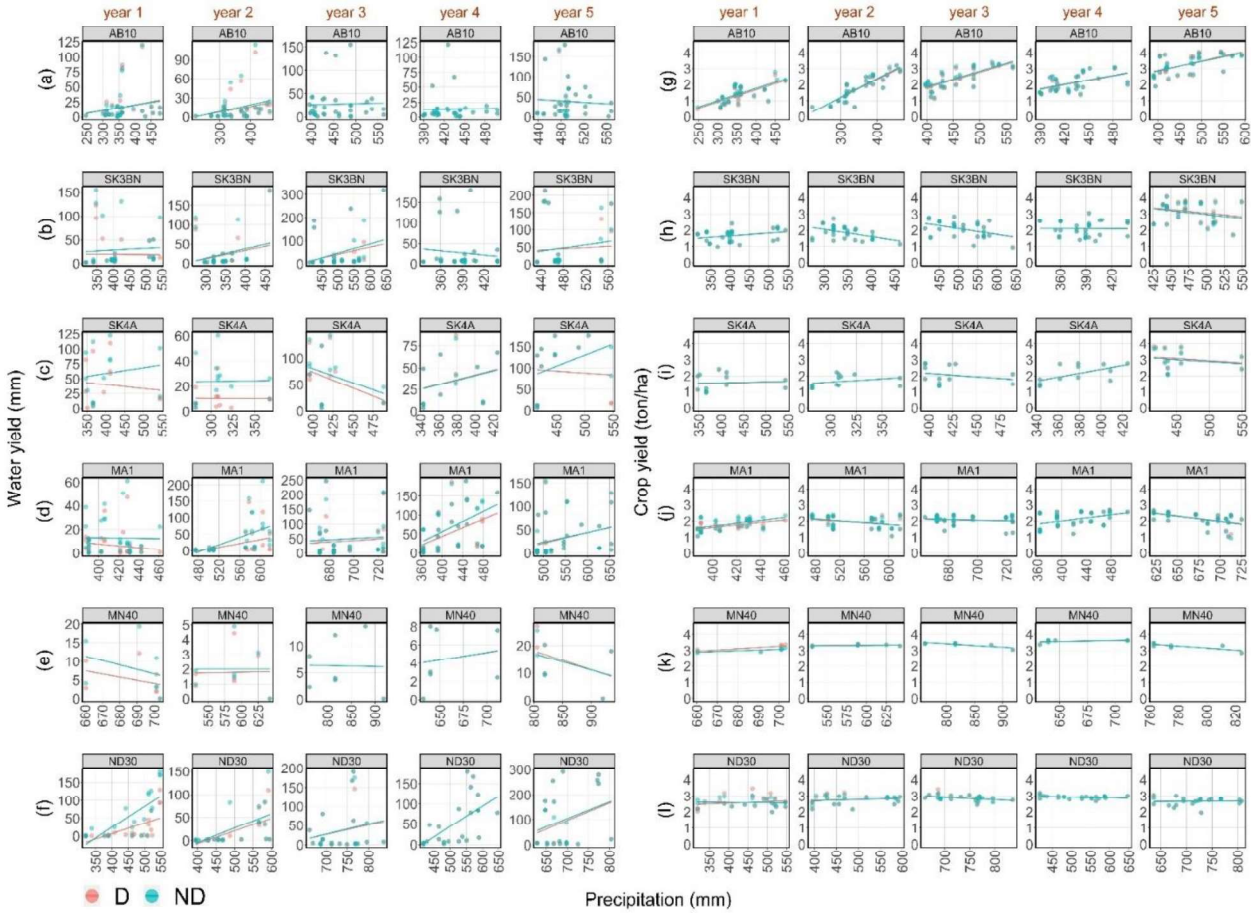

Figure A.10. Comparative analysis of water yield (mm) and crop yield (tonne/ha) for first to fifth post-drought years (D scenario) versus corresponding five-year periods assuming no prior drought (ND scenario) under historical period. Green dots and lines represent the ND scenario, while red dots and lines denote the D scenario across six selected CARs for comprehensive basin coverage. Each dot represents a sub-basin within a CAR.

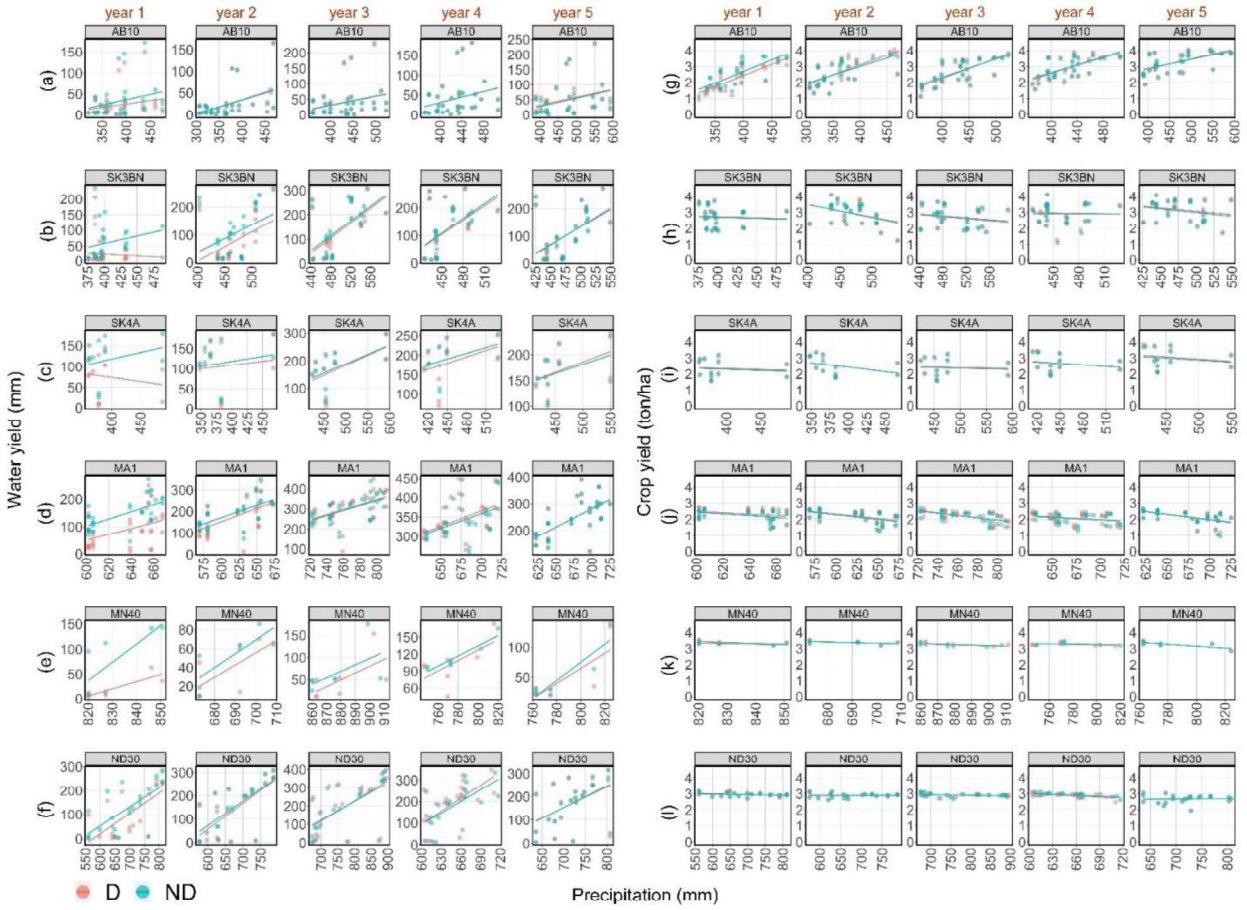

Figure A.11. Simulated WYLD (left) and Y (right) versus cumulative precipitation in six selected CARs across the basin. The data are presented for the five consecutive post-drought years (D scenario, red) and the same years assuming no prior drought (ND scenario, blue) under the SSP585 future scenario. Only spring wheat Y is presented due to its prevalence in the basin. Each dot represents a sub-basin within a CAR.

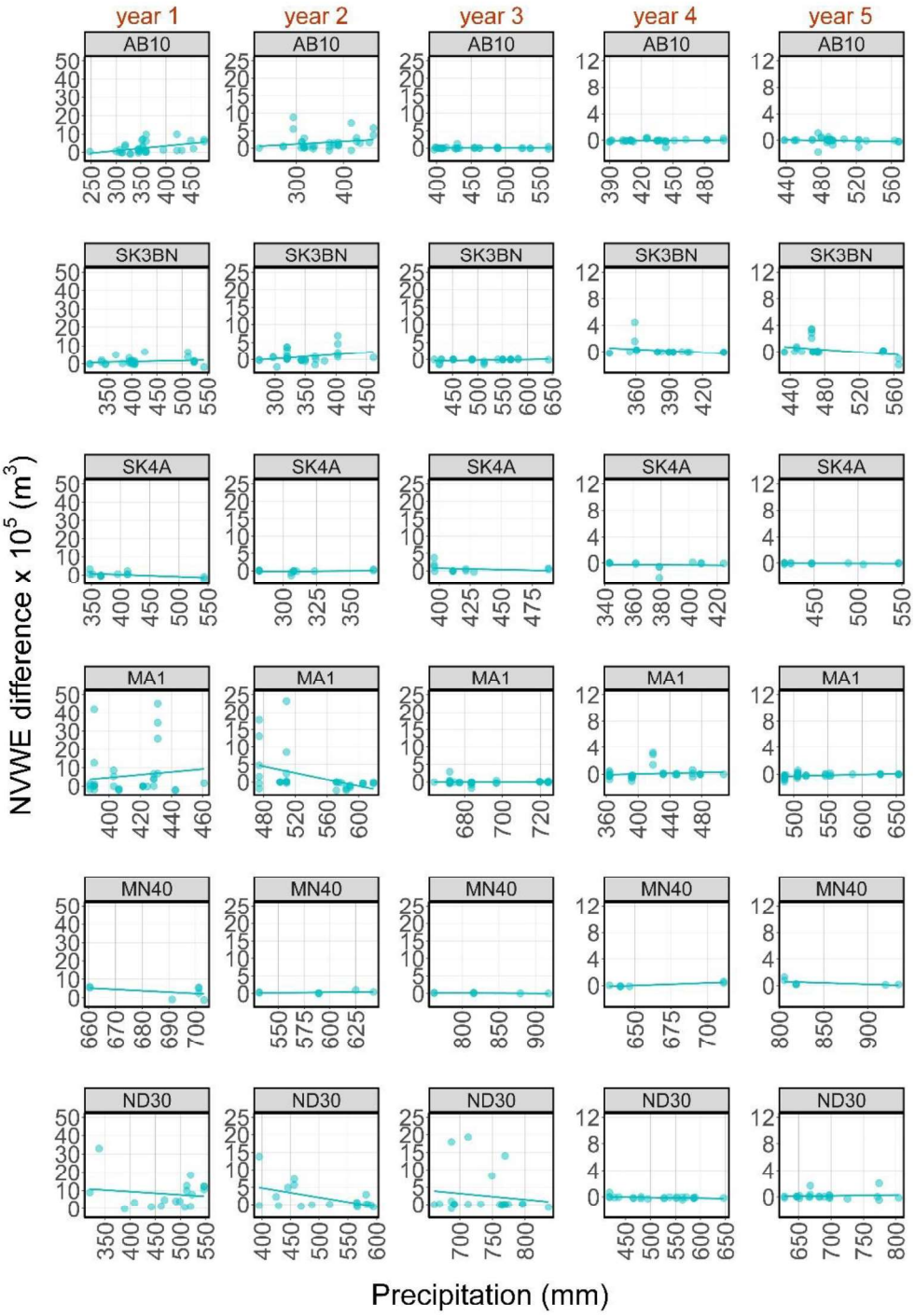

Figure A.12. Simulated net virtual water export (NVWE) anomalies between D and ND scenarios (i.e., calculated as NVWE (D) - NVWE (ND)) in six selected CARs across the basin. The data are presented for five consecutive post-drought years under the historical scenario. Only spring wheat NVWE anomalies ($\times 10^5$ m³) is presented due to its prevalence in the basin. Each dot represents a sub-basin within a CAR.

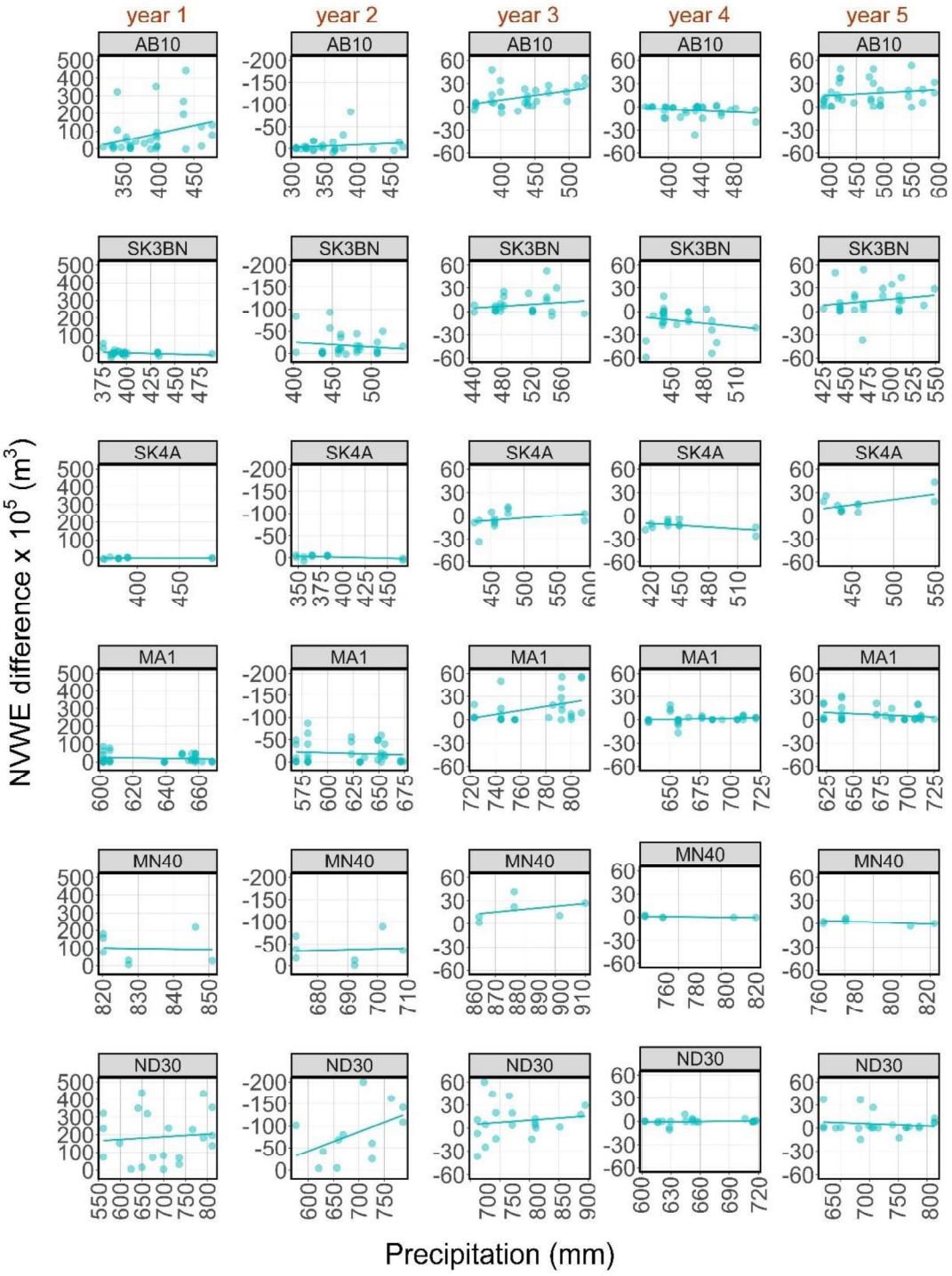

Figure A.13. Simulated net virtual water export (NVWE) anomalies between D and ND scenarios (i.e., calculated as NVWE (D) - NVWE (ND)) in six selected CARs across the basin. The data are presented for five consecutive post-drought years under the SSP585 scenario. Only spring wheat NVWE anomalies ($\times 10^5$ m³) is presented due to its prevalence in the basin. Each dot represents a sub-basin within a CAR.